Design and Assist-as-Needed Control of an Intrinsically Compliant Robotic Orthosis for Gait Rehabilitation

Shahid Hussain

November 2012

Supervisor: Prof. Shane Xie

Co-Supervisors: Assoc. Prof. Enrico Haemmerle

Assoc. Prof. Bruce Macdonald

A thesis submitted in partial fulfillment of the requirements for the degree of Doctor of Philosophy in Mechanical Engineering, The University of Auckland, 2012.

Abstract

Neurologic injuries, such as stroke and spinal cord injuries (SCI), cause damage to neural systems and motor function, which results in lower limb impairment and gait disorders. Subjects with gait disorders require specific training to regain functional mobility. Traditionally, manual physical therapy is used for the gait training of neurologically impaired subjects which has limitations, such as the excessive workload and fatigue of physical therapists. The rehabilitation engineering community is working towards the development of robotic devices and control schemes that can assist during the gait training. The initial prototypes of these robotic gait training orthoses use conventional, industrial actuators that are either extremely heavy or have high endpoint impedance (stiffness). Neurologically impaired subjects often suffer from severe spasms. These stiff actuators may produce forces in response to the undesirable motions, often causing pain or discomfort to patients. The control schemes used by the initial prototypes of robotic gait training orthoses also have a limited ability to provide seamless, adaptive, and customized robotic assistance. This requires new design and control methods to be developed to increase the compliance and adaptability of these automated gait training devices. This research introduces the development of a new robotic gait training orthosis that is intrinsically compliant. Novel, assist-as-needed (AAN) control strategies are proposed to provide adaptive and customized robotic assistance to subjects with different levels of neurologic impairments.

The new robotic gait training orthosis has six degrees of freedom (DOFs), which is powered by pneumatic muscle actuators (PMA). The device provides naturalistic gait pattern and safe interaction with subjects during gait training. New robust feedback control schemes are proposed to improve the trajectory tracking performance of PMAs. A dynamic model of the device and a human lower limb musculoskeletal model are established to study the dynamic interaction between the device and subjects.

In order to provide adaptive, customized robot assisted gait training and to enhance the subject's voluntary participation in the gait training process, two new control schemes are proposed in this research. The first control scheme is based on the impedance control law. The impedance control law modifies the robotic assistance based on the human subject's active joint torque contributions. The levels of robot compliance can be selected by the physical therapist during the impedance control scheme according to the disability level and

stage of rehabilitation of neurologically impaired subjects. The second control scheme is proposed to overcome the shortcomings of impedance control scheme and to provide seamless adaptive, AAN gait training. The adaptive, AAN gait training scheme is based on the estimation of the disability level of neurologically impaired subjects based on the kinematic error and adapts the robotic assistance accordingly. All the control schemes have been evaluated on neurologically intact subjects and the results show that these control schemes can deliver their intended effects. Rigorous clinical trials with neurologically impaired subjects are required to prove the therapeutic efficacy of the proposed robotic orthosis and the adaptive gait training schemes.

The concept of intrinsically compliant robotic gait training orthosis, together with the trajectory tracking and impedance control of robotic gait training orthosis are the important contributions of this research. The algorithms and models developed in this research are applicable to the development of other robotic devices for rehabilitation and assistive purposes. The major contribution of the research lies in the development of a seamless, adaptive AAN gait training strategy. The research will help in evolving the field of compliant actuation of rehabilitation robots along with the development of new control schemes for providing seamless, adaptive AAN gait training.

Acknowledgements

I would like to express my special thanks to my supervisor Prof. Shane Xie for his guidance, support and encouragement throughout this research work. His contagious enthusiasm for this project was the greatest motivation. The Medical and Rehabilitation Robotics research group established by him at the University of Auckland provided me with a valuable research experience. I would also like to thank my co-supervisors Assoc. Prof. Enrico Haemmerle, and Dr. Guangyu Liu for his devotion to the project during the first year. Being an inter disciplinary project, I would like to mention Dr. Yanxin Zhang at the Biomechanics lab, The University of Auckland and Dr. John Parsons at the School of Nursing, The University of Auckland for their valuable interactions; their experience and ideas have helped to tailor this project.

May I also offer thanks to those in the Medical and Rehabilitation Robotic research group with whom I have worked especially Dr. Parshant Jamwal and Dr. Yun Ho Tsoi for making it such an exciting environment. I have also benefited from my interactions with my office mate Dr. Andrew McDaid.

The fourth year honours students Boran Wang and Jiawen Liang at the Department of Mechanical Engineering, The University of Auckland played an important role in fabrication of the mechanical hardware. The Mechatronics laboratory technician Logan Stewart, at the University of Auckland also helped throughout this research in fabricating and improving the mechanical and electronic hardware. Also the IT staff especially Barry Fullerton and Craig Barton deserve a special thanks.

I am forever indebted to my parents for their guidance and support throughout my student life. My brothers, Zahid and Fahad also deserve a special place in these lines. My friends at the University of Auckland provided me with their valuable support and company.

Table of Contents

Abstract ii
Acknowledgements iv
List of Figures ix
List of Tables xii
List of Acronyms, Abbreviations and Mathematical Notations xiii
Chapter 1. Human Gait Rehabilitation: A Review 1
1.1. Human Gait 1
1.2. Spinal Cord Injuries and Stroke as Causes of Gait Disorders 2
1.3. Conventional Gait Rehabilitation: Theory and Practice 3
1.4. Robot Assisted Gait Rehabilitation 5
1.5. Robotic Orthoses for Treadmill Training 6
1.5.1. Commercial robotic orthoses 7
1.5.2. Research prototype robotic orthoses 8
1.6. Gait Training Strategies 10
1.6.1. Trajectory tracking 11
1.6.2. Impedance control 11
1.6.3. Adaptive control 13
1.7. Training Protocols and Evaluation Methods 15
1.8. Literature Findings and Research Motivation 17
1.8.1. Robotic orthosis Design 17
1.8.2. Trajectory tracking Control 19
1.8.3. Muscle activation patterns during robot assisted gait 19
1.8.4. Impedance control for interactive gait training 20
1.8.5. Assist-as-Needed gait training 21
1.9. Research Outline 22
1.9.1. Problem definition 22
1.9.2. Research objectives 23
1.10. Thesis Overview 24
1.11. Chapter Summary 26
Chapter 2. Robotic Orthosis Design 28
2.1. Introduction 28

2.2. Biomechanics of Human Gait 30
2.2.1. Gait cycle 30
2.2.2. Planes and axis division 31
2.2.3. Pelvic and hip complex 32
2.2.4. Kinematics and kinetics of gait cycle 33
2.3. Design Requirements 34
2.4. Mechanism Design and Actuation 36
2.5. Safety 41
2.6. Instrumentation 42
2.7. Visual Feedback 43
2.8. Design Capability Analysis 44
2.9. Conclusions 44
2.10. Acknowledgements 45
Chapter 3. Dynamics of the Robotic Orthosis 46
3.1. Introduction 46
3.2. Numerical Modeling of PMA 47
3.3. Dynamics of the Robotic Orthosis Powered by PMA 49
3.4. PMA Nominal Pressure for Desired Equilibrium Position of the Robotic Orthosis 52
3.5. Robotic Gait Training Orthosis Joint Compliance 53
3.6. Conclusions 55
Chapter 4. Trajectory Tracking Control of the Robotic Orthosis 56
4.1. Introduction 56
4.2. Boundary Layer Augmented Sliding Mode Control (BASMC) 58
4.2.1. Controller formulation 58
4.2.2. Chattering mitigation 61
4.3. Chattering Free Robust Variable Structure Control (CRVC) 62
4.3.1. Generalized CRVC 62
4.3.2. CRVC for the robotic gait training orthosis 63
4.4. Joint Compliance Control 64
4.5. Experimental Evaluation of Trajectory Tracking Controllers 65
4.5.1. Experimental protocol 65
4.5.2. BASMC 66
4.5.3. CRVC 69
4.6. Conclusions 72

Chapter 5. Modeling Muscle Activation Patterns during Robot Assisted Gait 74
5.1. Introduction 74
5.2. Musculoskeletal Gait Model 76
5.3. Robotic Orthosis Model and Control 77
5.4. Optimization 79
5.4.1. Simulation 82
5.5. Results 82
5.5.1. Kinematics 82
5.5.2. Kinetics 83
5.5.3. Robot induced torques 84
5.5.4. Muscle activation patterns 85
5.6. Effect of Cadence Regulation on Muscle Activation Patterns 88
5.6.1. Simulation 89
5.6.2. Results 89
5.7. Discussion 96
5.7.1. Muscle activation patterns 96
5.7.2. Cadence regulation 99
5.8. Conclusions 100
Chapter 6. Impedance Control of Robotic Orthosis for Interactive Gait Training 101
6.1. Introduction 101
6.2. Impedance Control 103
6.3. Inverse Dynamics 105
6.4. Interaction Torque Estimation 107
6.5. Experimental Evaluation 109
6.5.1. Subjects 109
6.5.2. Experiment protocol 109
6.5.3. Data analysis 111
6.6. Experimental Results 111
6.6.1. Joint kinematics 111
6.6.2. Joint compliance 115
6.6.3. Interaction torques 116
6.6.4. Inter subject variability 116
6.7. Related Work 118
6.8. Conclusions 119

Chapter 7. Assist-as-Needed Control of Robotic Gait Training Orthosis 121
7.1. Introduction 121
7.2. Compliance Adaptation 124
7.3. Assist-as-Needed Control 127
7.4. Experimental Protocol 128
7.4.1. Trajectory following experiment 128
7.4.2. AAN experiment 129
7.4.3. Data analysis 130
7.5. Experimental Results 130
7.5.1. Trajectory following experiment 130
7.5.2. AAN experiment 133
7.6. Discussion and Conclusion 136
7.6.1. Related work and significance of present work 137
7.6.2. Conclusions 139
Chapter 8. Conclusions 140
8.1. Contributions 142
8.1.1. Robotic orthosis design 142
8.1.2. Trajectory tracking control 142
8.1.3. Modeling muscle activation patterns during robot assisted gait 143
8.1.4. Impedance control for interactive gait training 143
8.1.5. Assist-as-Needed control 143
8.2. Limitations 144
8.3. Suggestions for Future Work 145
Appendix A. Stability Analysis of Adaptive Assist-as-Needed Control Scheme 146
Appendix B. Bill of Materials 148
Appendix C. Publication List 149
Appendix D. Ethics Approval 151
References 161

List of Figures

Figure 1-1. Body weight supported (BWS) manual treadmill training 4
Figure 1-2. LOKOMAT [7] 7
Figure1-3. (a). ALEX [6]. (b). LOPES [39] 9
Figure1-4. (a). ARTHUR [41, 43]. (b). PAM and POGO [46]. 10
Figure1-5. Overview of Robotic Gait Training 15
Figure 2-1. Phases of gait cycle (GC) 31
Figure 2-2. Plane and Axis [115]. 32
Figure 2-3. Joint angles in sagittal plane [3]. 33
Figure 2-4 Degrees of freedom possible during natural human gait. Flex/Ext. stands for flexion/extension, Inv. for inversion, Int./Ext. for internal/external and Abd. for abduction. (a) Front view of the human lower extremity. (b) Side view of the human lower extremity 34
Figure 2-5. Kinematic diagram of the robotic orthosis showing all the DOF. R5. Revolute ankle joint. R4. Revolute joint for knee flexion. R3. Revolute joint for hip flexion/extension. R2. Revolute joint for hip abduction/adduction. R1 (a,b,c,d). Revolute joints of the parallelogram mechanism for vertical translation. T. Sliders for lateral translation. 37
Figure 2-6. Robotic orthosis, its major components and all the degrees of freedom labelled. A: Parallelogram mechanism for vertical translation, B: Height adjustable frame, C: Hip sagittal plane revolute joint, D: Walker, E: Ankle sagittal plane revolute joint, F: Treadmill, G: Foot lifter, H: Knee sagittal plane revolute joint, I: Hip abduction/adduction revolute joint, J: Sliders for lateral translation. 38
Figure 2-7. Experimental setup of the robotic orthosis with a subject walking on a treadmill. 39
Figure 2-8. (a) Pneumatic muscle actuator (PMA). (b) Double groove aluminium disc. (c) Antagonistic disc-PMA (opposing pair configuration) mechanism. 42
Figure 2-9. A block diagram showing the instrumentation and connection overview of the robotic gait training orthosis. Load cells were only used for the impedance control scheme. 43
Figure 3-1. Schematic drawing of the PMA 47
Figure 3-2. Three element model of PMA [126] 48
Figure 3-3. Overall dynamics of the robotic gait training orthosis. The human subject interaction torques was not modeled in this Chapter. The estimation of human subject interaction torques is presented in Chapter 6. 49
Figure 3-4. (a) Antagonistic PMA configuration. (b) Robotic orthosis with PMA for hip and knee joint actuation 50
Figure 4-1. Robotic orthosis controller diagram. The controller was implemented in joint space. Trajectory tracking controllers based on BASMC and CRVC were developed. The reference joint compliance was selected to be minimum during the present study. 59
Figure 4-2. Hip and knee sagittal plane joint angle trajectories with healthy subjects as a percentage of GC obtained during trajectory tracking mode, averaged over all subjects. Normal gait trajectories taken as desired [3] and plotted against the trajectories obtained during walking in the robotic orthosis. (a) Hip joint. (b) Knee joint. 67
Figure 4-3. Trajectory tracking error at hip and knee sagittal plane joints during the trajectory tracking performance of Fig. 4-2. 67
Figure 4-4. Control effort produced at (a). Hip and (b). Knee sagittal plane joints during tracking performance of Fig. 4-2. 68

Figure 4-5. Hip and knee joint compliance, averaged over all subjects..... 69
Figure 4-6. Hip and knee joint angle trajectories with healthy subjects as a percentage of gait cycle obtained during trajectory tracking mode, averaged over all subjects. Normal gait trajectories taken as reference [3] and plotted against the trajectories obtained during walking in the robotic orthosis (a) Hip joint. (b) Knee joint. 70
Figure 4-7. Trajectory tracking error at hip and knee joints during the trajectory tracking performance of Fig. 4-6. 70
Figure 4-8. Control effort produced at (a). Hip and (b). Knee joints during tracking performance of 4-6. 71
Figure 4-9. Hip and knee joint compliance, averaged over all subjects..... 72
Figure 5-1. (a) Major muscle groups used in the musculoskeletal model. (b) Ground contact force model. Adapted from [113]..... 77
Figure 5-2. Robotic orthosis leg model to guide subject's limbs on reference trajectories (side view). 78
Figure 5-3. Sagittal plane joint angle trajectories obtained for hip, knee and ankle for a GC. A positive value indicates flexion and a negative value indicates extension at the hip and knee joints. A positive value indicates dorsiflexion and a negative value indicates plantarflexion at the ankle joint..... 83
Figure 5-4. Ground contact force (GCF) normalized to system mass for a GC. 83
Figure 5-5. (a) Torques at human hip, knee and ankle sagittal plane joints for a GC. (b) Torques induced by the robotic orthosis at sagittal plane hip, knee and ankle joint. A positive value indicates extension and a negative value indicates flexion at the hip and knee joints. A positive value indicates plantarflexion and a negative value indicates dorsiflexion at ankle joint. 84
Figure 5-6. Predicted muscle activations during robot assisted gait for a GC. Abbreviations: Hamstrings (HAM), rectus femoris (RF), gluteus maximus (GLU), uniarticular hip flexors (iliopsoas, IP), gastrocnemius (GAS), vasti (VAS), soleus (SOL) and tibialis anterior (TA)..... 86
Figure 5-7. (a) Perturbation torques at hip joint. Blue and red curves show a +5% and -5% perturbation, respectively. A small window shows the perturbation torques during 50-60% of gait cycle (b) Hip joint muscle activations produced in response to the perturbations..... 87
Figure 5-8. Joint angles of the subject with respect to % GC during slow, natural and fast cadence. (a) Hip angles (deg). (b) Knee angles (deg). (c) Ankle angles (deg). Flx: Flexion, Ext: Extension, Pf: Plantar flexion, Df: Dorsiflexion. 90
Figure 5-9. Vertical ground contact force (GCF) normalized to system mass for slow, natural and fast cadence with respect to % GC. 91
Figure 5-10. Torques (N-m/kg) during slow, natural and fast cadence at. (a) Hip joint. (b) Knee joint. (c) Ankle joint. 92
Figure 5-11. Torques induced by the robotic orthosis during slow, natural and fast cadence at. (a) Hip joint. (b) Knee joint. (c) Ankle joint. 93
Figure 5-12. Muscle activation patterns for a GC at slow, natural and fast cadence. (b). Mean activation patterns for a GC at slow, natural and fast cadence. 95
Figure 6-1. Impedance controller diagram. Position controller works on the basis of the CRVC law (Chapter 4). The inverse dynamics algorithm extracts the active human torque component (**Tha**) from remaining passive and kinetic effects. The proportional torque controller minimizes the error in $\mathbf{T - Tha}$. The impedance controller was implemented in joint space..... 104
Figure 6-2. Passive joint torque. (a). Hip joint. (b). Knee joint. Adapted from [112] 106
Figure 6-3. Average hip and knee sagittal plane joint angle trajectories with healthy subjects as a percentage of GC obtained during position control mode, averaged over all subjects for two GC.

Position controller works on the basis of CRVC. Normal gait trajectories taken as desired and plotted against the trajectories obtained during walking in the robotic orthosis. (a) Hip joint. (b) Knee joint. 112
Figure 6-4. Average hip and knee sagittal plane joint angle trajectories with healthy subjects as a percentage of GC obtained during zero impedance control mode, averaged over all subjects for two GC. Normal gait trajectories taken as desired and plotted against the trajectories obtained during walking in the robotic orthosis. (a) Hip joint. (b) Knee joint. 113
Figure 6-5. Average hip and knee sagittal plane joint angle trajectories with healthy subjects as a percentage of GC obtained during non-zero impedance control with high compliance, averaged over all subjects for two GC. Normal gait trajectories taken as desired and plotted against the trajectories obtained during walking in the robotic orthosis. (a) Hip joint. (b) Knee joint. 114
Figure 6-6. Average hip and knee sagittal plane joint angle trajectories with healthy subjects as a percentage of GC obtained during non-zero impedance control with low compliance, averaged over all subjects for two GC. Normal gait trajectories taken as desired and plotted against the trajectories obtained during walking in the robotic orthosis. (a) Hip joint. (b) Knee joint. 114
Figure 6-7. Hip sagittal plane joint compliance for four different control modes as a percentage of GC, averaged over all subjects for two GC. 115
Figure 6-8. Knee sagittal plane joint compliance for four different control modes as a percentage of GC, averaged over all subjects for two GC. 115
Figure 7-1. Assist-as-needed controller diagram. Position controller works on the basis of the CRVC control law (Chapter 4). The assist-as-needed torque decay term continuously decrease the amount of robotic assistance if trajectory tracking errors are small. The controller was implemented in joint space. 125
Figure 7-2. Radial Basis functions for the hip and knee sagittal plane joints. (a) Hip joint. (b) Knee joint. 126
Figure 7-3. Average hip and knee sagittal plane joint angle trajectories with healthy subjects as a percentage of GC obtained during position control mode (trajectory tracking), averaged over all subjects for two GC. The deviations from the reference trajectories were kept to be minimum. The shown trajectories are for the values of forgetting rate ($\boldsymbol{\tau = 8s}$) that still allows the robotic orthosis to move the subjects' limbs on reference trajectories. (a) Hip joint. (b) Knee joint. 131
Figure 7-4. Average hip and knee sagittal plane joint angle trajectories with healthy subjects as a percentage of GC obtained during zero-impedance control or backdrive mode, averaged over all subjects for two GC. No robotic assistance was provided during this mode. (a) Hip joint. (b) Knee joint. 132
Figure 7-5. Robot applied torque at hip and knee sagittal plane joints of healthy subjects as a percentage of GC obtained during AAN experiment for always active condition, averaged over all subjects for two GC. Trajectories with a forgetting term ($\boldsymbol{\tau = 8s}$) and without a forgetting term ($\boldsymbol{\tau = \infty}$) are shown. (a) Hip joint. (b) Knee joint. 134
Figure 7-6. Robot applied torque at hip and knee sagittal plane joints of healthy subjects as a percentage of GC obtained during AAN experiment for inactive to active condition, averaged over all subjects for two GC. Trajectories with a forgetting term ($\boldsymbol{\tau = 8s}$) and without a forgetting term ($\boldsymbol{\tau = \infty}$) are shown. The subjects' remained inactive (passive) during GC1. At the end of GC1 the subjects' participated actively in the gait training process during GC2. (a) Hip joint. (b) Knee joint. 135

List of Tables

Table 1-1. Overview of treadmill based robotic gait training orthoses. 6
Table2-1 Actuated, passive and blocked DOF of the robotic orthosis compared with natural human gait. 37
Table2-2. Maximum ranges of motions and joint moments of robotic orthosis [3]. 40
Table 4-1. Geometric and inertial parameters of test subjects. 65
Table 5-1. Mean kinematic and kinetic measures. 96
Table 6-1. Maximum Absolute Values of sagittal plane Joint Angular Deviations and Joint Interaction Moment Ranges Recorded for Different Control Modes and Averaged Over Subjects. 116
Table 6-2. Average of sagittal plane Joint Angles and Joint Interaction Moment Ranges (+ Standard Deviations) Recorded for Different Control Modes. Average values of 60 GC for All Subjects are Presented. 117
Table 6-3. Inter Subject Variability of sagittal plane Joint Angles and Joint Interaction Moment Ranges (+ Standard Deviations) Recorded for Different Control Modes. Variability for 60 GC is presented. 117
Table 7-1. Maximum Absolute Values of sagittal plane Joint Angular Deviations and Mean values of the controller output joint torque for Different Control Modes and Averaged Over Subjects during trajectory following experiment. The joint torque is the rough indicator of the robotic assistance provided to the subjects. Standard Deviations (+) are presented for within subject variability..... 132
Table 7-2. Maximum Absolute Values of sagittal plane Joint Angular Deviations and Maximum value of the controller output joint torque for Different Control Modes and Averaged Over Subjects during assist-as-needed experiment. The joint torque is the rough indicator of the robotic assistance provided to the subjects. Standard Deviations (+) are presented for within subject variability. Values for GC2 presented in Fig. 7-5 and 7-6 are provided. 136

List of Acronyms, Abbreviations and Mathematical Notations

Acronyms and Abbreviations

Active Leg Exoskeleton	ALEX
Ambulation-assisting Robotic Tool for Human Rehabilitation	ARTHUR
Assist-as-Needed	AAN
Body Weight Support	BWS
Boundary Layer Augmented Sliding Mode Control	BASMC
Chattering Free Robust Variable Structure Control	CRVC
Degrees of Freedom	DOFs
Drive Gait Orthosis	DGO
Gait Cycle	GC
Gastrocnemius	GAS
Gluteus Maximus	GLU
Ground Contact Force	GCF
Hamstrings	HAM
Iliopsoas	IP
Incomplete Spinal Cord Injuries	ISCI
Lower Extremity Powered Exoskeleton	LOPES
Pelvic Assist Manipulator	PAM
Physiological Cross-sectional Area	PCSA
Proxy Based Sliding Mode Control	PBSMC
Pneumatic Muscle Actuators	PMA
Pneumatically Operated Gait Orthosis	POGO

Rectus Femoris	RF
Spinal Cord Injuries	SCI
Sliding Mode Control	SMC
Soleus	SOL
Tibialis Anterior	TA
Vasti	VAS

Mathematical Notations

θ^*	Desired joint position
θ	Actual robot position
$\dot{\theta}$	Robot joint velocity
K	Stiffness matrix
B	Viscosity matrix
F	Force at the end-effector
M	Combined patient-orthosis inertia matrix
C	Coriolis and centrifugal torque
G	Gravity torques
T_a	Torque applied by actuator onto the orthosis
r	Radius of robotic orthosis joint disc
T_f and T_e	Torque due to each of the individual PMA
x_f and x_e	Lengths of two PMA
l_i	Length of i^{th} leg segment
I_i	Inertia of i^{th} leg segment
P_{MAX}	Maximum pressure that can be applied to the PMA
P_{0ei}, P_{0fi},	Nominal pressures
Δp_i	Controllable pressures
γ_i	Robotic orthosis joint compliance
ρ	Gain margin of the design
$S(t)$	Time varying sliding surface
$\emptyset_h$ and $\emptyset_k$	Boundary layer thicknesses

z	Vertical deformation of heel and toe
$\dot{z}$	Rate of vertical deformation of heel and toe
F_{ce}	Effective force provided by the contractile element
F_a^M	Muscle activations
$\tilde{T}_t$	Interaction torque between the robotic orthosis and the human subject
T_{ha}	Active human torque components
T_{hp}	Passive human torque components
g_{ni}	*nth* radial basis function
$\hat{\beta}$	Parameter estimate vector
$\frac{1}{\tau}$	Forgetting rate of the robotic orthosis

Chapter 1. Human Gait Rehabilitation: A Review

While the use of robotic manipulators has a long history in the automation of industrial processes, there is an increasing trend where robotic devices are used to provide health care services. An important area of health care services is the physical therapy of stroke and spinal cord injured (SCI) subjects. Physical therapy for gait rehabilitation of these subjects is an important task [1, 2]. For this reason, much research has been dedicated to the development of robotic devices that can aid in the gait rehabilitation of stroke and SCI subjects [1, 2]. The use of robotic devices in the field of gait rehabilitation may help in providing repetitive, systematic, prolonged and customized gait training sessions at a reasonable cost [1, 2]. The overall aim of this research is to develop a robotic device to facilitate the process of physical therapy for human gait rehabilitation. This chapter provides background knowledge on the issues relating to this research, starting with the basic definitions of human gait and the causes of gait disorders. An overview of the conventional gait training procedure is also provided. Study of the human gait, possible gait disorders and conventional gait rehabilitation practices is also important while investigating robot design and control specifications. State-of-the-art in the mechanism design, actuation and control strategies of robotic gait training devices is provided. Information regarding the training protocols used to evaluate these robotic devices is also provided. The motivations and objectives of this research, as well as the overview of this thesis, are provided at the end of this chapter.

1.1. Human Gait

Human gait can be defined as: ‘a particular way of walking, running, or moving along on foot’, or ‘shorter a manner of walking’[3]. In literature on rehabilitation, *gait* is usually a synonym for *walking*. This activity is so familiar, that it may seem excessive to define it in detail. The activity of walking itself is, however, much easier than the activity of defining it scientifically as a bio-mechanical and control process. A basic insight is that human gait is a dynamical process – sometimes described as a constantly prevented falling – in the way that it is not a semi-static motion of the legs, that, if stopped, instantly leads to a statically stable standing position [3, 4]. On the contrary, the body centre of mass is periodically brought further forward than the limit of static stability, causing the body to fall forward, and then, by placing a foot forward in time, an actual fall is prevented. This way of moving, uses gravity as the main driving force; therefore, is very economic with the use of muscle power.

Except for this forward direction, the body is also sideways instable. In fact, it strongly resembles a standing stick, always about to fall. This impels a human to not only constantly prevent a forward fall, but at the same time, using the same two feet, prevent a sideways fall. This has also to be attained by placing the feet in time at a position that assures stability. How difficult this combined stability problem is can both be seen from the difficulty children have in learning to walk as from the scientific literature on the issue [3, 5].

As the exact mechanisms in walking are complex and not fully understood, most research literature on walking is limited to the calculation and mutual relation of *gait parameters*, such as step length, step width, walking velocity, cadence, step frequency [3], to the observation over a *gait cycle* (GC) of averaged kinematics and kinetics; for example, motion profiles, calculated torque-profiles in joints, and the ground reaction forces. Such information allows identifying and quantifying disorders in walking. The background knowledge relevant to the biomechanics of human gait is provided in chapter 2 (section 2.2). The knowledge relevant to the biomechanics of human gait is important for the design, modeling and control of robotic gait training orthosis.

In the everyday life, walking, or in general 'the ability to move oneself around' is a very important condition for independent, personal functioning, both for private and societal objectives. Losing this ability severely affects ones functioning and well-being, as well as strongly increasing dependency on others. Therefore, there is usually significant personal as well as therapeutic effort in recovering gait, in case of disorders.

1.2. Spinal Cord Injuries and Stroke as Causes of Gait Disorders

Neurologic injuries, such as stroke and SCI, cause damage to neural systems and motor function, which results in lower limb impairment and gait disorders [6, 7]. Human *motor function or motor skill* is the ability to perform complex neuromuscular acts that produce movement [8-10]. There are more than 55 million survivors of stroke worldwide, with over half of these subjects having some form of stroke related disability [11]. Each year more than 780000 Americans suffer from a new or recurrent stroke [11]. Traumatic brain injuries and stroke are the third highest cause of death in New Zealand each year, and the highest cause of ongoing disability [12].

Current figures show that twenty New Zealanders suffer a new stroke each day and the rate is increasing [12]. Leading causes of hospitalization and rehabilitation are stroke and

SCI. Current trends suggest that if enough is not done to prevent stroke, the current rate will increase three times over the next thirty years, indicating sixty new strokes per day and, over 20,000 new strokes annually [13]. New Zealand has one of the highest rates of SCI in the western world and since 1979, this has been increasing [13]. Those who survive stroke and SCI often have a greater level of ongoing lower limb disability. Improvements in walking capabilities of SCI subjects are confirmed by recent studies [7, 14].

The rehabilitation and hospitalization costs for stroke and SCI are among the highest for all injuries [12, 13]. The costs of resulting disabilities to both individuals and society are staggering. Moreover, with advancing medical technology and increasing life expectancies, these costs are increasing at a rapid pace. Reports of costs related to SCI in Australia shows an annual spending of $250 million during the year 2006 [15]. The estimated cost of stroke recovery is $ 65.5 billion in US [11]. These costs pose a burden to society, and more should be done in the field of rehabilitation for affected subjects.

The neurologic injuries and the resulting disabilities have far reaching consequences on human life. For instance, stroke and SCI causes motor function disorders that would result in lower limb disability and mobility loss. Often, subjects are incapable of returning to their premorbid roles in society or may even require long term care and assistance. Much attention should be paid to regain walking capability at least in the home environment so that the subjects may not pose a burden to the society and can perform activities of daily living. The gait rehabilitation of neurologically impaired subjects is vital in order to reduce the economic burden on the health care system, as well as to provide more opportunities to the neurologically impaired subjects to participate actively in their private, social, and professional lives. The preliminary research has shown that the systematic and repetitive physical therapy of these subjects can help them in regaining functional mobility [16-23]. While stroke and SCI are the leading causes of long term lower limb disability in the modern world, there is no universally accepted gait rehabilitation approach [24]. The work at the Department of Mechanical Engineering, University of Auckland, focuses on the gait rehabilitation of stroke and SCI subjects.

1.3. Conventional Gait Rehabilitation: Theory and Practice

The traditional therapy methods used for SCI and stroke rehabilitation involve manual gait training of subjects. Body weight supported (BWS) manually assisted treadmill training

has been in practice for more than 20 years [25, 26] (Fig. 1-1). The BWS treadmill training usually starts four to six weeks after a neurologic injury, when the subjects are not yet capable of moving their legs themselves. Also, the subjects are incapable of supporting their body weight. During the BWS treadmill training, the trunk of subjects' is stabilized using a weight compensation system and a harness. BWS treadmill training requires a team of three or more physical therapists to guide subjects' legs on predefined paths and to stabilize subjects' pelvis. BWS manually assisted treadmill training has proven significant improvements in step length, endurance, and walking speed of neurologically impaired subjects [16-23].

Figure 1-1. Body weight supported (BWS) manual treadmill training

The BWS treadmill training may become more effective if the legs are moved in a reproducible, rhythmical, and physiological manner [7]. Thus, the role of physical therapist is vital in the treadmill training process. The quality of manually assisted BWS treadmill training is dependent on physical therapists' experience and judgment, which varies widely amongst therapists. Also, the training sessions are short due to physical therapists' fatigue and frequent complaints of back pain have been made by physical therapists. Also, the manual physical therapy does not have any proper method of recording subjects' progress and recovery.

1.4. Robot Assisted Gait Rehabilitation

Automated rehabilitation solutions have been researched lately to overcome the above mentioned shortcomings of manual physical therapy [7]. Robot assisted gait training has several advantages over manual physical therapy; it relieves the physical therapist from the strenuous task of manual assistance and facilitates in delivering well controlled repetitive, prolonged training sessions. The physical therapist's role is limited to supervision. The subjectivity of manually assisted training is eliminated by providing measurement of interaction forces and limb movements to assess the quantitative level of motor function recovery.

The history of robot assisted training started with the adaptation of industrial robotic manipulators to the field of rehabilitation [27-29]. Following that trend, various devices were designed for restoration of upper limb and gait functions. The industrial robotic manipulators are mainly designed for tasks such as pick and place, and are inherently stiff and massive. Robotic training devices, on the other hand, need compliant and safe human-machine interface. Subsequently, robots for applying suitable forces and capable of providing a safe interaction with the subject are developed [1, 7]. Most of these robots are wearable, and work in proximity with the subject's limbs. *Active orthosis* or *robotic orthosis* are more common terms for these wearable robotic devices [1, 6]. From the studies of gait biomechanics and manual physical therapy practice, different training strategies are incorporated in the robot control schemes to enhance motor function recovery [1]. *Passive orthoses*, such as gravity balancing orthosis (GBO) [30, 31] has also been developed to assist subjects with hemiparesis to walk through full or partial elimination of the effects of gravity. These passive orthoses [30, 31] use only passive elements like springs and do not have any motors or actuators on them. As passive orthosis cannot supply energy to the leg, they are limited in their ability compared to an active orthosis.

The field of robot assisted treadmill training has evolved significantly during the last decade. Rehabilitation engineering community is now evaluating different training strategies in combination with new actuation concepts for standardization of robot assisted treadmill training process. Our focus in this work is the robotic orthosis for treadmill training of neurologically impaired subjects.

1.5. Robotic Orthoses for Treadmill Training

Robotic orthoses are training devices that work in parallel with the human body and have mechanical actuation to apply forces to the human limbs. The history of robotic orthoses started in late 1970's. Early active orthoses were standard braces with added actuation mechanisms [32]. Among the first full lower limb robotic orthosis is the University of Wisconsin prototype [33]. The orthosis has universal joints at hip and ankle and provides sagittal plane flexion/extension motions by means of hydraulic cylinders. The remaining degrees of freedom (DOFs) are passively held by springs. A complete listing of the robotic gait training orthoses is provided in Table 1-1. Actuated DOFs, actuation mechanism and the gait training strategies, along with proper citations, are provided in Table 1-1. Robotic orthoses using functional electrical stimulation, [34] and those designed for a single joint like Ankle robot [35] are not discussed in this work.

Table 1-1. Overview of treadmill based robotic gait training orthoses.

Device	Actuation	Actuated Degrees of Freedom	Training Strategy	Citations
LOKOMAT	DC motor drive	2	Impedance based assistance, Adaptive Assistance	[36, 37]
Autoambulator	DC motor drive	2	-	[38]
LOPES	Series elastic actuation (SEA)	4	Impedance based assistance	[39, 40]
ALEX	Servo drive	2	Force field based impedance controller	[6, 41, 42]
ARTHUR	Servo drive	2	Impedance based adaptation	[43, 44]
PAM & POGO	Pneumatic Cylinders	7	Admittance based assistance	[45, 46]

1.5.1. Commercial robotic orthoses

The first modern automated BWS treadmill training system LOKOMAT was developed in the late 1990's and is commercially available (Fig. 1-2). The system has a wearable driven gait orthosis, (DGO) having mechanical actuation to power hip and knee sagittal plane rotations [7]. DC motors with a ball screw mechanism are used to power the hip and knee sagittal plane joints. Dorsiflexion to the ankle joint is provided by passive elastic bands and the hip abduction/adduction is kept free. DGO works on the assumption that the orthosis joints are in perfect alignment with subject's joints, and the joint positions are measured with encoders built into DC motors. The physical contact between DGO and subject is through two force-torque sensors placed in series with DC motors that move orthosis links. DGO is connected to the treadmill by a rotatable parallelogram linkage in order to stabilize subject's trunk. In this manner, the DGO moves only in vertical direction, avoiding any sideways tilt of trunk. BWS up to 40% of total body weight can be selected. Later on, an automated and adaptable BWS system was designed by the developers of LOKOMAT, which compensates the weight of the subject according to his weight bearing capabilities during the training process [47]. Also, a control method for automated treadmill speed adaptation is designed, which can adjust treadmill speed according to the subject's disability level and intention in real time [48].

Autoambulator is a similar treadmill training device developed by Health South for subjects with gait disorders, coordination, balance and postural problems [38]. This device also has direct current (DC) motor drives at hip and knee joints for sagittal plane rotations. Details relevant to the working of Autoambulator are not available.

Figure 1-2. LOKOMAT [7]

1.5.2. Research prototype robotic orthoses

1.5.2.1. Active leg exoskeleton

Recently a robotic orthosis, Active leg exoskeleton (ALEX) has been developed at the University of Delaware for gait training of stroke survivors [6] (Fig. 1-3 (a)). ALEX uses gravity balancing orthosis (GBO) [30] as its foundation. GBO is a passive device without any mechanical actuation and utilizes the conventional method of geometrically locating the center of mass by using a parallelogram mechanism. Zero free-length springs are then placed at appropriate positions to balance the effect of gravity [31]. Linear servo drives are used on the GBO for providing actuation at hip and knee joints for flexion/extension rotations in sagittal plane. Hip abduction/adduction and four trunk rotations are held passive by means of springs. ALEX also uses the position encoders built into servo drives and force sensors mounted in series with the servo drives that move orthosis segments. The use of gravity balancing makes the orthosis light weight and reduces the amount of force required from actuators. ALEX is also attached to a treadmill with a walker via parallelogram linkage. ALEX does not provide any actuation at the ankle joint for foot clearance during swing phase of gait; instead it uses the method of force field control for foot clearance.

1.5.2.2. Lower extremity powered exoskeleton

Lower extremity powered exoskeleton (LOPES) uses a Bowden cable based actuation system usually referred to as Series Elastic Actuation (SEA) [39] (Fig. 1-3 (b)). It is built on the idea of a light weight exoskeleton system having a pair of springs in series with an electric motor. The electric motor is coupled to the springs via Bowden-cables. Due to the cable based actuation, the electric motor is placed on a remote station and act as a low weight pure force source. The displacement of springs recorded by linear potentiometers is used as a force measurement. The actuated degrees of freedom include two pelvis rotations, hip sagittal and frontal plane rotations, and knee sagittal plane rotations. The results with actuated hip and knee sagittal plane rotations are available. The other degrees of freedom are blocked during experiments. LOPES don't provide any actuation for ankle joint. It is reported that the joint angle sensor readings are not accurate enough for inverse dynamic modeling [39]. Due to this problem, the joint torques may not be estimated properly, which results in inefficient control of the exoskeleton. Also, the displacement of springs is not an effective way of measuring actuator forces due to high exoskeleton joint friction [49]. A sensor pressure

distribution has also been carried out in order to estimate the human robot interaction during LOPES assisted gait [49]. Unfortunately, no clinical data has been reported for that study.

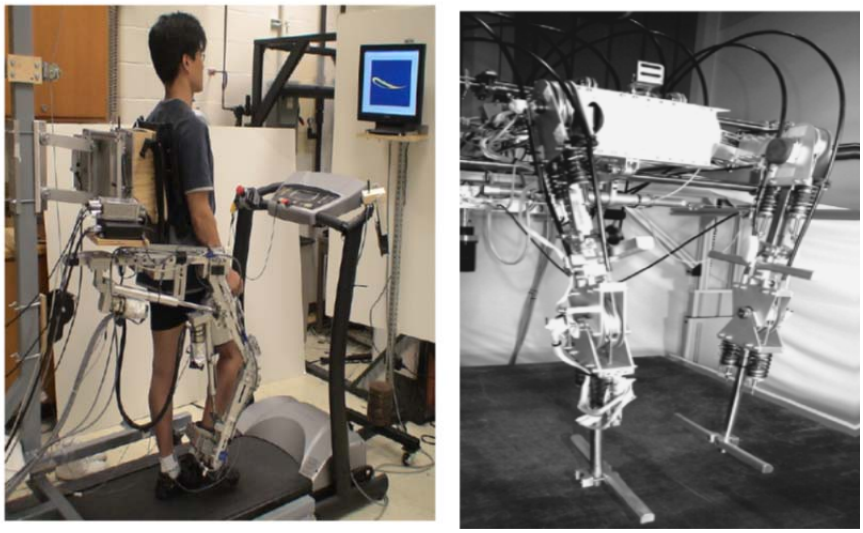

(a) **(b)**

Figure1-3. (a). ALEX [6]. (b). LOPES [39]

1.5.2.3. Ambulation-assisting robotic tool for human rehabilitation

Ambulation-assisting robotic tool for human rehabilitation (ARTHUR) is developed to mechanically interact with a single leg during treadmill training (Fig. 1-4 (a)). It consists of two moving coil brushless servo motors that drive either end of a two bar linkage [41, 43]. ARTHUR provides motions to knee and ankle joints in sagittal plane and is force and position controllable. The device can generate substantial force required for gait training purpose and is light weight. ARTHUR is limited to knee and ankle joint motions and don't address the need of proper hip joint actuation. Moreover, the designers of ARTHUR have not considered the pelvic motions as well as hip abduction/ adduction.

1.5.2.4. PAM and POGO

Pelvic Assist Manipulator (PAM) is developed to allow naturalistic movements to the human pelvis during gait training [46]. Two, 3-DOF robotic arms are used to assist the subject's pelvis during treadmill training (Fig. 1-4 (b)). These two robotic arms are placed at an angle to give the therapist access from sides and from behind. PAM uses pneumatic actuators to provide lateral and rotational pelvic movements to the subject. PAM is used in combination with pneumatically operated gait orthosis (POGO), a device which provides pneumatic actuation for hip and knee sagittal rotations. Pneumatic actuators have built-in

linear potentiometers to measure the cylinder lengths in order to solve the kinematics of the system. Force control is achieved by implementing nonlinear force tracking controllers to control the gas flow into and out of each cylinder [45]. A constant upward force is applied by pneumatic cylinders for gravity compensation of the device.

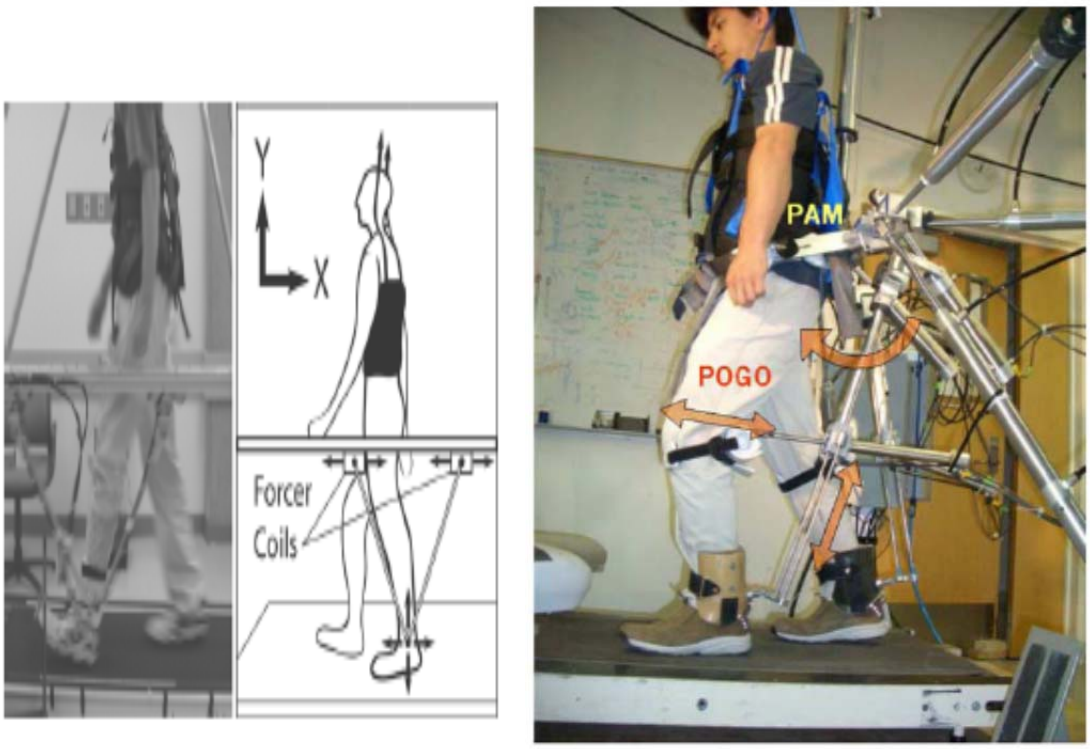

(a) **(b)**

Figure1-4. (a). ARTHUR [41, 43]. (b). PAM and POGO [46].

1.6. Gait Training Strategies

The goal of robot assisted gait training is to reinstate motor function so that the human movement capability could be improved. Although successful determinants of gait training are largely unknown, repetitive and task oriented training strategies may result in significant improvements [50, 51]. These determinants have been formulated by drawing concepts from rehabilitation, neuroscience, and motor learning literature [52, 53]. Gait training is to be provided according to the level of disability while encouraging subject's active participation in the training process. Various robot control strategies have been developed for providing gait training according to the disability level and stage of rehabilitation of neurologically impaired subjects [1]. Robot assisted treadmill training utilizes trajectory tracking, impedance and adaptive control based training strategies.

1.6.1. Trajectory tracking

Trajectory tracking or *position control* is widely implemented by robotic gait training devices [7, 54]. Trajectory tracking works on the principle of guiding the subject's limbs on fixed reference gait trajectories. It mainly consists of proportional feedback position controllers with joint angle gait trajectories as input [55-57]. The proportional feedback controller limits the difference between the reference trajectories and the actual trajectories (*i.e.* kinematic error). For trajectory tracking, the issue of determining the reference trajectory is important. Mathematical models of normative gait trajectories and prerecorded trajectories from healthy individuals are commonly used [7, 46, 58, 59]. A teach and replay technique is introduced by the designers of ARTHUR in which a joint angle trajectory is recorded during manual assistance and is then replayed during robotic assistance [41]. Recently, a reference trajectory generation method is developed for hemiparetic subjects. Desired trajectory for the impaired limb is generated online based on the movement of an unimpaired contralateral limb [60].

Trajectory tracking is suitable for gait training of wheel chair bound subjects with SCI or acute stroke when they have no muscular strength to move their limbs. A potential issue with this method is the imposition of a predefined trajectory which limits kinematic error, an important parameter that drives human motor learning [44, 61, 62]. This may result in abnormal gait pattern generations and would leave the subject unable to adapt to physiological gait [63].

Subject's active participation and involvement in the robotic gait training process is important to improve motor function [44, 64]. The terms of *patient cooperative*, *assist as needed* (AAN), *adaptive, and interactive* robot assisted gait training are used in literature [37, 39, 65]. Robot assisted gait training utilizes impedance and adaptation based control strategies to actively involve the human subjects in training process.

1.6.2. Impedance control

The relationship between the force exerted by the actuators and resulting motion is generally known as *Mechanical Impedance* [36, 37]. The concept of impedance control in the field of robotics is first introduced by Hogan [66]. Impedance control work on the principle of force based impedance control and is mostly implemented in the form of an outer position

feedback loop and inner force feedback loop. The impedance based assistance controller work on the basis of 2-D control law:

$$\mathrm{F} = \mathrm{K}(\theta^* - \theta) - \mathrm{B}\dot{\theta} \tag{1.1}$$

where F is the force at the end-effector, θ is the robot actual position, θ^* is the desired position, $\dot{\theta}$ is the robot velocity, K is the stiffness matrix, and B is the viscosity matrix.

LOKOMAT uses the impedance controller [37]. For gait training purpose, the idea behind impedance control is to allow variable deviation from reference gait trajectory depending on the patient's resistance. As long as the patient is on the reference trajectory with minimum deviations, the robot should not intervene. After a set limit is exceeded, an adjustable moment is applied at each joint to keep the leg within a defined range along the reference trajectory. The impedance values are chosen by the physical therapist based on their experience and patient's disability level. For higher impedance values, the concept of admittance control is also utilized by LOKOMAT [67]. Admittance controller as opposed to impedance control works on the principle of position based impedance control.

A variant of impedance control is impedance based triggered assistance. This allows the patient to begin movement without any robotic assistance and if the patient is unable to achieve a threshold value, then the robotic assistance could be triggered. The threshold value could be the trajectory tracking error or minimum force generated by the patient. This form of impedance based assistance encourages self-initiated movement by patients [68]. A similar approach is used by the developers of PAM and POGO while using pneumatic actuators [46].

More recent forms of impedance controllers use the concept of viscous force fields [69, 70]. For ALEX, a force field controller is developed for applying tangential and normal forces at patient's ankle. The linear actuators mounted at the hip and knee joints, simulate the forces applied at the ankle. Tangential forces help to move the patient along the trajectory and normal forces simulate virtual walls around the desired ankle trajectory in the plane containing human thigh and shank [6, 42]. An impedance control based path control strategy is recently proposed by developers of LOKOMAT[71]. In this strategy, compliant virtual walls keep patient's legs within a tunnel around the desired spatial path, whereas ALEX simulates the virtual walls around the subject's foot only.

LOPES also uses impedance control for its *patient in charge* and *robot in charge* modes [39]. Robot in charge mode is the trajectory tracking mode in which the controller impedance is increased, so the patient is not in a compliant environment. During patient in charge mode low impedance values are used.

1.6.3. Adaptive control

The potential issue with trajectory tracking and impedance control based training is that they do not tune controller parameters based on real time judgment of the patient's disability level [1, 37]. Adaptive assistance is utilized to enhance patient's active participation in the training process [61]. The basis of adaptive assistance is to modify the robot motion in a way that is desired by the patient. Moreover, the adaptive assistance will provide robotic gait training according to the disability level and stage of rehabilitation of neurologically impaired subjects. The adaptive robotic assistance may help in increasing the rate of recovery of neurologically impaired subjects [37].

The term adaptation is used for real time tuning of the controllers designed for robotic actuators to match patient's disability level and to actively involve him/her in the training process. Robot motion is initiated from the physical interaction between the patient and orthosis. As disability level varies from subject to subject, online estimation of patient-orthosis interaction force is the most crucial task in adaptive assistance paradigm. In most of the gait training orthoses, this interaction force is estimated from the combined patient-orthosis dynamic model:

$$\mathrm{M}(\theta)\ddot{\theta} + \mathrm{C}(\theta, \dot{\theta})\dot{\theta} + \mathrm{G}(\theta) + \mathrm{F}(\dot{\theta}) = \mathrm{T}_a + \tilde{\mathrm{T}}_t \qquad (1.2)$$

where M is the combined patient-orthosis inertia matrix, C is a term for coriolis and centrifugal torque, G is a term representing gravity torques, and F is orthosis joint friction. T_a is the torque applied by actuator onto the orthosis, $\tilde{\mathrm{T}}_t$ is the patient-orthosis interaction torque or the resistance offered by patient to applied actuator forces and θ is the generalized position vector representing joint angles. $\dot{\theta}$ and $\ddot{\theta}$ are joint velocity and acceleration, respectively.

Different methods are used to estimate patient-orthosis interaction torque component $\tilde{\mathrm{T}}_t$ from eq.1.2. LOKOMAT use a moving average based exponential forgetting technique for interaction torque estimation. After obtaining this estimate, various reference joint angle adaptation algorithms are formulated to adapt reference gait trajectory parameters by online

optimization [36]. These algorithms include; inverse dynamics based joint angle adaptation, direct dynamics based joint angle adaptation, and impedance control based joint angle adaptation [36]. The reference joint angle trajectories are parameterized through variable scaling factors to obtain different hip and knee joint angle trajectories. The impedance control based joint angle adaptation algorithm works on the basis of an inner proportional integral (PI) force control loop and an outer proportional derivative (PD) position control loop [36]. However, the extent of reference trajectory modification is an important research question, as it may not yield in the development of physiological trajectories.

Later, an impedance magnitude adaptation algorithm is formulated for LOKOMAT [37]. This algorithm works on the basis of impedance magnitude adaptation with constant reference joint angle trajectories. In case of a small patient resistance torque ($\tilde{T}_t$) estimate, the controller impedance is set high to guide the patient's limbs on reference trajectory [37]. Impedance magnitude is reduced in the case of larger $\tilde{T}_t$ estimates, and larger deviations from reference trajectory are allowed.

ARTHUR uses an approach of manual teach and replay for robot assisted gait training. Physical therapists are asked to provide manual gait training to subjects first, and the kinematic and kinetic gait parameters are recorded. These recorded parameters are then used during robotic gait training to adapt the stiffness and damping of a proportional derivative (PD) force controller as a function of trajectory tracking error [41]. The orthosis-patient interaction force is estimated by an error based control law with a forgetting factor *f*, which shows that patient attempts to complete a movement with reduced effort. This forgetting factor will help in reducing the robotic assistance if trajectory tracking error is small:

$$F_{n+1} = fF_n + g(\theta - \theta^*) \tag{1.3}$$

where is F_{n+1} is the robot impedance at present time step, F_n is the robot impedance at nth step, *f* is the forgetting factor varying between 0 and 1 and *g* is the learning gain. The effectiveness of the manual teach and replay for robot assisted treadmill training is not proven, because the process of obtaining a reference gait trajectory depends on physical therapist's experience and judgment. The uniformity of this process is not guaranteed during different training sessions, even in the case of a team of same physical therapists.

The adaptive algorithms discussed above estimate the patient-orthosis interaction force from the combined dynamic model of the patient and orthosis mechanism. The quality of

interaction force estimation is dependent on the accuracy of force and joint position sensors and also on the estimation algorithm [72]. The abrupt forces like muscle spasms arising from patient and resulting actuator *non-back-drivability* presents a major problem to the interaction torque estimation. *Back-drivability* is the ability of the robot to be moved by the patient with low mechanical impedance, allowing patient's voluntary movements [73].

1.7. Training Protocols and Evaluation Methods

The evaluation of efficacy of robotic gait training devices and training strategies is a difficult task, and many training protocols are proposed to carry out these evaluations. This section presents a summary of these evaluation methods and training protocols. An overview of robotic gait training process is proposed in Fig. 1-5. Biomechanics data from clinical gait analysis is used in the design of robotic gait training orthosis as well as in defining the reference physiological trajectories. The assistance mode and the level of robotic assistance can be selected according to the disability level and stage of rehabilitation of neurologically impaired subjects.

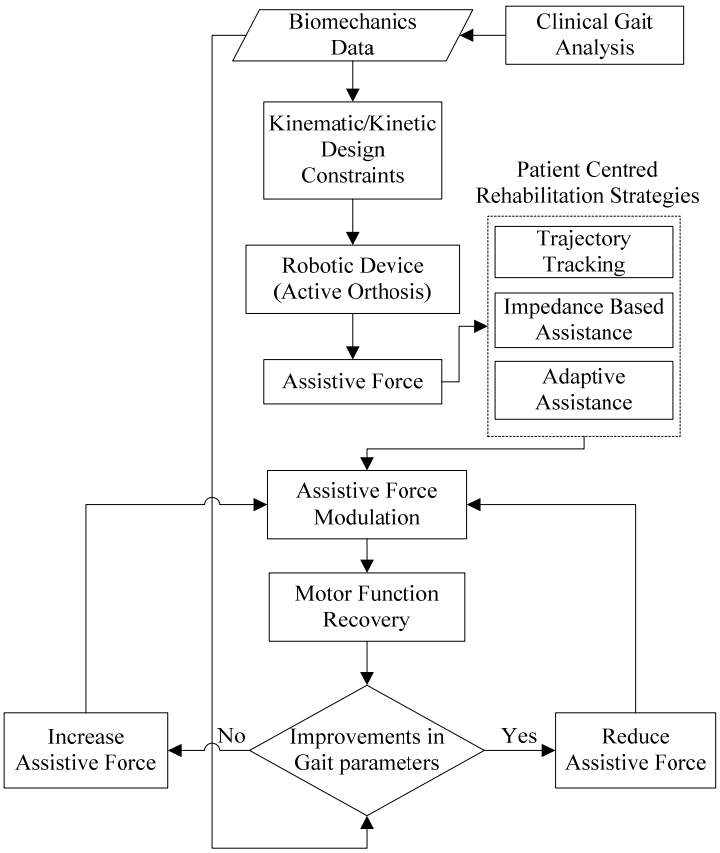

Figure1-5. Overview of Robotic Gait Training

The autonomic nervous system response (ANS) of stroke and cervical spondylotic myelopathy (CSM) patients is evaluated during LOKOMAT's trajectory tracking training mode by Magagnin et al. [74, 75]. The evaluation protocol include the measurement of ECG and respiratory signals during six phases: sitting position, standing position, standing position with total BWS, LOKOMAT assisted walking at two different velocities with 50% BWS and recovery in standing position with 0% BWS. Partial recovery of cardiovascular control is achieved in stroke and CSM patients as a result of LOKOMAT assisted BWS treadmill training [75]. LOKOMAT's trajectory tracking training mode is also evaluated on patients with Parkinson's disease. Freezing of gait is reduced and improvement in gait velocity, stride length, rhythmicity, and coordination is observed [76]. A study is performed on incomplete spinal cord injured (ISCI) patients using LOKOMAT trajectory tracking training mode and changes in motor impairment, functional limitations, and locomotor disability is monitored on a weekly basis. The majority of the patients regained normal over ground walking, and the remaining have improved gait speed and endurance [77].

A limited evidence of clinical trials of impedance and adaptive gait training strategies is reported in literature. Most of the studies are conducted to validate the concept of impedance and adaptive training strategies. LOKOMAT's impedance controller is tested on healthy subjects and incomplete paraplegic patients [37]. The comparison is performed between stiff (trajectory tracking) and complaint (impedance controlled) modes. The results of zero impedance and position control on intact and contralateral limb respectively are available. The trajectory tracking training mode produced higher joint moments as compared to impedance controlled mode. PAM and POGO's trigger based impedance controller is evaluated on SCI patients [46]. The patients are observed to start walking out of phase with the device and take shorter and quicker steps due to unexpected forces applied by the robotic device. This happens because the patients want to stabilize themselves against the applied actuator forces while remaining in stance phase for longer duration. A synchronization algorithm is formulated and assessed on SCI patients and positive observations are reported. ALEX force field controller is evaluated on healthy subjects [78] and stroke patients [6]. Results show significant increase in the size of patient's gait pattern, increased knee and ankle joint excursions, and increase in gait velocity. LOKOMAT's path control algorithm is evaluated on ISCI patients to prove the feasibility of training strategy and is found suitable for 85% of the participants [71]. LOPES impedance controller is evaluated on healthy subjects who walked unhindered in the device. Kinematics and EMG muscle activation

patterns are studied to compare the gait in LOPES with the normal treadmill gait and are found moderately similar [79].

LOKOMAT's adaptive gait training strategies are evaluated on SCI patients. Evaluation parameters include the extent of trajectory adaptation and interaction force parameters. The impedance based joint angle adaptation algorithm provides best performance [80]. Although in some cases the adapted joint angle gait trajectories remain unphysiological, concern about the merit of these adaptation algorithms are raised. The manual teach and replay training strategy of ARTHUR is studied on SCI patients [41]. The EMG activity, level of BWS, and kinematic data is collected during the experiments, and the patients walk with greater variability while maintaining the physiological gait patterns.

The substantiation of effectiveness of robot assisted gait training against manual physical therapy is sparse. Husemann *et al.* evaluated LOKOMAT trajectory tracking training mode on stroke patients and compared that with patients who received manual physical therapy [81]. The performance indices evaluated are gait velocity, cadence, stride duration, single limb support time, and body tissue composition. No significant difference in performance indices of both the groups is observed after the treatment, although the LOKOMAT group shows an advantage of improvement in gait abnormality and body tissue composition. A decrease in metabolic costs is also observed in case of LOKOMAT's trajectory tracking training of SCI patients when compared to manual physical therapy [82]. Similar clinical trials are also performed on stroke patients by using LOKOMAT to compare the effectiveness of robot assisted gait training with manual physical therapy, and no significant differences are reported [83, 84]. In case of some studies conducted on stroke patients, the manual physical therapy is proven to be more effective than robot assisted gait training in terms of gains in cadence and symmetry [85, 86].

1.8. Literature Findings and Research Motivation

1.8.1. Robotic orthosis Design

The initial commercial prototypes of robotic gait training orthoses, such as LOKOMAT, [7] allows motion only in one plane thus kinematically constraining the motion of human subjects during gait training. Actuation mechanisms are also imperative in the design and functioning of the robotic gait training orthoses. Most of the robotic gait training orthoses [6, 7] are driven by geared electric motors that have high endpoint impedance (stiffness) [43] and

are extremely heavy. These high endpoint impedance actuators are more suitable for industrial applications. Neurologically impaired subjects often suffer from severe spasms. These stiff actuators may produce large forces in response to the undesirable motions produced by spasms (position errors) [87, 88]. As a result, the subject may feel pain or discomfort. Adding compliance to the actuation mechanism would help in absorbing large position errors and would insure safety of the subject [87, 88]. The compliant actuation also provides impact resistance during events like heel strike. The robotic orthosis with inherent compliant actuation are important for gait rehabilitation, because they allow after-effects to be measured [89]. More generally, a wide range of dynamic environments can be created by using the actuators with inherent compliant actuation [2]. *Intrinsic, inherently compliant or back-drivable* robotic orthosis will allow deviations from its own equilibrium position, depending on the applied external force [88, 90].

The designers of LOPES came up with a light weight robotic gait training orthosis to overcome the limitations of high end point impedance actuators. The concept of Bowden cable based light weight SEA [91-94] has been used for the design of LOPES [39, 40]. The highly variable friction forces in the Bowden cables [95], inefficient transfer of power, non-durability of actuation transfer mechanism, (cables) and lack of precise control are the drawbacks associated with this approach [1]. Moreover, most of the above mentioned robotic gait training orthoses do not possess intrinsic compliance (elasticity) [1].

Pneumatic muscle actuators (PMA) present a promising solution for the development of rehabilitation robots. They are light weight and have high power/weight and power/volume ratios compared to existing actuators [96, 97]. PMA possess intrinsic elasticity that can be used in providing compliant actuation [90]. PMA have a highly nonlinear and time-varying behaviour that present a control problem, but in the presence of the above mentioned advantages, these limitations become secondary. PMA have been used in the design of various upper extremity robotic orthoses [87, 98] and single joint robotic orthoses for lower limb [99]. However, the potential of PMA in the design and control of multijoint robotic gait training orthoses has not been fully explored. In this research, we have developed a multijoint intrinsically compliant and light weight robotic orthosis for gait training of neurologically impaired subjects. The robotic orthosis is capable of providing compliant and safe gait training. The robotic orthosis allows kinematic freedom to the human subjects' so that the resulting gait patterns are close to normal gait.

1.8.2. Trajectory tracking Control

The purpose of the robotic orthosis is to guide the subject's limbs on reference physiological trajectories in order to re-train them to achieve normal gait for activities of daily living. The problem with the trajectory tracking control of the conventional robotic gait training orthoses [7, 37, 100] is that it works on the basis of infinite and constant compliance (impedance) values [37]. These constant and infinite impedance values produce large forces in response to the undesirable motions produced by spasms [87, 88]. As a result, the subject may feel pain or discomfort. Therefore, there is a need to develop trajectory tracking control schemes that can provide variable compliance during the robot assisted gait training [88]. This variable compliance is beneficial for human-robot interaction applications and would help in absorbing large position errors and would insure safety of the subject [87, 88]. A trajectory tracking control scheme for the robotic gait training orthosis is proposed in this work. The novelty of the proposed control scheme is that it allows the robotic orthosis joint compliance to be controlled independently of the trajectory tracking control.

Most of the upper limb and single joint robotic orthoses for lower limb [87, 98, 99] have used PMA in a feed forward open loop control configuration which may not result in development of physiological trajectories [87]. As the proposed robotic gait training orthosis is powered by PMA which have a highly nonlinear and time-varying behaviour. This behaviour of PMA presents a control problem in terms of guiding the subject's limbs on reference trajectories with minimum tracking error. In this work, we have developed trajectory tracking controller (feedback controller) based on the robust control laws in order to guide the subjects' limbs on reference trajectories.

1.8.3. Muscle activation patterns during robot assisted gait

Neurologic injuries, such as stroke and SCI, often result in damage to neuromuscular system and muscle coordination discrepancies [101-103]. The survivors have lower limb impairment and gait disorders and are unable to perform activities of daily living. One of the important goals of gait rehabilitation is to re-train muscle coordination and function for motor performance improvement [104]. Robot assisted gait training is an emerging rehabilitation practice, and several robotic orthoses have been developed for BWS treadmill training of neurologically impaired subjects [1, 6, 7].

These robotic orthoses kinematically constrain subject's limbs; therefore, the behaviour of resulting gait dynamics and muscle activation patterns is unclear [105-107]. An enhanced understanding of the correlation between muscle coordination abnormalities, gait pattern deviations, [108] and torques applied by robotic orthoses could facilitate in customized motor re-training as well as improvement of robotic gait training strategies. A limited number of studies performed in the biomechanics laboratories to analyse muscle coordination patterns during robot assisted gait have been reported in literature. A dynamic model of human musculoskeletal system and robotic orthosis was developed to study the muscle activation patterns during this research.

1.8.4. Impedance control for interactive gait training

The initial prototypes of robotic gait training orthoses, such as LOKOMAT, work on the basis of pure trajectory tracking control [7]. The problem with the trajectory tracking control is that it forces the subject's limbs on predefined trajectories without taking into account the subject's disability level and voluntary participation. The disability level of subjects suffering from neurologic impairments varies from subject to subject and for the same subject during the course of rehabilitation. The individual effort of the subject needs to be estimated, and the robotic orthosis torques needs to be adjusted accordingly so that the subject can contribute more towards the rehabilitation process [109]. Subsequently, several control strategies have been developed for the above mentioned robotic gait training orthoses to provide robotic assistance according to the subject's disability level and to enhance the subject's voluntary participation in the gait training process [1].

A patient-cooperative gait training strategy requires interactive robot-patient control and is mostly achieved by the use of impedance control [66]. The developers of LOKOMAT have implemented an impedance control scheme for their high endpoint impedance actuators to provide interactive, AAN gait training [36, 37]. However, the LOKOMAT has not been originally built to function as an impedance controlled device [79]. The designers of LOPES came up with a light weight robotic gait training orthosis [39, 40] to overcome the limitations of impedance control of LOKOMAT. LOPES has its patient-in-charge (zero impedance mode) mode during which the actuator stiffness is kept low, and a robot-in-charge mode (position control mode) during which the actuator stiffness is set high. However, the findings from LOPES robot-in-charge mode and AAN gait training based on impedance control have not been reported in literature [39, 79]. Also, a closed-loop force controller has been

implemented to make LOKOMAT and LOPES backdrivable [79], which results in an increased control complexity. An impedance control scheme has also been developed for ARTHUR [41]. However, the manual assistance during the impedance control of ARTHUR introduces subjectivity in the robotic gait training process, which may not be a desirable aspect for providing seamless robotic assistance [41]. In the present, research we have developed and implemented an impedance control scheme for the robotic gait training orthosis powered by PMA.

1.8.5. Assist-as-Needed gait training

The most common AAN robotic gait training strategies are based on impedance control [66]. The developers of LOKOMAT have implemented an impedance control scheme for their high endpoint impedance actuators to provide compliant AAN gait training [36], but this attempt has added an extra layer of control complexity [110]. The impedance control strategy has a limited ability to create accurate joint movements when large forces are required at the subject's limbs to complete these movements, such as situations in which the subject's limbs exhibit substantial tone. The impedance controlled robotic devices, such as LOKOMAT, address the problem of moving compliantly against the gravity by adding an offset term proportional to the weight or a fixed model of the subject's lower extremity dynamics [37]. However, the offset term or fixed model needs to be manually adjusted for each patient [65]. Also this approach does not address the issue of large forces required to overcome abnormal muscle tone. *Muscle tone* is the continuous and passive partial contraction of the muscles or the muscle's resistance to passive stretch during resting state [111]. Also, the impedance control has only been implemented for the swing phase of LOKOMAT assisted gait, as the inverse dynamics algorithm is not able to properly extract the active torque component contributed by the patient during the stance phase of gait cycle (GC) [37]. It is also evident that the lower limb joint stiffness relationship [112, 113] used in the inverse dynamics algorithm of LOKOMAT [37] is most likely not quantitatively identical to that observed in a particular user, as a large variability can be found in the physical properties of the human lower limb joints. Also, a limited evidence of the evaluation of impedance magnitude adaptation algorithm of LOKOMAT has been reported in literature.

A force field control scheme [42] has been used by the developers of ALEX for the AAN gait training of stroke patients [6]. This control scheme reduces the amount of robotic assistance as the training process progresses in a subjective manner without effectively taking

into account the patient's movement capability and disability level. ALEX force field [6] and LOKOMAT impedance controllers (virtual impedance) [36] are also dependent on physical therapist's decision to increase or decrease the amount of robotic assistance [6, 37]. The force field control scheme also address the problem of moving compliantly against the gravity by adding an offset term proportional to the weight or a fixed model of the subject's lower extremity dynamics [14, 37, 71]. These control approaches do not provide seamless adaptive AAN robotic assistance during gait training.

PAM and POGO have used the concept of *triggered assistance* [46]. The goal of triggered assistance is to allow the patient to first attempt the movement, and then provide robotic assistance to complete the movement, either automatically or initiated by a therapist , after a certain amount of time or when the patient is not able to voluntarily complete the movement. The discrete event nature of this approach, however, requires decision either by a programmed rule set or by an observing physical therapist. In other words, this approach breaks the movement into a subject driven part and a robot driven part, rather than providing a seamless level of robotic assistance to the subject-driven part. Another limitation of PAM and POGO is that they work with a low compliance level and guide the subject's limbs on predefined trajectories without subjectively taking into consideration his disability level.

This thesis proposes AAN control architecture for providing seamless adaptive robotic assistance during gait training process. The adaptive AAN controller takes into account the patient's disability level and voluntary participation and adapts the robotic assistance accordingly, in a seamless manner in real time. The seamless, adaptive AAN controller does not require any manual adjustment of control parameters during the robot assisted gait training.

1.9. Research Outline

1.9.1. Problem definition

Currently no multijoint robotic gait training orthosis is available that is intrinsically compliant as well as allows naturalistic motions to the neurologically impaired subjects. Also no seamless AAN gait training strategy is available that learns in real time the disability level and voluntary participation of human subjects and adapts the robotic assistance accordingly. At the same time it is evident that the robotic gait training orthoses and the AAN gait training strategies are vital for objectifying, intensifying, and optimizing gait training. The major

scientific contribution of this work involves the combination of an intrinsically compliant robotic orthosis mechanism with an AAN control scheme.

1.9.2. Research objectives

The ultimate goal of this research was to develop an intrinsically compliant robotic gait training orthosis that allows more naturalistic gait patterns to the neurologically impaired subjects, and provides gait training according to the disability level and stage of rehabilitation of neurologically impaired subjects. The research goal can be further explained with the help of following research objectives:

1.9.2.1. Development of the robotic gait training orthosis

A robot gait training orthosis will be developed. The biomechanics of human gait will be studied in order to select which degrees of freedom are required to be actuated and which are required to be left free in order to allow a natural walking pattern; i.e., which degrees of freedom can be blocked without disturbing the natural walking pattern too much. Also a study will be carried out to decide which design concept is best suited for an intrinsically compliant robot interacting with a human subject for the purpose of gait training, concerning basic control outline, actuation principles, and safety and compliance. Unlike the previous robotic gait training orthoses mentioned in literature [6, 7], the robotic orthosis will be light weight, intrinsically compliant, and will allow more naturalistic walking patterns.

1.9.2.2. Trajectory tracking control

During the initial phases of gait rehabilitation the purpose of the robotic orthosis is to guide the neurologically impaired subjects' limbs on reference physiological trajectories. In order to operate the robotic orthosis in trajectory tracking mode, suitable control algorithm will be studied. Evaluation of these trajectory tracking control algorithms will be carried out with neurologically intact subjects.

1.9.2.3. Modeling muscle activation patterns during robot assisted gait

In order to study the muscle activation patterns, a musculoskeletal model of the human gait will be developed along with the robotic orthosis model. The effect of cadence regulation on muscle activation patterns during robot assisted gait will also be studied by using these dynamic simulations. *Cadence* is the number of steps per minute during the human gait [3].

1.9.2.4. Impedance control scheme for interactive gait training

In order to provide interactive robotic gait training according to the disability level and stage of rehabilitation of neurologically impaired subjects, an impedance control scheme will be developed. The impedance control scheme will estimate the human subject disability level and participation of human subject and adjust the robotic orthosis torques accordingly. The impedance control scheme will be able to provide robotic gait training at low compliance to severely impaired subjects and vice versa. Subsequently, experiments with neurologically intact subjects will be performed to evaluate the performance of the impedance control scheme.

1.9.2.5. Assist-as-needed control scheme

In order to overcome the limitations of impedance control scheme, an AAN control scheme will be developed. The AAN control scheme will provide seamless, adaptive robotic assistance and will adjust the robotic assistance according to the subject's kinematic error in real time. If the kinematic error is small, the AAN control scheme will decrease the robotic assistance and vice versa. Experiments with neurologically intact subjects will be performed to evaluate the performance of the AAN control scheme.

An important research question will be how well the robotic orthosis prototype and the adaptive AAN gait training strategy satisfy the stated goals. This can be considered a clinical question that can be only answered by extensive clinical trials with neurologically impaired subjects. This is true, but beyond the scope of this thesis. The ultimate evaluation test within this thesis will be carried out with neurologically intact subjects to assess how well the proposed robotic orthosis and the AAN gait training strategies provide seamless, adaptive gait training. However, the developed system will be capable of providing subject specific, task oriented, and repetitive gait training during which the physical therapist has a supervisory role.

1.10. Thesis Overview

This thesis details the work carried out in this research to meet the above objectives. Chapter 2 describes the mechanism design, actuation and instrumentation of robotic gait training orthosis. The robotic gait training orthosis is powered by PMA. An overview of biomechanics of human gait is also presented in order to provide the background knowledge used in the design, modeling, and control of robotic gait training orthosis.

Since the robotic orthosis is powered by PMA, which presents a highly nonlinear behaviour, dynamic modeling of robotic gait training orthosis is a crucial task. Chapter 3 describes the dynamic modeling of robotic gait training orthosis powered by PMA. The dynamic model of the robotic gait training orthosis is required for the trajectory tracking, impedance and AAN control tasks.

The purpose of the robotic gait training orthosis is to guide the subject's limbs on reference physiological trajectories and is generally referred to as trajectory tracking control. Trajectory tracking control is important for the gait rehabilitation of severely impaired subjects. Trajectory tracking control of robotic gait training orthosis powered by PMA is a crucial task due to the highly nonlinear and time varying behaviour. Chapter 4 describes the two robust control methods for the trajectory tacking control of the robotic gait training orthosis in the presence of structured uncertainties in the model of PMA. The dynamic model of the robotic orthosis developed in Chapter 3 was used for the trajectory tracking control of robotic orthosis.

The robotic gait training orthosis kinematically constrains the limbs of human subjects, so the resulting gait kinematics, dynamics, and muscle activation patterns are not clear. The understanding of these parameters is important in order to further develop the robotic orthosis mechanism and gait training strategies. The understanding of these parameters can be further enhanced by developing dynamic simulations of robot assisted gait. Chapter 5 presents the modeling of muscle activation patterns during robot assisted gait. Dynamic simulations were used in order to further enhance the understanding of muscle activation patterns. Also the effect of cadence regulation on muscle activation patterns during robot assisted gait was studied by using dynamic simulations. The robotic orthosis model developed in Chapter 3 and the trajectory tracking control scheme developed in Chapter 4 was used in order to study the muscle activation patterns.

The disability level of subjects varies from subject to subject and also for the same subject during the course of rehabilitation. The disability level and individual subject effort needs to be estimated and the robotic assistance needs to be modified in order to suit the needs of a wide population of neurologically impaired subjects. Thus, the trajectory tracking control is not a suitable option for the above mentioned task. Chapter 6 describes the concept of impedance control of robotic orthosis for interactive gait training. The impedance control scheme estimates the disability level of human subjects and adjusts the robotic assistance

accordingly. The trajectory tracking control scheme developed in Chapter 4 of this thesis was used as a basic potion controller in the overall impedance control scheme.

In order to overcome the limitations of impedance control scheme and to enhance the voluntary participation of human subjects in the gait training process, Chapter 7 presents the concept of AAN control scheme. The proposed AAN control scheme provides seamless adaptive robotic gait training and encourages active subject participation in the robotic gait training process. The trajectory tracking control scheme developed in Chapter 4 of this thesis was used as a basic position controller in the overall AAN control scheme.

Chapter 8 contains the outcomes, conclusions and contributions of this research, together with relevant future works that can be done to further enhance the capabilities of the developed gait rehabilitation system. This research had produced publications in international journals, peer reviewed international conferences, and an invited book chapter (Appendix C). Certain sections of this thesis, are therefore, based on these published works.

1.11. Chapter Summary

This chapter presents the background knowledge on human gait, neurologic injuries, and human gait impairments. The conventional gait rehabilitation practice based on BWS manually assisted treadmill training is discussed. The need of robotic gait rehabilitation solutions is emphasized, and a review of the available robotic gait training orthoses is presented. Also presented is the review of robot control strategies that are used to provide robotic assistance according to the disability level and stage of rehabilitation of neurologically impaired subjects. The training protocols used to evaluate these robotic orthosis and control strategies are also discussed. The important challenges in the fields of design, actuation and control of the robotic gait training are emphasized and the motivations of this research are discussed.

The goal of this research is presented along with main research objectives. The first objective set for the research was to develop a robotic gait training orthosis that will be intrinsically compliant and allows naturalistic walking patterns. The trajectory tracking control of robotic gait training orthosis was the second objective of this research. Development of dynamic simulations in order to study the muscle activation patterns during robot assisted gait was considered as the third objective for this research. The impedance control of robotic orthosis for interactive gait training was the fourth objective of this

research. Lastly, the final objective of this research was to develop an AAN control scheme that will be capable of providing seamless, adaptive robotic assistance according to the disability level and active participation of neurologically impaired subjects. An overview of the subsequent chapters of this thesis is provided in the end.

Chapter 2. Robotic Orthosis Design

This chapter presents the new intrinsically compliant robotic orthosis powered by PMA for treadmill training of neurologically impaired subjects. An introduction to biomechanics of human gait is presented in order to provide the background knowledge used in the design of robotic gait training orthosis. The orthosis has hip and knee sagittal plane rotations actuated by antagonistic configuration of PMA. It has passive mechanisms to allow vertical and lateral translations of the trunk, and a passive hip abduction/adduction joint. A foot lifter with a passive spring mechanism was used to ensure sufficient foot clearance during swing phase. The orthosis is a new addition to the rapidly advancing field of robotic orthoses for treadmill training.

2.1. Introduction

Robot assisted gait training has several advantages over manual physical therapy [6, 7]. It relieves the physical therapist from the strenuous task of manual assistance and facilitates in delivering well controlled repetitive and prolonged training sessions. The physical therapist's role will then be to supervise the gait training process and to set up the devices. The subjectivity of manually assisted training is then eliminated by providing objective measurement of interaction forces and limb movements to assess the quantitative level of motor function recovery.

The initial commercial prototypes of robotic gait training orthoses such as, LOKOMAT [7] and Autoambulator [23], kinematically constrain the limbs of human subjects and allow motion only in one plane. This kinematically constrained motion may not be the best way for rapid recovery of neurologically impaired subjects. The robotic orthosis should allow gait training close to natural gait so that the recovery process of subjects' may become fast. In this work, the study of biomechanics of human gait was carried out to design a robotic orthosis mechanism that can help in providing a naturalistic gait pattern to the neurologically impaired subjects.

Actuators also hold a paramount importance in the design and functioning of these robotic orthoses. Two approaches have been used in the design of robotic gait training orthoses [1]. In one of the approaches, the actuators have been placed on a remote station, and the actuation has been transferred to the orthosis joints via cables, rigid linkages, [39,

114] and pneumatic or hydraulic systems [46]. LOPES [39], PAM [46], ARTHUR [43] and the cable-driven locomotor training system [114] are the rehabilitation devices using this approach. In the second approach, actuators have been directly mounted on the orthosis frame. LOKOMAT [7] and ALEX [6] use this approach of actuator mounting.

The benefit of the first approach is no limitations on actuator weight and hence the power capacity of the actuators. Lack of precise control, inefficient transfer of power, and non-durability of actuation transfer mechanism (cables) are the drawbacks associated with this approach [1]. Also, the highly variable friction forces in the Bowden cables present a control problem [95]. The main advantage of the second approach is the efficient transfer of power and a better alignment of orthosis joints with subject joints [1]. However, the disadvantage is the use of geared electric motors that are either extremely heavy [1] and have high endpoint impedance (stiffness) [114]. The use of heavier electric motors and gear assembly increases the overall weight of the robotic orthosis, which is not suitable for implementing advance control strategies, such as impedance control [39]. If light weight electric motors are used, the force and torque generation capabilities of the robotic orthosis are seriously compromised [1]. Also, these high endpoint impedance electric motors are more suitable for industrial applications. Neurologically impaired subjects often suffer from severe spasms. These stiff actuators produce large forces in response to the undesirable motions produced by spasms (position errors) [87, 88]. As a result, the subject feels pain or discomfort. The robotic orthosis with low endpoint impedance is important for gait rehabilitation, because they allow after-effects to be measured [89]. More generally, a wide range of dynamic environments can be created by using the actuators with low impedance [2].

The second approach of directly mounting the actuators on orthosis frame may become more beneficial if the limitations on the weight and endpoint impedance of the actuators could be overcome. Also adding compliance to the actuation mechanism would help in absorbing large position errors and would insure safety of the subject. The compliant actuation also provides impact resistance during events like heel strike as well as a realistic stepping experience [88, 90]. A closed-loop force controller has been implemented to make LOKOMAT and LOPES compliant (backdrivable) [79], which results in an increased control complexity. Also, the highly variable friction forces in the Bowden cables present a control problem [95]. Moreover, most of the above mentioned robotic gait training orthoses do not possess intrinsic compliance [1].

PMA are promising tools in the field of rehabilitation robotics. They are light weight and have high power/weight and power/volume ratios compared to all the existing actuators [96]. PMA have intrinsic elasticity that can be used in providing compliant actuation. PMA possess a highly nonlinear and time-varying behaviour that presents a control problem, but in the presence of above mentioned advantages, these limitations become secondary. PMA have been used in the design of various upper extremity robotic orthoses [87, 98] and single joint robotic orthoses for lower limb [99]. However, the potential of PMA in the design of robotic orthoses for treadmill training has not been fully explored. In this work we developed a new multijoint robotic orthosis powered by PMA for treadmill training of neurologically impaired subjects. The mechanism design and actuation concepts used for the robotic gait training orthosis are presented.

A brief description of the biomechanics of human gait is presented in the beginning of the chapter to provide the background knowledge used in the design and control of robotic gait training orthosis. Design requirements of the robotic gait training orthosis are then presented. This follows with the mechanism design, actuation, instrumentation, and design capability analysis of the robotic gait training orthosis.

2.2. Biomechanics of Human Gait

The basic knowledge of human gait biomechanics is necessary as the robotic orthosis is a wearable device and has to interact with human lower limb during gait rehabilitation. Therefore, a brief study of human gait fundamentals and its kinematic and kinetic details is presented. The knowledge of the biomechanics of human gait would be used in the design, modeling, and control of robotic orthosis.

2.2.1. Gait cycle

There are two requisites for human walking; continuing ground reaction forces that support the body, and periodic movement of each foot from one position of support to the next in the direction of progression. A *gait cycle* (GC) is the sequence of events from heel strike of one foot to the heel strike of same foot (Fig. 2-1). It is defined in terms of time interval and is usually expressed as a percentage of gait events taking place. Walking consists of a cycle of repeated events of foot strike and foot off. The event of foot strike usually begins with heel strike and is an indication of load bearing. Foot off begins with the toe pressing against the ground while preparing for load transfer to the contra lateral limb (Fig. 2-

1). The four events in human gait cycle are; foot strike (FS), opposite foot off (OFO), opposite foot strike (OFS), and foot off (FO). The gait cycle is considered to be initiated at heel strike.

The GC consists of two phases; stance and swing (Fig. 2-1). *Stance phase* is defined by the percentage of gait cycle when the foot is in contact with the ground, and *swing phase* by the time when the foot is in air and is not bearing any load. 62% of the gait cycle consists of stance and 38% of swing phase.

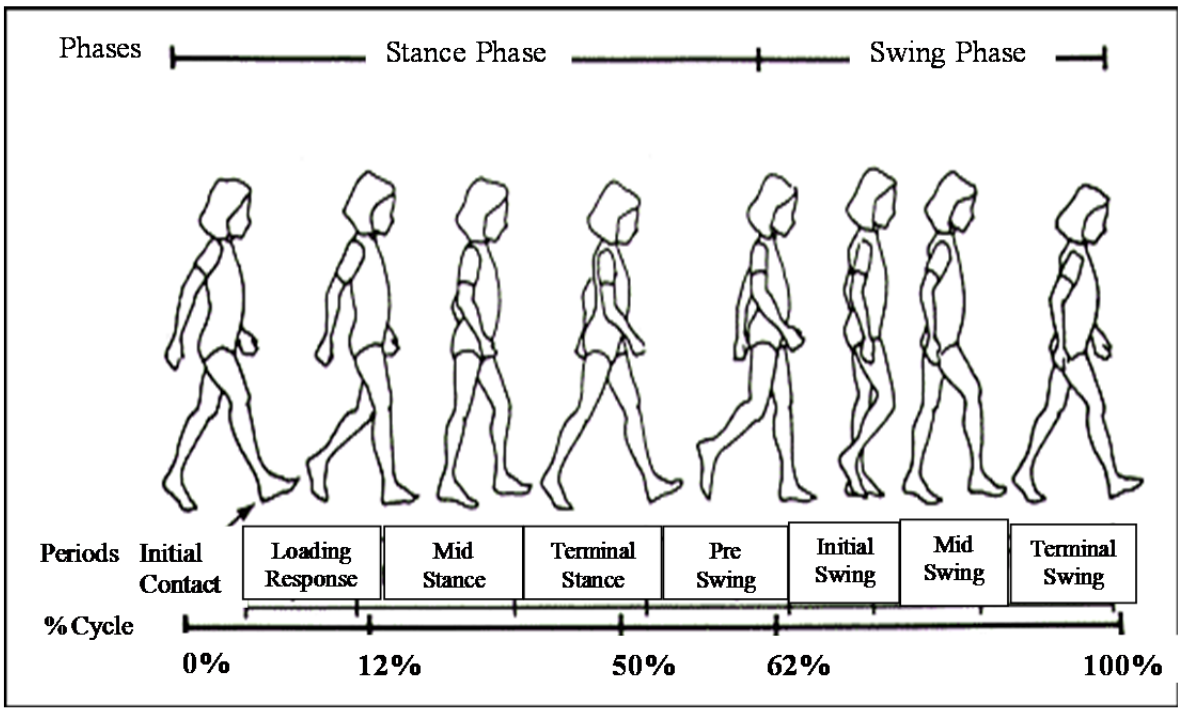

Figure 2-1. Phases of gait cycle (GC)

2.2.2. Planes and axis division

The three planes which divide the human body in six parts are (Fig. 2-2):

- *Sagittal* Plane bisects the body into right and left halves. Movements occur about the *mediolateral* axis running side to side through the centre of mass of the body.
- *Frontal or Coronal* plane bisects the body into front and back halves. Movements occur about *anteroposterior* axis that runs anterior and posterior from the plane.
- *Transverse or horizontal* plane bisects the body to create upper and lower halves. Movements occurring in this plane are primarily rotations about a *longitudinal* axis.

2.2.3. Pelvic and hip complex

Pelvic girdle and hip joints act as a part of closed kinetic chain; in which forces travel up from the lower extremity through the hip and the pelvis into the trunk or vice versa. The pelvic girdle supports the weight of the body, helps in the lower limb coordination, and maintains equilibrium.

The pelvis has following movements;

- *Anterior tilt* of the pelvis occurs when the trunk flexes or the thighs extend and is defined as forward tilting and downward movements of pelvis.
- *Posterior tilt* is created through trunk extension or thigh flexion, which occurs as the pelvis moves posteriorly.

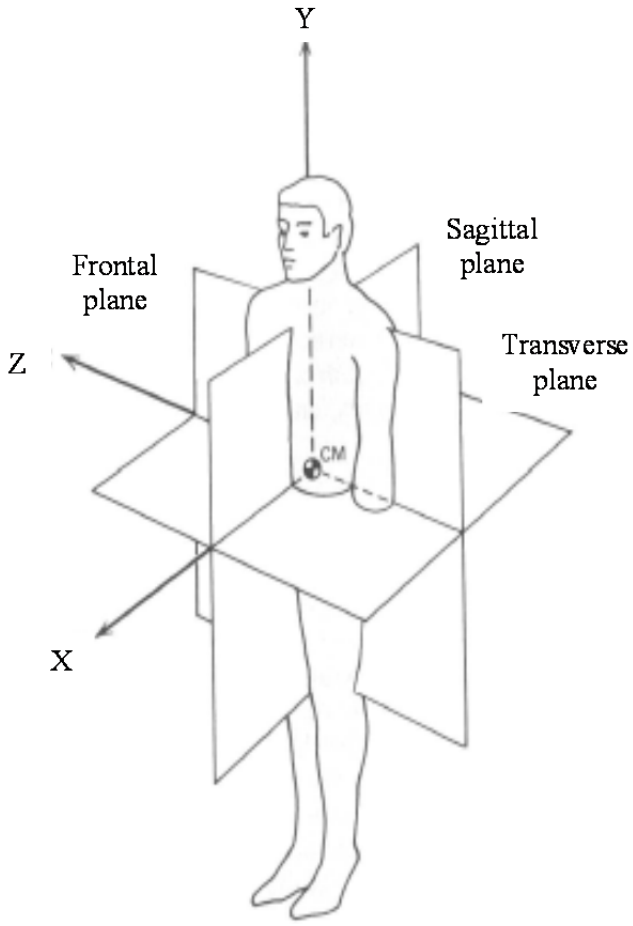

Figure 2-2. Plane and Axis [115].

- *Lateral tilt or pelvic obliquity* is controlled by muscles like gluteus medius. The pelvis would try to tilt to the right when weight is supported by the left limb.

- *Pelvic rotation* would take place as the left limb swings forward, and the pelvis rotates to the left.

The final joint in the pelvic girdle is the hip joint that has three degrees of freedom. The hip joint allows the thigh to move through a wide range of motion in three directions.

2.2.4. Kinematics and kinetics of gait cycle

The joint *kinematics* describes relative position of one body segment with respect to the adjoining one. Relative orientation of one body segment to the other one defines joint angles. The majority of these displacements occur in the sagittal plane. Relative joint angles in the sagittal plane are shown in Fig. 2-3. Sign conventions used for each joint angle is measured as positive counter clockwise displacement of proximal link from the distal link (zero in anatomical position). The position presented in Fig. 2-2 presents the *quite standing posture* [115]. This quite standing posture will be taken as the *equilibrium or home position* during robot assisted gait training. During the quite standing posture all the joint angles will be taken as $\theta = 0^{o}$ (Fig. 2-3).

Kinetics deals with individual muscle forces and moments generated by these forces across each joint, mechanical power, and energy patterns. Moment is measured as positive acting counter clockwise on the distal link.

Robotic orthosis uses human walking data to specify the design requirements at the orthosis joints. The biomechanical data is obtained with the help of external markers that are affixed to each body segment, whose axes define the position of these body segments. Cameras track and record marker trajectories, as the subject walks along a marked walkway.

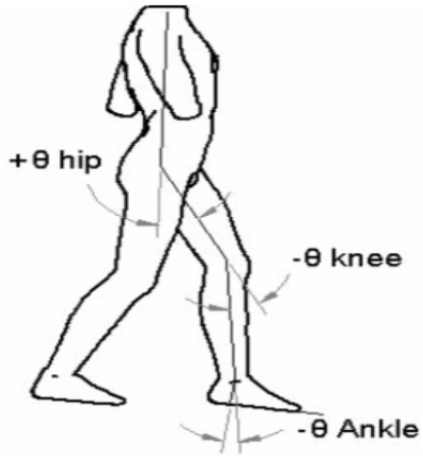

Figure 2-3. Joint angles in sagittal plane [3].

Gait kinetic results are difficult to understand as they cannot be directly observed. Force plates are used along the pathway on which the subject walks for kinetic data collection. For this project, sagittal plane motions are of interest as they form the actuated degrees of freedom of the robotic orthosis.

Hip joint can provide motions in all the three planes as hip flexion/extension in the sagittal plane, abduction/adduction in frontal plane and rotation in transverse plane (Fig. 2-4). Knee joint has major rotations in the sagittal plane as flexion/extension and provide rotations in transverse plane (Fig. 2-4). The ankle is a complex joint and, owing to its variable centre of rotation, the axes of motion are not simply three Euclidean axes (Fig. 2-4). The most important one is plantar /dorsiflexion in the sagittal plane for ground clearance during swing phase. The sagittal plane joint ranges of motion and moments contribute most during the gait cycle and are provided in (Table 2-2).

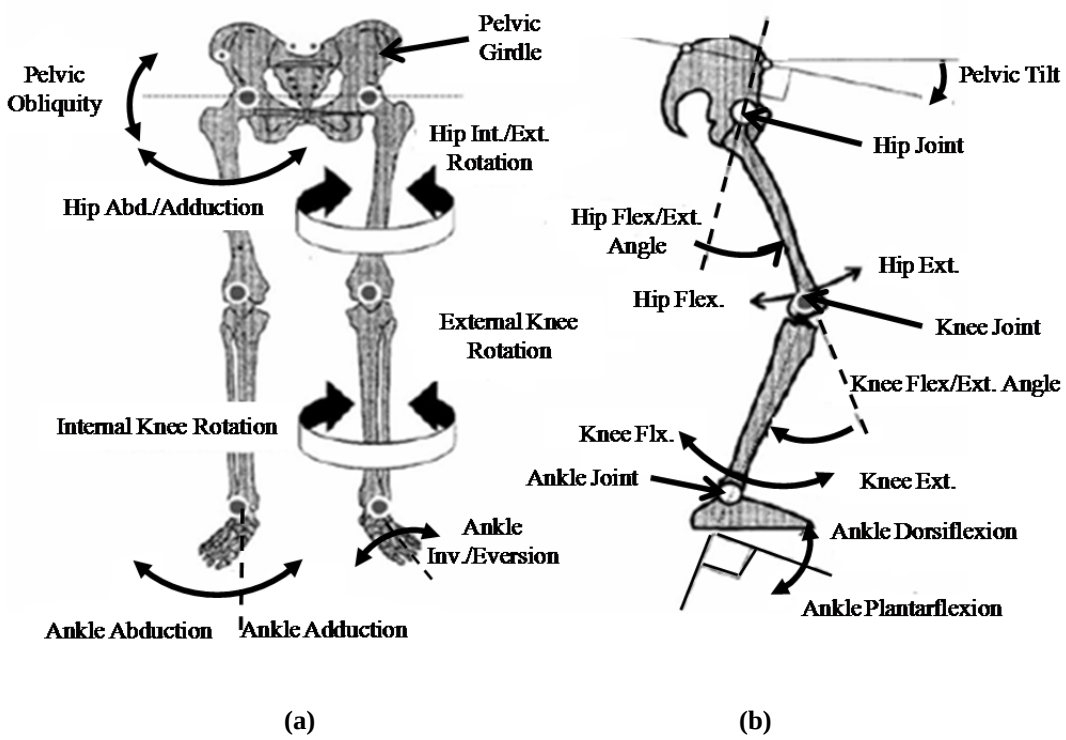

Figure 2-4 Degrees of freedom possible during natural human gait. Flex/Ext. stands for flexion/extension, Inv. for inversion, Int./Ext. for internal/external and Abd. for abduction. (a) Front view of the human lower extremity. (b) Side view of the human lower extremity.

2.3. Design Requirements

In order to address the functional, structural, and cosmetic limitations of current robotic gait orthoses for treadmill training and to meet the clinical requirements of the treadmill

training of neurologically impaired subjects, the new intrinsically compliant robotic orthosis was designed based on the following criteria.

To begin with, the robotic orthosis should provide a realistic stepping experience. The realistic stepping experience could be achieved by determining an optimal number of DOFs of the robotic gait training orthosis. The realistic stepping experience is important so that the human subject feels minimum kinematic constraint during robot assisted gait training. The realistic stepping experience may also help in increasing the rate of recovery of neurologically impaired subjects. It is important to mention here that there is no scientific evidence available regarding the optimal number of DFOs of robotic gait training orthosis required for realistic stepping experience. The robotic orthosis joints should allow sufficient ranges of motion to the human subjects' anatomical joints. The joint ranges of motion provided by robotic gait training orthosis is important so that the realistic stepping experience could be achieved. The robotic orthosis should also inhibit excessive knee extension and hip flexion/extension. It is important to inhibit excessive knee extension and hip flexion/extension motions, as the excessive motion may cause damage to the neuromuscular system of the neurologically impaired subjects [116].

The robotic gait training orthosis actuation system should be powerful enough to guide the subject's limbs on reference trajectories and be able to produce required joint torques. Actuators should be highly compliant with low mechanical impedance in order to accommodate abrupt forces arising from clonus. *Clonus* is a series of involuntary muscle contractions and relaxations due to neurologic injuries, such as stroke and SCI. The robotic orthosis and the actuation mechanism should be light weight so that the advance control strategies such as impedance control [39, 40] could be implemented. The decrease in weight of robotic orthosis mechanism will also help in better alignment of robotic orthosis joints with subject's anatomical joints. Moreover, since this robotic orthosis is to be used by subjects of different anthropometric features and age groups, its design features should be adaptable. Safety is also a major concern, and it should be considered at every stage of robotic orthosis development. Regarding the cosmetic requirements and ease of use, the robotic orthosis should be easy to wear and comfortable.

The robotic gait training orthosis joints should work in good alignment with the subject's anatomical joints. The subject may feel uncomfortable without the correct alignment of robotic orthosis and anatomical joints [117]. Alignment may also take 20-30 minutes, cutting

into the valuable rehabilitation time available for each subject. It is important to mention here that it is difficult to achieve good alignment of subject's joints with robotic orthosis joints as the exact location of anatomical joints cannot be seen from outside without the help of imaging devices. Bony landmarks can only provide a general approximation of the location of rotation axes of anatomical joints, with significant difference between subjects. Moreover, the positioning of robotic orthosis on human lower limb may differ between therapy sessions, thus always requiring final adjustments, even if robotic orthosis settings are stored for later recollection. However, even if close alignment is achieved before therapy session is started; the cuffs may slip during usage, requiring further adjustments [7].

With the objective to develop a pragmatic and feasible design for the robotic gait training orthosis, meetings were arranged with physical therapists and biomechanics experts in the School of Nursing and the Department of Sports and Exercise Science, respectively at The University of Auckland, Auckland. Regular meetings with practicing stakeholders such as physical therapists and biomechanics experts were important for a practical design solution.

2.4. Mechanism Design and Actuation

The biomechanics of human gait is studied in order to design a robotic orthosis that can provide training close to natural gait [3]. The DOFs of the human lower extremity are provided in Fig. 2-4. The hip, knee, ankle and pelvis DOFs are shown in Fig. 2-4 for three anatomical planes. The study of these anatomical DOFs is necessary in order to choose an optimal set of DOFs for the robotic orthosis that can provide naturalistic gait training.

Based on the study of biomechanics of human gait, the above mentioned design requirements, and analyzing the experiences with existing robotic orthoses, the design of robotic gait training orthosis was carried out. Table 2-1 describes the DOFs that are possible for natural human gait; which of these are actuated in the robotic orthosis, which are left passive, and which are blocked. During the design of robotic orthosis, an optimal set of DOFs was chosen in order to allow for a human subject to walk normally and safely in the device. For the pelvis motion, only vertical and lateral translations were included in the robotic orthosis design, and all the other DOFs were blocked (Table 2-1). For the hip joint, flexion/extension and abduction/adduction motions were included in the robotic orthosis design while the Exo./Endo rotations were blocked (Table 2-1). Similarly, knee flexion/extension was included in the robotic orthosis design and the Exo./Endo rotations

were blocked. For the ankle joint, the only motion included in the robotic orthosis design was the sagittal plane plantar/dorsi flexion while the motions in other two planes were blocked (Table 2-1).

Table2-1 Actuated, passive and blocked DOF of the robotic orthosis compared with natural human gait.

Degree of Freedom	**Natural Gait**	**Robot Design**		
		Actuated	Passive	Blocked
Pelvis to fixed world	3 rotations 3 translations	-	Lateral translation Vertical translation	All rotations Forward/Backward
Hip	3 rotations	Flex/Extension	Abd/Adduction	Exo/Endo rotation
Knee	2 rotation	Flex/Extension	-	Exo/Endo rotation
Ankle	3 rotations	-	Plantar/Dorsi Flexion	Abd/Adduction Inv/Eversion

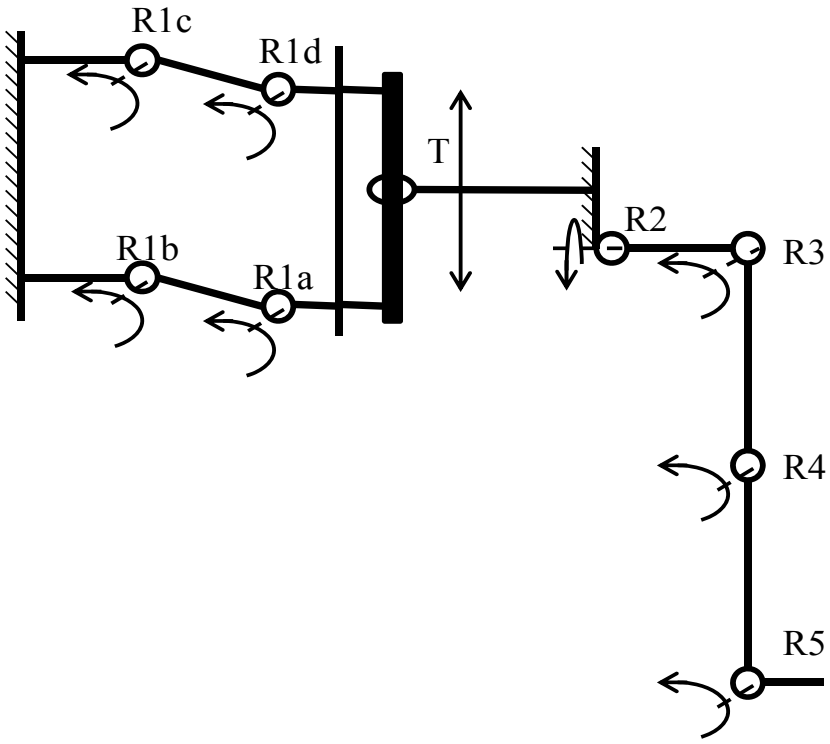

Figure 2-5. Kinematic diagram of the robotic orthosis showing all the DOF. R5. Revolute ankle joint. R4. Revolute joint for knee flexion. R3. Revolute joint for hip flexion/extension. R2. Revolute joint for hip abduction/adduction. R1 (a,b,c,d). Revolute joints of the parallelogram mechanism for vertical translation. T. Sliders for lateral translation.

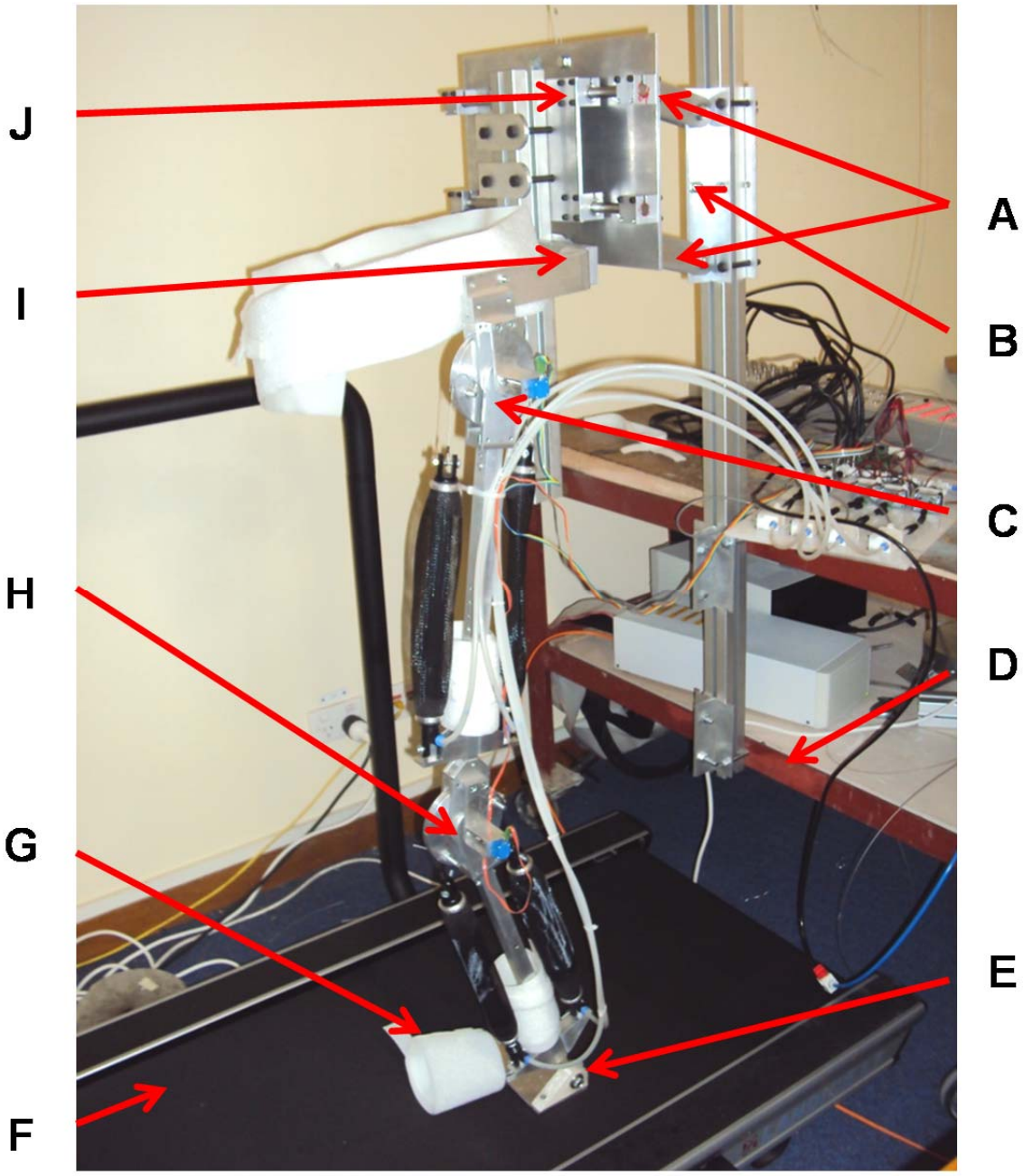

Figure 2-6. Robotic orthosis, its major components and all the degrees of freedom labelled. A: Parallelogram mechanism for vertical translation, B: Height adjustable frame, C: Hip sagittal plane revolute joint, D: Walker, E: Ankle sagittal plane revolute joint, F: Treadmill, G: Foot lifter, H: Knee sagittal plane revolute joint, I: Hip abduction/adduction revolute joint, J: Sliders for lateral translation.

A kinematic diagram of the DOFs of the robotic orthosis is shown in Fig. 2-5. These DOFs (Fig. 2-5) were considered to be sufficient for the robotic gait training orthosis and can help in achieving a more naturalistic stepping experience. The complete design description of the robotic orthosis is shown in Fig. 2-6 and 2-7. A height adjustable frame was used to match the subject's height. The trunk of the robotic orthosis has two DOFs, namely vertical and lateral translations. The thigh segment of the orthosis has two DOFs with respect to the trunk of the orthosis; one for flexion/extension and other for abduction/adduction motion.

The thigh segment and hip brace are telescopic and can be adjusted to match anthropometric features of a wider population range. The telescopic shank segment has one DOF with respect to the thigh segment for knee flexion. A foot lifter is attached to the shank section with a revolute ankle joint to ensure sufficient dorsiflexion during swing phase of gait.

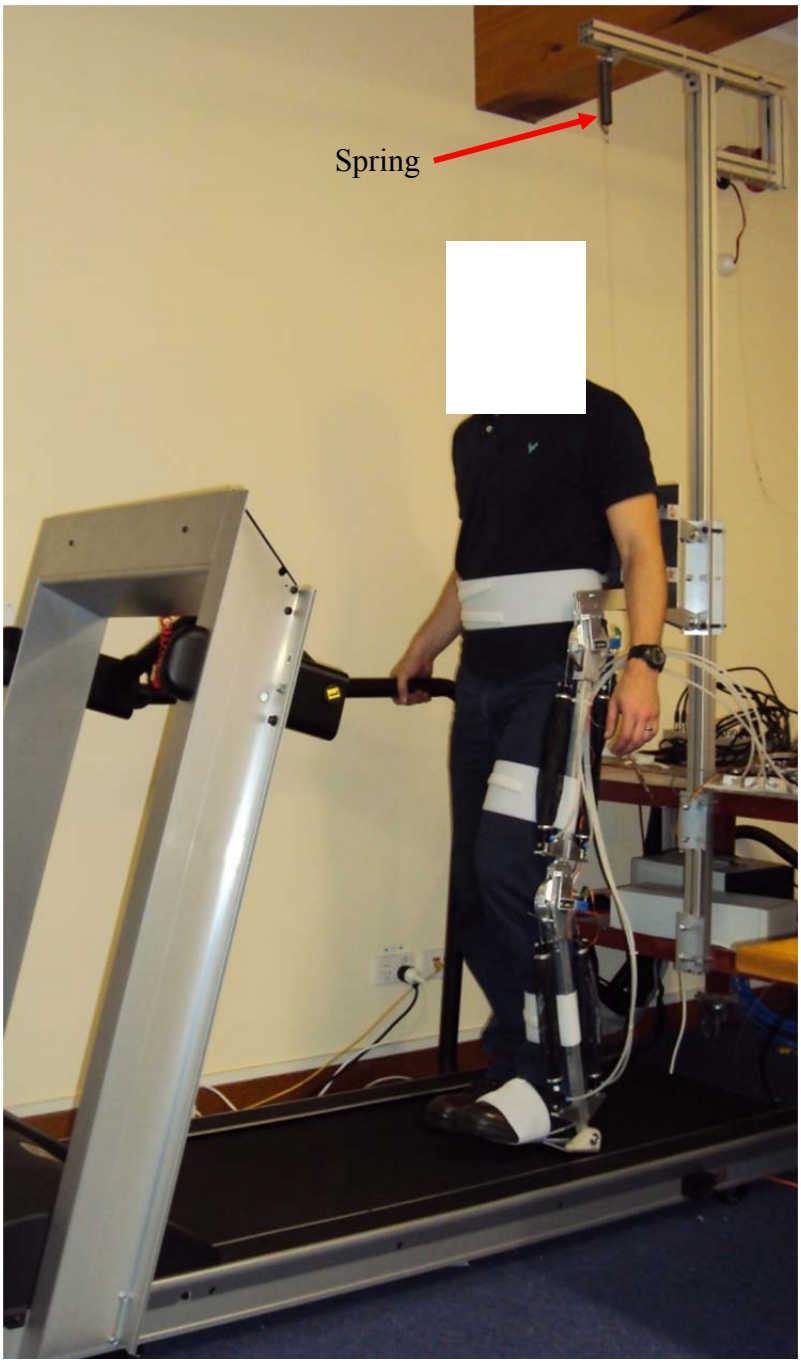

Figure 2-7. Experimental setup of the robotic orthosis with a subject walking on a treadmill.

Actuated and passive DOF for the robotic orthosis were decided based on the joint ranges of motion. The major rotations during gait cycle are in the sagittal plane [3]. The actuated DOF were hip and knee sagittal plane rotations (Table 2-1). The maximum joint ranges of

motion for the actuated and passive DOFs were selected from the studies reported in literature [3] (Table 2-2). Similarly, the maximum joint moment ranges for the actuated DOFs were also selected from the studies of normal human gait reported in literature [3] (Table 2-2). All other DOFs were kept free (Table 2-1). A provision was made in the robotic orthosis design that any of these DOFs can be blocked during the gait training based on the observation and decision of physical therapist.

Table2-2. Maximum ranges of motions and joint moments of robotic orthosis [3].

Degree of Freedom	Range of Motion	Joint Moment
Hip Flexion/Extension	$+60^0/-30^0$	50 N-m
Knee Flexion/Extension	$+0^0/-90^0$	50 N-m
Hip Abduction/Adduction	$+15^0/-15^0$	Passive motion
Lateral Translation	+0.30m/-0.30m	Passive motion
Vertical Translation	+0.10m/-0.10m	Passively weight compensated
Ankle Dorsiflexion	$+20^0/-45^0$	Passive spring mechanism

PMA was used for providing actuation to robotic orthosis (Fig. 2-8 (a)). PMA possess the characteristics of skeletal muscles and generate force upon contraction. To provide actuation at hip and knee joints, various mechanisms were studied to transfer the actuation from PMA to the orthosis joints. Double groove aluminium discs (Fig. 2-8 (b)) were employed at hip and knee joints for sagittal plane motions. An antagonistic disc-PMA mechanism was selected for actuation purpose (Fig. 2-8 (c)). The vertical translation was realized by a passive parallelogram mechanism.

A spring was mounted on the parallelogram mechanism (Fig. 2-7). The purpose of the spring was to compensate the weight of the robotic orthosis, which would help in reducing the relative slip between the robotic orthosis joints and the subject's anatomical joints. This reduction in relative slip may help in achieving a better alignment between the robotic orthosis joints and the subject's anatomical joints. A passive slider mechanism was used to allow the lateral translation. The additional DOFs for pelvis translations and hip abduction/adduction may become beneficial for gait training as they allow to leave the balance related control tasks to the subject [82].

The orthosis frame was made from lightweight aluminium rectangular tubing to meet the strength requirements for torque transmissions. The orthosis frame was connected to the subjects' limbs with two braces; one at the thigh section and other at the shank section. Hip straps were used to secure the robotic orthosis with the subject's hip. All the braces have soft straps to provide a comfortable feel to the subject.

The ankle joint was not actuated. The rationale for eliminating an actuated ankle joint was that it is not necessary to provide an ankle push-off in the robotic orthosis in order to walk safely. For subject safety, the only necessary ankle function is to assure enough dorsiflexion during swing phase for foot clearance [7]. This could be realized by simpler means such as elastic straps or spring mechanisms. A foot lifter with a passive spring mechanism was designed to provide the necessary dorsiflexion during swing phase for foot clearance. The robotic orthosis is a unilateral device and only attachment to the left leg was considered. Robotic devices such as Anklebot [35] or Ankle-foot orthosis [118] can be added to the robotic gait training orthosis if the ankle joint actuation appears crucial from the clinical point of view.

A kinematic model of the lower extremity was developed using Open SIMM [119]. The model was used to study the effects of insertion/origin locations of the PMA on the joint ranges of motion. Based on the anthropometric data of an average man, [120], the required length and braid diameter (Fig. 2-8 (a)) of each PMA to generate the desired range of motion for the hip and knee joints were 34 cm and 3 cm, respectively. These PMA can provide peak joint torques of 50Nm, which was sufficient for the proposed application (Table 2-2). If larger torque is required larger diameter PMA can be used under the safety constraints.

2.5. Safety

Safety is a key concern for the robotic devices working in close proximity with human subjects. As the proposed robotic orthosis was designed to work in close proximity with neurologically impaired subjects, several safety features were incorporated in the robotic orthosis mechanism and control hardware. Mechanical stops were placed on the hip and knee joint discs to avoid the orthosis to go beyond the physiological ranges of motion (maximum ranges between $30^o/60^o$ and $90^o/0^o$ for hip and knee flexion/extension, respectively). These mechanical stops can withstand the maximum torques applied by the PMA. Also, an independent safety circuit was created that can power the system down in case of any danger

or if the subject feels uncomfortable in the device. Two emergency switches were wired so that, a single push can stop the whole system by exhausting the air from each PMA. One switch button was held by the subject while the other was held by the person invigilating the training process.

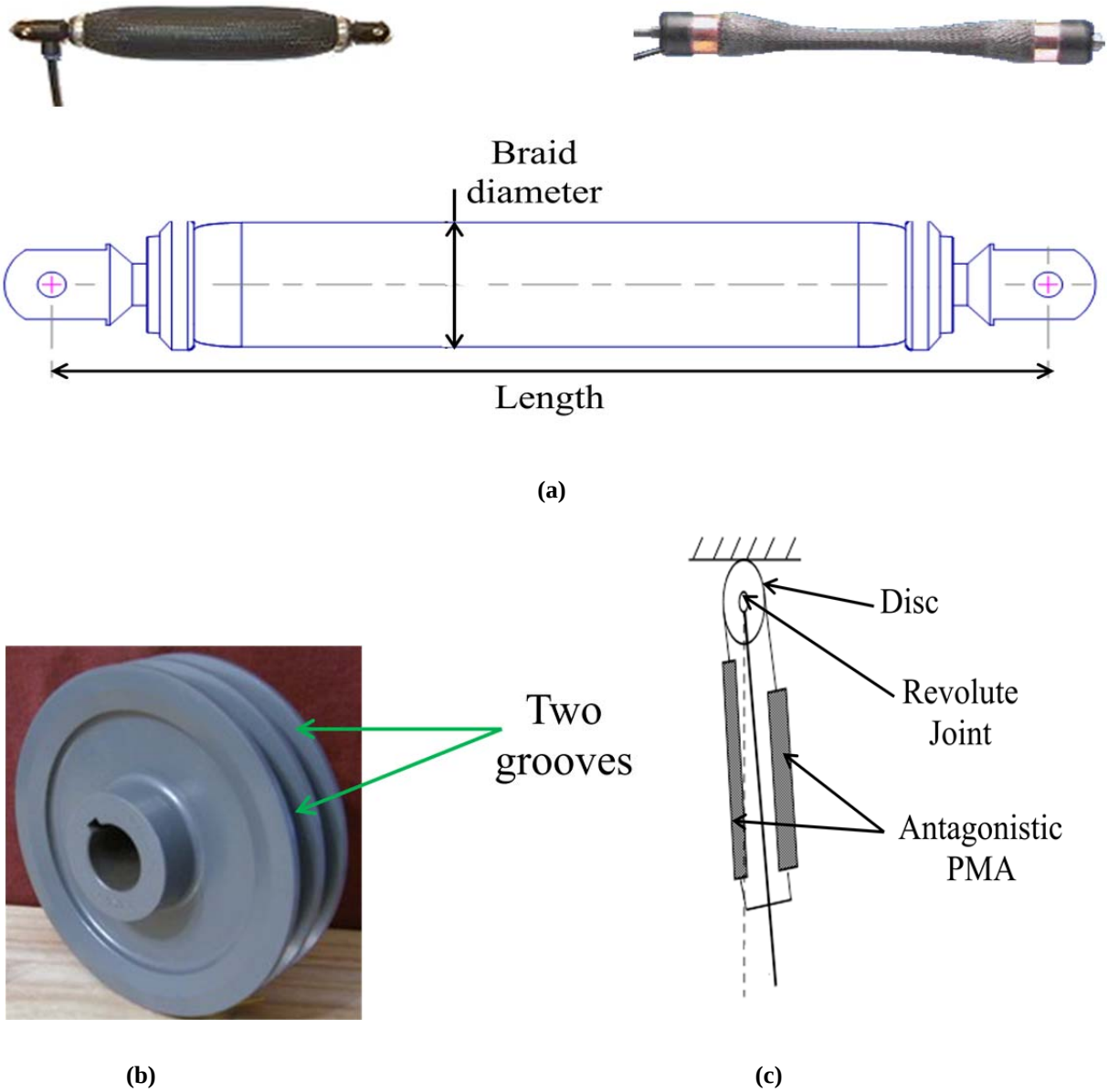

Figure 2-8. (a) Pneumatic muscle actuator (PMA). (b) Double groove aluminium disc. (c) Antagonistic disc-PMA (opposing pair configuration) mechanism.

2.6. Instrumentation

Matrix 820 solenoid 2/2 valves were used for the control of pressure in PMA. Each PMA was equipped with gauge pressure sensor and joint encoders were used to measure hip and knee joint angle trajectories. The joint angle measurements were used to calculate and control

the lengths of PMA. A tension/compression load cell was placed in series with each PMA. Load cells were only used during the experimental evaluation of impedance control scheme. All the hardware was controlled by using a DSPACE, Ds1103 operating system (Fig. 2-9). Landice gait rehabilitation treadmill was used to carry out the robotic gait training process. A bill of materials is provided in Appendix B.

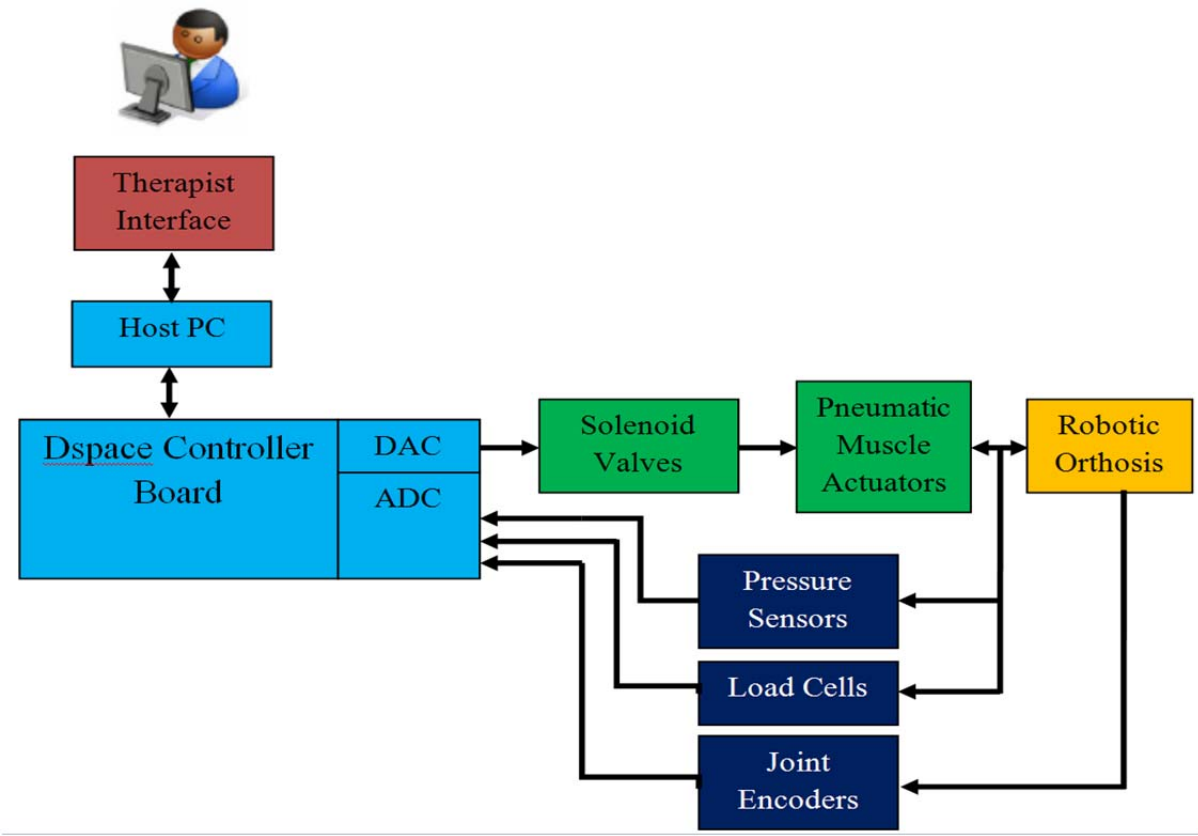

Figure 2-9. A block diagram showing the instrumentation and connection overview of the robotic gait training orthosis. Load cells were only used for the impedance control scheme.

2.7. Visual Feedback

Visual feedback to the human subjects was provided using a display placed in front of them. The visual feedback is important in order to encourage the subjects to participate more actively in the gait training process during impedance control and AAN control modes. The visual feedback was provided in the form of plots of reference hip and knee sagittal plane joint angle trajectories against the actual hip and knee sagittal plane joint angle trajectories. Hip and knee joint angles are generated at DAC (digital to analog) channels in the DSPACE panel. Similarly, a visual feedback system was also developed for the physical therapist in order to facilitate him. The physical therapist can also observe the subjects' performance in the form of plots of reference hip and knee sagittal plane joint angle trajectories against the

actual hip and knee sagittal plane joint angle trajectories. The physical therapist also has access to all the important controller parameters, and the treadmill speed that could be changed by using a therapist interface.

2.8. Design Capability Analysis

The design of the robot gait training orthosis was analyzed for two important requirements; i.e., joint ranges of motion and robotic orthosis moment exerting capacities. Careful measurements were carried out from the readings of position and force sensors and the obtained results were analyzed. It was observed that the robotic orthosis design is able to provide the estimated joint range of motion, with a maximum hip flexion/extension of $+60^0/-30^0$ and maximum knee flexion/extension of $+0^0/-90^0$. The experimental validation of these joint ranges of motion is also provided in Chapter 4 (Section 4.5). The passive foot lifter provided sufficient dorsiflexion during the swing phase of gait cycle, and the cases of foot dragging against the treadmill were not recorded. Similarly, subjects reported comfortable hip abduction and adduction motion as well as the trunk translations.

Moment exerting capacity of the robotic gait training orthosis design was also evaluated by considering the maximum joint moments available from the actuators. First of all, the maximum moments that can be applied at hip and knee sagittal plane joints were found, while the robot was moved to trace the entire joint space. It is important to note here that this moment analysis was carried out on hip and knee sagittal plane joints in joint space. The antagonistic actuation of PMA provided maximum achievable joint moments of 50 Nm, which is sufficient for the proposed application. The hip and knee sagittal plane mechanical joint stops were also tested against the maximum joint moments. The joint stops were able to withstand the maximum robot applied moments, thus inhibiting excessive hip flexion/extension and knee extension. The spring mounted on the parallelogram mechanism, and the light weight nature of the robotic gait training orthosis helped in reducing the relative slip between the robotic orthosis joints and anatomical joints. However, it was not possible to completely eliminate the slip between the robotic orthosis joints and anatomical joints.

2.9. Conclusions

In this chapter, we discussed the motivation and need to build the intrinsically robotic gait training orthosis that can aid in gait rehabilitation of neurologically impaired subjects. Useful inferences were drawn from the study of biomechanics of human gait to conceptualize a

robotic gait training orthosis. The mechanical design of the robotic gait training orthosis has been presented in detail. The robotic orthosis is hypothesized to allow more naturalistic gait patterns to the neurologically impaired subjects. Actuators used in this robotic orthosis were intrinsically compliant, back-drivable, safe for human-robot interaction and exhibit skeletal muscle like behavior. Since the robotic gait training orthosis has mechanical actuators, several safety features were incorporated to ensure the safety of the neurologically impaired subjects. Any of the DOFs of the robotic orthosis can be blocked within minutes based on the observation and decision of the physical therapist. The design of the robotic orthosis was analyzed in terms of joint ranges of motion and robotic orthosis moment exerting capacities, in order to validate its suitability for the gait training task. It was found that the robotic orthosis can provide the required joint ranges of motion and required moments. According to the author's best knowledge, no intrinsically compliant multijoint robotic orthosis for treadmill training, powered by PMA, has been reported in literature before. In the next chapter, the dynamic model developed for the robotic gait training orthosis is described in detail.

2.10. Acknowledgements

The fourth year honours students Boran Wang and Jiawen Liang at the Department of Mechanical Engineering, The University of Auckland played an important role in fabrication of the mechanical hardware. The Mechatronics laboratory technician Logan Stewart, at the University of Auckland also helped throughout this research in fabricating and improving the mechanical and electronic hardware.

Chapter 3. Dynamics of the Robotic Orthosis

Dynamic modeling of robotic gait training orthosis is an important task in order to design the robust and adaptive control schemes. This chapter presents the dynamic modeling of the robotic gait training orthosis. The numerical model of the PMA, consisting of a nonlinear friction, nonlinear spring, and a nonlinear contractile element was used in order to derive the dynamic model of robotic gait training orthosis. Nominal pressure of PMA for the desired equilibrium position of the robotic gait training orthosis was derived. It is necessary to derive the nominal pressures so that robotic orthosis will revert to the desired equilibrium position if the control is lost. This will enhance the safety of the human subjects during the gait training process. The concept of joint compliance of the robotic gait training orthosis is also presented. The joint compliance of the robotic gait training orthosis is an important concept and will be used in providing variable compliance during the robot assisted gait training (Chapter 4).

3.1. Introduction

The dynamic model of robotic orthosis [121] formulates the relationship between the inputs to the robotic orthosis and the corresponding outputs. Classical control methods [122] require a dynamic model of the robotic orthosis to design control architecture. Dynamic modeling of the robotic orthosis, powered by PMA, is a crucial task because of the nonlinear elasticity of the bladder contained within the braided sheath and the mechanical characteristics of bladder/sheath combination under pressure [96, 123, 124] .

The first important work related to the modeling of PMA has been carried out by Chou *et al.* [96]. The static PMA model has been derived on the principle of virtual work [96]. Tondu *et al.* have also used the principle of virtual work [96] for the PMA modeling [123]. In addition to the model developed by Chou *et al.* [96], Tondu *et al.* have included a term accounting for the non-cylindrical form of PMA ends, which appeared during the excitation phase. Klute *et al.* have modeled the PMA based on the nonlinear material characteristics [125]. This model has yielded improved accuracy of the model developed by Chou and Hannaford [125]. Recently a PMA static model has been developed by Doumit *et al.* [124] by considering the constitutive material properties of PMA. These types of analytical models developed for PMA are more suitable for mechanical design of the PMA, but as these

equation parameters cannot be measured during actuation of the PMA, it does not help model the system for the purpose of actuator control that, is important for classical nonlinear control.

The most significant work regarding the modeling of PMA has been carried out by Reynolds *et al*. [126] and a phenomenological model of the dynamic behavior of PMA has been proposed. The dynamic characteristic of PMA has been modeled as a three element model on the basis of Voight visco elastic model of the skeletal muscle [126]. The PMA model proposed by Reynolds *et al*. will be used for deriving a dynamic model of the proposed robotic gait training orthosis.

Numerical modeling of PMA is presented in the beginning of this chapter. This follows with the dynamics of the robotic orthosis powered by PMA. The concepts of nominal pressure and the joint compliance of the robotic gait training orthosis are also defined.

3.2. Numerical Modeling of PMA

Modeling of the robotic orthosis with PMA (Fig. 3-1) was a crucial task, as they exhibit highly nonlinear force-length characteristics. For this work, we considered the PMA numerical model developed by Reynolds *et al.* [126], although other approaches to modeling also exist [96, 123, 124]. The model developed by Reynolds *et al*. is easy to apply to robotic systems powered by PMA [127]. The dynamic behavior of the PMA hanging vertically and actuating a mass *M* has been modeled as a combination of a nonlinear friction, a nonlinear spring, and a nonlinear contractile element (Fig. 3-2). The equation describing the dynamics of this PMA hanging vertically actuating a mass is

$$M\ddot{x} + B(P)\dot{x} + K(P)x = F(P) - Mg \tag{3.1}$$

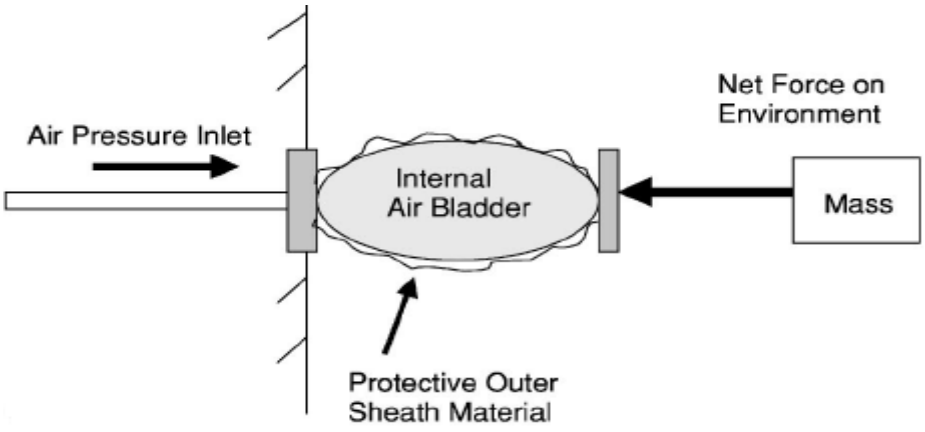

Figure 3-1. Schematic drawing of the PMA

where *x* is the amount of PMA contraction and where the coefficients for spring element *K(P),* damping element *B(P)* and contractile force element *F(P)* are given in [126] as function of pressure *P*

$$K(P) = K_0 + K_1 P \tag{3.2}$$
$$= 5.71 + 0.0307P$$
$$B(P) = B_{0i} + B_{1i} P \tag{3.3}$$
$$= 1.01 + 0.00691P$$
$$B(P) = B_{0d} + B_{1d} P \tag{3.4}$$
$$= 0.6 - 0.000803P$$
$$F(P) = F_0 + F_1 P \tag{3.5}$$
$$= 179.2 + 1.39P$$

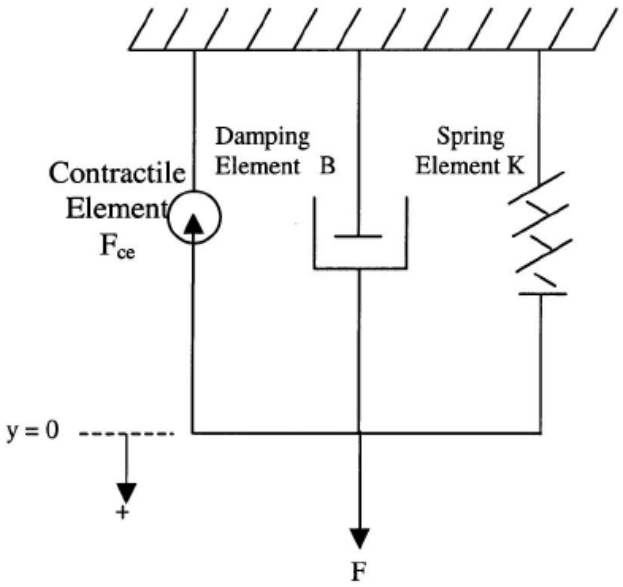

Figure 3-2. Three element model of PMA [126]

From eq. (3.1) the total force exerted by the PMA on the mass is

$$\beta = F(P) - B(P)\dot{x} - K(P)x \tag{3.6}$$

For the antagonistic configuration of PMA (Fig. 3-4 (a)) the torque (T_i) imparted to the robotic orthosis hip and knee joint by the PMA pair is

$$T_i = T_f - T_e = (\beta_f - \beta_e)r \tag{3.7}$$

where T_f and T_e are the torque due to each of the individual PMA and are given by:

$$T_f = (F_f - K_f x_f - B_f \dot{x}_f) r \quad (3.8)$$

$$T_e = (F_e - K_e x_e - B_e \dot{x}_e) r \quad (3.9)$$

In eq.(3.8) and eq.(3.9) x_f and x_e are the lengths of two PMA and r is the radius of disc. Thus the relation for total torque becomes:

$$T_i = (F_f - K_f x_f - B_f \dot{x}_f - F_e + K_e x_e + B_e \dot{x}_e) r \quad (3.10)$$

3.3. Dynamics of the Robotic Orthosis Powered by PMA

The dynamics of robotic orthosis is given by (Fig. 3-3). The dynamic model of the robotic orthosis formulates the relationship between the pressure applied to the PMA (P) and the resulting human subject hip and knee sagittal plane joint angle accelerations ($\ddot{\theta}$) (Fig. 3-3). The input pressure (P) entering the PMA model generates the total force exerted by PMA (β) (Fig. 3-3). The PMA force (β) applied to the robotic orthosis joints in the form of antagonistic PMA configuration generates the joint torques (T_i) (Fig. 3-3). The joint torques applied by the robotic gait training orthosis accelerates ($\ddot{\theta}$) the human subject sagittal plane hip and knee joints (Fig. 3-3). It is important to mention here that the joint torques generated by the human subjects is not included in the present dynamic model. Details regarding the joint torques generated by human subjects are presented in Chapter 6. The dynamics of the robotic gait training orthosis was modeled as a double pendulum (Fig. 3-4 (b)) using Newton-Euler formulation [121] and is given by the following equation

$$D_i(\theta)\ddot{\theta} + C_i(\theta, \dot{\theta})\dot{\theta} + G_i(\theta) = T_i \quad (3.11)$$

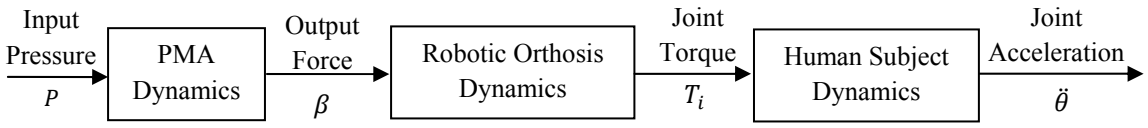

Figure 3-3. Overall dynamics of the robotic gait training orthosis. The human subject interaction torques was not modeled in this Chapter. The estimation of human subject interaction torques is presented in Chapter 6.

where the subscript *i=1(hip),2 (knee)*. $D_i(\theta)$, C_i and G_i are the mass, centrifugal and Coriolis, gravitational matrices of the system. The mass, centrifugal and Coriolis, gravitational matrices were combined for the robotic orthosis and human subject in the dynamic model given by eq.(3.11). Geometric values of the human subject were measured before the experiments. Human subject mass parameters were estimated from the regression equations

proposed by Zatsiorsky *et al*. [128]. T_i is the vector of torque applied by robotic orthosis on human joints. By expanding the matrices D_i , C_i and G_i and vectors $\ddot{\theta}$ and $\dot{\theta}$, we get

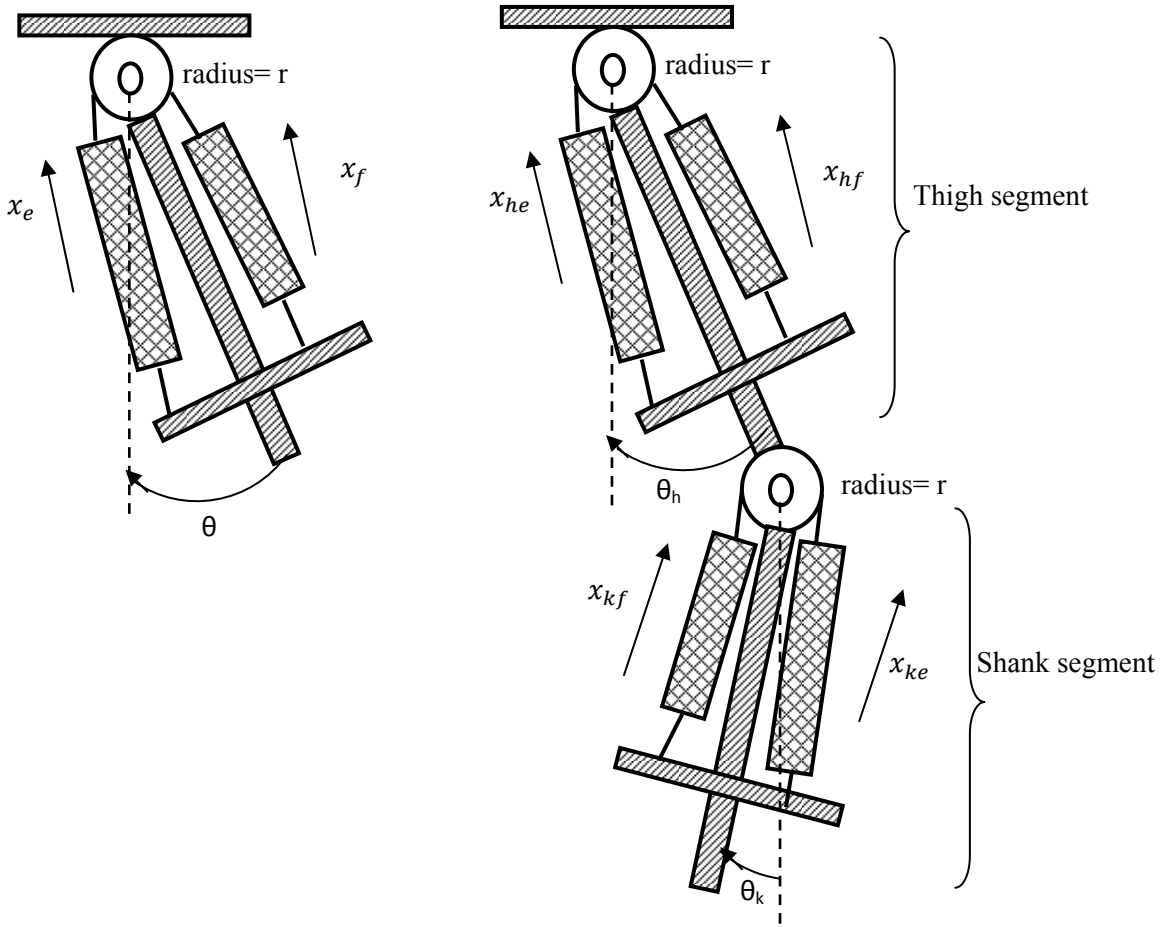

Figure 3-4. (a) Antagonistic PMA configuration. (b) Robotic orthosis with PMA for hip and knee joint actuation.

$$\begin{bmatrix} D_{11} & D_{12} \\ D_{21} & D_{22} \end{bmatrix} \begin{bmatrix} \ddot{\theta}_1 \\ \ddot{\theta}_2 \end{bmatrix} + \begin{bmatrix} C_{11} & C_{12} \\ C_{21} & C_{22} \end{bmatrix} \begin{bmatrix} \dot{\theta}_1 \\ \dot{\theta}_2 \end{bmatrix} + \begin{bmatrix} G_1 \\ G_2 \end{bmatrix} = \begin{bmatrix} T_1 \\ T_2 \end{bmatrix} \tag{3.12}$$

where

$$D_{11} = I_1 + m_2 l_1^2 + m_2 l_1 l_2 C_2 + I_2$$

$$D_{12} = D_{21} = 0.5 \times m_2 l_1 l_2 C_2 + I_2$$

$$D_{22} = I_2$$

$$C_{11} = -m_2 l_1 l_2 S_2 \dot{\theta}_1 \dot{\theta}_2$$

$$C_{12} = -0.5 \times m_2 l_1 l_2 S_2 \dot{\theta}_2{}^2$$

$$C_{21} = 0.5 \times m_2 l_1 l_2 S_2 \dot{\theta}_1{}^2$$

$$C_{22} = 0$$

$$G_1 = g[0.5 \times m_1 l_1 C_1 + m_2 l_1 C_1 + 0.5 \times m_2 l_2 C_{12}]$$

$$G_2 = g \times 0.5 \times m_2 l_2 C_{12}$$

where

l_i= length of i^{th} leg segment.

I_i= inertia of i^{th} leg segment.

m_i= mass of i^{th} leg segment including the mass of subject's leg segments.

The arrangement of the PMA on the robotic orthosis is shown in Fig. 3-4 (b). Under these conditions, the hip and knee sagittal plane torques T_h and T_k, respectively can be expressed using eq.(3.7).

$$T_h = (F_h - K_h x_{fh} - B_{fh}\dot{x}_{fh} - F_h + K_h x_{eh} + B_{eh}\dot{x}_{eh})\, r \tag{3.13}$$

$$T_k = (F_k - K_k x_{fk} - B_{fk}\dot{x}_{fk} - F_k + K_k x_{ek} + B_{ek}\dot{x}_{ek})r \tag{3.14}$$

The joint angle measurements were converted into the lengths of PMA by using the following relation

$$x_{ei} = r\left(\theta_i + \frac{\pi}{2}\right) \tag{3.15}$$

$$x_{fi} = r\left(\theta_i - \frac{\pi}{2}\right) \tag{3.16}$$

where x_{ei} and x_{fi} are lengths of hip and knee flexion and extension PMA expressed in terms of θ_i. The input pressures to the PMA actuating hip and knee joints can be expressed as:

$$0 \le P_{ei} = P_{0ei} + \Delta p_i \le P_{MAX} \tag{3.17}$$

$$0 \le P_{fi} = P_{0fi} - \Delta p_i \le P_{MAX} \tag{3.18}$$

$$P_{oi} = P_{0ei} - P_{0fi}$$

where P_{0ei}, P_{0fi}, are nominal pressures and Δp_i are the controllable pressures represented as arbitrary functions of time. P_{MAX} is the maximum pressure that can be applied to the PMA. From eq.(3.13)-(3.18), the hip and knee joint torques can be written as

$$T_i = T_{0i} + T_{1i}\Delta p_i \tag{3.19}$$

where

$$T_{0i} = [F_{0i} + F_{1i}P_{0fi} - (K_{0i} + K_{1i}P_{0fi})x_{fi} - (B_{0i} + B_{1i}P_{0fi})\dot{x}_{ti} - F_{0i} - F_{1i}P_{0ei} + (K_{0i} + K_{1i}P_{0ei})x_{ei} + (B_{0i} + B_{1i}P_{0ei})\dot{x}_{ei}]\, r \tag{3.20}$$

$$T_{1i} = [-F_{1i} + K_{1i}x_{fi} - B_{1i}\dot{x}_{fi} - F_{1i} + K_{1i}x_{ei} + B_{1i}\dot{x}_{ei}]\, r \tag{3.21}$$

Combining eq.(3.11) and eq.(3.17)-(3.21), the dynamics of robotic orthosis actuated by PMA can be written as:

$$\begin{bmatrix}\ddot{\theta}_1\\ \ddot{\theta}_2\end{bmatrix} = \begin{bmatrix}a_1\\ a_2\end{bmatrix} + H\begin{bmatrix}\Delta p_1\\ \Delta p_2\end{bmatrix} \tag{3.22}$$

where

$$\begin{bmatrix}a_1\\ a_2\end{bmatrix} = D^{-1}\left(-C\dot{\theta} - G + \begin{bmatrix}T_{01}\\ T_{02}\end{bmatrix}\right) \tag{3.23}$$

$$H = D^{-1}\begin{bmatrix}T_{11} & 0\\ 0 & T_{12}\end{bmatrix} \tag{3.24}$$

The dynamic model of robotic orthosis given by eq.(3.22) provides output in the form of hip and knee joint accelerations ($\ddot{\theta}$). The model output in the form of joint accelerations will be integrated to calculate the hip and knee joint velocities ($\dot{\theta}$) and joint angles (θ). This information will be used to find the difference between the reference joint angles and velocities and the actual joint angles and velocities. This difference or trajectory tracking error will then be used in the design of robust and adaptive control schemes. The experimental results of these control schemes are provided in Chapters 4, 6 and 7.

3.4. PMA Nominal Pressure for Desired Equilibrium Position of the Robotic Orthosis

The hip and knee joint nominal pressures P_{0bi}, P_{0ti}, were derived so that the robotic orthosis has an equilibrium point at a desired constant hip and knee angle (θ_{ieq}). These nominal pressures at the equilibrium points were necessary because if the control is lost, the robotic orthosis will revert to the desired equilibrium position [129]. In order to find the proper nominal pressures between antagonistic configurations of PMA relationships between these PMA were established to balance the steady-flexion and extension torques about the hip and knee as functions of the desired equilibrium joint angles. From eq.(3.13)-(3.15) and eq.(3.20)-(3.21), the total steady state flexion and extension torques about the hip and knee joints are

$$T_{0if} = \left[F_{1i}P_{0ti} - (K_{0i} + K_{1i}P_{0ti})r\left(\theta_{ieq} + \frac{\pi}{2}\right)\right]r + G_i \tag{3.25}$$

$$T_{0ie} = \left[F_{1i}P_{0bi} - (K_{0i} + K_{1i}P_{0bi})r\left(\theta_{ieq} - \frac{\pi}{2}\right)\right]r \tag{3.26}$$

where G_i is the flexion torque imparted to the hip by gravity. Equating the flexion and extension torques results in the following relationship between P_{0ti} and P_{0bi}

$$P_{0ti} = m_i P_{0bi} + j_i \tag{3.27}$$

where

$$m_i = \frac{\left[F_{1i} - K_{1i}r\left(\theta_{ieq} + \frac{\pi}{2}\right)\right]}{\nabla_i} \tag{3.28}$$

$$j_i = \frac{\left(K_{0i}r\left(2\theta_{ieq} - \frac{\pi}{2}\right) + \frac{G_i}{r}\right)}{\nabla_i} \tag{3.29}$$

and

$$\nabla_i = F_{1i} - K_{1i}r\left(\theta_{ieq} - \frac{\pi}{2}\right) \tag{3.30}$$

The relationships between the nominal flexion and extension PMA pressures are given by eq.(3.27) and depend on the system coefficients and the desired equilibrium angles. Therefore, for a given equilibrium angle θ_{ieq}, one of the nominal hip PMA pressure (say P_{0ti}) was chosen arbitrarily, and the other nominal pressure (P_{0bi}) was derived according to the relation given in eq.(3.27). The significance of these nominal pressures was that the robotic orthosis will revert to its quite standing posture if there is no control input or if the control is lost (i.e. Δp_i=0). For the control of robotic orthosis the hip and knee equilibrium angles in the quite standing posture according to anatomical conventions (i.e. θ_{ieq}=0^o) were selected. The nominal pressures P_{0th} and P_{0tk} chosen for the hip and knee joint were 150 KPa. The nominal pressure of 150 KPa was selected according to the operational pressure range of PMA [126].

3.5. Robotic Gait Training Orthosis Joint Compliance

The stiffness property of a PMA is dominated by the nominal pressure from its air supply. The compliance control of the robotic orthosis was performed by regulating the nominal pressure of the hip and knee flexion/extension muscles for their operating ranges. This method of controlling the compliance of a 2-DOF, PMA actuated planar manipulator has also been used by Choi *et al*. in [127, 130]. The torque of the joint's spring force term was derived by extracting the spring terms from eq. (3.20) and eq.(3.21).

$$T_{is} = (K_{0i} + K_{1i}P_{0fi})x_{fi}.r - (K_{0i} + K_{1i}P_{0ei})x_{ei}.r + K_{1i}(x_{ei} + x_{fi})r.\Delta p_i = \delta_i.\theta_i \quad (3.31)$$

where T_{is} is the spring torque derived from the three element model of the PMA. δ_i is the stiffness value at the hip and knee joints. By combining eq.(3.15)-(3.21) and eq.(3.31), spring torque equation for hip and knee joint is derived like

$$T_{is} = S_i.\theta_i = 2r^2K_{0i}\theta_i + K_{1i}(r^2\pi P_{0fi} - P_{oi}x_{ei}r) + K_{1i}r^2\Delta p_i \quad (3.32)$$

The joint compliance was derived as

$$\gamma_i = \frac{1}{\delta_i} = \frac{\theta_i}{2r^2K_{0i}\theta_i + K_{1i}(r^2\pi P_{0fi} - P_{oi}x_{ei}r) + K_{1i}r^2\Delta p_i} \quad (3.33)$$

In order to control the joint compliance, it was assumed that $P_{0fi} = P_{0ei} = P_i$, typically by setting the nominal position of the orthosis to the initial standing posture (i.e. θ_i=0^o). Joint compliance was then determined for hip and knee joint as

$$\gamma_i = \frac{\theta_i}{2r^2K_{0i}\theta_i + K_{1i}r^2\pi(P_i + \Delta p_i)} \quad (3.34)$$

Joint compliance depends only on P_i because Δp_i is determined by the trajectory tracking controller (see Chapter 4 for details). The control laws for P_i for the desired joint compliance γ_i were directly determined form the following equation

$$P_i = \frac{\theta_i - r^2(2K_{0i}\theta_i + K_{1i}\pi\Delta p_i)\gamma_i}{K_{1i}r^2\pi C_i} \quad (3.35)$$

$$|\Delta p_i| \le P_i \le P_{MAX} - |\Delta p_i| \quad (3.36)$$

such that $\forall\theta_i \in (-\pi/2, \pi/2)$. Also $\forall\gamma_i \in (\gamma_{iMIN}, \gamma_{iMAX})$ where γ_{iMIN} and γ_{iMAX} were determined by using eq.(3.34)-(3.36). γ_{iMAX} was at $P_i = |\Delta p_i|$. Γ_{iMIN} was at $P_i = P_{MAX} - |\Delta p_i|$:

$$\gamma_{iMIN} = \frac{|\theta_i|}{2r^2K_{0i}|\theta_i| + 2K_{1i}r^2\pi P_{MAX}} \quad (3.37)$$

$$\gamma_{iMAX} = \frac{|\theta_i|}{2r^2K_{0i}|\theta_i| + 2K_{1i}r^2\pi|\Delta p_i|} \quad (3.38)$$

where γ_{iMAX} and γ_{iMIN} represent the maximum and minimum joint compliance of the robotic orthosis, respectively. The minimum joint compliance of the robotic orthosis (γ_{iMIN}) can be achieved by selecting the applied pressure to be maximum (P_{MAX}), whereas the maximum compliance (γ_{iMAX}) can be achieved by selecting the applied pressure to be $|\Delta p_i|$.

3.6. Conclusions

This chapter proposed a dynamic model of the robotic gait training orthosis. The robotic orthosis hip and knee sagittal plane motions were powered by antagonistic configuration of PMA. Three element numerical model of the PMA was used to formulate the model of robotic gait training orthosis. The nominal pressures of PMA for desired equilibrium position of the robotic gait training orthosis were also derived. These nominal pressures are important from the safety point of view. If the subject feels uncomfortable during the robotic gait training process or something goes wrong with the robotic hardware or software, the robotic orthosis will revert to these equilibrium positions, and the safety of the subject is ensured. The robotic orthosis joint compliance was also derived for the hip and knee sagittal plane rotations. This compliance is beneficial for human-robot interaction and will be further used during the AAN control of robotic gait training orthosis. In the next chapter, the trajectory tracking controllers developed for the robotic gait training orthosis are described.

Chapter 4. Trajectory Tracking Control of the Robotic Orthosis

Trajectory tracking control of robotic gait training orthosis is important for guiding the limbs of severely impaired subjects on reference trajectories. This Chapter presents a new trajectory tracking control scheme that allows the robotic orthosis joint compliance to be controlled independently of the trajectory tracking control. Trajectory tracking control laws based on the boundary layer augmented sliding control law (BASMC) and the chattering free robust variable structure control law (CRVC) was developed in joint space to guide the subject's limbs on reference physiological gait trajectories. The experimental evaluation of the BASMC and the CRVC was carried out on neurologically intact subjects. The results show that the robotic orthosis is able to guide the subjects' limbs on reference physiological trajectories while using the BASMC and the CRVC control laws. It is also demonstrated that the presented control scheme can provide variable compliance during robot assisted gait training.

4.1. Introduction

One of the main purposes of the robotic gait training orthosis is to guide the limbs of severely impaired subjects on reference physiological trajectories [7, 39, 79]. The control schemes that are used to guide the subjects' limbs on reference physiological trajectories are generally regarded as trajectory tracking or position controllers [1, 7]. The trajectory tracking control is important for the gait rehabilitation, especially at the initial phases of training when subjects are not capable of contributing any effort towards the gait training process [7, 54]. The trajectory tracking control scheme may help in providing an optimal afferent input to the neuromuscular system, which may result in motor function improvement [7].

The trajectory tracking control scheme of conventional robotic orthoses, such as LOKOMAT [37] and ALEX, [100] works on the basis of a proportional-derivative (PD) control law with an infinite and constant impedance (compliance) value. These infinite and constant impedance values produce large forces in response to the undesirable motions produced by spasms [87, 88]. As a result, the subject may feel pain or discomfort. Therefore, there is a need to develop trajectory tracking control schemes that can provide variable compliance during the robot assisted gait training [88]. This variable compliance is beneficial for human-robot interaction applications and would help in absorbing large position errors

and would insure safety of the subject [87, 88]. A novel trajectory tracking control scheme for the robotic gait training orthosis is proposed in this work. The novelty of the proposed control scheme is that it allows the robotic orthosis joint compliance to be controlled independently of the trajectory tracking control (Fig. 4-1). The control of compliance will provide variable compliance during the robot assisted gait training.

The hip and knee sagittal plane rotations of the robotic orthosis are powered by PMA. PMA possess a highly nonlinear and time-varying behaviour that presents a control problem [96, 126]. This control problem has been approached via various methodologies. In [131], an antagonistic PMA actuation has been used to actuate a leg-like swinging pendulum in the lab. The PMA are actuated in a periodic manner to mimic walking movements, and the action has been controlled by a proportional digital pole placement controller. The approach used in [131] is not suitable for the control of PMA, as they have structured uncertainties [126]. The structured uncertainties in the model of PMA exist due to its inherent material properties [96, 126]. The proportional digital pole placement controller [131] does not take into account the structured uncertainties in the model of PMA.

For the trajectory tracking control of robotic manipulators powered by PMA, sliding mode control law (SMC) has been commonly used in literature [129, 130, 132-134]. SMC is ideal for PMA applications because the PMA model has structured uncertainties [126], non-linear and time varying, necessitating the application of some robust control algorithm. The sliding mode control guarantees the stability of the system, and a reasonably good tracking performance in the presence of structured uncertainties in the model of PMA as well as external disturbances [127]. In [134], sliding mode control (SMC) has been simulated to control the joint angles in PMA antagonistic configuration.

It is well known that sliding control law produce chattering [122], that is undesirable, as it usually excites the high frequency unmodeled dynamics of the systems powered by PMA. This chattering needs to be mitigated for the controller to perform properly. Different methods of mitigating chattering have been proposed in literature. BASMC is one of these methods. In [127, 129, 134], a BASMC has been used to control the position of robotic manipulators powered by PMA. BASMC has shown reasonable tacking performance for the robotic manipulators powered by PMA [129]. BASMC of PMA actuated robotic systems [129, 130] has the advantage to mitigate the control chattering, which can significantly improve tracking performance. The variation of manipulated load could pose a problem to the

application of BASMC. To take into account the variable loading effect, an adaptive control algorithm has been simulated by Lilly *et al.* [135]. Later, Lilly *et al.* has also shown the robustness of BASMC against variable loading [129]. This makes the BASMC an appropriate choice for the control of the robotic gait training orthosis, powered by PMA.

In [136], a proxy-based SMC (PBSMC) has been used to provide safety and achieve tracking of a 2-DOF planar manipulator powered by PMA. The PBSMC has the disadvantage of low tracking performance for a large initial error owing to its delayed positioning [136]. This delayed positioning is not acceptable in the case of a robotic gait training orthosis, as the test subjects may start walking out-of-phase with the robotic orthosis [46]. A chattering free robust variable structure controller (CRVC) has also been proposed by *Xu.* [137]. CRVC carries all the advantages of conventional BASMC and eliminates the chattering effect by utilizing a novel feedback function, which is continuous in time domain.

For the trajectory tracking control of robotic gait training orthosis the controllers developed were (1) BASMC. (2) CRVC. The chapter starts with the formulation of BASMC and CRVC control laws for the trajectory tracking control of robotic gait training orthosis. Then the control of robotic orthosis joint compliance is presented. This follows with the experimental evaluation of the BASMC and CRVC control laws for the trajectory tracking control of robotic gait training orthosis. Experiments with neurologically intact subjects were performed. The contribution of this work includes the development of a control scheme that allows the robotic orthosis joint compliance to be controlled independently of the trajectory tracking control.

4.2. Boundary Layer Augmented Sliding Mode Control (BASMC)

A BASMC was developed for the robotic gait training orthosis in joint space to guide the subjects' limbs on reference physiological trajectories ($\theta_i^*, \dot{\theta}_i^*$) (Fig. 4-1). The goal of the BASMC is to minimize the trajectory tracking errors ($\tilde{\theta}_1, \dot{\tilde{\theta}}_1$) in the presence of structured uncertainties in the model of PMA (Chapter 3).

4.2.1. Controller formulation

Assume that we have imperfect knowledge of a_i and H due to the structured uncertainties in the model of PMA (eq.3.22-3.24). Suppose the extent of imprecision on a_i and H is bounded by known continuous functions of θ_i and $\dot{\theta}_i$. Assuming that we have estimates

$\tilde{a}_h, \tilde{a}_k$ of a_h and a_k such that the estimation error on a_h and a_k is bounded by some known function A_i $(\theta_i, \dot{\theta}_i)$

$$|\tilde{a}_i - a_i| \leq A_i \tag{4.1}$$

The control gain H was unknown but of known bounds, we had the estimate $\tilde{H}$ for it such that

$$0 < H_{min} \leq H \leq H_{max} \tag{4.2}$$

As the control input enters multiplicatively in the system dynamics, it is usual to have estimate $\tilde{H}$ of gain H as the geometric mean of above bounds

$$\tilde{H} = \sqrt{H_{min} H_{max}} \tag{4.3}$$

The bounds (eq.4.2) can be written in the form

$$\rho^{-1} \leq \frac{\tilde{H}}{H} \leq \rho \tag{4.4}$$

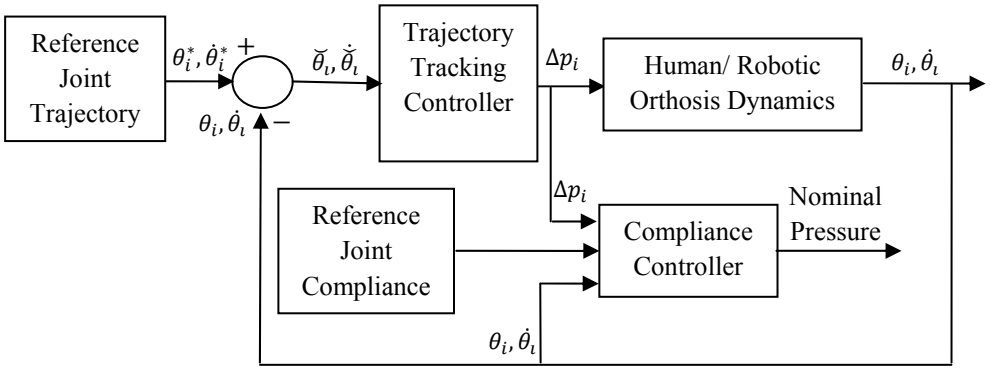

Figure 4-1. Robotic orthosis controller diagram. The controller was implemented in joint space. Trajectory tracking controllers based on BASMC and CRVC were developed. The reference joint compliance was selected to be minimum during the present study.

where

$$\rho = \sqrt{\frac{H_{max}}{H_{min}}} \tag{4.5}$$

The control law was designed to be robust against the bounded multiplicative uncertainty (eq.4.4), where ρ was the gain margin of the design. ρ was time varying or state dependent, and we also have

$$\rho^{-1} \leq \frac{H}{\tilde{H}} \leq \rho \tag{4.6}$$

The control problem was formulated by defining a time varying sliding surface *S(t)* in state space R^n by the scalar equation $s(\theta; t) = 0$, where

$$s_i(\theta_i; t) = (\frac{d}{dt} + \lambda)^{n-1}\tilde{\theta}_i \tag{4.7}$$

For a second order system,

$$s_i = \dot{\tilde{\theta}}_i + \lambda\tilde{\theta}_i \tag{4.8}$$

Differentiating eq.(4.8)

$$\dot{s}_i = \ddot{\tilde{\theta}}_i + \lambda\dot{\tilde{\theta}}_i \tag{4.9}$$

where $\tilde{\theta}_i = \theta_i - \theta_i^*$ are the tracking errors at hip and knee joints. Also θ_i^* and θ_i represents the desired and actual trajectories for the hip and knee joints, respectively (Fig. 4-1).

The simplified problem of maintaining the scalar *s* at zero can now be achieved by selecting the pressure inputs Δp_h and Δp_k such that outside *S(t)*,

$$\frac{1}{2}\frac{d}{dt}{s_i}^2 \leq -\eta|s_i| \tag{4.10}$$

where η is a strictly positive constant. The best approximation $\Delta\tilde{p}_h$ and $\Delta\tilde{p}_k$ of continuous control laws that can achieve $\dot{s} = 0$ is thus

$$\begin{bmatrix}\Delta\tilde{p}_h \\ \Delta\tilde{p}_k\end{bmatrix} = \tilde{H}^{-1}\left(-\begin{bmatrix}\tilde{a}_h \\ \tilde{a}_k\end{bmatrix} + \begin{bmatrix}\ddot{\theta}_h^{\,*} \\ \ddot{\theta}_k^{\,*}\end{bmatrix} - \begin{bmatrix}\lambda_h\dot{\tilde{\theta}}_h \\ \lambda_k\dot{\tilde{\theta}}_k\end{bmatrix}\right) \tag{4.11}$$

where λ_h and λ_k are positive scalar design parameters. From (4.11) $\Delta\tilde{p}_h$ and $\Delta\tilde{p}_k$ can be interpreted as our best estimate of the equivalent control. In order to satisfy sliding condition (eq.4.10) despite the uncertainty on the dynamics a_i, we add to $\Delta\tilde{p}_h$ and $\Delta\tilde{p}_k$ a term discontinuous across the surface $s = 0$:

$$\begin{bmatrix}\Delta p_h \\ \Delta p_k\end{bmatrix} = \tilde{H}^{-1}\left(\begin{bmatrix}\Delta\tilde{p}_h \\ \Delta\tilde{p}_k\end{bmatrix} - \begin{bmatrix}l_h\,\mathrm{sgn}(s_h) \\ l_k\,\mathrm{sgn}(s_k)\end{bmatrix}\right) \tag{4.12}$$

where l_h and l_k are positive constants and *sgn* is the sign function:

$$\begin{aligned} \mathrm{sgn}(s_i) &= +1 \qquad \text{if } s > 0 \\ \mathrm{sgn}(s_i) &= -1 \qquad \text{if } s < 0 \end{aligned} \tag{4.13}$$

By selecting $l_i(\theta_i, \dot{\theta}_i)$ in eq.(4.12) to be large enough, it can be guaranteed that eq.(4.10) was verified. From eq.(4.8), eq.(4.11) and eq.(4.12), it was verified

$$\frac{1}{2}\frac{d}{dt}{s_i}^2 = \dot{s}_i.\,s_i = [a_i - \tilde{a}_i - l_i\mathrm{sgn}(s_i)]s_i = (a_i - \tilde{a}_i)s_i - l_i|s_i| \tag{4.14}$$

By letting

$$l_i = A_i + \eta \tag{4.15}$$

Eq.(4.1) yields eq.(4.10), as desired. Also with the estimated gain margin $\tilde{H}^{-1}$

$$l_i \geq \rho(A_i + \eta) + (\rho - 1)|\Delta\tilde{p}_i| \tag{4.16}$$

satisfies the sliding condition. Using eq.(4.12) in the expression of $\dot{s}_i$ leads to

$$\dot{s}_i = \left(a_i - H\tilde{H}^{-1}\tilde{a}_i\right) + \left(1 - H\tilde{H}^{-1}\right)\left(-\ddot{\theta}_1^{*} + \lambda_i\dot{\tilde{\theta}}_i\right) - H\tilde{H}^{-1}l_i sgn(s_i) \tag{4.17}$$

So that l_i must verify

$$l_i \geq \left|H^{-1}\tilde{H}a_i - \tilde{a}_i + \left(H^{-1}\tilde{H} - 1\right)\left(-\ddot{\theta}_1^{*} + \lambda_i\dot{\tilde{\theta}}_i\right)\right| + \eta H^{-1}\tilde{H} \tag{4.18}$$

As $a_i = \tilde{a}_i + (a_i - \tilde{a}_i)$, where $|\tilde{a}_i - a_i| \leq A_i$, this in turn leads to

$$l_i \geq H^{-1}\tilde{H}A_i + \eta H^{-1}\tilde{H} + |H^{-1}\tilde{H} - 1|.\left(\tilde{a}_i - \ddot{\theta}_1^{*} + \lambda_i\dot{\tilde{\theta}}_i\right) \tag{4.19}$$

thus to eq.(4.18). The idea behind eq.(4.7) and eq.(4.10) was to pick up a well behaved function of the trajectory tracking error, $\tilde{\theta}_1$, according to eq.(4.7) and then select the feedback control law Δp_i in eq. (3.22), such that $\tilde{\theta}_1^{2}$ remains a Lyapunov-like function of the closed-loop system, despite the presence of structured uncertainties in the model of PMA.

4.2.2. Chattering mitigation

The sliding control law given by eq.(4.12) is known to produce chattering due to the discontinuities across the sliding surfaces. This chattering needs to be mitigated for a proper functioning of the controller. To mitigate this chattering, a thin boundary layer was introduced in the area surrounding the sliding surfaces. Inside the boundary layer, the control laws are linear and continuous.

$$B_h(t) = \{(\theta_h, \dot{\theta}_h), |s_h(\theta_h, \dot{\theta}_h)| \leq \emptyset_h\}222211 - 3$$

$$B_k(t) = \{(\theta_k, \dot{\theta}_k), |s_k(\theta_k, \dot{\theta}_k)| \leq \emptyset_k\} \tag{4.20}$$

where $\emptyset_h$ and $\emptyset_k$ are the boundary layer thicknesses for the hip and knee sagittal plane joints, respectively. Replacing the term of $sgn(s_h)$ and $sgn(s_k)$ in the expression eq.(4.12) with $s_h/\emptyset_h$ and $s_k/\emptyset_k$, the sliding control law becomes

$$\begin{bmatrix}\Delta p_h \\ \Delta p_k\end{bmatrix} = \tilde{H}^{-1}\left(\begin{bmatrix}\Delta\tilde{p}_h \\ \Delta\tilde{p}_k\end{bmatrix} - \begin{bmatrix}l_h sat(s_h/\emptyset_h) \\ l_k sat(s_k/\emptyset_k)\end{bmatrix}\right) \tag{4.21}$$

and *sat* is the saturation function:

$$\text{sat}(y) = y \qquad \text{if } |y| \leq 1$$
$$\text{sat}(y) = \text{sgn}(y) \qquad \text{otherwise} \tag{4.22}$$

Outside this boundary layer, the control law was the same as represented by eq.(4.12), which guaranteed that the boundary layer was attractive and invariant. By introducing this boundary (eq.4.21) layer, it was guaranteed that the SMC law remains robust to high frequency, unmodeled dynamics of the robotic orthosis.

4.3. Chattering Free Robust Variable Structure Control (CRVC)

A CRVC control scheme was also developed in joint space for the trajectory tracking control of robotic gait training orthosis (Fig. 4-1). The goal of the CRVC was to minimize the trajectory tracking errors ($\tilde{\theta}_1, \dot{\tilde{\theta}}_1$) in the presence of structured uncertainties in the model of PMA.

4.3.1. Generalized CRVC

For a general nonlinear *n*-dimensional system

$$x_i^{n_i} = a_i(x_1, \dots\dots, x_m, t) + \sum_{j=1}^{m} h_{ij}(x_1, \dots\dots, x_m)u_j,$$
$$i, j = 1, \dots\dots, m. \tag{4.23}$$

The estimated system dynamics are represented by

$$\tilde{x}_i^{n_i} = \tilde{a}_i(x_1, \dots\dots, x_m, t) + \sum_{j=1}^{m} \tilde{h}_{ij}(x_1, \dots\dots, x_m)u_j,$$
$$i, j = 1, \dots\dots, m. \tag{4.24}$$

where '∼' in eq.(4.24) presents the estimated parameter information. The PMA model has structured uncertainties and the parameters a_i and h_{ij} represented in eq.(3.22) are imprecise but the imprecision is bounded by the following functions

$$H = (1 + \Delta)\tilde{H}$$
$$\Delta_{ij} \leq \eta_{ij} \leq 1 \tag{4.25}$$

where $\eta = [\eta_{ij}] \in R^{m\times m}$ and $\tilde{H} = [\tilde{h}_{ij}(x_1, \dots\dots, x_m)] \in R^{m\times m}$. The parametric uncertainties on the input matrix are bounded by η. Similarly, for $[a_i]^T$ we have estimates $[\tilde{a}_i]^T$ such that the estimation error on a_i is bounded by some known function $A_i(\theta_i, \dot{\theta}_i)$

$$|\tilde{a}_i - a_i| \leq A_i \tag{4.26}$$

The sliding manifold for the above mentioned *n*-dimensional system has been defined as

$$s_i = \sum_{p=0}^{n_i-1} C_{n-1}^{p}\, \mu_{ip} e_i^{n_i-1-p}$$

$$S = [s_1, \dots\dots, s_m]^T \in R^m \tag{4.27}$$

The control law for the target system has been determined as

$$U = \tilde{H}^{-1}\left[-\tilde{a} + x_d^{(n)} - \sum_{p=1}^{n-1} C_{n-1}^{p}\, \mu_p e^{(n-p)} - K\sum_{p=0}^{n-1} C_{n-1}^{p}\, \mu_p e^{(n-1-p)}\right] \tag{4.28}$$

where $K = [K_1, \dots\dots, K_m]^T \in R^m$ is the continuous feedback gain. The important concept behind CRVC was to use a continuous and smooth feedback gain in contrast to the conventional method of BASMC by eliminating the *saturation function (sat) or signum function* (*sgn*) (eq.4.22) [122]. Feedback gain has been determined from the following conditions, which satisfies the Lyapunov stability condition [137]. If *s* is a positive value then

$$A_i + \sum_{j=1}^{m} \eta_{ij}\left|x_{j,d}^{(n_i)} - \tilde{a}_j - \sum_{p=1}^{n_j-1} C_{n_j-1}^{p}\mu_{jp} e_j^{n_j-p}\right| + \psi_i s_i = k_i s_i - \sum_{j=1}^{m} \eta_{ij}\left|k_j s_j\right| \tag{4.29}$$

If *s* is a negative value then

$$-A_i - \sum_{j=1}^{m} \eta_{ij}\left|x_{j,d}^{(n_i)} - \tilde{a}_j - \sum_{p=1}^{n_j-1} C_{n_j-1}^{p}\mu_{jp} e_j^{n_j-p}\right| + \psi_i s_i = k_i s_i + \sum_{j=1}^{m} \eta_{ij}\left|k_j s_j\right| \tag{4.30}$$

4.3.2. CRVC for the robotic gait training orthosis

A CRVC control law was developed for the robotic gait training orthosis in joint space to guide the subjects' limbs on reference physiological trajectories (Fig. 4-1). The CRVC was rearranged for the robotic orthosis that was represented by a second order system eq.(3.22). The control input to the system is Δp_i eq.(3.22) (Fig. 4-1). For hip and knee sagittal plane joints, it was assumed the coefficients *H* and *a* represented in eq.(3.22) were bounded by the constraints of eq.(4.25) and eq.(4.26). Then, the sliding surface was determined by using eq.(4.27):

$$s_i = \mu_{i0}\dot{e}_i + \mu_{i1}e_i \tag{4.31}$$

where μ_{i0} and μ_{i1} can be any positive number. $\mu_{i0} = 1$ is usually selected. Also a smaller μ_{i1} and a larger k_n decrease transient time.

For the above mentioned sliding condition, the control law Δp_i for the robotic orthosis hip and knee joints (Fig. 4-1) was determined as

$$\Delta p_i = \tilde{H}^{-1}[-a_i + x_d'' - K.\mu.e - (\mu + K)e'] \tag{4.32}$$

where $K = [K_1\ K_2]^T$ was decided from the following by merging eq.(4.29) and eq.(4.30) using the $|s_n|$ notation to avoid separated conditions:

$$k_n = \frac{a_n + \eta_n\left|x_{nd}'' - \mu_n e_n' - \tilde{a}_n\right| + \psi_n|s_n|}{(1-\eta_n)|s_n|}$$

$$k_n = \frac{(1-\eta_n)^{-1}\left(a_n + \eta_n\left|x_{nd}'' - \mu_n e_n' - \tilde{a}_n\right|\right)}{|s_n|} + (1-\eta_n)^{-1}\psi_n \tag{4.33}$$

k_n can be rearranged as a simple form like

$$k_n = (1-\eta_n)^{-1}\xi/|s_n| + (1-\eta_n)^{-1}\psi_n \tag{4.34}$$

where ξ is $a_n + \eta_n\left|x_{nd}'' - \mu_n e_n' - \tilde{a}_n\right|$ and ψ_n are user parameters involving system performance. A larger ψ_n will cause a faster transient but with a larger feedback gain k_n. Essentially, k_n was varied by the current distance to the sliding manifold continuously by employing the sliding manifold information. Other conventional approaches have generally used a simplified form of

$$k_n = (1-\eta_n)^{-1}\xi + (1-\eta_n)^{-1}\psi_n \tag{4.35}$$

This difference makes the CRVC control law smoother than the BASMC, eliminating the sliding manifold information using *signum* or *saturation* function (eq.4.22) [129, 130, 134].

4.4. Joint Compliance Control

There is a strong need to provide customized robotic assistance as the level of neurologic impairment varies from subject to subject [1, 6, 37]. The robotic orthosis should be capable of providing gait training to severely impaired subjects by guiding their limbs on reference physiological trajectories. This training mode is usually referred as position control or trajectory tracking mode [79]. During position control mode, the robotic orthosis is run under 100% guidance forces with maximum stiffness so that the deviations from the reference

trajectories should be minimum [37]. On the other hand, the robotic orthosis should provide gait training with a reduced level of assistance to less severely impaired subjects who are more capable of voluntarily contributing movements towards the robotic gait training process [6]. For these subjects, the robotic orthosis compliance should be kept high so that the subjects have more freedom to voluntarily participate in the gait training. Therefore, compliance, stiffness or impedance variation of robotic gait training orthoses is an important task and has also been emphasized in the work by Riener *et al.* [37] and Asseldonk *et al.* [79]. During the current research, we also present the concept of compliance control of the robotic gait training orthosis (Fig. 4-1).

The stiffness property of a PMA is dominated by the nominal pressure. The control scheme shown in Fig. 4-1 made it possible to control the robotic orthosis joint compliance independently of the trajectory tracking control. The compliance control of the robotic orthosis was performed by regulating the nominal pressure (P_i) (eq. 3.35) of the hip and knee flexion/extension muscles for their operating ranges (Fig. 4-1). For the compliance control purpose the control pressures (Δp_i) and sagittal plane hip and knee joint angles (θ_i) were recorded. Joint compliance depends only on P_i because Δp_i is determined by the trajectory tracking controller (Fig. 4-1). The joint compliance relations for the robotic gait training orthosis are provided in Section 3.5 (eq. 3.37 and 3.38). It is important to mention here that the reference joint compliance was selected to be minimum (γ_{iMIN}) (eq.3.37) during the trajectory tracking experiments.

Table 4-1. Geometric and inertial parameters of test subjects.

Age (years)	25 to 42
Gender	Male
Height (m)	1.61 to 1.79
Body weight (kg)	62 to 81

4.5. Experimental Evaluation of Trajectory Tracking Controllers

4.5.1. Experimental protocol

In order to evaluate the performance of the robotic orthosis design and trajectory tracking controllers, preliminary experiments with neurologically intact subjects were performed. Three healthy (Table 4-1), neurologically intact subjects gave written informed consent and

participated in the study. The experimental protocol was approved by The University of Auckland, Human Participants Ethics Committee (Appendix D).

The subjects were asked to walk within the passive (unpowered) robotic orthosis for 20 minutes so that they should become familiar with the robotic orthosis and training environment. Similar procedure was repeated for the robotic orthosis in trajectory tracking (active) mode. Hip and knee physiological gait trajectories reported by *Winter* in [3] were used to define the reference joint angle trajectories. These joint angle trajectories are scalable in time, amplitude offset, and range in order to adjust it to the individual gait parameters of subjects. The subjects were asked to remain passive within the robotic orthosis and allow it to guide the trajectory of their legs during the trajectory tracking mode. Walking speed was set to 0.6 m/s. After the initial 20 minute session, the data for 60 GC during the trajectory tracking mode was recorded for analysis purpose. No BWS was used during the experiment as the test subjects had no neurological impairment and did not require any external support.

4.5.2. BASMC

The BASMC was designed according to the sliding control law given by (4.21) with the robotic orthosis dynamics given by (3.22). The ideal values of *K, B* and *F* given by eq. (3.2)-(3.5) were used. For the structured uncertainties in the model of PMA, maximum parameter error of 20% was selected eq.(3.22) for the matrix $[a_h\ a_k]^T$ eq.(3.23) and *H* eq.(3.24). For the sliding controller parameters, we used λ=12, η=0.3 for both joints and $\emptyset_i$=0.8. The control frequency was set to 60 Hz and the data from pressure sensors, as well as the data from joint encoders and reference trajectories, was recorded at the same sampling rate. P_{MAX} was selected to be 550 KPa.

Fig. 4-2 shows the reference and measured hip and knee joint angles of healthy subjects walking in the robotic orthosis during trajectory tracking mode. The joint angle trajectories averaged over all subjects are presented in Fig. 4-2. The tacking performance at hip and knee joints was acceptable as the recorded gait trajectories remained physiological. The passive foot lifter provided sufficient clearance during the swing phase and no cases of foot touching the treadmill were observed during the experiments. The subjects also reported comfortable trunk motions in the vertical and lateral planes.

The trajectory tracking errors obtained for the complete GC are shown in Fig. 4-3. The maximum trajectory tracking errors at the hip and knee sagittal plane joints during the

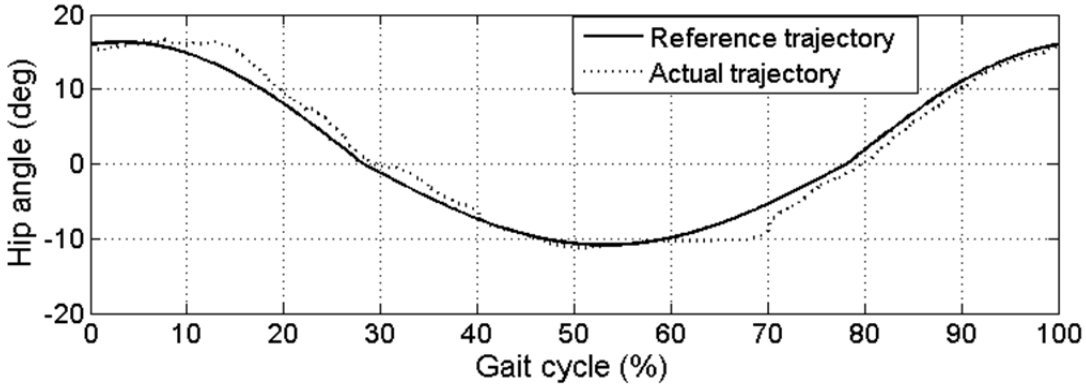

(a)

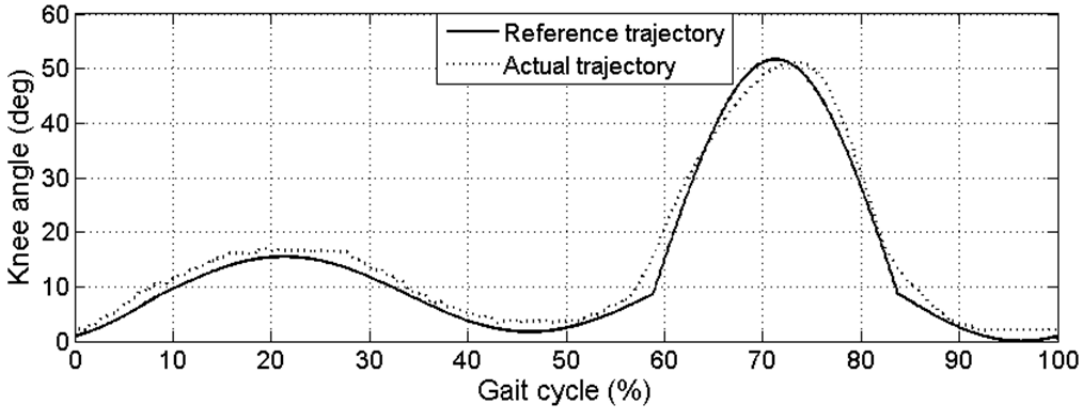

(b)

Figure 4-2. Hip and knee sagittal plane joint angle trajectories with healthy subjects as a percentage of GC obtained during trajectory tracking mode, averaged over all subjects. Normal gait trajectories taken as desired [3] and plotted against the trajectories obtained during walking in the robotic orthosis. (a) Hip joint. (b) Knee joint.

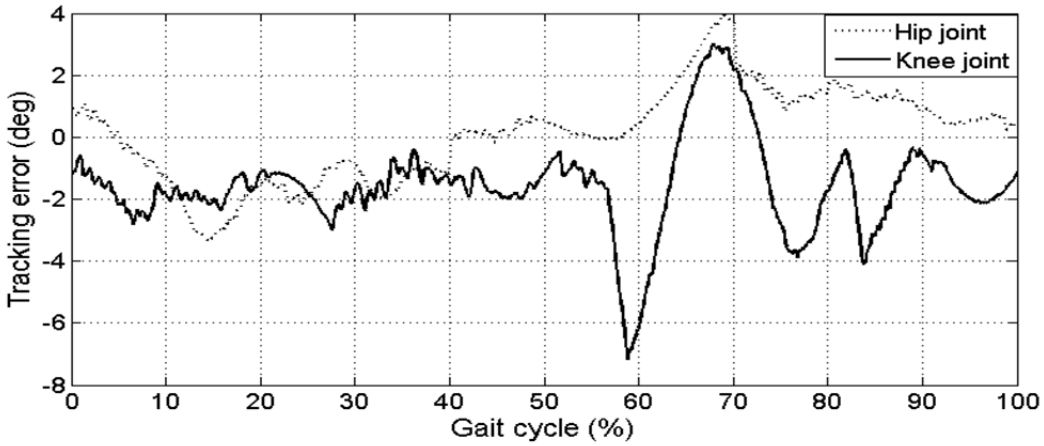

Figure 4-3. Trajectory tracking error at hip and knee sagittal plane joints during the trajectory tracking performance of Fig. 4-2.

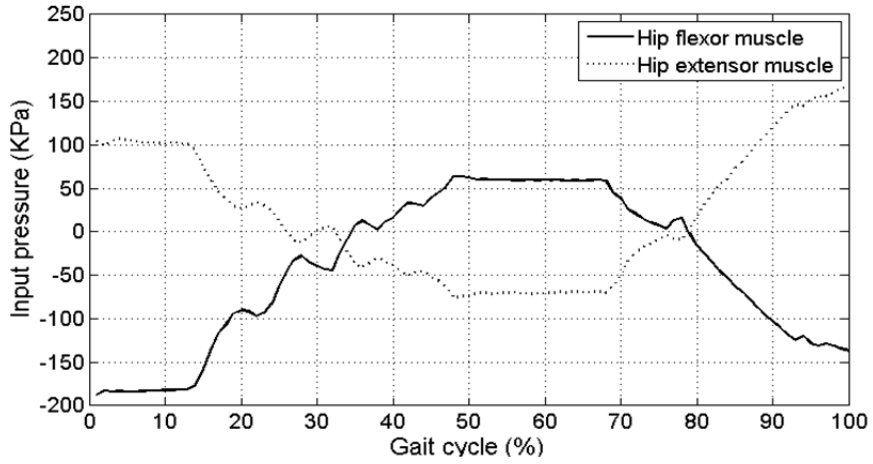

(a)

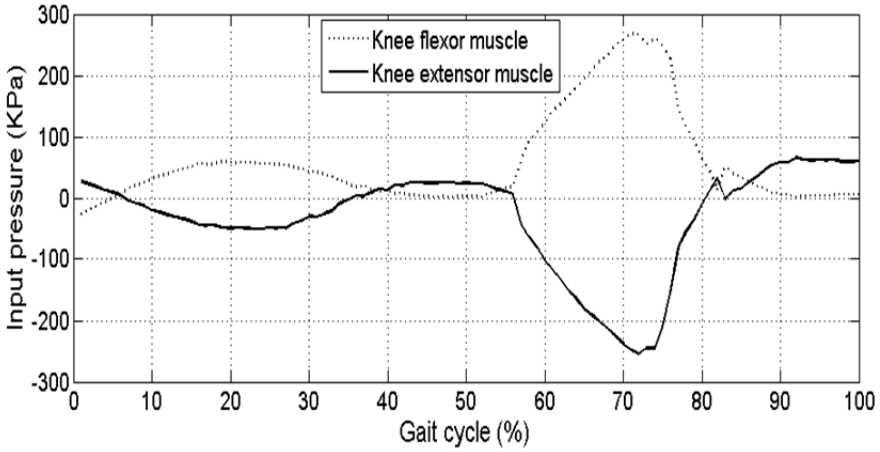

(b)

Figure 4-4. Control effort produced at (a). Hip and (b). Knee sagittal plane joints during tracking performance of Fig. 4-2.

BASMC control were less than 10^{o} (Fig. 4-3). Peak errors at the hip and keen joint occurred during the pre and initial-swing phases that involve the leg raising task (Fig. 4-3). The gravity effect during the swing phase may be a contributing factor to these peak errors. During the pre and initial-swing phase, the magnitudes of hip and knee joint angles also started to increased. The gravity effect started to grow during the pre and initial-swing phases with an increase in the magnitude of hip and knee joint angles. The structured uncertainties in the model of PMA also contributed to the trajectory tracking error and has also been reported in literature previously [129].

Fig. 4-4 shows the control signals Δp_h and Δp_k that produced the tracking performance of Fig. 4-2. The control signals for the hip and knee flexion/extension PMA are presented. Fig.

4-5 shows the hip and knee joint compliance for a gait cycle. As the compliance of the robotic orthosis is a function of joint angles, it increased with an increase in joint ranges of motions. It is important to mention here that the presented results are for the minimum reference compliance (γ_{iMIN}) (eq.3.37) of the robotic orthosis.

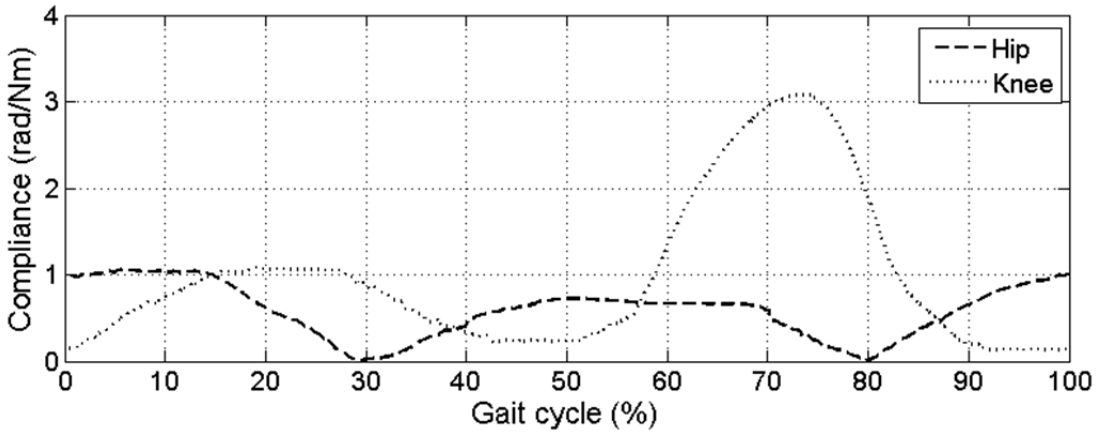

Figure 4-5. Hip and knee joint compliance, averaged over all subjects.

4.5.3. CRVC

The CRVC was designed according to the law given by (4.32) with the robotic orthosis dynamics given by eq.(3.22). The ideal values of *K*, *B* and *F* given in eq.(3.2)-(3.5) were used. For the structured uncertainties in the model of PMA, maximum parameter error of 20% was selected eq.(3.22) for the matrix $[a_h\ a_k]^T$ eq.(3.23) and *H* eq.(3.24). For the CRVC parameters, we used μ_{i1}=5.6, η=0.3 for both joints (found by trial and error) for desired positioning performance. The control frequency was set to 60 Hz, and the data from pressure sensors, as well as the data from joint encoders and reference trajectories, was recorded at the same sampling rate. P_{MAX} was selected to be 550 KPa.

Fig. 4-6 shows the reference and measured hip and knee joint angles of healthy subjects walking in the robotic orthosis during trajectory tracking mode. The joint angle trajectories averaged over all subjects are presented in Fig. 4-6. The representative subject showed the maximum trajectory tracking errors. The tracking performance at hip and knee joints was acceptable as the recorded gait trajectories remained physiological. The passive foot lifter provided sufficient clearance during the swing phase and no cases of foot touching the treadmill were observed during the experiments. The subjects also reported comfortable trunk motions in the vertical and lateral planes.

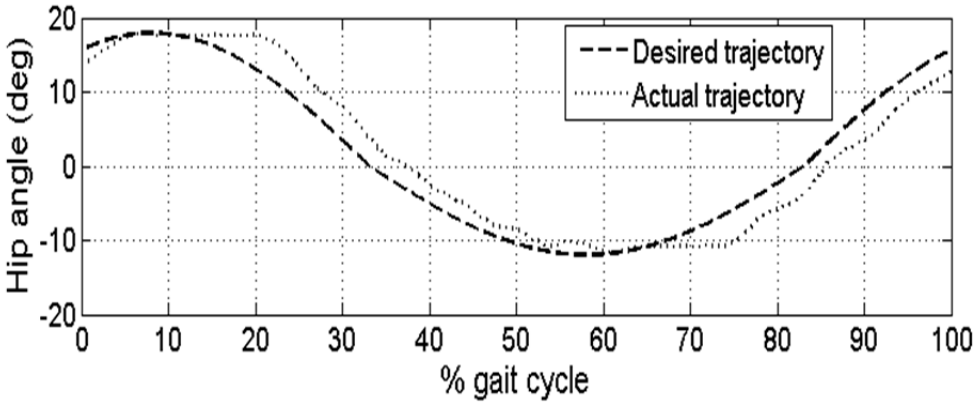

(a)

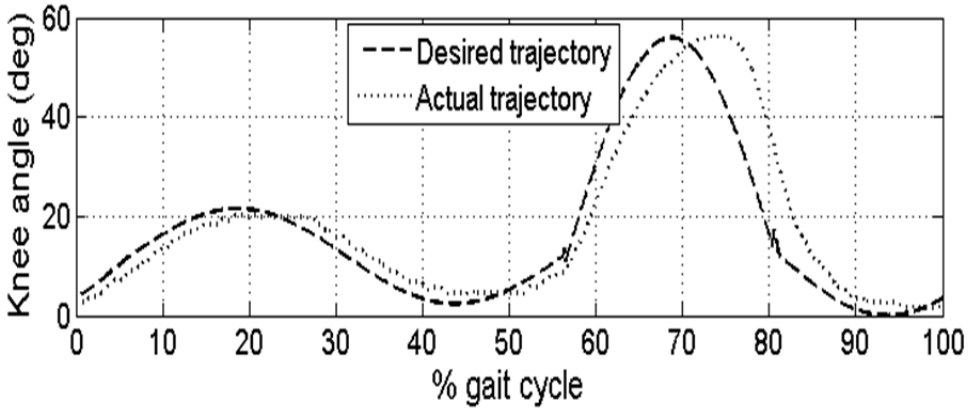

(b)

Figure 4-6. Hip and knee joint angle trajectories with healthy subjects as a percentage of gait cycle obtained during trajectory tracking mode, averaged over all subjects. Normal gait trajectories taken as reference [3] and plotted against the trajectories obtained during walking in the robotic orthosis (a) Hip joint. (b) Knee joint.

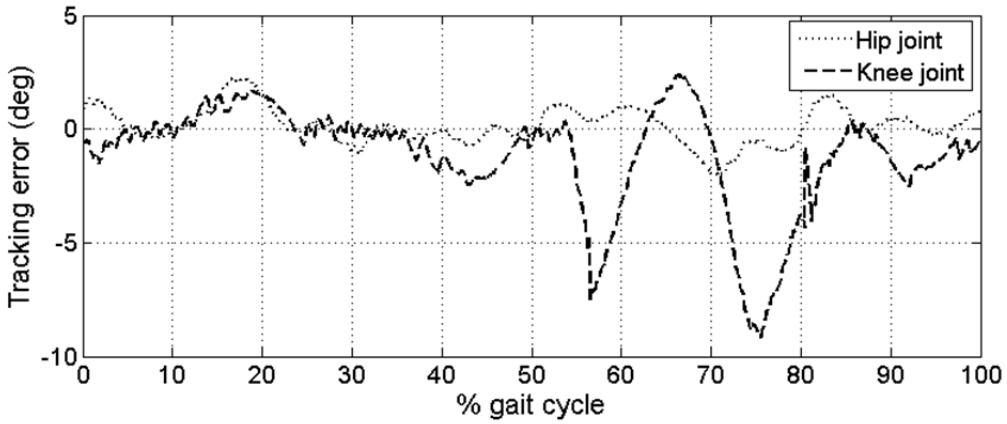

Figure 4-7. Trajectory tracking error at hip and knee joints during the trajectory tracking performance of Fig. 4-6.

The trajectory tracking errors obtained for the complete GC are shown in Fig. 4-7. The maximum trajectory tracking errors at the hip and knee sagittal plane joints during the CRVC

control was less than 10^{o} (Fig. 4-7). Like the BASMC, peak errors during the CRVC law at the hip and knee joint occurred during the pre-swing and swing phases that involve leg raising task (Fig. 4-7). The gravity effect during the swing phase may also be a contributing factor to these peak errors. During the pre-swing and swing phase, the magnitudes of hip and knee joint angles also started to increase. The gravity effect started to grow during the pre and initial-swing phases, with an increase in the magnitude of hip and knee joint angles. The structured uncertainties in the model of PMA also contributed to the trajectory tracking error and has also been reported in literature previously [129].

Fig. 4-8 shows the control signals Δp_h and Δp_k that produced the tracking performance of Fig. 4-6. The control signals for the hip and knee flexion/extension PMA are presented. Fig. 4-9 shows the hip and knee joint compliance for a GC. As the compliance of the robotic orthosis is a function of joint angles, it increased with an increase in joint ranges of motions. It is important to mention here that the presented results are for the minimum reference compliance (γ_{iMIN}) (eq.3.37) of the robotic orthosis.

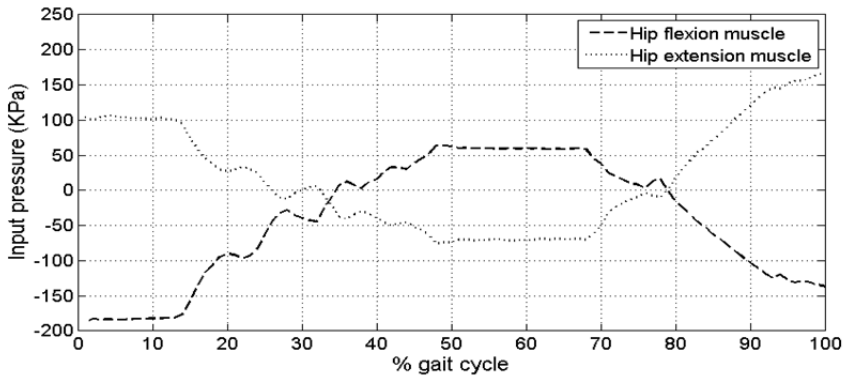

(a)

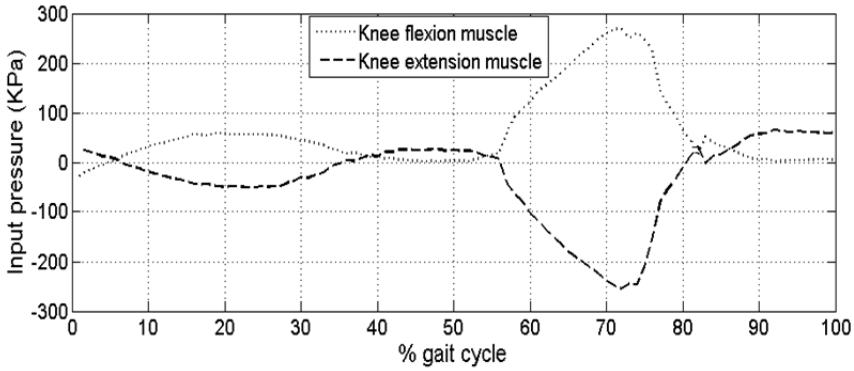

(b)

Figure 4-8. Control effort produced at (a). Hip and (b). Knee joints during tracking performance of 4-6.

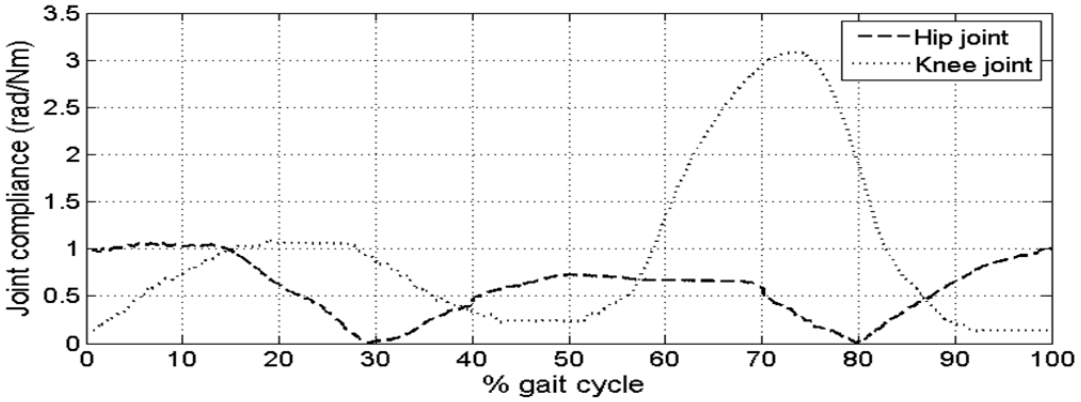

Figure 4-9. Hip and knee joint compliance, averaged over all subjects.

4.6. Conclusions

A trajectory tracking control scheme was developed to guide the subject's limbs on reference physiological trajectories. The proposed control scheme allows the robotic orthosis joint compliance to be controlled independently of the trajectory tracking control. Trajectory tracking controllers based on the BASMC law and CRVC were implemented in joint space for the robotic gait training orthosis. The proposed control scheme was evaluated on three neurologically intact subjects. The reference compliance of the robotic orthosis was selected to be minimum (γ_{iMIN}) (eq.3.37) during the evaluation of trajectory tracking controllers. The compliance levels can be chosen by the physical therapist, based on the level of recovery and rehabilitation stage of the neurologically impaired subjects.

Experimental results illustrate the performance of the robotic orthosis and the trajectory tracking control. It was shown that the BASMC and CRVC laws were successfully able to guide the subjects' limbs on reference physiological gait trajectories in the presence of structured uncertainties in the model of PMA. The maximum trajectory tracking errors obtained both for BASMC and CRVC were less than 10^{o}. This trajectory tracking performance is appropriate because of the fact that PMA have the structured uncertainties in their model and have a highly nonlinear behavior (Chapter 3). This trajectory tracking performance is also in accordance with other gait rehabilitation orthoses, such as LOKOMAT, for which the maximum trajectory tracking errors during trajectory tracking control mode "must be below 15^{o}" [37]. It is important to mention here that the extent of allowable trajectory tracking error during robot assisted gait training is an important and open research question [37, 42] that, still needs to be answered. CRVC carries all the advantages of conventional BASMC and eliminates the chattering effect by utilizing a novel feedback

function that is continuous in time domain. The CRVC control law is smoother than BASMC, eliminating the sliding manifold information using *signum* or *saturation* function. For this reason CRVC was used as a basic trajectory tracking (position) controller for the implementation of impedance (Chapter. 6) and AAN (Chapter. 7) controllers.

The proposed control scheme presents advancement on the current trajectory tracking control schemes of the state-of-the-art robotic gait rehabilitation orthoses [1, 37, 100]. The trajectory tracking control scheme of conventional robotic orthoses [37, 100] works on the basis of an infinite and constant impedance (compliance) value, whereas the proposed control scheme provides variable compliance (Fig. 4-5 and 4-9) during the robot assisted gait training. This variable compliance is beneficial for human-robot interaction applications [88] and would help in absorbing large position errors and would insure safety of the subject. According to the author's best knowledge, no multijoint robotic gait training orthoses powered by PMA has been operated in a trajectory tracking or feedback control configuration prior to this research.

Chapter 5. Modeling Muscle Activation Patterns during Robot Assisted Gait

Gait training is performed to reinstate muscle coordination for motor performance improvement and also to extract information relevant to muscle activation patterns that can be used to improve rehabilitation treatments. The aim of this study was to investigate the muscle activation patterns during robot assisted unimpaired gait using dynamic simulations. A two-dimensional (2-D) musculoskeletal model of human gait, along with existing ground contact force (GCF) model, was used. Also, a 2-D model of a robotic orthosis was developed that provides actuation to the sagittal plane hip, knee and ankle joints to guide the subject's limbs on reference trajectories. A custom inverse dynamics algorithm was developed, along with a quadratic minimization algorithm, to obtain a feasible set of muscle activation patterns. To analyze the sensitivity of the skeletal muscle activation solution vector for changes in joint torques, a perturbation analysis was carried out, and the variations in the muscle activations were found to be of the same order as of the perturbations. The effects of cadence variation on muscle activation patterns during robot assisted unimpaired gait were also studied using dynamic simulations. These dynamic simulations can lead to a better understanding of the biomechanics of gait in a robotic orthosis and provides the foundation for investigating neuromuscular parameters of interest during robot assisted gait.

5.1. Introduction

Neurologic injuries, such as stroke, often result in damage to neuromuscular system and muscle coordination discrepancies [101, 102]. The survivors have lower limb impairment and gait disorders, and are unable to perform activities of daily living. One of the important goals of gait rehabilitation is to re-train muscle coordination and function for motor performance improvement [104]. Robot assisted gait training is an emerging rehabilitation practice, and several robotic orthoses have been developed for BWS treadmill training of neurologically impaired subjects [1].

The robotic orthoses kinematically constrain subject's limbs; therefore, the behaviour of resulting gait dynamics and muscle activation patterns is unclear [105-107]. An enhanced understanding of correlation between muscle coordination abnormalities, gait pattern deviations [108] and torques applied by robotic orthoses could facilitate in customized motor

re-training as well as improvement of robotic gait training strategies. A limited number of studies related to muscle coordination patterns during robot assisted gait training have been reported in literature. Electromyography (EMG) measurements of healthy subjects have been recorded during LOKOMAT [7] assisted treadmill training and compared with those exhibited during normal treadmill walking [105]. Muscle activations of hemiparetic stroke subjects have also been recorded during LOKOMAT assisted gait [107]. Still, the vital question of how the robot assisted gait training affectd muscle coordination patterns, largely remains unanswered. Also, the ankle plantar and dorsiflexor muscle activations during robot assisted gait training have not been studied, as the current robotic gait training orthoses do not provide actuation at ankle joint [7, 39].

Dynamic simulations of human walking provide a useful tool for determining aspects of muscle function and coordination patterns that are difficult or impossible to measure non-invasively [138-140]. Dynamic simulations for specific neurological impairments have been developed to identify abnormalities in muscle function and compared with those of normal gait simulations to infer the causes of deviation from normal gait pattern [141, 142]. Further, these evaluations can help in precisely planning as well as devising better gait rehabilitation treatments. A dynamic simulation of unimpaired gait in a passive ankle foot orthosis has been developed by Charles et al. [143]. However, according to the authors' best knowledge, no extant work on dynamic simulations of robot assisted gait has been reported in literature.

The objective of this study was to investigate muscle activation patterns during robot assisted unimpaired gait. A dynamic simulation of robot assisted gait was produced to estimate the muscle activation patterns. A two dimensional (2-D) musculoskeletal model of human gait was developed along with a 2-D model of robotic orthosis. These models were used along with a custom inverse-dynamics algorithm [107], and a quadratic minimization algorithm [144] to identify muscle activation patterns during robot assisted gait. The information obtained from this simulation is important for proper elucidation of clinical studies involving robotic gait training orthoses.

The contributions of this work include the development of the first dynamic simulation of robot assisted gait. Also, a new static optimization technique [145, 146] was developed that worked on the basis of minimization of norm of the error in the target torques (required torques) and the actual torques.

The chapter begins with the musculoskeletal gait model. This follows with the robotic orthosis model and control. Then, the optimization algorithm used to find the muscle activation patterns is presented. The results of such simulation are presented afterwards. Later in the chapter, the effect of cadence regulation on muscle activation patterns is also studied. The chapter ends with the discussion and conclusion sections.

5.2. Musculoskeletal Gait Model

A 2-D musculoskeletal model was developed for simulation purpose. The body segments included in the model were trunk, thigh, shank, and foot. Trunk was included as a single rigid body to account for the upper extremity inertial parameters. The segments were connected with revolute joints, and the gait was considered as purely sagittal [Fig.5-1 (a)]. The model was developed for a subject 1.78 m tall and weighing 77.9 kg, according to the segment lengths and inertial parameters reported in [120]. The dynamical equation of motion [139] was derived by Newton-Euler Principle and is given by

$$\mathrm{M_1(q)\ddot{q} + C_1(q,\dot{q}) + G_1(q) + R(q)F^M + F(q,\dot{q}) = 0} \tag{5.1}$$

where q, $\dot{q}$ and $\ddot{q}$ are vectors of generalized position, velocity and acceleration, respectively. $M_1(q)$ is the system mass matrix; C_1 is a vector of centrifugal and Coriolis torques and G_1 is the vector of gravitational torques. F^M is a vector of muscle activations; $R(q)$ is the matrix of muscle moment arms, and $F(q,\dot{q})$ is a vector of GCF.

Eight major muscle groups of each leg were selected for simulation purpose in this study [Fig.5-1 (a)]: soleus (SOL), gastrocnemius (GAS), tibialis anterior (TA), hamstrings (HAM), vasti (VAS), gluteus maximus (GLU), uniarticular hip flexors (iliopsoas, IP), and Rectus Femoris (RF). The muscle attachment parameters were determined according to anatomical data reported in [120]. All the muscles were modeled as mass-less wires. The ground contact (GCF) was modeled as nonlinear visco-elastic spring damper arrangement [Fig. 5-1 (b)]. The spring damper arrangement was positioned vertically at the heel and toe of each foot [147] and was characterized according to the relation

$$\mathrm{F_z = cz^3(1 - b\dot{z})} \tag{5.2}$$

where z and $\dot{z}$ was the vertical deformation and rate of vertical deformation of heel and toe, respectively. The values of c and b were 0.25×10^9 N/m^3 and 1.0 s/m, respectively.

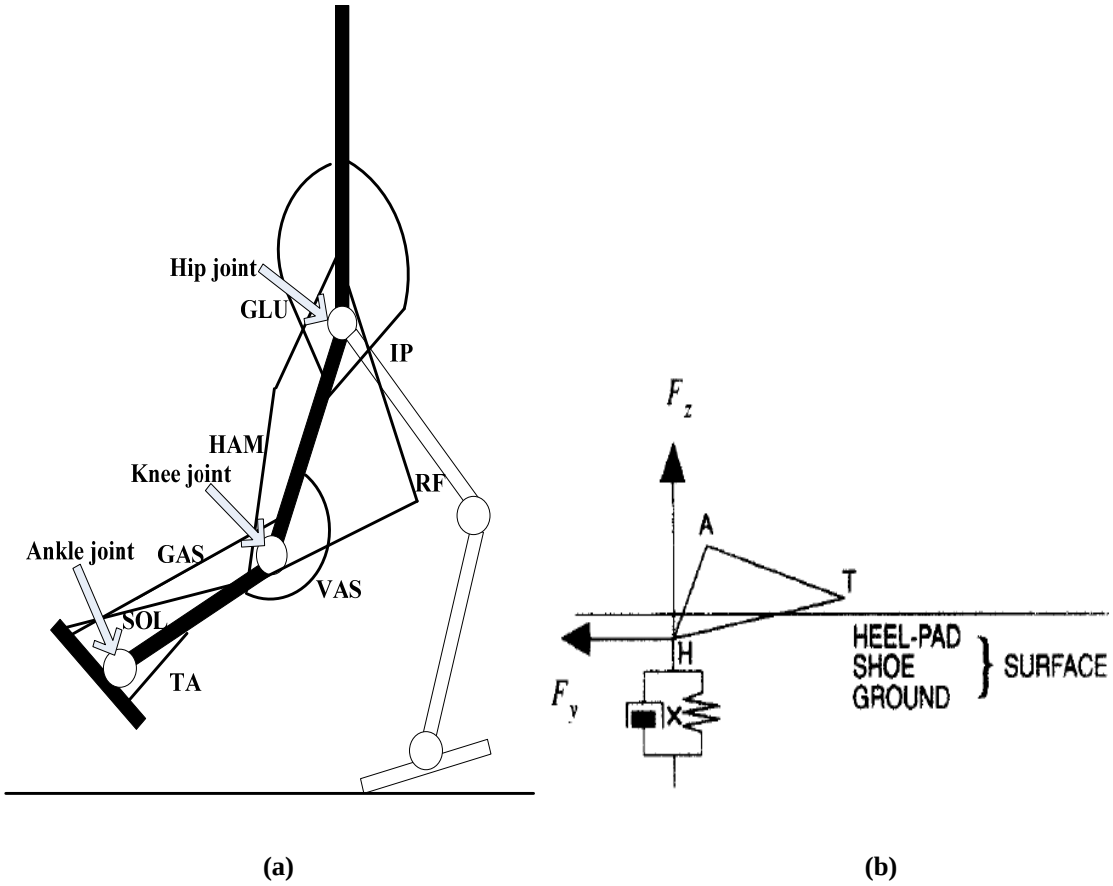

Figure 5-1. (a) Major muscle groups used in the musculoskeletal model. (b) Ground contact force model. Adapted from [113].

5.3. Robotic Orthosis Model and Control

The purpose of a robotic orthosis is to guide subject's limbs on reference trajectories. Each leg of the robotic orthosis weighing 9.8 kg was modeled as a double pendulum with an additional shoe section [Fig. 5-2]. The robotic orthosis have revolute joints at hip, knee and ankle to provide motion in sagittal plane. The orthosis joints were modeled to be in perfect alignment with musculoskeletal model joints. The dynamics of robotic orthosis is given by

$$\mathrm{M_2(q)\ddot{q} + C_2(q,\dot{q}) + G_2(q) = T_{rob}} \tag{5.3}$$

where $M_2\ (q)$ is the orthosis mass matrix, C_2 is a vector of orthosis centrifugal and Coriolis torques; G_2 is a vector of orthosis gravitational torques. $\mathrm{T_{rob}}$ is the vector of torque applied by robotic orthosis. The orthosis joint friction torques was not modeled.

The mass matrices, centrifugal, Coriolis and gravitational torques from musculoskeletal and orthosis model (eq. (5.1) and (5.3)) were combined to form an integrated dynamic model of the system and is represented by

$$M(q)\ddot{q} + C(q,\dot{q}) + G(q) + F(q,\dot{q}) - T_{rob} = R(q)F^{M} = T_{j} \quad (5.4)$$

where *M*, *C* and *G* are the combined terms for robotic orthosis and subject. The maximum joint ranges of motion were kept under anatomical constraints by the orthosis torques. T_j is the human joint torque vector. The robotic orthosis torques at hip, knee and ankle joint was produced by the antagonistic actuation of PMA [Fig. 5-2]. For the purpose of this study, a three element dynamic model of PMA developed by Reynolds *et al.* in [126] was used, (Chapter 3) and is given by

$$M_i\ddot{x} + B(P)\dot{x} + K(P)x = F_{ce}(P) - Mg \quad (5.5)$$

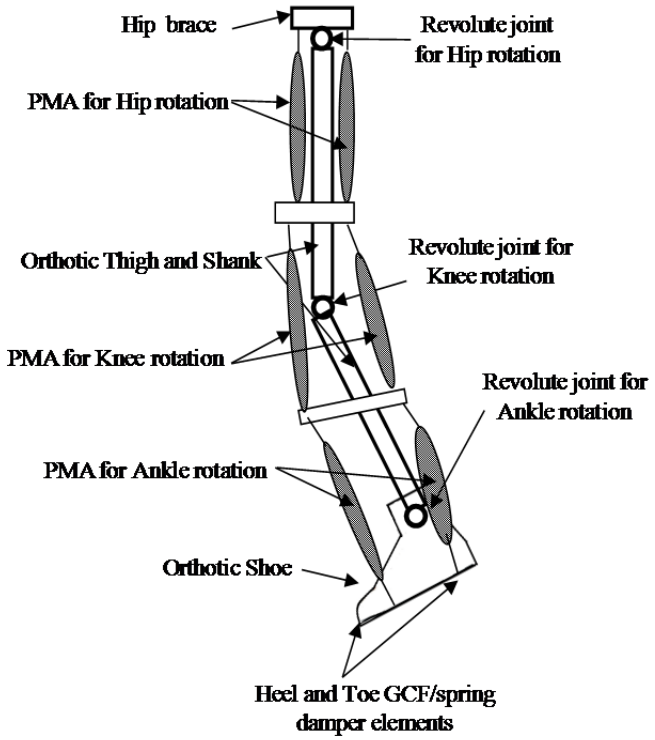

Figure 5-2. Robotic orthosis leg model to guide subject's limbs on reference trajectories (side view).

where *x,* $\dot{x}$, $\ddot{x}$, is the amount of PMA contraction, contraction velocity, and acceleration, respectively. F_{ce} is the effective force provided by the contractile element, *K* and *B* are spring and damping coefficients, respectively. All these coefficients are functions of pressure (*P*). M_i is the inertial load and Mg is the load due to the weight of the system. Readers are guided to [126] for the further details of the three element model of PMA.

To guide the subject's limbs on reference trajectories, a trajectory tracking controller was implemented. Reference joint angle trajectories for natural cadence (105±6 steps/min) reported by Winter in [3], were used. An error was measured between the reference trajectory $\mathrm{q_{ref}}$, and the measured trajectory q. The reference trajectory and the measured trajectory were numerically differentiated to find joint velocities. The CRVC controller (Chapter 4) generates the torque necessary ($\mathrm{T_{rob}}$) to guide the subject's limbs on these reference trajectories. The controller was implemented in joint space

The kinematic parameters were combined with all the forces and torques acting on the subject as shown in eq.(5.4) into a custom inverse dynamic model. This model was used to calculate the joint torques that the subject was generating during the gait cycle, as well as the torques induced by the robotic orthosis on the subject's joints. This method has also been used for LOKOMAT in [107].

5.4. Optimization

Joint motions in the human body are achieved by the antagonistic activation of group of skeletal muscles. Fundamentally, to actuate a joint, coordinated action of tension and compression activations in the muscles is required. However the skeletal muscles are flexible and cannot provide compressive forces. Owing to this limitation, joint motions with requisite torques are required to be realized by the application of positive activation vector. Interestingly, our musculoskeletal system has a redundant number of muscles acting at the joints, and hence the null space solution of the muscle activations gets extra degrees of freedom that could be used efficiently to get tension or positive muscle activations [98]. Due to redundant actuation, it is possible to obtain vectors of muscle activations comprising only tension forces for requisite joint torques. Therefore, the objective of the present optimization is to find a unique positive muscle activation vector from the redundant solution space.

In previous research mentioned in the literature, it has been hypothesized that the skeletal muscles follow the optimality principle that further means the muscles are activated in a manner so that minimum energy is consumed [98, 146]. Consequently, in most of the earlier works, the norm of muscle stresses/activations has been minimized under the constraints that the activations so obtained are able to provide required torque and lie within given bounds [98]. Nevertheless, in the present work, a different approach was carried out wherein norm of the error in the target torques (actual torques) and the torques obtained from our optimized

activation solution has been minimized. Quadratic minimization algorithm was used to optimize muscle activations while constraining it between two bounds [144]. Since the muscle activation vector was required to be positive, the lower bound was kept at zero. Upper bound values of the muscle activations (f_{max}), on the other hand, were proportional to the physiological cross-sectional area (PCSA) and were calculated separately for individual muscle using eq.(5.15). The formulation and methodology of the optimization problem is discussed below.

Sagittal motion of hip, knee and ankle joints individually has a single degree of freedom, realized by eight skeletal muscles. The resulting Jacobian matrices of these joints, which map the joint motions to the activations, were all non-square matrices. The extra degrees of freedom in the null space of Jacobian matrices can be utilised to obtain non-zero muscle activations. To begin with, all possible solutions for muscle activations (F_a^M), producing a particular joint moment, were obtained using eq.5.7, which is an underdetermined system.

$$T_j = J^T F_a^M \tag{5.6}$$

$$F_a^M = \bar{J} T_j \tag{5.7}$$

where $\bar{J} = J(J^T J)^{-1}$ is the pseudo inverse of J^T, which is given below using singular value decomposition

$$J^T = U\Sigma \begin{bmatrix} V_1^T \\ V_0^T \end{bmatrix} \tag{5.8}$$

Next, at each point of the desired trajectory of the joint motion, the quadratic minimization algorithm was used to obtain a unique activation vector as explained below:

Without loss of generality, the torque provided by the optimized unique muscle activation vector (F_c^M) can be written as eq. (5.9). In eq. 5.11-5.14, V_1 and U are matrices containing the input and output basis vectors corresponding to non zero singular values of J^T. Comparing eq.(5.6) with eq.(5.9) produced (eq.(5.10) and eq.(5.11)) where V_0 is the null vector of J^T. Additionally, η and ε are vectors specifying the components of ΔF along the column vectors of V_1 and V_0, respectively.

$$T_i = R \times F_c^M \tag{5.9}$$

$$\text{where} \quad F_c^M = \begin{bmatrix} n_1 f_1 \\ n_2 f_2 \\ n_3 f_3 \\ | \\ n_i f_i \end{bmatrix}$$

$$\Delta T = T_j - T_i \tag{5.10}$$

$$\Delta F = F_a^M - F_c^M = V_1 \eta + V_0 \varepsilon \tag{5.11}$$

The relationship between eq.(5.10) and eq.(5.11) can be written as:

$$\Delta T = J^T \Delta F \tag{5.12}$$

$$\Delta T = U\Sigma \begin{bmatrix} V_1^T \\ V_0^T \end{bmatrix} [V_1 \; V_0] \begin{bmatrix} \eta \\ \varepsilon \end{bmatrix} \tag{5.13}$$

$$\Delta T = U[\text{diag}(\sigma_1, \sigma_2, \sigma_3)]\eta \tag{5.14}$$

Using singular value decomposition ΔT can be factorized in three vectors, wherein Σ is a diagonal vector of singular values expressed as $\sigma_1, \sigma_2, \sigma_3$. From the above analysis, following objective function, describing the norm of error in moments, can be deduced.

$$\text{Minimize} \qquad \Delta T^T \Delta T = \eta^T [\text{diag}(\sigma_1^2, \sigma_2^2, \sigma_3^2)]\eta$$

$$\text{Subjected to} \qquad 0 \leq F^M \leq f_{max}$$

$$\Rightarrow 0 \leq \left[\bar{J} T_j + \varepsilon V_0 + V_1 \eta \right] \leq f_{max}$$

$$\text{where} \qquad f_{max} = a.\, n_i \tag{5.15}$$

F^M is the vector of muscle activations $(f_1, f_2, \ldots, f_i)$, wherein multipliers $n_1, n_2, \ldots, n_i$ were used to account for the muscle PCSA. It was assumed that the muscle endurance is proportional to its PCSA [145]. The muscle PCSA reported by Friederich *et al.* were used in the present work [148], where a is a constant of proportionality and is given by,$a = 0.7 \times 10^6 \; N/m^2$ according to [145].

Subsequently, a perturbation analysis was carried out to analyze the sensitivity of the skeletal muscle activation solution vector for changes in joint torques. In this analysis, 200 perturbations ranging between -5% and +5% (magnitude of joint torque values), were applied

to the hip joint torque, and their effect on the optimization approach, providing the muscle activation vector, was observed and analyzed.

5.4.1. Simulation

Dynamic simulations of robot assisted gait were performed. The lower extremity joint angles, joint torques, GCF, and muscle activation patterns were monitored during the simulation. In total 300 simulation cycles were performed and the results after the 299^{th} simulation cycle was selected for analysis purposes. The first 298 cycles were not selected in order to allow some time for the static optimization routine.

Initial conditions of the simulation had the model in quite standing posture. Initial step was performed by the right foot. The duration of the simulation was set to complete eight gait cycles (GC). The first step from initial standing posture was eliminated, and the remaining seven GC were utilized for analysis purpose. All the simulations were performed by implementing appropriate models in Matlab- Simulink R2009b, using fourth-order Runge-Kutta algorithm (The MathWorks, Inc: Natick, Ma, USA). The frame rate of simulation was set at 100 Hz. Data from the right GC was formatted for presentation purpose.

5.5. Results

5.5.1. Kinematics

The tracked sagittal plane joint angle trajectories (θ) for hip, knee and ankle at three different cadences as a percentage of GC are shown in Fig. 5-3. The robotic orthosis generated appropriate joint torques to guide the subject's limbs on the reference trajectories. A CRVC controller was selected to minimize the deviations from desired trajectory by developing corrective torques. The maximum hip joint angle was 22^{o} and occurred during the terminal swing phase. For the knee joint, the maximum angle was 65^{o} and occurred during the initial swing phase. For the ankle joint, the maximum plantar flexion angle was 19^{o} and occurred during initial swing phase. The maximum trajectory tracking error for hip, knee and ankle joint was always within $\pm 4^{o}$ across the GC.

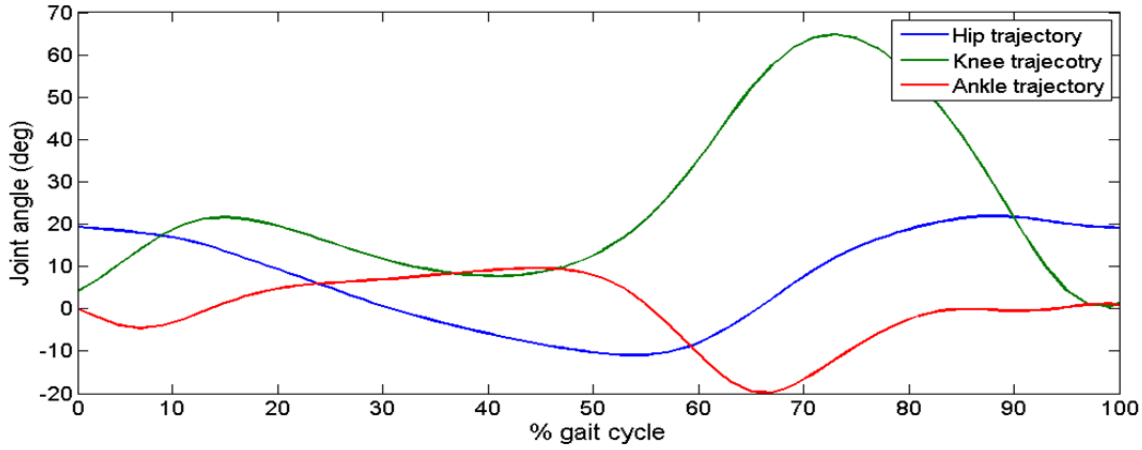

Figure 5-3. Sagittal plane joint angle trajectories obtained for hip, knee and ankle for a GC. A positive value indicates flexion and a negative value indicates extension at the hip and knee joints. A positive value indicates dorsiflexion and a negative value indicates plantarflexion at the ankle joint.

5.5.2. Kinetics

The vertical GCF normalized to the total mass of the system is shown in Fig. 5-4. The GCF model did not produce the familiar double hump pattern, although the weight-acceptance hump is more pronounced compared to the second hump. This may had happened due to the external push-off provided by the robotic orthosis.

The sagittal plane hip, knee and ankle joint torques in terms of % GC is shown in Fig.5-5 (a). The peak hip extension torque was during the pre-swing phase, which subsequently increased to the peak flexion torque during the terminal swing. For the knee joint, the peak

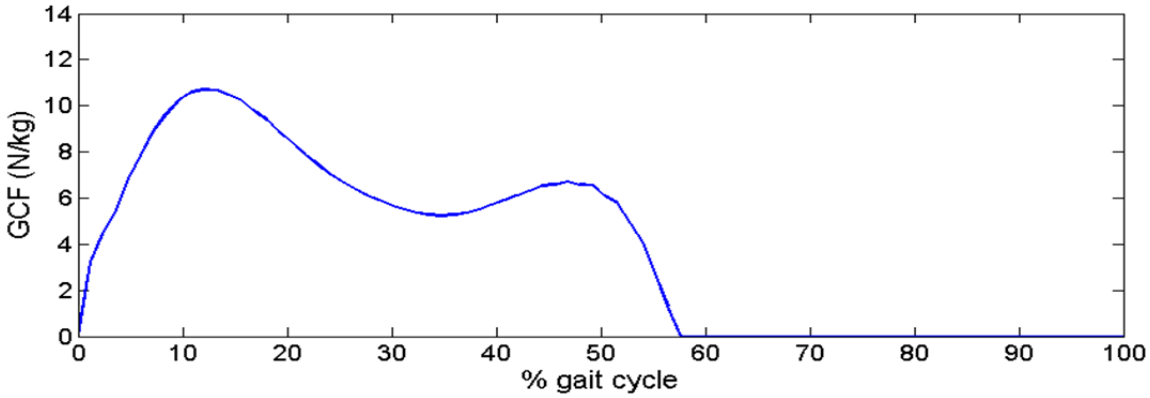

Figure 5-4. Ground contact force (GCF) normalized to system mass for a GC.

flexion toque was observed during the loading phase. For the ankle joint, the peak dorsiflexion torque was during the pre-swing phase.

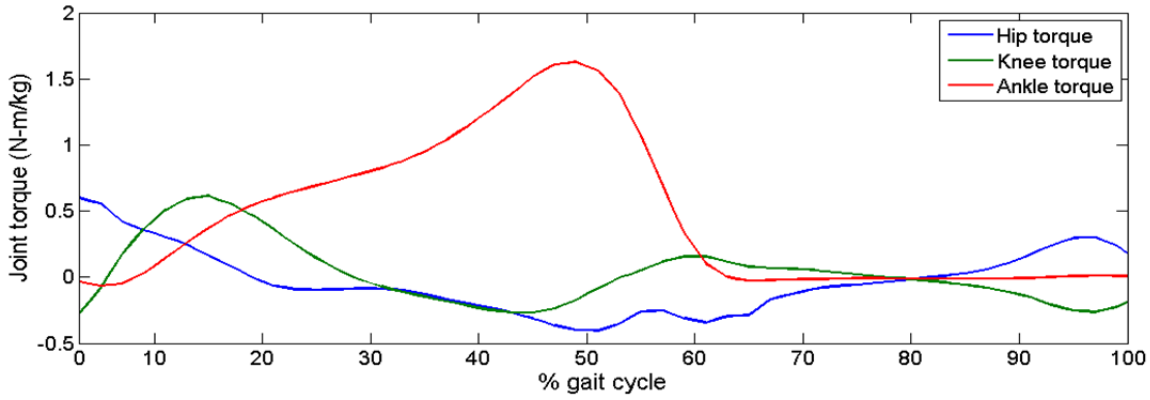

(a)

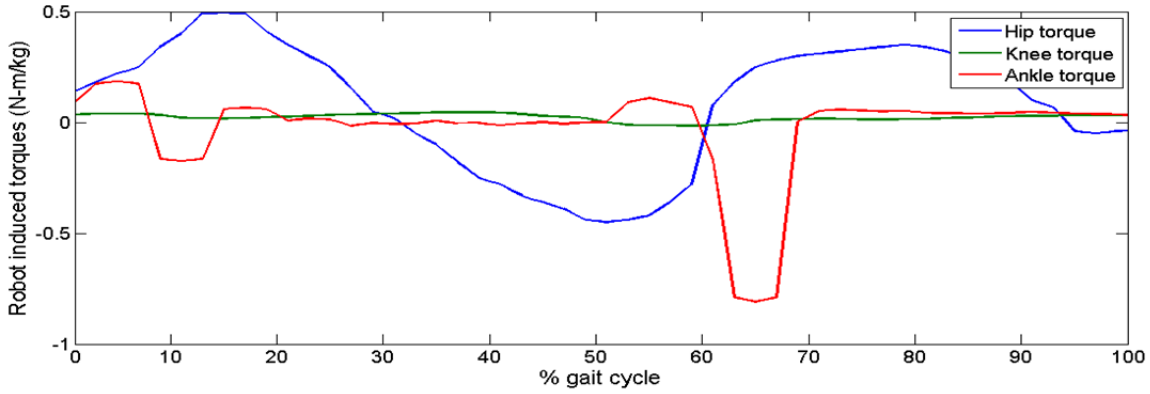

(b)

Figure 5-5. (a) Torques at human hip, knee and ankle sagittal plane joints for a GC. (b) Torques induced by the robotic orthosis at sagittal plane hip, knee and ankle joint. A positive value indicates extension and a negative value indicates flexion at the hip and knee joints. A positive value indicates plantarflexion and a negative value indicates dorsiflexion at ankle joint.

5.5.3. Robot induced torques

Torques induced by robotic orthosis at hip, knee and ankle sagittal plane joints in terms of % GC is illustrated in Fig. 5-5(b). At the hip joint, the robotic orthosis induced an extension torque at the heel strike, which peaked during loading phase and returned to zero by the end of mid stance. From mid to late stance phase, the robotic orthosis induced a flexion torque at the hip joint, which is followed by another extension torque peak through swing. At the knee joint, the robotic orthosis induced low levels of torque throughout the gait cycle. At the ankle joint, the robotic orthosis induced low level of plantarflexion torques at heel strike, which returned to zero by the mid loading phase and is followed by a dorsiflexion torque at the end of loading phase. The robotic orthosis also applied a dorsiflexion torque during the initial swing phase.

5.5.4. Muscle activation patterns

Muscle activation patterns during robot assisted gait versus % GC are illustrated in Fig. 5-6. These optimized muscle activations reproduced the joint torques. Hip, knee and ankle torques were reproduced with an RMS error of the order of 10^{-32} N-m. HAM showed an activity during the initial stance phase and during the terminal swing phase. RF activity peaked during the terminal stance phase and at the start of swing phase. GLU showed similar activation pattern as of HAM, although the magnitude of GLU activation pattern is slightly higher than the HAM activation patterns. IP showed peak activations at the end of mid stance phase and during the initial swing phase. GAS activity also peaked during the terminal stance and pre swing phase. SOL had the similar activation pattern as GAS, but with a higher peak magnitude. VAS activity also peaked during the mid stance phase and was silent during the rest of the GC. TA showed peak activity during the loading phase and was silent during the rest of swing phase. TA also showed activity during most of the swing phase.

The results of perturbation analysis are illustrated in [Fig. 5-7 (a,b)]. Muscle activations obtained by inducing perturbation in the joint torques [Fig. 5-7(a)] are displayed. Apparently, variations in the muscle activations [Fig. 5-7(b)] were of the same order as the perturbations. Further, as the perturbed activation values changed around the nominal activation values, the optimization method was robust against perturbations in the joint torque values. Another important inference drawn from these illustrations was that, since there were no extreme variations observed in the perturbed activation vector, the optimization method was able to provide a unique solution of muscle activations for given joint torques.

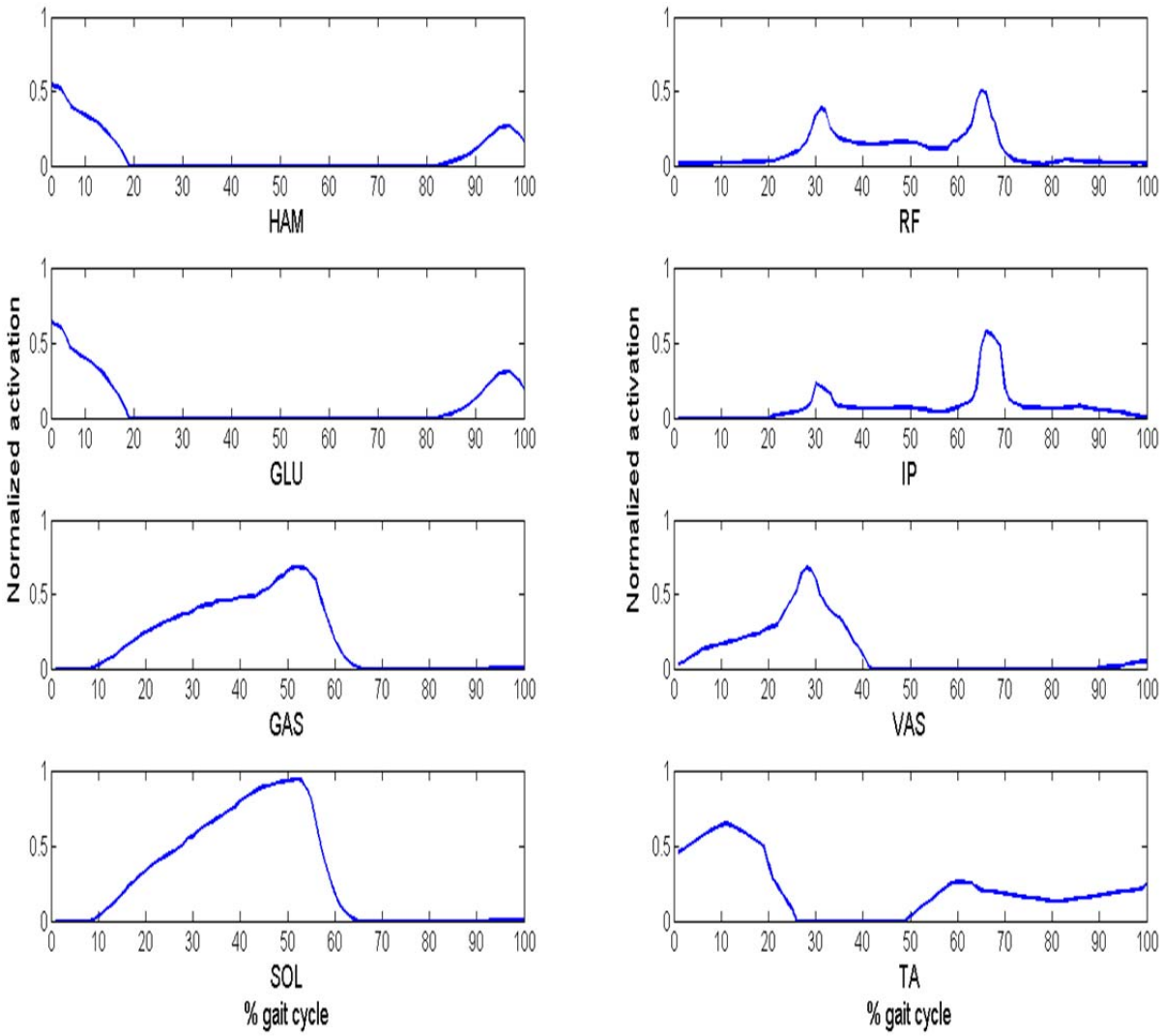

Figure 5-6. Predicted muscle activations during robot assisted gait for a GC. Abbreviations: Hamstrings (HAM), rectus femoris (RF), gluteus maximus (GLU), uniarticular hip flexors (iliopsoas, IP), gastrocnemius (GAS), vasti (VAS), soleus (SOL) and tibialis anterior (TA).

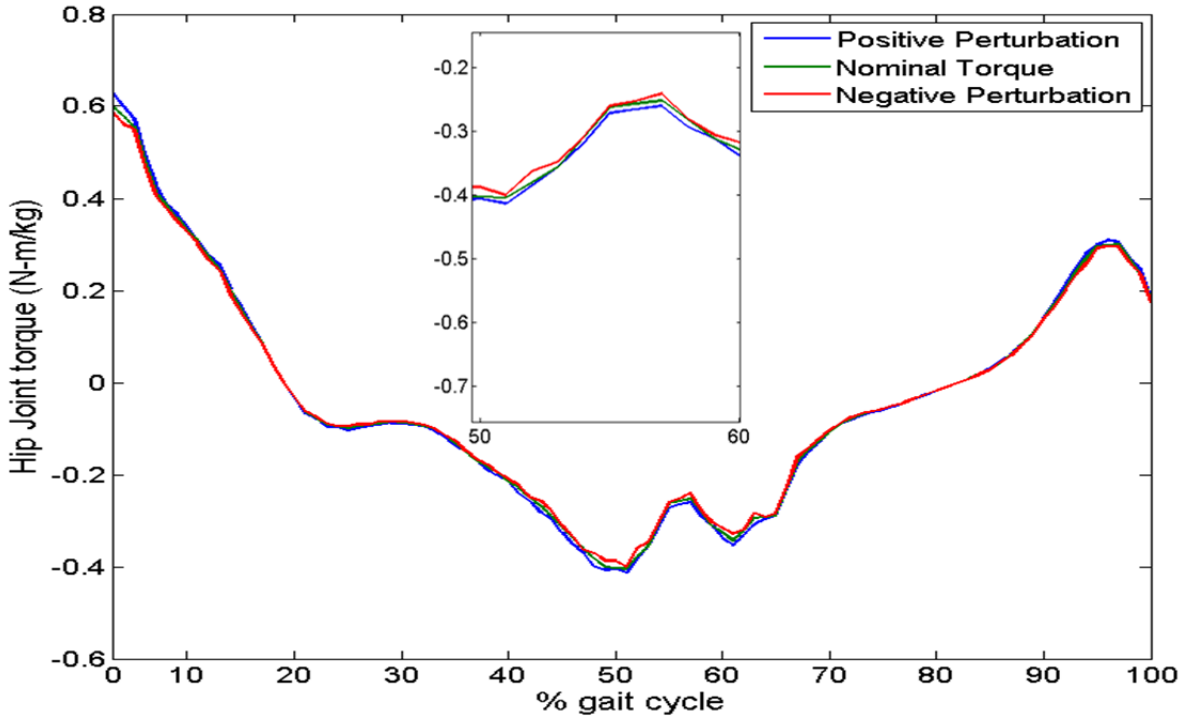

(a)

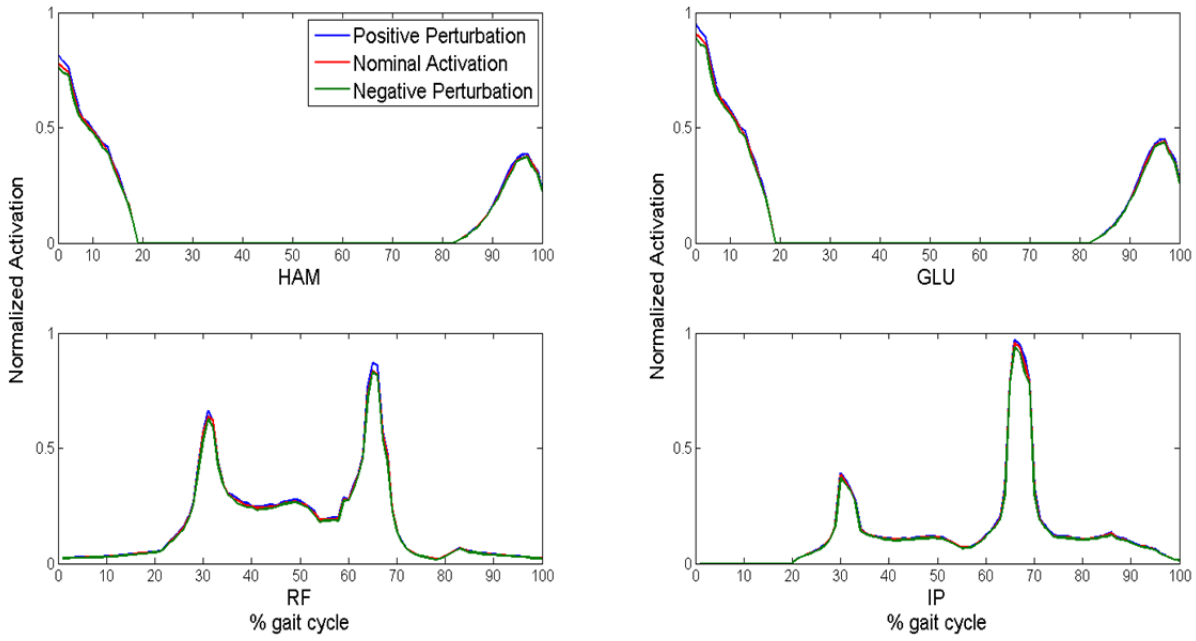

(b)

Figure 5-7. (a) Perturbation torques at hip joint. Blue and red curves show a +5% and -5% perturbation, respectively. A small window shows the perturbation torques during 50-60% of gait cycle (b) Hip joint muscle activations produced in response to the perturbations.

5.6. Effect of Cadence Regulation on Muscle Activation Patterns

Variation of cadence also influences muscle coordination and the muscle activity generally increases with an increase in cadence [149-151]. Unfortunately, a limited number of studies analyzing the effects of cadence regulation on muscle activation patterns during robot assisted gait have been reported in literature. Electromyography (EMG) activity of healthy subjects has been recorded with no BWS during LOKOMAT assisted treadmill training at different gait speeds. No significant statistical difference in the magnitude of EMG has been reported for these variable speeds [105]. On the other hand, a similar study has been conducted with the LOKOMAT at different stride frequencies with variable BWS, which presents significant variance in the magnitude of EMG activity [106]. Apparently, the question of how the robot assisted gait training at different cadence affect muscle activations still remains largely unanswered. As has been stated earlier that cadence regulation is important with regards to gait rehabilitation process, the present study is an attempt to investigate the effects of cadence regulation on muscle activation patterns during robot assisted gait training.

Dynamic simulation of human gait is a useful tool for determining aspects of muscle functions and coordination patterns that are otherwise difficult or impossible to measure non-invasively [142, 146, 152-154]. Dynamic simulations have been developed to analyze the effects of cadence regulation on muscle activations during unassisted normal and impaired gait [151, 155, 156]. However, results from dynamical simulations of robot assisted gait at variable cadence would be more appropriate in devising better robotic gait rehabilitation protocols. Unfortunately, to the best knowledge of authors, no extant work on such studies is available in the literature and the proposed work is a step towards addressing this research question.

Therefore, the objective of this study was to investigate the effects of cadence regulation on muscle activation patterns during robot assisted unimpaired gait. A dynamic simulation of robot assisted gait was produced to evaluate the muscle activation patterns at slow, natural and fast cadence. A 2-D musculoskeletal model of human gait was developed along with a 2-D model of robotic orthosis. These models were used along with a custom inverse-dynamics algorithm [107, 157] and a quadratic minimization algorithm [144] to identify muscle activation patterns at variable cadence, during robot assisted gait. The information obtained from this simulation is important for proper elucidation of clinical studies involving robotic

gait training orthoses, and to develop a better understanding of the effects of cadence regulation on muscle function.

5.6.1. Simulation

Dynamic simulations of robot assisted gait at variable cadence were performed. The lower extremity sagittal plane joint angles, joint torques, GCF and muscle activation patterns were monitored during the simulations.

Initial conditions of the simulation had the model in quite standing posture. Initial step was performed by the right foot. The duration of the simulation was set to complete eight gait cycles (GC). The first step from initial standing posture was eliminated and the remaining seven GC were utilized for analysis purpose. All the simulations were performed by implementing appropriate models in Matlab- Simulink R2009b, using fourth-order Runge-Kutta algorithm (The MathWorks, Inc: Natick, Ma, USA). The frame rate of simulation was set at 100 Hz. Data from the right GC was formatted for presentation purpose.

5.6.2. Results

5.6.2.1. Kinematics

The tracked sagittal plane joint angle trajectories (θ) for hip, knee and ankle at three different cadences as a percentage of GC are shown in Fig. 5-8 (a), (b) and (c), respectively with mean values found in Table 5-1. The robotic orthosis generated appropriate joint torques to guide the subject's limbs on the reference trajectories. A CRVC controller was selected to minimize the deviations from desired trajectory by developing corrective torques. The maximum hip joint angles during slow, natural, and fast cadence were 19^o, 22^o and 21^o, respectively and occurred during the terminal swing phase (88% GC) [Fig. 5-8(a)]. For the knee joint, the maximum angles for slow, natural and fast cadence were 63^o, 65^o and 67^o, respectively and occurred during the initial swing phase (72% GC) [Fig. 5-8(b)]. For the ankle joint, the maximum plantar flexion during slow, natural and fast cadence was 18^o, 19^o and 20^o, respectively and occurred during initial swing phase (66 % GC) [Fig. 5-8(c)]. The maximum trajectory tracking error for hip, knee and ankle joint at all three cadences was always within $\pm 4^o$ across the GC.

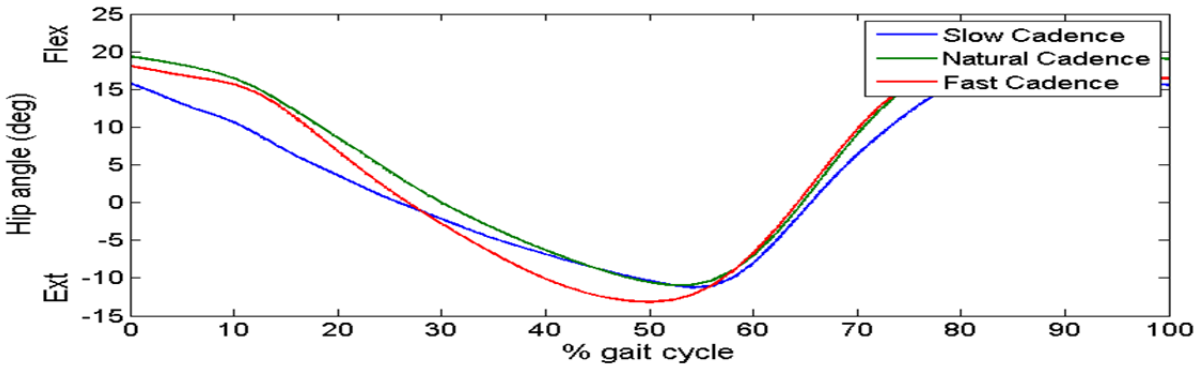

(a)

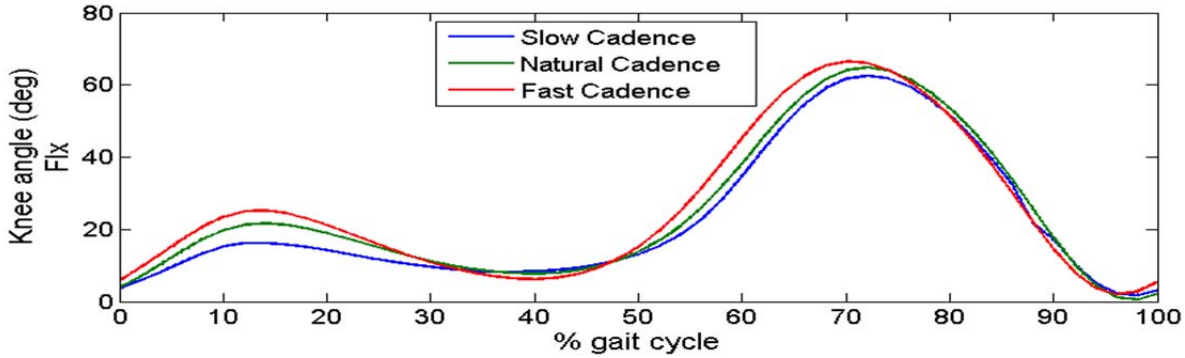

(b)

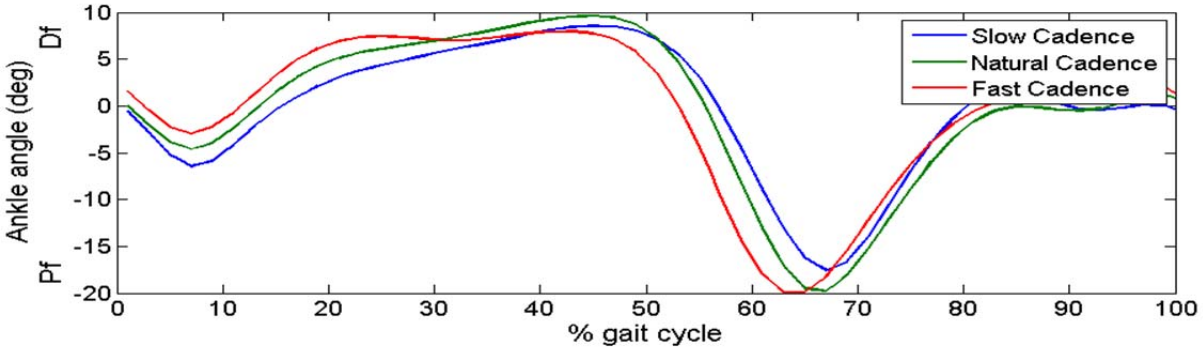

(c)

Figure 5-8. Joint angles of the subject with respect to % GC during slow, natural and fast cadence. (a) Hip angles (deg). (b) Knee angles (deg). (c) Ankle angles (deg). Flx: Flexion, Ext: Extension, Pf: Plantar flexion, Df: Dorsiflexion.

5.6.2.2. Kinetics

The vertical GCF normalized to the total mass of the system is shown in Fig. 5-9. The GCF model did not produce the familiar double hump pattern although the weight-acceptance hump is more pronounced compared to the second hump. This may had happened due to the

external push-off provided by the robotic orthosis. The magnitude of GCF increased with the increase of cadence (Table 5-1), while the weight acceptance hump appeared approximately at the same time for all three cadences.

The sagittal plane limb joint torques for slow, natural, and fast cadence in terms of % GC is shown in Fig.5-10. (a-c) with mean absolute values provided in Table 5-1. For all three cadences, hip joint torques follow quite similar pattern throughout the GC, with an increase in magnitude with increasing cadence. Although the increase in hip joint torque from slow to natural cadence was small, the increase in joint torque at fast cadence torque was more significant, particularly, during the terminal stance and pre-swing phases (40-60% GC) [Fig. 5-10(a)]. For the knee joint, the torque patterns were quite similar throughout the GC at all three cadences, with an increase in magnitude from slow to fast cadence. The most significant difference in knee joint torques at three cadences was during the loading and mid-stance phases (5-20% GC), during which the torque magnitude at fast cadence doubles compared to the torque at natural cadence [Fig. 5-10(b)]. There was no considerable difference in magnitude of the knee joint torques during swing phase at all three cadences. The ankle joint torques follow a similar pattern during the complete GC at three cadences [Fig. 5-10(c)]. The observable difference in magnitude of ankle joint torques at three cadences was during the terminal-stance and pre-swing phases. During the terminal stance phase, the magnitude of the ankle joint torques at slow and natural cadence was greater compared to fast cadence. During the pre-swing phase, the magnitude of ankle joint torque becomes greater at fast cadence as compared to slow and natural cadence. There was no observable difference in the magnitude of ankle joint torques during the swing phase at all three cadences.

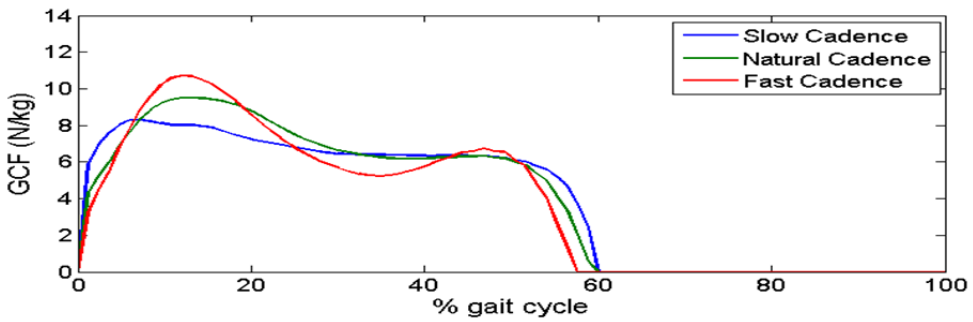

Figure 5-9. Vertical ground contact force (GCF) normalized to system mass for slow, natural and fast cadence with respect to % GC.

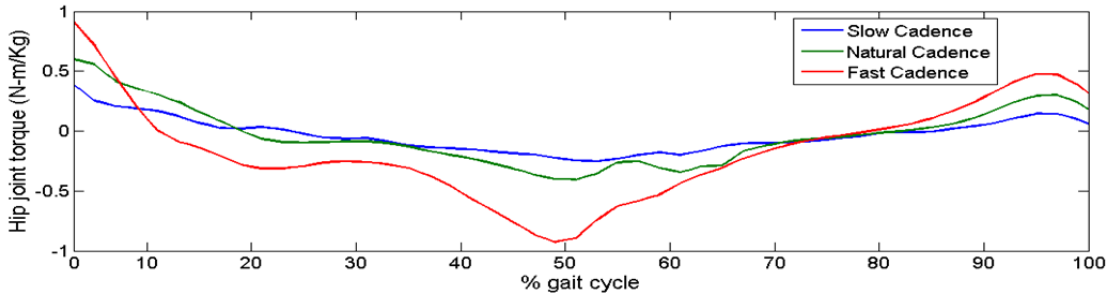

(a)

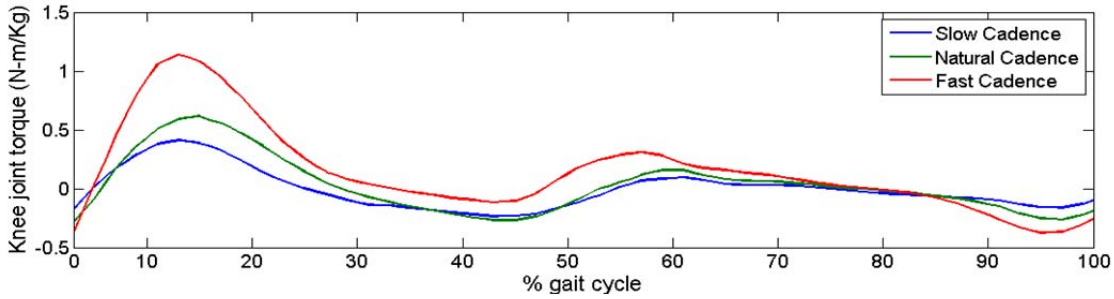

(b)

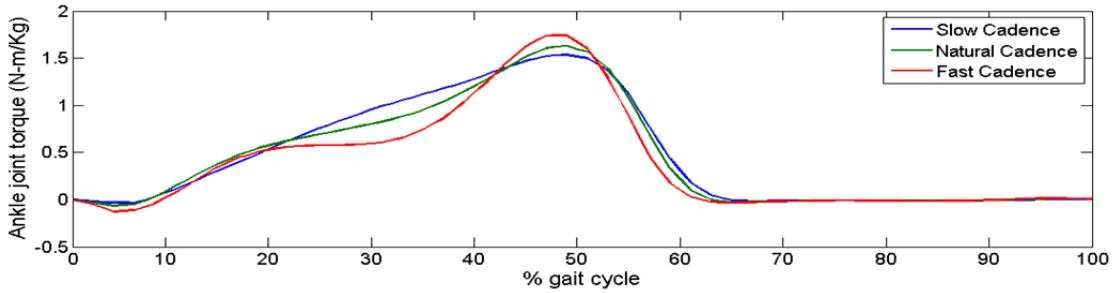

(c)

Figure 5-10. Torques (N-m/kg) during slow, natural and fast cadence at. (a) Hip joint. (b) Knee joint. (c) Ankle joint.

5.6.2.3. Robot induced torques

The torques induced by the robotic orthosis at the sagittal plane hip, knee, and ankle joints of the subject at three cadences throughout the gait cycle are shown in Fig. 5-11 (a-c). At the hip joint, the robotic orthosis induced torque has the same patterns at all three cadences, but higher magnitude torques at slow and natural cadence were induced compared to fast cadence during the loading and initial swing phases [Fig. 5-11(a)]. The magnitude of induced hip torques at slow, natural, and fast cadence was quite similar during the rest of stance, initial, and terminal swing phases. At the knee sagittal plane joint, the robot orthosis

induced torques also followed the same pattern at all three cadences [Fig. 5-11(b)]. The magnitude of torque induced at the knee joint increased during loading and terminal swing phases at slow and natural cadence

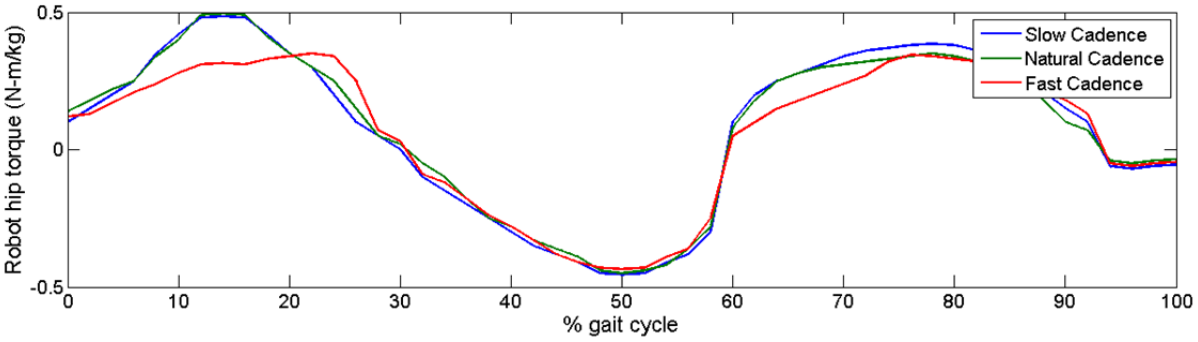

(a)

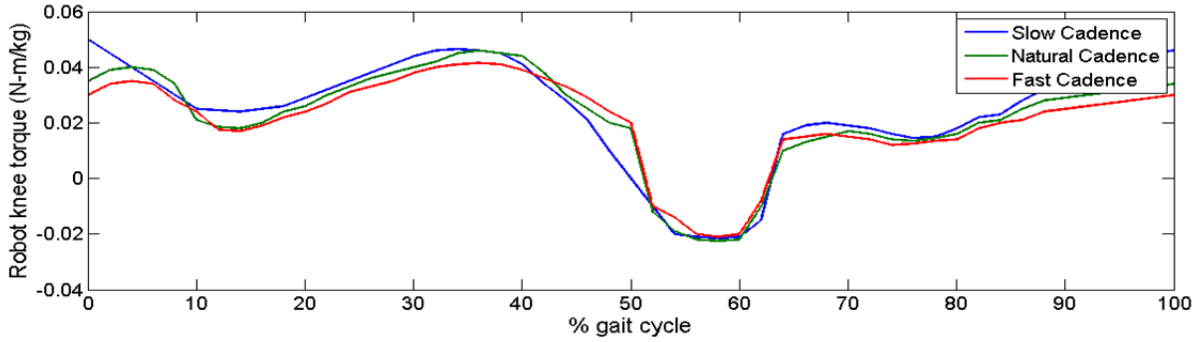

(b)

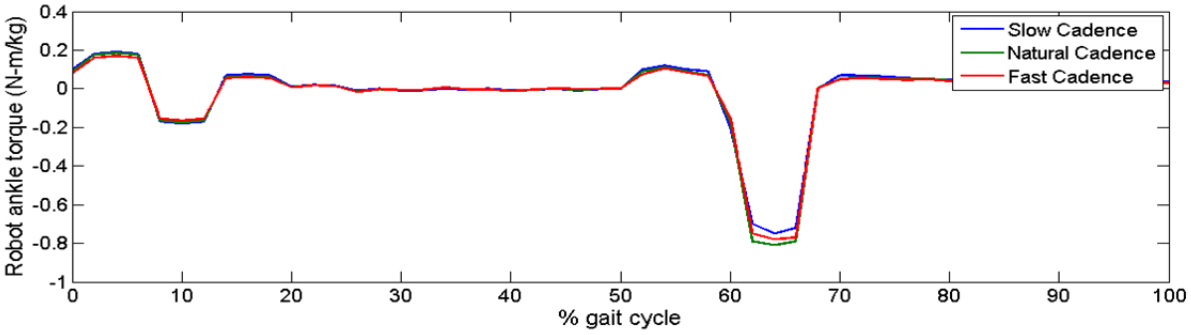

(c)

Figure 5-11. Torques induced by the robotic orthosis during slow, natural and fast cadence at. (a) Hip joint. (b) Knee joint. (c) Ankle joint.

compared to fast cadence, while during rest of the GC the magnitude of torques remained approximately same at all three cadences. For the ankle joint, the robot induced torques also followed the same pattern and there was no considerable difference among the magnitude of these torques at all three cadences [Fig. 5-11(c)].

5.6.2.4. Muscle activation patterns

Normalized activation patterns of eight major muscle groups produced during robot assisted gait at slow, natural, and fast cadence throughout the GC are illustrated in Fig. 5-12(a). These optimized muscle activities reproduced the joint torques. Hip, knee, and ankle torques were reproduced with an RMS error of the order of 10^{-32} N-m/kg. For the most part of the gait cycle, the muscle activation patterns are quite similar for all three cadences, although a small phase variation was observed in the activity of ankle plantar flexors (40-60% GC) and hip extensors (10-25% GC). HAM activity magnitude generally increased with an increase in cadence and showed a higher activity during loading and terminal swing phases at fast cadence compared to slow and natural cadence. GLU showed similar activation patterns to HAM, although the magnitude of GLU activation patterns is slightly lower than the HAM activation patterns. RF activity also increased with an increase in cadence. The most considerable difference in RF activity magnitude was during the loading and mid stance phases, during which the magnitude of muscle activation at fast cadence was nearly twice the magnitude at slow and natural cadence. The magnitude of IP activity at fast cadence was greater than slow and natural cadence during the mid stance phase. The magnitude of IP activity during initial swing phase was greater for slow and natural cadence compared to fast cadence. The magnitude of GAS and SOL also remained the same throughout the GC at all three cadences, but a small increase was observed during the terminal swing phase at fast cadence. The magnitude of VAS activity also increased at fast cadence during the mid stance phase compared to slow and natural cadence. The magnitude of TA activity remained the same during the major phase of GC except during the loading and terminal swing phases when the magnitude at fast cadence was greater than the magnitude at slow and natural cadence. The mean activations of the muscle for the complete GC are shown in Figure 5-12(b). The mean activations of HAM, RF, GLU, IP, SOL, and TA increased with cadence. However, the cadence variation had no significant effect on the mean activations of VAS and GAS.

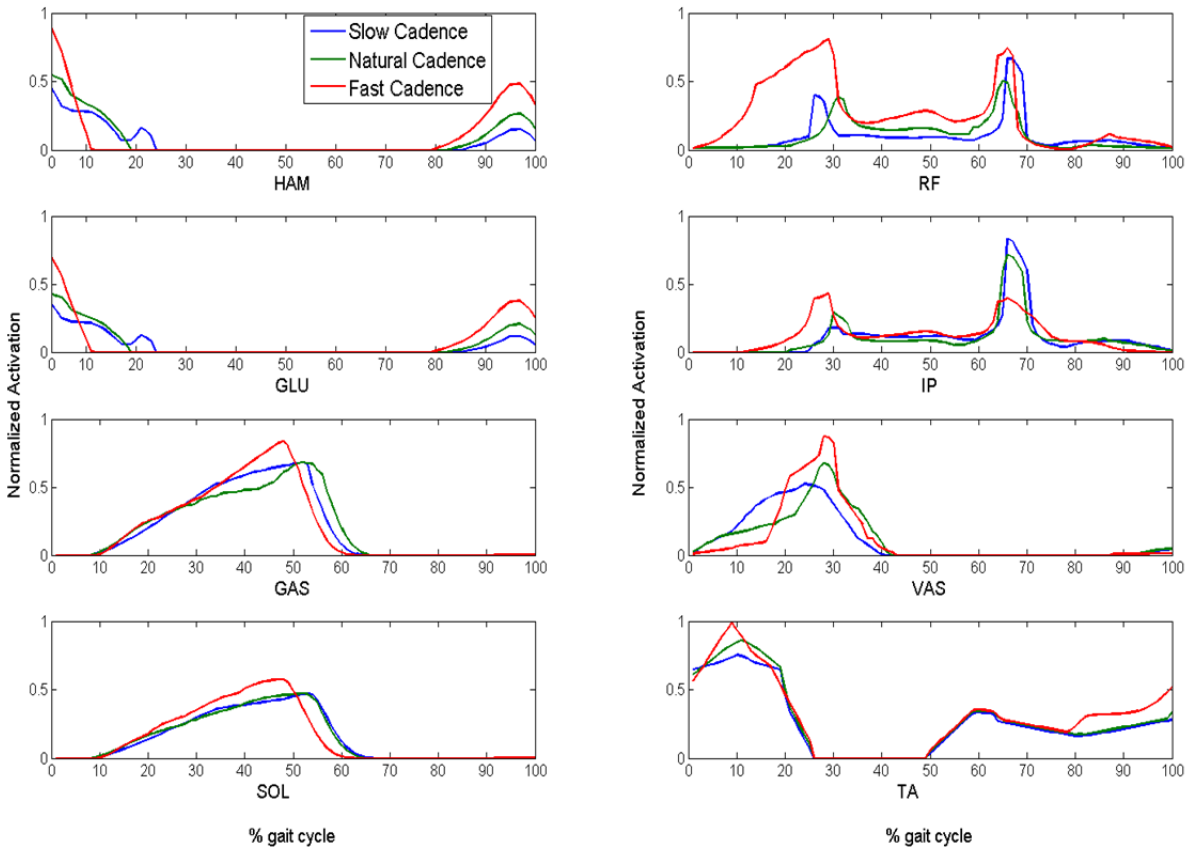

(a)

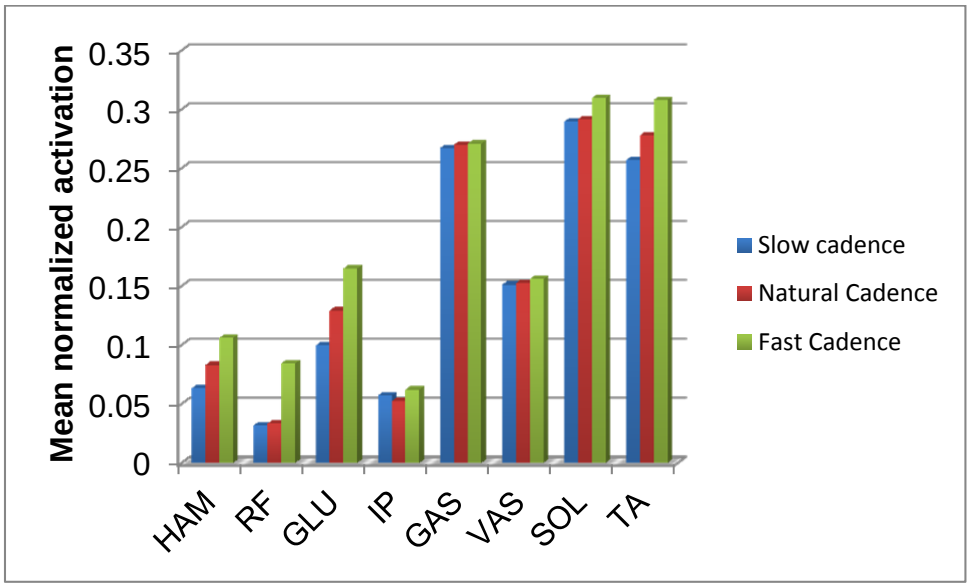

(b)

Figure 5-12. Muscle activation patterns for a GC at slow, natural and fast cadence. (b). Mean activation patterns for a GC at slow, natural and fast cadence.

Table 5-1. Mean kinematic and kinetic measures.

	Slow Cadence	Natural Cadence	Fast Cadence
Hip angle	9.5602	11.7598	11.7713
Knee angle	22.7686	24.7668	25.9720
Ankle angle	5.2548	6.1152	6.0963
GCF max.*	8.3	9.5	10.7
Hip torque (abs)**	0.1205	0.2035	0.3635
Knee torque (abs)	0.1293	0.1791	0.2671
Ankle torque (abs)	0.4747	0.4603	0.4220

*Maximum (max) values are provided for GCF. ** Absolute (abs) values are given for hip, knee and ankle joint torques.

5.7. Discussion

5.7.1. Muscle activation patterns

Neurologic injuries, such as stroke and SCI, often result in neuromuscular damage and disorders in muscle functions. Lower limb disability and gait disorders are the major issues arising from these neurologic injuries. Robot assisted gait therapy is an emerging rehabilitation practice, and one of the important goals of robot assisted gait therapy is to reinstate the muscle coordination and function for motor performance improvement [104]. However, our understanding of muscle functions during the robot assisted gait is limited and dynamic simulations of human gait [138-140, 158] provide a useful tool to study these muscle functions during robot assisted gait.

In this study, we developed the first ever dynamic simulation of robot assisted unimpaired gait to develop better understanding of muscle activation patterns. A 2-D musculoskeletal model of human gait was used which had eight major muscle groups. A 2-D robotic orthosis was modeled to provide actuation at the hip, knee, and ankle sagittal plane joints. These two models were used along with a custom inverse dynamics algorithm to determine sagittal plane joint torques. Muscle activation patterns were obtained using the quadratic minimization algorithm (static optimization). This algorithm worked on the basis of minimization of the norm of the error in the target joint torques (required joint torques) and the actual joint torques. The combination of dynamic modeling of musculoskeletal system and robotic orthosis, position control, inverse dynamics, and quadratic minimization

algorithm provides considerable insight into the muscle activation patterns of robot-assisted unimpaired gait.

It is important to mention that the static optimization method used in this research is different from the Crowninshield method [145]. In the Crowninshield method, the norm of muscle stresses/activations has been minimized under the constraints that the activations so obtained are able to provide required torques and lie within given bounds [98, 145]. In the present research, a static optimization approach was used in which the error in the target torques (required torques) and the actual torques produced by our optimized activation solution has been minimized. Further, the optimization algorithm also ensures that the muscle activation patterns obtained are positive and lie within given bounds. A perturbation analysis was also carried out to analyze the sensitivity of the skeletal muscle activation solution vector for changes in joint torques. The findings from the perturbation analysis show that the static optimization method was robust against the perturbations in the joint torque values.

Previous attempts at analyzing muscle activation patterns during robot assisted gait are limited to the use of EMG signals, recorded in biomechanics laboratories [105, 107]. This method of analyzing muscle activation patterns has its own limitations [138, 154, 159]. First, the EMG signals recorded during robot assisted gait are not reliable, as the attachment of robotic orthosis to human limbs leaves limited space for the attachment of EMG surface electrodes. This limitation of EMG signals could be overcome by designing robotic orthosis mechanisms that do not hinder the placement of EMG surface electrodes. The second reason associated with the poor reliability of EMG recording method is the lack of good alignment of robotic orthosis joints with the subject's joints [160]. This poor alignment of robotic orthosis joints with the subject's joints causes a shift in robotic orthosis applied joint torques from subject's joints. Also, the above mentioned studies based on EMG signals do not consider the activation of ankle plantar and dorsiflexor muscles, as the previous robotic gait training orthoses overlook the actuation of ankle joint [7, 39].

The musculoskeletal gait and robotic orthosis model used in this study was 2-D. Future work shall involve the musculoskeletal and robotic orthosis model with hip abduction/adduction joints to facilitate the study of frontal plane muscle activation patterns. It is worth stating that most of the available robotic orthoses do not provide actuation for hip abduction/adduction motion [36]. The robotic orthosis was operated in pure position control (trajectory tracking) mode, and the advanced assist-as-needed [6] or patient-cooperative

robotic gait training strategies [36] were not included in the present simulation study. A similar method of operating the LOKOMAT in pure position control mode for studying muscle activities (EMG) has also been used in [106, 107]. Body weight support (BWS) was not applied during the presented simulations as is commonly done during robot assisted gait training of neurologically impaired subjects. The reason for not applying BWS was that the BWS has also shown to alter the muscle activation patterns [106], and we did not want to introduce any other biases that could potentially alter the behaviour exhibited by walking in the robotic orthosis. Also other than the muscle activation constraints, the physiological muscle properties were not included in the musculoskeletal model, because the muscle physiology has a small effect on the characteristics of static optimization solutions [146].

It is problematic and difficult to validate the above mentioned muscle activation patterns with the EMG signals recorded during the robot assisted gait. Some of the reasons include the poor placement of EMG surface electrodes in conjunction with robotic orthosis which may not provide the reliable EMG activities of some muscle groups for validation purpose. The relative movement of the robotic orthosis joints with the subject's joints also creates a shift in the robotic orthosis applied torques [160], which may not present the true picture of muscle activities. The rehabilitation engineering community is working towards the development of robotic orthosis mechanisms that have better alignment with the subject's joints. The available robotic gait training orthosis, such as LOKOMAT, also do not provide actuation to the ankle joint. Therefore, the activity of some important muscles, such as bi-articular GAS, TA and SOL, cannot be compared with the EMG signals recorded during LOKOMAT assisted gait [105]. Moreover, the EMG recordings of some large muscles, such as vastus medialis, are not reliable, as they are hidden by other muscles closer to the skin [159]. Due to the above mentioned reasons and the availability of the reliable EMG data only for superficial muscles, we could not validate the muscle activations obtained from the dynamic simulations developed in this study with the EMG signals recorded during robot assisted gait.

In summary, the presented study demonstrated an approach to studying the muscle activation patterns during robot assisted gait using dynamic simulations. We have tried to overcome the limitations of existing methods of studying muscle activation patterns during robot assisted gait that mostly relies on the measurement of EMG signals. We believe that the dynamic simulations of robot assisted gait will enhance our understanding of muscle activation patterns in a kinematically constrained walking environment. Furthermore, these simulations can enable us to develop better robotic better robotic gait training orthoses that

are kinematically compatible and would allow naturalistic gait patterns [39, 79]. However, the kinematic compatibility of robotic gait training orthoses itself is an important research question that largely depends on the disability level and stage of rehabilitation of neurologically impaired subjects [39].

Although only a trajectory tracking controller was implemented in the present study, these dynamic simulations can also be used to study the muscle activation patterns of subjects walking in the robotic gait training orthoses during advance assist-as-needed [6] or patient-cooperative [1, 37] gait training strategies, such as impedance control [66]. The role of advance assist-as-needed robotic gait training strategies is still under investigation in context of motor function recovery [6]. These dynamic simulations can be used to establish a theoretical frame work in order to enhance the understanding of changes in muscle functions when the neurologically impaired or healthy subjects are provided with more freedom to modify their gait patterns during assist-as-needed gait training.

5.7.2. Cadence regulation

Dynamic simulations of robot assisted gait at three different levels of cadence were performed. Analysis of these simulations showed an overall increasing trend in the mean muscle activations, with an increase in cadence. However, no significant variation in mean activations of VAS and GAS was observed [Fig. 6(b)]. Also, the hip extensors and ankle plantar flexors showed a phase change in muscle activations, with a change in cadence.

The muscle coordination patterns during robot assisted gait at variable gait speeds have also been studied earlier. A study conducted by Hidler *et al.* on healthy subjects has shown no significant difference in EMG patterns of LOKOMAT assisted gait at different walking speeds while no body weight support has been provided [105]. Another study conducted by Klarner et al. on healthy subjects to examine the effects of variable stride frequency and BWS during LOKOMAT assisted gait has shown a decrease in EMG intensity, with an increase in stride frequency and BWS [106]. The results from our simulation showed an increase in mean muscle activations, with an increase in cadence with no BWS.

The decrease in EMG intensity reported by Klarner *et al.* [106] may have resulted due to the additional bias of BWS on variable stride frequency which was not considered in the present study. On the other hand, the invariance of EMG magnitude with change in walking speed reported by Hidler *et al.* may have happened due to the narrow range of walking speeds

used in the study [105]. To make the difference in muscle activation magnitudes more pronounced at different cadences, a wider range of cadence was used in this study. The increase in mean muscle activations, with an increase in cadence during robot assisted gait is in accordance with normal unassisted gait. During normal gait, the magnitude of muscle activations generally increases with an increase in cadence or stride frequency [149-151].

5.8. Conclusions

In this work, the muscle activation patterns during robot assisted unimpaired gait were studied. Also, the effect of cadence regulation on muscle activation patterns during robot assisted gait was also studied. According to the author's best knowledge, the dynamic simulations of robot assisted gait have not been reported in literature. The proposed dynamic simulation involves a 2-D musculoskeletal model of human gait and a 2-D robotic orthosis model along with a custom inverse dynamics algorithm and a quadratic minimization algorithm that worked on the basis of minimization of norm of the error in the target joint torques (required joint torques) and the actual joint torques. The proposed dynamic simulation can lead to a profound understanding of the biomechanics of gait in a robotic orthosis and provides the foundation for investigating neuromuscular parameters of interest during robot assisted gait training. The information obtained from these dynamic simulations is particularly useful in the design of new robotic gait training orthoses, which may provide improved physiological gait training. These dynamic simulations may also aid in the development of better robotic gait training strategies and protocols for the treatment of different types and levels of neurologic injuries.

Chapter 6. Impedance Control of Robotic Orthosis for Interactive Gait Training

Interactive or AAN gait training encourages neurologically impaired subjects' active involvement and voluntarily participation in the robotic gait training process which may aid in rapid motor function recovery. In this chapter, an AAN gait training paradigm based on impedance control was developed to provide interactive robotic gait training. The proposed AAN gait training paradigm allows subjects to modify the robot imposed motions, according to their level of disability. The robotic orthosis was operated in four gait training modes, namely position control, zero-impedance control, non-zero-impedance control with high compliance, and non-zero-impedance control with low compliance to evaluate the performance of proposed impedance control scheme. The impedance control scheme is evaluated on neurologically intact subjects. The experimental results show that an increase in robotic compliance encouraged the subjects to participate more actively in the gait training process.

6.1. Introduction

The initial prototypes of robotic gait training orthoses, such as LOKOMAT, work on the basis of pure trajectory tracking (position) control [7]. The problem with the trajectory tracking control is that it forces the subject's limbs on predefined trajectories without taking into account the subject's disability level. The disability level of subjects suffering from neurologic impairments varies from subject to subject and for the same subject during the course of rehabilitation. The individual impairment of a subject needs to be estimated and the torque outputs of the robotic orthosis need to be adjusted accordingly so that the subject can contribute more towards the rehabilitation process [109]. Several control strategies have been developed for the above mentioned robotic gait training orthoses to provide robotic assistance according to the subject's disability level and to enhance subject's voluntary participation in the gait training process [1]. The terms of *compliant*, *AAN, interactive* or *patient cooperative* gait training strategies have been used in literature for this purpose [1, 6, 37].

An AAN or patient-cooperative gait training strategy requires interactive robot-patient control and is mostly achieved by the use of *impedance control*. The concept of impedance control in the field of robotics has been introduced by Hogan [66]. By adjusting the

impedance of the robotic gait training orthoses, the behavior of the robot can be adjusted from very stiff to very compliant. The robot behavior can be made more compliant if the subject has less severe neurological impairment so that the subject can contribute more effort to the robotic gait training process. Similarly, the robot behavior can be made stiff if the subject is unable to achieve the required degree of motion during the gait training process. The relationship between robotic orthosis applied moment and the joint angle is more generally called *mechanical impedance* [37, 66]

The developers of LOKOMAT have implemented an impedance control scheme for their high endpoint impedance actuators to provide AAN gait training [36, 37]. However, the LOKOMAT has design issues, such as the heavy weight, high friction [40, 132], and high endpoint impedance or stiffness (*i.e.* low compliance) of actuators [2, 89]. These design issues limit the ability of LOKOMAT to function as an impedance controlled device [79]. The designers of LOPES came up with a light weight and compliant robotic gait training orthosis to overcome the limitations of impedance control of LOKOMAT [39, 79]. LOPES has its *patient-in-charge* (zero impedance mode) mode, during which the actuator stiffness is kept low, and it also has a *robot-in-charge* mode (position control mode), during which the actuator stiffness is set high. However, the findings from the LOPES robot-in-charge mode and AAN gait training based on impedance control have not been reported in literature [39, 79].

An impedance control scheme has also been implemented for ARTHUR assisted gait rehabilitation of SCI subjects [41, 43]. The impedance control scheme of ARTHUR requires external support in the form of manual assistance from the physical therapists [41]. The physical therapists increase or decrease the amount of manual assistance, based on their experience during the adaptive impedance control of ARTHUR [41]. The manual assistance during the impedance control of ARTHUR introduces subjectivity in the robotic gait training process, which may not be a desirable aspect.

In this work, we have developed and implemented an impedance control scheme for the robotic orthosis powered by PMA. The chapter begins with the concept of impedance control of robotic gait training orthosis. Then, inverse dynamics algorithm used to estimate the human active torque component will be introduced. This follows with the interaction toque estimation method that is used in the inverse dynamics algorithm. The experimental evaluation of the impedance control scheme is presented. The impedance control scheme was

evaluated on neurologically intact subjects. According to the author's best knowledge, impedance control of robotic gait rehabilitation orthoses powered by PMA has not been reported in literature before. In the context of interactive gait training, this work is an advance on the current state-of-the-art in the compliant actuation of robotic gait rehabilitation orthoses.

6.2. Impedance Control

The combined dynamics of robotic orthosis and human subject is given by

$$M(\theta)\ddot{\theta} + C(\theta, \dot{\theta})\dot{\theta} + G(\theta) = T_{rob} + \tilde{T}_t \tag{6.1}$$

where θ,$\dot{\theta}$ and $\ddot{\theta}$ are vectors of generalized position, velocity and acceleration, respectively. M (θ) is the system mass matrix. C is a vector of centrifugal and Coriolis torques, and G is the vector of gravitational torques. T_{rob} (Fig. 6-1) is the vector of torque outputs of the robotic orthosis to guide the subject's limbs on reference trajectories. The dynamic model of the robotic gait training orthosis, powered by PMA, is presented in Chapter 3. The term $\tilde{T}_t$ represents the interaction torque between the robotic orthosis and the human subject.

Robotic gait rehabilitation process involves complex human-robot interactions due to the variability in the disability level of neurologically impaired subjects. The torques applied by the robotic orthosis can be adjusted according to the individual's disability level to provide AAN gait training. Impedance control of the robotic orthosis [66] is a well-established method to modify the robotic assistance, according to the subject's disability level by taking into account the joint torques applied by the subject. The concept behind impedance control of robotic gait training orthosis is to allow the subject to deviate from the reference physiological gait trajectories. The extent of deviation from reference physiological gait trajectories is decided on the basis of the subject disability level and effort. If the deviation from reference trajectories increases from a certain extent, an adjustable moment is applied to track the leg back to the reference trajectories. This applied moment is usually either a zero order (stiffness) or higher order (first or second order) function of joint angles and their gradients. This relationship between moment and angle is generally known as *mechanical impedance* [36]. In this impedance control mode, the robotic orthosis is capable of providing assistance at low compliance level to severely impaired subjects and can adapt the compliance to an increased level for subjects with less severe impairments. The relations for

low and high joint compliance of the robotic manipulators, actuated by PMA, have been discussed in Chapter 3**.**

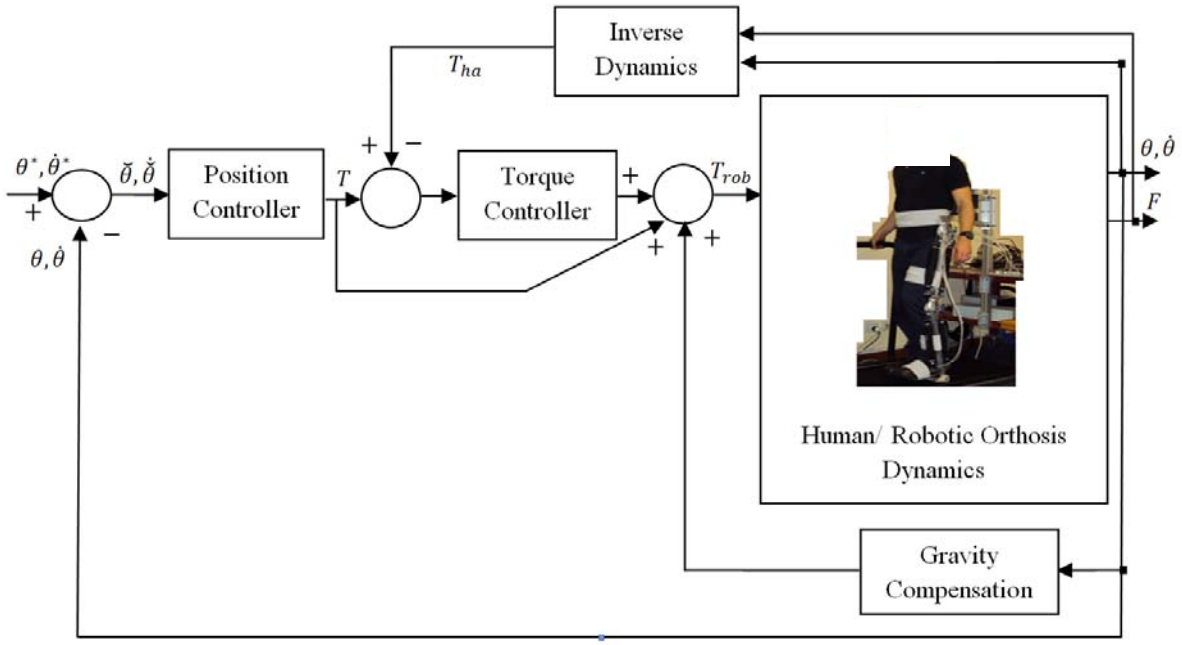

Figure 6-1. Impedance controller diagram. Position controller works on the basis of the CRVC law (Chapter 4). The inverse dynamics algorithm extracts the active human torque component ($\mathbf{T_{ha}}$) from remaining passive and kinetic effects. The proportional torque controller minimizes the error in $\mathbf{T - T_{ha}}$. The impedance controller was implemented in joint space.

The impedance control architecture implemented to provide assist-as-needed robotic gait training is shown in Fig. 6-1. The impedance controller was developed in joint space. The joint encoders were used to measure hip and knee joint angle trajectories θ_i *(i=hip, knee)*. The robotic orthosis joints were assumed to be in alignment with the subject's joints. The joint angle measurements were used to calculate the lengths of PMA. Joint angular velocities ($\dot{\theta}_i$) were computed by using numerical differentiation of joint angular trajectories (θ_i). The hip and knee sagittal plane physiological gait trajectories, reported by *Winter* in [3], were used to define the reference joint angle trajectories (θ_i^*). These joint angle trajectories are scalable in time, amplitude offset, and range in order to adjust it to the individual gait parameters of each subject. The trajectory tracking errors from joint angles $\breve{\theta}_i$ ($\breve{\theta}_i = \theta_i^* - \theta_i$) as well as the joint velocities $\dot{\breve{\theta}}_i$, were used to calculate the joint torques T that guide the lower limbs to follow the predefined reference trajectories. The CRVC control law (Chapter 4) was used as a basic position controller to guide the subject's limbs on reference trajectories, in the presence of structured uncertainties in the model of PMA (Fig. 6-1).

6.3. Inverse Dynamics

The torques outputs of the robotic orthosis T_{rob} are controlled by a torque control strategy (Fig. 6-1). The load cells placed in series with each PMA provide the interaction torques $\check{T}_t$ acting between the robotic orthosis and the human subject. The forces provided by the load cells comprised of gravitational and inertial components as well as the torques produced by subject's joints T_h. The human torque component T_h is further divided into the *active* and *passive torque* components. Active torque component was generated by the human skeletal muscles, and the passive torque component was generated by the viscoelastic components like ligaments and other tissues surrounding the hip and knee sagittal plane joints

$$T_h = T_{ha} + T_{hp} \tag{6.2}$$

where T_{ha} and T_{hp} represents the active and passive human torque components, respectively. The passive joint torque component (T_{hp}) has been modeled by a double exponential equation (Fig. 6-2) by Reiner *et al*. [112] and was implemented in this study. The model developed by Reiner *et al*. (Fig. 6-2) presents the relationship between sagittal plane joint angles and sagittal plane passive joint moments. Experimental data for neurologically intact subjects have been used while developing the model of passive hip and knee sagittal plane joint moments (Fig. 6-2). The model developed by Reiner *et al*. [112] was implemented because the impedance control scheme developed in this study will also be evaluated on neurologically intact subjects. For the evaluation of impedance control scheme on neurologically impaired subjects the passive joint moment model developed by Edrich *et al.* [113] should be used.

An inverse dynamics model (Fig. 6-1) of the robotic orthosis and human subject was developed to extract the active human torque component (T_{ha}) from the remaining passive and kinetic effects.

$$\check{T}_{ha} = \check{M}(\theta)\ddot{\theta} + \check{C}(\theta, \dot{\theta}) + \check{G}(\theta) - \check{T}_{hp} - \check{T}_t \tag{6.3}$$

where $\check{M}(\theta)\ddot{\theta}, \check{C}(\theta, \dot{\theta})$ and $\check{G}(\theta)$ are the estimates of the combined robotic orthosis and human subject inertial, coriolis and gravitational torques, respectively. Geometric values of the human subject were measured before the experiments. Human mass parameters were estimated from the regression equations proposed by Zatsiorsky *et al*. [128]. The inverse dynamics model was required to isolate the active human joint torque component from the

passive joint torque component as well as gravitation and inertial torque components of the robotic orthosis and the human subject. In this way, the torque controller (Fig. 6-1) can avoid responding to passive effects, as the aim of assist-as-needed gait training is to allow deviations only from the active muscle contributions of the human subject.

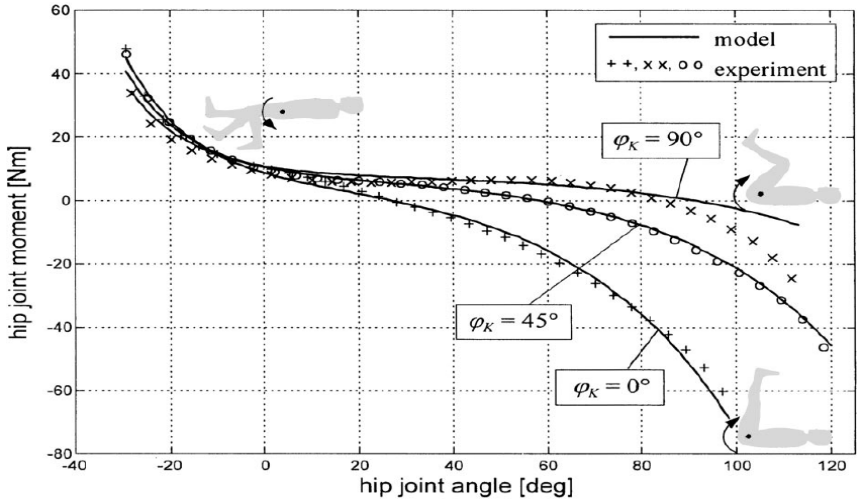

(a)

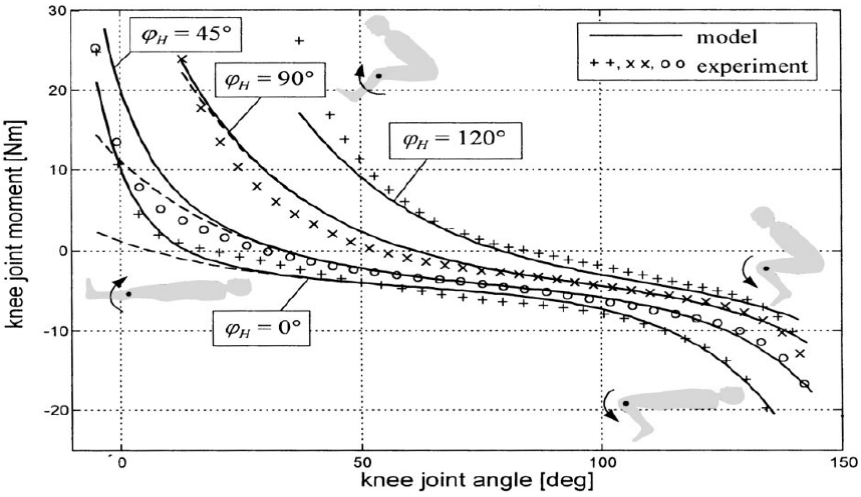

(b)

Figure 6-2. Passive joint torque. (a). Hip joint. (b). Knee joint. Adapted from [112]

The estimation of active human joint torque component was only valid for the swing phase of the GC, as the ground reaction forces cannot be measured in the present experimental setup. During the stance phase of GC, the data from load cells was mainly corrupted by the horizontal ground reaction forces so that the estimated torques were only rough approximations of human subject contributions. A proportional torque controller with feedforward of the desired torque T was used to minimize the error $T - T_{ha}$ (Fig. 6-1). In

order to improve the performance of the torque controller, additional feedback loops were used to partially compensate gravitational effects (Fig. 6-1). Gravitation effects were identified in the inverse dynamic model.

6.4. Interaction Torque Estimation

The interaction torque $\tilde{T}_t$ estimation during the gait training process is an important task as it contains the degree of activity of the human subject walking in the robotic orthosis [161]. It was estimated as the product of force measured by the load cells and the lever arm. Lever arm is equal to the length of human subject's thigh and shank sections. A tension/compression load cell was placed in series with each PMA. The lever arm is a function of robotic orthosis joint angle (eq.3.15 and eq.3.16).

For the purpose of measuring interaction torque, two neurologically intact subjects were asked to walk in the robotic orthosis in two different modes. During the first mode, the subjects were asked to walk actively with the robotic orthosis running in passive mode (active walking). The subjects were shown the reference joint angle trajectories (θ_i^*) on a display and were encouraged to match these trajectories. For the second mode the subjects were asked to walk with the robotic orthosis and allow it to guide the trajectory of their legs during the position control mode (passive walking). The CRVC control law was used as a basic position controller to guide the subjects' limbs on reference trajectories (Chapter 4). The subjects were asked not to contribute any movement during the second mode. Data from the hip and knee joint load cells was recorded for 60 GC during the each mode. By averaging the subject-robotic orthosis interaction torques for all subjects, a reference torque profile representing active walking and passive walking was calculated.

As the gait dynamics and interaction torques varies from subject to subject and for the same subject during the course of rehabilitation, a generalized model of the reference torque profiles is required. A generalized model of the reference interaction torques was developed to account for these variations during the active and passive walking states. The model generates *P* torque profiles for the active state and passive state with *l* samples per GC with the data spread around the reference torque profiles $\tilde{T}_t^{active}$ and $\tilde{T}_t^{passive}$, respectively. The generation of these torque profiles $q_i^v[.]$ with $v \in r\,active, passive\}$ and $P \in \{1,100\}$ is defined for the hip and knee sagittal plane joints

$$q_i^v[l] = \tilde{T}_t^v[l] + \beta_l^v.\left(q_i^v[l-1] - \tilde{T}_t^v[l-1]\right) + u[l] \tag{6.4}$$

where $\tilde{T}_t^v$is the reference torque profile of the state v. β_l^v is a factor to control the distribution of the data and u[l] is a Gaussian noise term. The magnitude of the initial value $q_i^v[1]$ is based on a Gaussian distribution around the initial value of the reference torque profile $\tilde{T}^v[1]$ with

$$q_i^v[1] = \tilde{T}_t^v[1] + r \tag{6.5}$$

where $r \sim K(0, \gamma_{q[0]}^2)$. The magnitude of the generated torque profile at the time instant $q_i^v[l]$ was calculated as the sum of reference torque profile $\tilde{T}_t^v[l]$ and the weighted difference between the generated torque profile and the reference torque profile of the previous time point $q_i^v[l-1] - \tilde{T}_t^v[l-1]$. The distance between the generated torque profile $q_i^v[l-1]$ and the reference torque profile $\tilde{T}_t^v[l-1]$ was multiplied by the factor $\beta_l^v \epsilon R^+$ to control the distribution of the data. The distance between the reference torque profile and the generated torque profile remains unchanged when $\beta_l^v = 1$. The generated torque profile approaches the reference torque profile when $0 < \beta_l^v < 1$ and departs from it when $\beta_l^v > 1$. β_l^v is based on the observed variance of the interaction torques measured among the different subjects during this study. A high variance was created in the sections of the generated torque profile where a high variance was observed in the measured interaction torques. The Gaussian noise term u[l] was included to model the variability in the course of the generated torque profiles. With this method, bundles of *P=100* toque profiles for the hip and knee joints for the active and passive states were generated.

To estimate the degree of subject activity walking within the robotic orthosis, the measured torque profile for the subject for one GC g[.] was matched to the generated torque profiles describing the active and passive state, respectively. The best fitting generated torque profile of the active and passive state was identified by calculating the Euclidian distance between the measured torque profile g[.] and each of the generated torque profile q_i^v for the stance and swing phase and for the hip and knee joint separately

$$\hat{q}_{stance}^{active} = \arg\min_{q_i^{active}} \sqrt{\sum_{l=1}^{550}(g[l] - q_i^{active}[l])^2} \tag{6.6}$$

$$\hat{q}_{swing}^{active} = \arg\min_{q_i^{active}} \sqrt{\sum_{l=551}^{1000}(g[l] - q_i^{active}[l])^2} \tag{6.7}$$

$$\hat{q}_{stance}^{passive} = \arg\min_{q_i^{passive}} \sqrt{\sum_{l=1}^{550}(g[l] - q_i^{passive}[l])^2} \tag{6.8}$$

$$\hat{q}_{swing}^{passive} = \arg\min_{q_i^{passive}} \sqrt{\sum_{l=551}^{1000}(g[l] - q_i^{passive}[l])^2} \quad (6.9)$$

where $l \in \{1,550\}$ for the stance phase and $l \in \{551,1000\}$ for the swing phase of GC.

After identifying the best fitting generated torque profile for the active and passive state, a further step was performed to estimate and quantify the subject's degree of activity. The estimation was based on the relative position of the measured torque profile compared to the best fitting generated torque profiles by

$$tb_{swing} = dist\left(\hat{q}_{swing}^{passive}, g_{swing}\right) - dist\left(\hat{q}_{swing}^{active}, g_{swing}\right) \quad (6.10)$$

$$tb_{swing} = \sqrt{\sum_{l=1}^{550}(\hat{q}_{swing}^{passive}[l] - g[l])^2} - \sqrt{\sum_{l=1}^{550}(\hat{q}_{swing}^{active}[l] - g[l])^2} \quad (6.11)$$

where tb_{swing} represents the quantification of the degree of the activity of the subject. It was determined in the swing phase whether the measured torque profile g_{swing} better matched the generated torque profile of the passive state $\hat{q}_{swing}^{passive}$ or active state $\hat{q}_{swing}^{active}$ by calculating their Euclidian distance $dist$ from the measured torque profile g_{swing}. The difference between Euclidian distances then represent a quantitative estimate of whether the subject is more likely to be in an active state with a positive value or in a passive state with a negative value. During the stance phase of GC, the data from load cells was mainly corrupted by the horizontal ground reaction forces so that the quantified torques were only rough approximations of human subject contributions.

6.5. Experimental Evaluation

6.5.1. Subjects

Three healthy, neurologically intact subjects with no history of neurologic disorders gave written informed consent and participated in the preliminary study (Table 4-1). This experimental protocol was approved by The University of Auckland, Human Participants Ethics Committee (Appendix D).

6.5.2. Experiment protocol

The subjects were asked to walk within the passive (unpowered or zero assistance condition) robotic orthosis for 20 minutes so that they should become familiar with the device

and training environment. A similar procedure was repeated for the robotic orthosis in trajectory tracking (active) mode. No BWS was used during the experiments as the test subjects had no neurological impairment and did not require any external support. The following experimental protocol was developed to evaluate the performance of impedance control scheme.

Experiments with healthy subjects were performed for the four gait training modes (control modes) namely position control, zero-impedance control, non-zero-impedance control with high compliance, and non-zero-impedance control with low compliance. The sagittal plane hip and knee joint angle trajectories, trajectory tracking errors, hip and knee sagittal plane joint compliance, the magnitude of interaction torques $\Delta\tilde{\mathrm{T}}_{\mathrm{t}} = \tilde{\mathrm{T}}_{\mathrm{t,max}} - \tilde{\mathrm{T}}_{\mathrm{t,min}}$ acting between the subjects, and the robotic orthosis at the hip $\Delta\tilde{\mathrm{T}}_{\mathrm{t,hip}}$ and knee $\Delta\tilde{\mathrm{T}}_{\mathrm{t,knee}}$ sagittal plane joints during the four control modes were determined.

Prior to impedance control mode, the robotic orthosis was operated in position control mode. It is important to mention here that the impedance control scheme (Fig. 6-1) was not used during the position control mode. This, in other words, means that the active human joint torque component ($\mathrm{T_{ha}}$) was not utilized to adjust the robot applied torques ($\mathrm{T_{rob}}$). The purpose of the position control mode is to guide the subjects' limbs on reference trajectories with minimum tracking errors. The CRVC was used as a position controller (Chapter 4). The subjects were asked to walk with the robotic orthosis and allow it to guide the trajectory of their legs during the position control mode. The robotic orthosis compliance was selected to be minimal during the position control mode to ensure that the deviation from reference trajectories was minimal. The position control mode is also important for the rehabilitation of severely impaired subjects [65]. The robotic orthosis was operated in position control mode with minimum compliance so that the comparisons can be done between the position control mode, impedance control mode at different levels of compliance, and zero-impedance control mode.

During the zero-impedance control mode, the robotic orthosis was completely passive (*T=0* as shown in Fig. 6-1) and subjects should be able to voluntarily drive the robotic orthosis. Full range leg movements should be possible during zero-impedance control mode. During the non-zero-impedance control with high compliance (Fig. 6-1), the robotic orthosis stiffness was selected to be low, whereas during the non-zero-impedance control with low compliance (Fig. 6-1), the robotic orthosis stiffness was selected to be high. The relations for

low and high joint compliance of the robotic orthosis, actuated by PMA, are provided in Chapter 3. These compliance values can be chosen by the physical therapist based on their experience and the stage of rehabilitation of neurologically impaired subjects. The impedance control scheme (Fig. 6-1) should reduce the robotic assistance if more active participation from the human subjects (T_{ha}) is measured and vice versa.

6.5.3. Data analysis

The evaluation of impedance control scheme was carried out with three neurologically intact subjects. To study the inter subject variability, standard deviation over the values for different GC for each separate control mode for the sagittal plane joint angular ranges of motion and interaction torques was assessed. Also from the measured 60 GC for each control mode, the data was averaged over two GC for all subjects for presentation purpose. All the statistical tests were performed using Matlab- R2009b (The MathWorks, Inc: Natick, Ma, USA).

6.6. Experimental Results

In this section the preliminary results of the impedance control scheme developed for the robotic orthosis are presented.

6.6.1. Joint kinematics

Fig. 6-3 shows the desired and measured hip and knee sagittal plane joint angle trajectories during position control mode. The trajectories were averaged over all subjects for two GC. The compliance of the robotic orthosis was selected to be low during the position control mode so that the deviations from the desired trajectories should be minimum. During position control mode, the maximum angular deviations from desired hip and knee joint angle trajectories were below 10^{o} (Table 6-1). These angular deviations are due to the structured uncertainties in the model of PMA [126]. Fig. 6-4 shows the desired and measured hip and knee joint angle trajectories during the zero impedance control mode. These trajectories were recorded after setting the impedance control parameters to zero so that the robotic orthosis can provide gait training with maximum compliance. Fig. 6-5 and Fig. 6-6 shows the desired and measured hip and knee joint angle trajectories during the non-zero impedance control with high compliance and non-zero impedance control with low compliance, respectively. No

complaints about the pain or discomfort were reported by the subjects during four control modes.

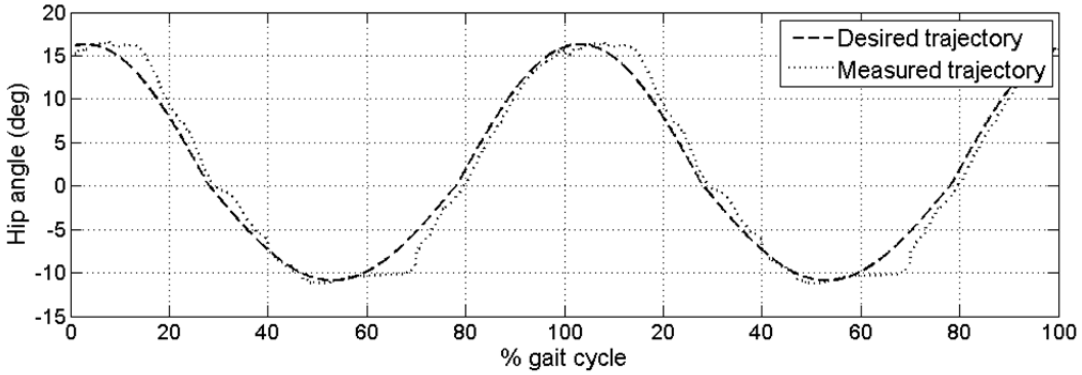

(a)

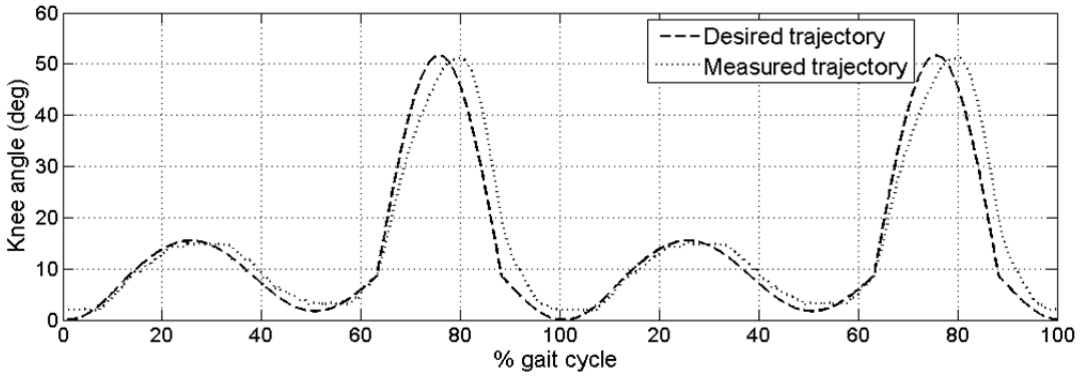

(b)

Figure 6-3. Average hip and knee sagittal plane joint angle trajectories with healthy subjects as a percentage of GC obtained during position control mode, averaged over all subjects for two GC. Position controller works on the basis of CRVC. Normal gait trajectories taken as desired and plotted against the trajectories obtained during walking in the robotic orthosis. (a) Hip joint. (b) Knee joint.

The absolute values of maximum angular deviations at hip $|\breve{\theta}_{\text{hip}}|_{\max}$ and knee joint $|\breve{\theta}_{\text{knee}}|_{\max}$ during the four control modes (Fig. 6-3,6-4,6-5,6-6) averaged over all subjects are given in Table 6-1. The minimum angular deviations at the hip and knee joints (3.96^{o} and 9.31^{o}, respectively) were for the position control mode (Table 6-1). The maximum angular deviations at the hip and knee joints (18.78^{o} and 28.24^{o}, respectively) were for the zero-impedance control mode (values depicted in Table 6-1), during which the robotic orthosis was completely passive, and the subjects have the liberty to drive the robotic orthosis freely. The angular deviations increased with an increase in robot compliance, as the subjects tried to move with more freedom compared to position control mode (values depicted in Table 6-1).

As the robot compliance was increased, the robotic orthosis applied smaller joint torques, and the subjects showed deviations from the reference trajectories.

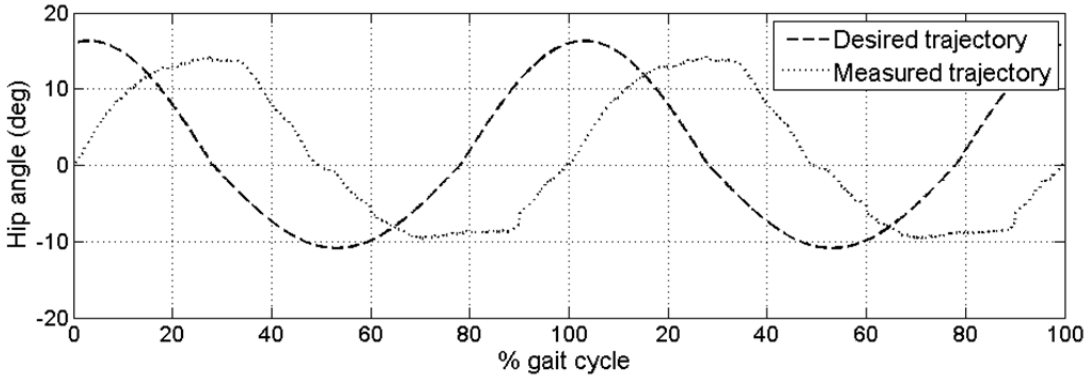

(a)

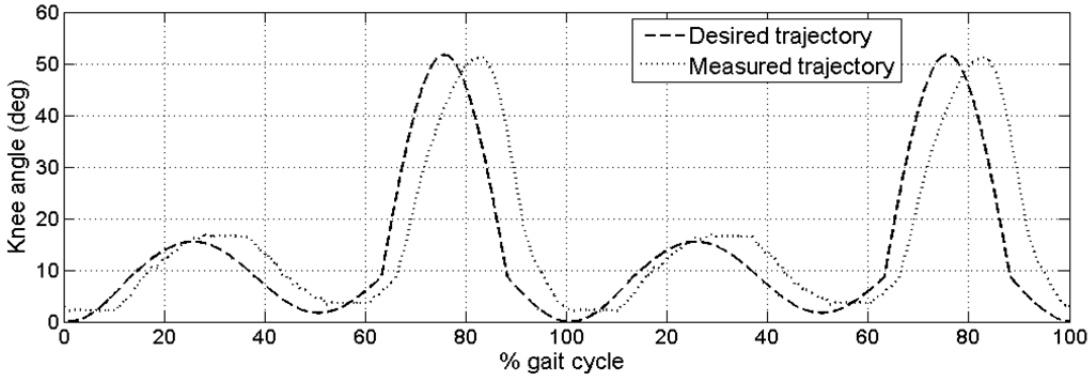

(b)

Figure 6-4. Average hip and knee sagittal plane joint angle trajectories with healthy subjects as a percentage of GC obtained during zero impedance control mode, averaged over all subjects for two GC. Normal gait trajectories taken as desired and plotted against the trajectories obtained during walking in the robotic orthosis. (a) Hip joint. (b) Knee joint.

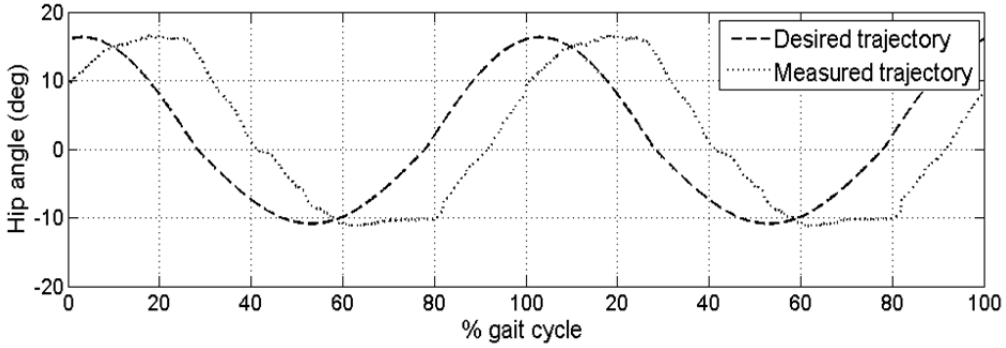

(a)

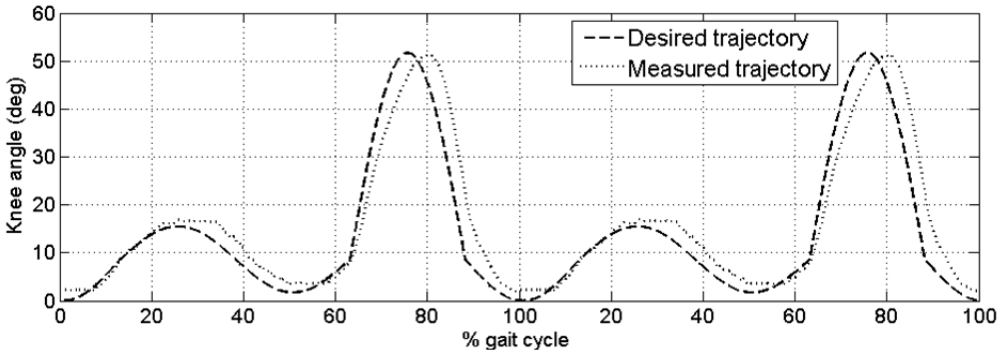

(b)

Figure 6-5. Average hip and knee sagittal plane joint angle trajectories with healthy subjects as a percentage of GC obtained during non-zero impedance control with high compliance, averaged over all subjects for two GC. Normal gait trajectories taken as desired and plotted against the trajectories obtained during walking in the robotic orthosis. (a) Hip joint. (b) Knee joint.

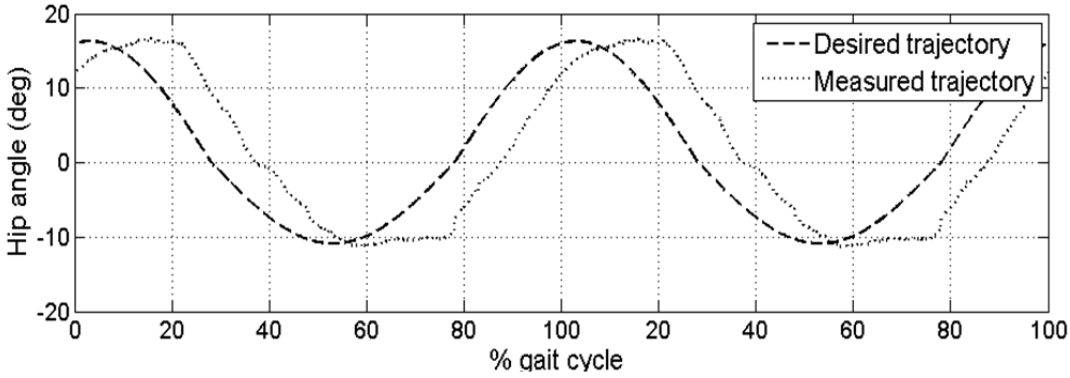

(a)

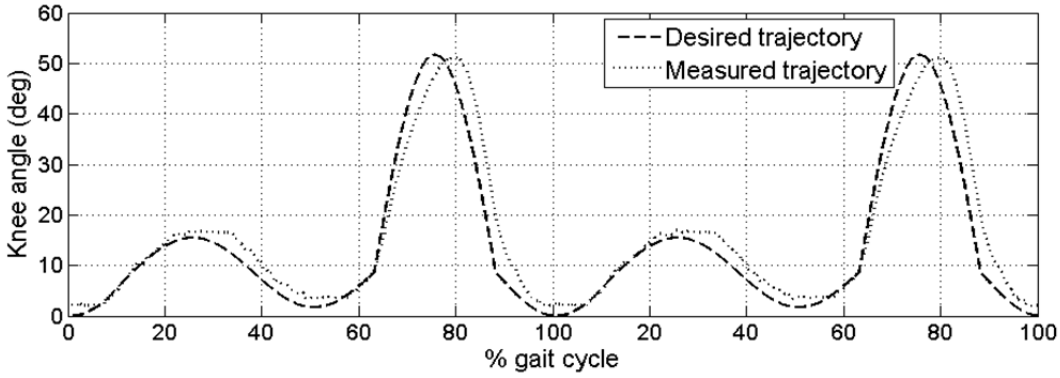

(b)

Figure 6-6. Average hip and knee sagittal plane joint angle trajectories with healthy subjects as a percentage of GC obtained during non-zero impedance control with low compliance, averaged over all subjects for two GC. Normal gait trajectories taken as desired and plotted against the trajectories obtained during walking in the robotic orthosis. (a) Hip joint. (b) Knee joint.

6.6.2. Joint compliance

The robotic orthosis compliance during the four control modes at the hip and knee joints averaged over all subjects are given in Fig. 6-7 and Fig. 6-8, respectively. The robotic orthosis compliance was maximum (4.35 rad/Nm for hip and 12 rad/Nm for knee joint) during the zero-impedance control mode and was minimum (1 rad/Nm for hip and 3.1 rad/Nm for knee joint) during the position control mode (Fig. 6-7 and Fig. 6-8). The impedance control scheme was further evaluated, with a high and low level of compliance. The relations for low and high joint compliance of the robotic manipulators, actuated by PMA, are provided in Chapter 3. The maximum pressure during position control and non-zero-impedance control with low compliance was selected to be 550 KPa. The impedance controller remained stable at both levels of compliance (non-zero-impedance control with high compliance and non-zero-impedance control with low compliance), and no performance issues were experienced during the experiments.

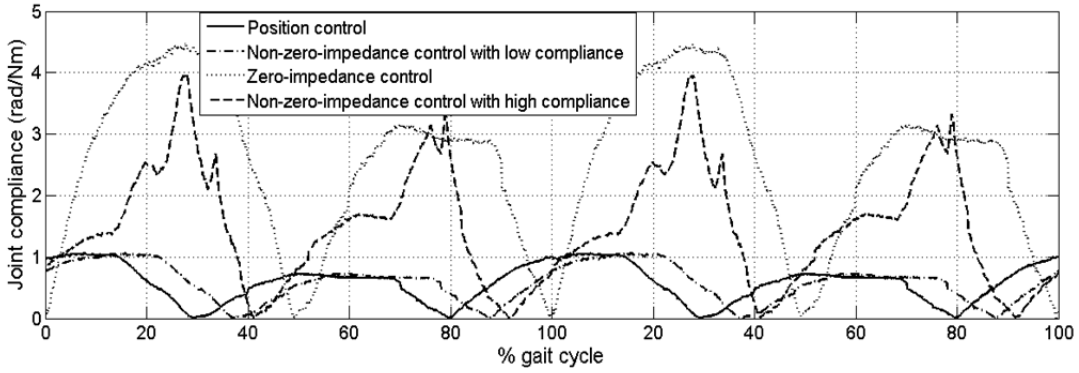

Figure 6-7. Hip sagittal plane joint compliance for four different control modes as a percentage of GC, averaged over all subjects for two GC.

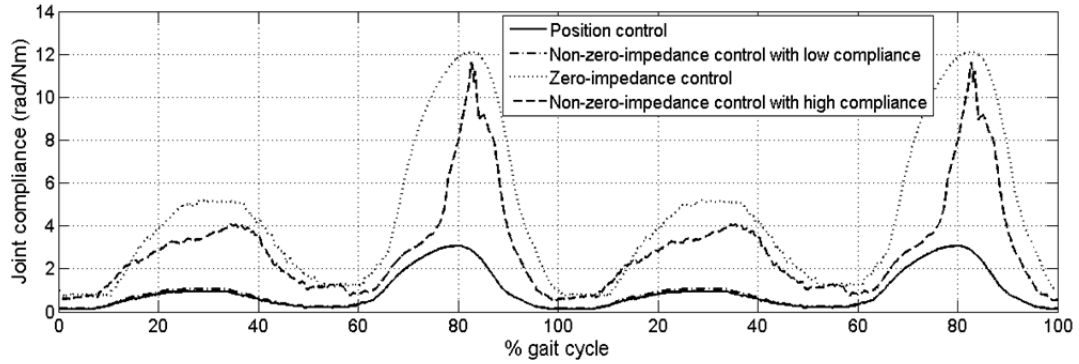

Figure 6-8. Knee sagittal plane joint compliance for four different control modes as a percentage of GC, averaged over all subjects for two GC.

The high or low compliance levels (Chapter 3) can be selected by the physical therapist based on the disability level and training performance of the neurologically impaired subjects.

6.6.3. Interaction torques

The values of interaction torques $\Delta\breve{T}_t = \breve{T}_{t,max} - \breve{T}_{t,min}$ acting between the subjects and the robotic orthosis at the hip $\Delta\breve{T}_{t,hip}$ and knee $\Delta\breve{T}_{t,knee}$ joints during the four control modes averaged over all subjects are provided in Table 6-1. The highest magnitude of joint torques (48 Nm) was observed during the position control mode as the robotic orthosis forces the subjects' limbs on reference trajectories with a minimum compliance (values depicted in Table 6-1). The values of joint torques decrease with an increase in robotic compliance (values depicted in Table 6-1), as the robotic orthosis allows more freedom to the subjects' to modify their gait trajectories. During zero-impedance control or robot-passive mode, the joint torques were greater than zero (11.4 Nm) (values depicted in Table 6-1). This behavior was not surprising as the human torque component $\breve{T}_{ha}$ (Fig. 6-1) was minimized and not the joint torque resulting from the interaction $\breve{T}_t$ between the human subject and robotic orthosis.

Table 6-1. Maximum Absolute Values of sagittal plane Joint Angular Deviations and Joint Interaction Moment Ranges Recorded for Different Control Modes and Averaged Over Subjects.

Gait parameter	Position control	Non-zero-impedance control with low compliance	Non-zero-impedance control with high compliance	Zero-impedance control
$\lvert\breve{\theta}_{hip}\rvert_{max}$	3.96^o	10.16^o	14.22^o	18.78^o
$\lvert\breve{\theta}_{knee}\rvert_{max}$	9.31^o	12.48^o	15.0^o	28.24^o
$\Delta\breve{T}_{t,hip}$	48 Nm	29.3 Nm	20.8 Nm	11.4 Nm
$\Delta\breve{T}_{t,knee}$	45.7 Nm	31 Nm	23 Nm	10.1 Nm

6.6.4. Inter subject variability

Standard deviation over the values for different GC for four separate control modes was assessed, in order to study the inter subject variability. Table 6-2 presents the average values of joint angles and joint interaction moment ranges with standard deviations recorded for four control modes. Average values of 60 GC for all subjects are presented (values depicted in Table 6-2). The minimum magnitude of inter variability was recorded during the position control mode ($\pm$1.2^o for hip and $\pm$3.4^o for knee joint) (values depicted in Table 6-2). The maximum magnitude of inter subject variability was recorded during the zero-impedance control mode ($\pm$ 7.5^o for hip and $\pm$13^o for knee joint) (values depicted in Table 6-2). The joint interaction moments also showed the same pattern (values depicted in Table 6-2). The

deviations from the average values increases over the 60 GC for all subjects, with an increase in robotic compliance. This could be explained by the fact that the robotic orthosis allows more freedom to the subjects to modify their gait patterns, with an increase in compliance.

Table 6-2. Average of sagittal plane Joint Angles and Joint Interaction Moment Ranges (± Standard Deviations) Recorded for Different Control Modes. Average values of 60 GC for All Subjects are Presented.

Gait parameter	Position control	Non-zero-impedance control with low compliance	Non-zero-impedance control with high compliance	Zero-impedance control
θ_{hip}	$27.7^{o}\pm1.2$	$28.0^{o}\pm2.7$	$29.2^{o}\pm4.3$	$27.17^{o}\pm7.5$
θ_{knee}	$53.2^{o}\pm3.4$	$52.8^{o}\pm8.6$	$51.6^{o}\pm11.4$	$54.6^{o}\pm13.0$
$\Delta\tilde{T}_{t,hip}$	48 Nm±2.8	29.3 Nm ± 4.1	20.8 Nm ± 5.3	11.4 Nm ±6.7
$\Delta\tilde{T}_{t,knee}$	45.7 Nm ± 3.2	31 Nm ± 3.9	23 Nm ± 4.8	10.1 Nm ± 5.4

Table 6-3. Inter Subject Variability of sagittal plane Joint Angles and Joint Interaction Moment Ranges (± Standard Deviations) Recorded for Different Control Modes. Variability for 60 GC is presented.

Gait parameter	Position control	Non-zero-impedance control with low compliance	Non-zero-impedance control with high compliance	Zero-impedance control
θ_{hip}	$1.3^{o}\pm0.4$	$2.5^{o}\pm0.6$	$3.8^{o}\pm0.9$	$5.2^{o}\pm1.3$
θ_{knee}	$1.9^{o}\pm0.3$	$3.4^{o}\pm0.5$	$5.8^{o}\pm0.7$	$7.3^{o}\pm1.1$
$\Delta\tilde{T}_{t,hip}$	1.2 Nm ± 0.2	2.3 Nm ±0.5	4.7 Nm ± 0.4	5.4 Nm ±0.6
$\Delta\tilde{T}_{t,knee}$	1.7 Nm ±0.4	2.9 Nm ±0.6	5.2 Nm ±0.3	6.1 Nm ±0.5

Table 6-3 presents the inter subject variability of joint angles and joint interaction moment ranges, with standard deviations recorded for four control modes. Inter subject variability for 60 GC is presented (values depicted in Table 6-3). The inter subject variability was minimum during the position control mode, as the robotic orthosis forces the subjects limbs on reference trajectories with minimum compliance. An inter subject variability of $\pm0.4^{o}$ for hip joint and $\pm0.3^{o}$ for knee joint was recorded during the position control mode (Table 6-3). The inter subject variability also increases with an increase in robotic orthosis compliance, as each subject contributed in a different manner toward the gait training process (values depicted in Table 6-3). Among the four control modes, the maximum magnitude of inter subject variability ($\pm1.3^{o}$ for hip joint and $\pm1.1^{o}$ for knee joint) was recorded during the zero-impedance control mode (Table 6-3). The inter subject variability of joint interaction

moments also showed the same pattern (Table 6-3). The increase in inter subject variability during the zero-impedance control mode was due to the fact that the robotic orthosis was completely passive and subjects have more freedom to drive the robotic orthosis voluntarily.

6.7. Related Work

It is important to mention here that an impedance control algorithm has also been used for LOKOMAT by Riener *et al.* [37]. However, "the LOKOMAT was originally not designed to function as an impedance controlled device" [79]. The LOKOMAT is powered by electric motors that are not back-drivable [7]. The reason for the non-back-drivability of the electric motor is that the friction and damping force in the lead screw of the motor gets magnified by its high transmission ratio. The ability to back-drive electric motors is important for interactive control schemes, as it makes it easier for the human subjects to move their legs without sizeable resistance from the robotic orthosis. The impedance control scheme of LOKOMAT requires a friction compensation method to make the motors back-drivable [37]. The friction compensation method is based on a friction model [162]. The friction compensation model is only an approximation, and actual friction force has a complicated dependency on the load applied to the motor and on the current configuration of the device [163, 164]. This friction compensation method increases the overall complexity of impedance control scheme. The impedance control scheme developed in this work does not require friction compensation, as the robotic gait training orthosis is intrinsically compliant (*i.e.* back-drivable).

The impedance control scheme used in this study is different from the control scheme used by Riener *et al.* in that a PD controller has been used as a basic position controller in the overall impedance control architecture [37]; whereas in this study, the CRVC (Chapter 4) was used as the basic position controller in the overall impedance control architecture. It was necessary to use the robust CRVC as the basic position controller in the overall impedance control scheme because of the structured uncertainties in the model of PMA [129, 134]. Four gait training modes (control modes), namely position control, zero-impedance control, non-zero-impedance control with high compliance, and non-zero-impedance control with low compliance were used to evaluate the impedance control scheme. Similarly, the position control mode, zero-impedance control mode and impedance control mode have also been used during the evaluation of LOKOMAT by Riener *et al.* in [37].

A maximum trajectory tracking error of less than 10^{o} was achieved during the position control mode with minimum compliance. This performance is in accordance with the other gait rehabilitation orthoses, such as LOKOMAT, for which the maximum trajectory tracking errors during the position control mode with maximum impedance "must be below 15^{o}" [37]. The maximum values of joint interaction moments recoded during the present study for the zero-impedance control mode were 11.4 Nm and 10.1 Nm for hip and knee joints, respectively. This behaviour during the zero-impedance control mode is in accordance with other robotic gait rehabilitation orthoses, such as LOKOMAT, for which the maximum values of joint interaction moments at hip and knee joints are 42 Nm and 28 Nm, respectively [37]. It is important to mention here that the joint interaction moment ranges ($\Delta\tilde{T}_t$) acting between the robotic orthosis and human subjects were greater than zero during the zero-impedance control mode. This behaviour is not unexpected, because the active torque component was minimized (T_{ha}) rather than the moment ranges resulting from the interaction ($\tilde{T}_t$) between the robotic orthosis and human subjects. A similar behaviour was observed during the zero-impedance control mode of LOKOMAT [37].

6.8. Conclusions

Interactive gait training strategy based on impedance control was developed for an intrinsically compliant light weight robotic orthosis powered by PMA. The CRVC control law, developed in Chapter 4, was used as a basic position controller to guide the subject's limbs on reference trajectories, in the presence of structured uncertainties in the model of PMA. Experiments were performed with three neurologically intact subjects to evaluate the performance of impedance control scheme. In order to evaluate the impedance control scheme the robotic orthosis was operated in four control modes, namely position control, zero-impedance control, non-zero-impedance control with high compliance, and non-zero-impedance control with low compliance. Experimental results showed that the impedance control scheme can deliver its intended effect. Subjects walked in the robotic orthosis during four control modes. All subjects showed greater deviations from the reference joint angle trajectories with an increase in robotic compliance. This happened because the impedance control scheme helped in enhancing subjects' voluntary participation in the gait training process. The impedance control scheme was only valid for the swing phase of GC, as during the stance phase, the data from load cells was mainly corrupted by the horizontal ground reaction forces.

The main contribution of this research is the development and application of impedance control on robotic gait rehabilitation orthosis powered by PMA. According to the author's best knowledge, neither previous work has developed nor implemented the impedance control on PMA driven robotic gait rehabilitation orthoses. This work will also help in further developing interactive rehabilitation strategies for robotic orthoses powered by intrinsically compliant actuators. In the next chapter, a seamless, adaptive AAN control scheme is described for the gait training of neurologically impaired subjects.

Chapter 7. Assist-as-Needed Control of Robotic Gait Training Orthosis

This chapter presents the development of an adaptive seamless, AAN control scheme for the robot assisted gait training. The AAN control scheme learns in real time the disability level of human subjects based on the trajectory tracking errors and adapts the robotic assistance accordingly. The overall AAN control architecture works on the basis of a robust adaptive control approach. The performance of seamless AAN control scheme was evaluated during treadmill training with the compliant robotic orthosis (Chapter 2). Two experiments namely trajectory following experiment and the AAN experiment, were carried out to evaluate the performance of seamless adaptive AAN control scheme. The trajectory following experiment was designed to evaluate whether the robotic orthosis can guide the limbs of severely impaired subjects on reference trajectories. The AAN experiment was designed to evaluate whether the robotic orthosis can increase or decrease the assistance based on the extent of voluntary participation from human subjects. Both experiments were performed with neurologically intact subjects. It was found that the robotic orthosis is capable of guiding the subjects' limbs on reference trajectories during the trajectory following experiment. Also, a variation in robotic assistance was recorded during the AAN experiment based on the voluntary participation of human subjects. Further trials with neurologically impaired subjects are required to prove the therapeutic efficacy of the proposed seamless adaptive AAN control scheme. This work is an advance on the current state of the art in the compliant actuation of robotic gait rehabilitation orthoses in the context of seamless AAN gait training.

7.1. Introduction

The most common AAN robotic gait training strategies are based on impedance control [66]. The developers of LOKOMAT have implemented an impedance control scheme for their high endpoint impedance actuators to provide compliant AAN gait training [36], but this attempt has added an extra layer of control complexity [110]. We have also developed an impedance control strategy for interactive gait training (Chapter 6). The impedance control strategy has a limited ability to create accurate joint movements, when large forces are required at subject's limbs to complete these movements, such as situations in which the subject's limbs exhibit substantial tone. The impedance controlled robotic devices, such as LOKOMAT, address the problem of moving compliantly against the gravity by adding an

offset term proportional to the weight or a fixed model of the subject's lower extremity dynamics [37]. However, the offset term or fixed model needs to be manually adjusted for each subject [65]. Also this approach does not address the issue of large forces required to overcome abnormal muscle tone. Moreover, the impedance control has only been implemented effectively for the swing phase of LOKOMAT assisted gait, as the inverse dynamics algorithm is not able to properly extract the active torque component contributed by the subject during the stance phase of GC [37]. It is also evident that the lower limb joint stiffness relationship [112, 113] used in the inverse dynamics algorithm of LOKOMAT [37] is most likely not quantitatively identical to that observed in a particular user, as a large variability can be found in the physical properties of the human lower limb joints.

A force field control scheme [42, 109] has been used by the developers of ALEX [6, 132] and LOKOMAT [14, 71] for the AAN gait training of stroke and SCI subjects. This control scheme reduces the amount of robotic assistance, as the training process progresses in a subjective manner without effectively taking into account the subject's movement capability and disability level. ALEX force field [6] and LOKOMAT impedance controllers (virtual impedance) [36] are also dependent on physical therapist's decision to increase or decrease the amount of robotic assistance [6, 37]. The force field control scheme also address the problem of moving compliantly against the gravity by adding an offset term proportional to the weight or a fixed model of the subject's lower extremity dynamics [14, 37, 71]. However, the offset term or fixed model needs to be manually adjusted for each subject [65]. Also, this approach does not address the issue of large forces required to overcome abnormal muscle tone. The force field control scheme developed for LOKOMAT [71] and ALEX [6, 132] also requires a friction compensation model to make the motors back-drivable [37]. The friction compensation model is only an approximation, and actual friction force has a complicated dependency on the load applied to the motor and on the current configuration of the device [163, 164], thus increasing the overall complexity of force field control scheme. Hence, the above mentioned control approaches do not provide seamless adaptive, AAN robotic assistance during gait training.

Later, robotic orthoses powered by inherently more compliant actuators have been developed. Pneumatic cylinders have been used in the design of PAM and POGO [46, 165] to provide compliant actuation to the pelvis and assistance during leg swing. PAM and POGO have used the concept of *triggered assistance* [46]. The goal of triggered assistance is to allow the subject to first attempt the movement, and then provide robotic assistance to

complete the movement, either automatically or initiated by a therapist , after a certain amount of time or when the subject is not able to voluntarily complete the movement. The discrete event nature of this approach, however, requires decision either by a programmed rule set or by an observing physical therapist. In other words, this approach breaks the movement into a subject driven part and a robot driven part rather than providing a seamless level of robotic assistance to the subject-driven part. Moreover, for the robot driven part, a relatively stiff controller has been used to achieve necessary assistance, so that the subject is not in a compliant environment when assistance is being provided.

We have also developed a light weight robotic gait training orthosis powered by PMA (Chapter 2) [54]. In this chapter, we have developed AAN control architecture for providing seamless adaptive robotic assistance during gait training process. The AAN controller takes into account the subject's disability level and voluntary participation, and adapts the robotic assistance accordingly, in a seamless manner in real time. The overall AAN control architecture consists of a robust adaptive controller. The basic position controller in the overall AAN control architecture works on the basis of the robust CRVC control law (Chapter 4). The adaptive controller in the overall AAN control architecture was developed to adapt the robotic assistance according to subjects' disability level.

Experiments were performed with healthy subjects to evaluate the performance of the AAN controller developed for the robotic gait training orthosis powered by PMA. The adaptive AAN controller was evaluated in terms of variation in robotic assistance depending upon the extent of voluntary participation by human subjects in the gait training process. The robotic orthosis is capable of providing assistance at high level to severely impaired subjects and can adapt the assistance to a decreased level for subjects with less severe impairments.

The chapter begins with the concept of compliance adaptation. This follows with the AAN control architecture. After that, the experimental protocol used to evaluate the AAN control strategy is elaborated. Then, the experimental results of the AAN control strategy are presented. The experiments were performed with neurologically intact subjects. The chapter ends with the discussion and conclusion section.

The contributions of this work include the development of a seamless adaptive AAN controller that does not need a physical therapist's decision to switch between different assistance modes, unlike the above mentioned robotic gait training orthoses [6, 37, 39]. According to the best knowledge of the author, the seamless adaptive, AAN control of

robotic orthoses powered by PMA has not been previously reported in literature. Unlike the above mentioned robotic gait training orthoses [6, 37], the adaptive AAN controller developed in this work does not require expensive force/torque sensors for human-robot interaction or human subject voluntary effort estimation. This work will also help in further developing AAN gait rehabilitation strategies for robotic orthoses powered by intrinsically compliant actuators.

7.2. Compliance Adaptation

The combined dynamics of robotic orthosis and human subject is given by

$$M(\theta)\ddot{\theta} + C\left(\theta, \dot{\theta}\right)\dot{\theta} + G(\theta) = T_{rob} + T_h \tag{7.1}$$

where θ,$\dot{\theta}$ and $\ddot{\theta}$ are vectors of generalized position, velocity and acceleration, respectively. *M (θ)* is the system mass matrix. *C* is a vector of centrifugal and Coriolis torques and *G* is the vector of gravitational and frictional torques. T_{rob} is the vector of torque applied by robotic orthosis. T_h is the vector of torque applied by human subject.

The adaptive compliance controller uses the sliding surface *s* and the desired trajectory *v* [122]. Here *s* and *v* are defined as

$$s_i = \dot{\tilde{\theta}}_i + \lambda_i \tilde{\theta}_i \tag{7.2}$$

$$v_i = \theta_i^* - \lambda_i \tilde{\theta}_i \tag{7.3}$$

where the subscript *i=h (hip),k (knee)*. $\tilde{\theta}_i = \theta_i - \theta_i^*$ is the tracking errors at hip and knee joints. Also θ_i^* and θ_i represents the desired and actual trajectories for the hip and knee joints, respectively. Also, λ_i are positive scalar design parameters. It was assumed that the joint angles of robotic orthosis correspond to the joint angles of human subject. Joint angular velocities were calculated by numerical differentiation. The adaptive control law for the desired robotic joint torque can be written as (Fig.7-1.)

$$T_{rob} = \Upsilon\left(\theta, \dot{\theta}, v, \dot{v}\right)\hat{\beta} - w \tag{7.4}$$

The CRVC control law (w) was used to guide the subject's limbs on reference trajectories in the presence of structured uncertainties in the model of PMA (Chapter 4).

$\Upsilon\hat{\beta}$ is a model of the robotic orthosis and human leg combination, including the torques generated by the human subject during gait training process and is defined as

$$\Upsilon\hat{\beta} = \breve{M}\dot{v} + \breve{C}v + \breve{G} - \breve{T}_h \tag{7.5}$$

where $\breve{M}$, $\breve{C}$ and $\breve{G}$ are the estimated parameters of the combined robotic orthosis and human lower limb. Υ is a $1 \times q$ vector of known functions of $\theta, \dot{\theta}, v$ and $\dot{v}$. $\hat{\beta}$ is a $q \times 1$ vector of estimated parameters of the real system parameters β.

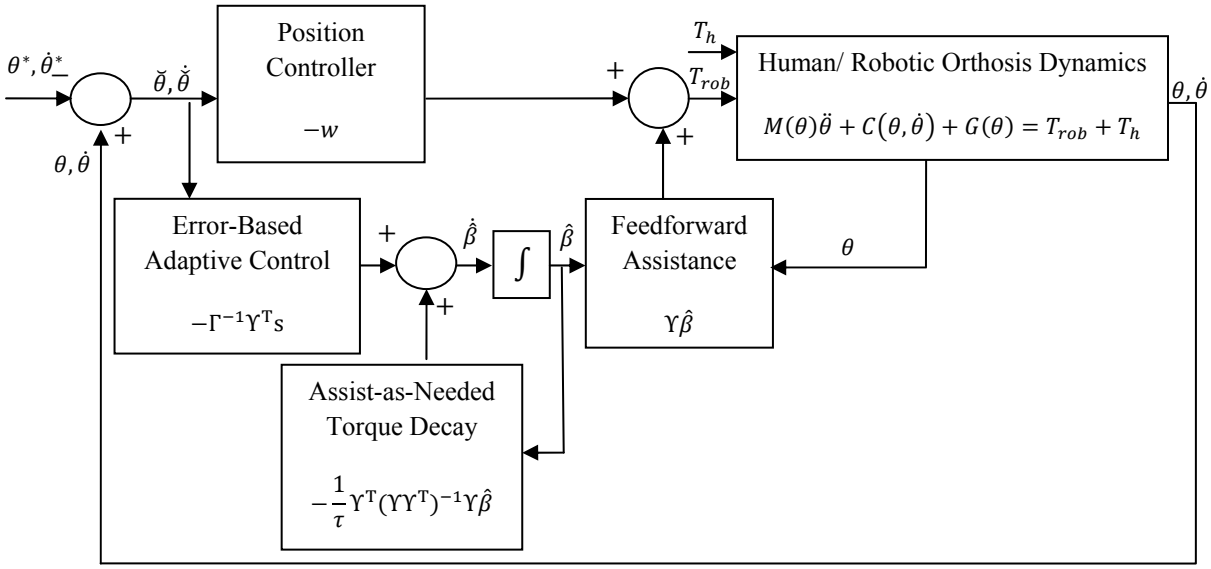

Figure 7-1. Assist-as-needed controller diagram. Position controller works on the basis of the CRVC control law (Chapter 4). The assist-as-needed torque decay term continuously decrease the amount of robotic assistance if trajectory tracking errors are small. The controller was implemented in joint space.

Conventionally, the dynamic model ($\Upsilon\hat{\beta}$) has been developed by using classical dynamic modelling methods. The dynamic model, which includes the human joint torque component (T_h), should have sufficient resolution to adapt to different types and levels of neurological impairments. The dynamic model developed for the robotic gait training orthosis in this study used a Gaussian radial basis functions to model the human joint torque component. The Gaussian radial basis functions are defined as

$$g_{ni} = \exp\left(-\frac{|\theta_i - \mu_n|}{2\sigma^2}\right) \tag{7.6}$$

where g_{ni} is the *nth* radial basis function, θ_i is the current location of the subject's joint and σ is a scalar smoothing constant that determined the width of the basis function. For the robotic gait training orthosis, six grid divisions of radial basis functions, each for hip and knee sagittal plane joint motion, was implemented (Fig. 7-2). The grid divisions were equally spaced at 12^o apart with $\sigma = 5.096^o$. For smaller values of σ, the function approximation was observed to be not desirable. The vector of all the Gaussian radial basis functions is defined as

$$\Upsilon = [g_1\ g_2 \dots \dots \dots . g_{l\times m}\ ]^T \tag{7.7}$$

The parameter estimate vector $\hat{\beta}$ is a $q \times 1$ vector, with the parameters representing the amount of torque the subject is unable to provide to complete the desired joint motions. The standard parameter update law for this method is

$$\dot{\hat{\beta}} = -\Gamma^{-1}\Upsilon^T s \tag{7.8}$$

where Γ is a symmetric, positive definite gain matrix that determined the overall error based adaptation rate. Similarly, λ_i determines the ratio of position error adaptation to velocity error adaptation. When all the gravitational and inertial components from eq.(7.7) are included and the torque output from the human subject remains time independent, the controller defined by eq.(7.4) and eq.(7.8) is asymptotically stable, following an analysis similar to [166]. However, for the implementation of robotic gait training orthosis, the human subject torque is most certainly time dependent. However, it is possible to show that the system does exhibit uniform ultimate boundedness, with the tracking errors limited by the bounds of the system dynamics and by the bounds of the torque output from the human subject.

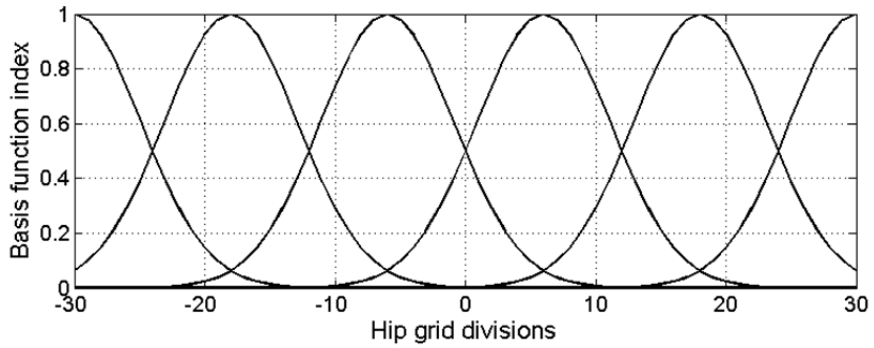

(a)

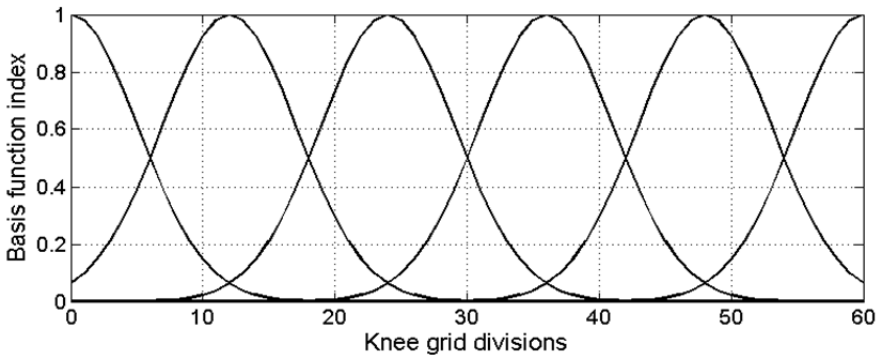

(b)

Figure 7-2. Radial Basis functions for the hip and knee sagittal plane joints. (a) Hip joint. (b) Knee joint.

7.3. Assist-as-Needed Control

The parameter update law eq.(7.8) was modified in order to decrease the torques applied to the subject when the tracking errors are small. This modification decays the torque applied by the robotic orthosis when the subject is able to complete the movements without assistance (Fig. 7-1). In order to achieve this robotic torque decay, we specified that the partial derivative of the robot applied torque with respect to time; when tracking error is zero, behave according to

$$\frac{\partial}{\partial t}\left(\Upsilon\hat{\beta}\right) = \Upsilon\dot{\hat{\beta}} = -\frac{1}{\tau}\Upsilon\hat{\beta} \tag{7.9}$$

where $\Upsilon\hat{\beta}$ is the model based feed forward torque applied by the robotic orthosis to the subject's joints. $\frac{1}{\tau}$ is the forgetting rate of the robotic orthosis ($\tau = \text{time constant}$). Using partial derivative of $\Upsilon\hat{\beta}$ limits the change in $\hat{\beta}$ so that it is no longer a function of changes in the regressor matrix Υ. This allows information learned from the previous motion to remain in the parameter vector $\hat{\beta}$ so that when the subject returns to similar motions in time, the assistance learned during the previous training trials is still available.

There are an infinite number of solutions available for $\dot{\hat{\beta}}$ that satisfy eq.(7.9). By seeking the minimum norm solution for $\dot{\hat{\beta}}$, the parameters that change are those that are most influential on the torque output at a given joint angle. This allows the controller to learn a model of the neuromuscular impairment and subject effort as a general function of desired position, velocity and acceleration of the lower limb in joint space. The minimum norm solution for $\dot{\hat{\beta}}$ was found by solving the constrained minimization problem

$$\min_{\dot{\hat{\beta}}}: \{f = \frac{1}{2}\dot{\hat{\beta}}^T\dot{\hat{\beta}}: g = -\Upsilon\dot{\hat{\beta}} - \frac{1}{\tau}\Upsilon\hat{\beta} = 0\} \tag{7.10}$$

The minimization solution to eq.(7.10) is

$$\dot{\hat{\beta}} = -\frac{1}{\tau}\Upsilon^T(\Upsilon\Upsilon^T)^{-1}\Upsilon\hat{\beta} \tag{7.11}$$

This term is added to eq.(7.8) to create the modified parameter update law

$$\dot{\hat{\beta}} = -\frac{1}{\tau}\Upsilon^T(\Upsilon\Upsilon^T)^{-1}\Upsilon\hat{\beta} - \Gamma^{-1}\Upsilon^T s \tag{7.12}$$

The two terms on the right side of eq.(7.12) create an adaptive controller with competing interests, with the first term attempting to reduce effort and the second term attempting to reduce error. The second term on the right side of eq.(7.12) is the standard adaptive control

law and is required for Lyapunov stability analysis. This second term adapts the parameters based on the trajectory tracking error. The first term on the right side of eq.(7.12) is the assist-as-needed modification of standard adaptive control law. This term decays the torque output with a time constant τ.

Lyapunov stability analysis of the adaptive, AAN control scheme is provided in Appendix A. The human torque component in the AAN controller is certainly time dependent. The presence of time dependent human torque component results in an overall control system that is not globally asymptotically stable. However, the AAN controller can be shown to exhibit uniform ultimate boundedness, with the tracking errors limited by the bounds of the system dynamics and by the bounds of the torque output from the human subject (Appendix A).

7.4. Experimental Protocol

Three healthy, neurologically intact subjects (Table 4-1) gave written informed consent and participated in the preliminary study. This experimental protocol was approved by The University of Auckland, Human Participants Ethics Committee (Appendix D).

The subjects were asked to walk within the passive (unpowered or zero assistance mode) robotic orthosis for 20 minutes so that they should become familiar with the robotic orthosis and training environment. Similar procedure was repeated for the robotic orthosis in trajectory tracking (active) mode. Hip and knee sagittal plane physiological gait trajectories, reported by *Winter* in [3], were used to define the reference joint angle trajectories. These joint angle trajectories are scalable in time, amplitude offset and range in order to adjust it to the individual gait parameters of subjects. Walking speed was set to 0.6 m/s during all experiments. Sensor data for all the experiments was collected at 1 KHz. No BWS was used during the experiments, as the test subjects had no neurologic impairments and did not require any external support [105, 132]. The following experimental protocol was developed to evaluate the performance of AAN control scheme.

7.4.1. Trajectory following experiment

During the first experiment, the subjects were asked to track the reference joint angle trajectories in a passive robotic orthosis (zero assistance mode). During the zero assistance mode, the robotic orthosis was operated in the *zero impedance* or *zero force* mode. The terms

of *backdrive* [65], *patient-in-charge* [39], and *zero-impedance* control [37] have also been used for this zero assistance mode in literature. In this mode, the robotic gait training orthosis balanced its own weight and the net torque at the joint level was zero. Visual feedback was used to show the subjects their tracking performance and encourage them to track the reference trajectories. After the initial 20 minute session, the data for 60 GC during the trajectory tracking mode was recorded for analysis purpose. During the second experiment, (position control or trajectory tracking mode) the subjects were instructed to remain passive within the robotic orthosis and allow it to guide the trajectory of their legs during the AAN control mode. The forgetting rate τ for the AAN controller was chosen by trial and error. The value of τ was slowly decreased until the controller could no longer move the subject's limbs on reference trajectories. This position control mode is important for the gait training of severely impaired subjects who cannot voluntarily participate towards the gait training process. Visual feedback was not used during the trajectory tracking mode. The value of forgetting rate, $\tau = 8\text{s}$ or $(1/\tau = 0.125)$ that can still guide the subject's limbs on reference trajectories was used for subsequent AAN experiments.

7.4.2. AAN experiment

One more experiment was designed to evaluate if the AAN control scheme could learn the torques necessary to assist the subjects in achieving the desired ranges of motion, while allowing the subject to remain as actively involved in the motions as possible. For the first condition, (always active mode) visual feedback was used, and the subjects were asked to track the reference joint angle trajectories for 60 GC. The aim of always active mode was to see if the AAN control can learn the torques necessary to aid the subjects in tracking the joint angle trajectories, while allowing the subjects to be more actively involved in the gait training process. For the second condition, (*inactive to active mode*) the subjects were instructed to remain passive within the robotic orthosis and allow it to guide the trajectory of their legs during the first 20 GC. During these 20 GC, the controller learned the model of the torques necessary to guide the subject's limbs on reference trajectories. After the first 20 GC, the subjects were asked to actively track the joint angle trajectories while using visual feedback for 40 GC. The objective of inactive to active mode was to determine if the controller can reduce its torque output (T_{rob}) to allow more voluntary participation from the subjects.

7.4.3. Data analysis

To study the inter subject variability, standard deviation over the values for different GC for each separate experimental mode for the sagittal plane maximum joint angular deviations ($|\breve{\theta}_{hip}|_{max}$, $|\breve{\theta}_{knee}|_{max}$) and sagittal plane robotic joint torques $|T_{rob}|$ was assessed. All the statistical tests were performed using Matlab- R2009b (The MathWorks, Inc: Natick, Ma, USA).

7.5. Experimental Results

An adaptive AAN control scheme was developed for the robot assisted gait training. The AAN control scheme works on the basis of adaptive control law and provides the robotic gait training according to the disability level of neurologically impaired subjects. Two experiments were designed to evaluate the AAN control scheme. In the first experiment known as trajectory following experiment, the performance of the robotic orthosis was evaluated to see whether the robotic orthosis is capable of guiding the subjects' limbs on reference joint angle trajectories, even when the subjects are not capable enough for completing these movements. In the second experiment, the AAN control scheme was evaluated in terms of allowing the subjects to participate more voluntarily in the gait training process. The AAN control scheme should decay the robot applied torques if the subjects have the ability to track the desired trajectories.

7.5.1. Trajectory following experiment

The desired and measured hip and knee sagittal plane joint angle trajectories during position control mode are shown in Fig. 7-3. The subjects were instructed to remain passive during the position control mode and not to contribute any motions towards the robotic gait training process. The position control mode was evaluated with no forgetting rate ($\tau = \infty$), as well as with a forgetting rate ($\tau = 8s$) included in the AAN controller, to evaluate the effect of the forgetting rate. The presented results (Fig. 7-3) are for the minimum value of forgetting rate ($\tau = 8s$) that can still provide sufficient robotic assistance to guide the subject's limbs on reference trajectories. This minimum value of the forgetting rate was also used in the AAN experiments. The trajectories (Fig. 7-3) were averaged over all subjects for two GC. The angular deviations ($|\breve{\theta}_{hip}|_{max}$, $|\breve{\theta}_{knee}|_{max}$) form the reference joint angle trajectories averaged over all subjects are provided in Table 7-1 (mean of maximum errors is provided).

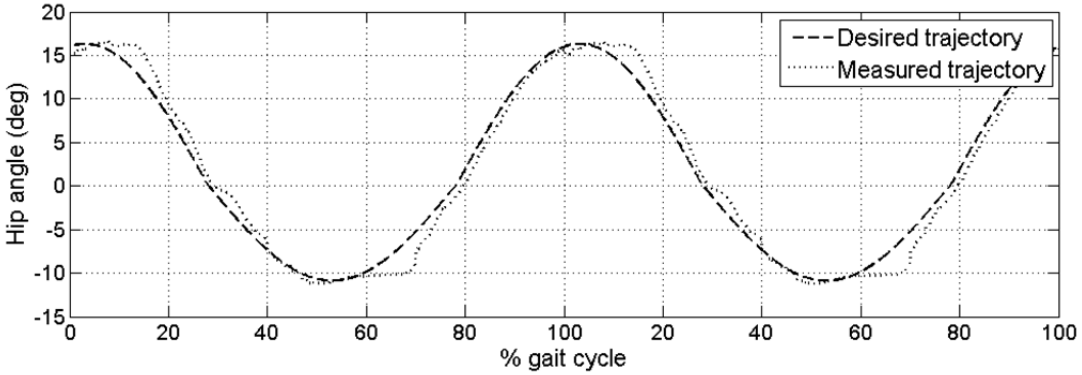

(a)

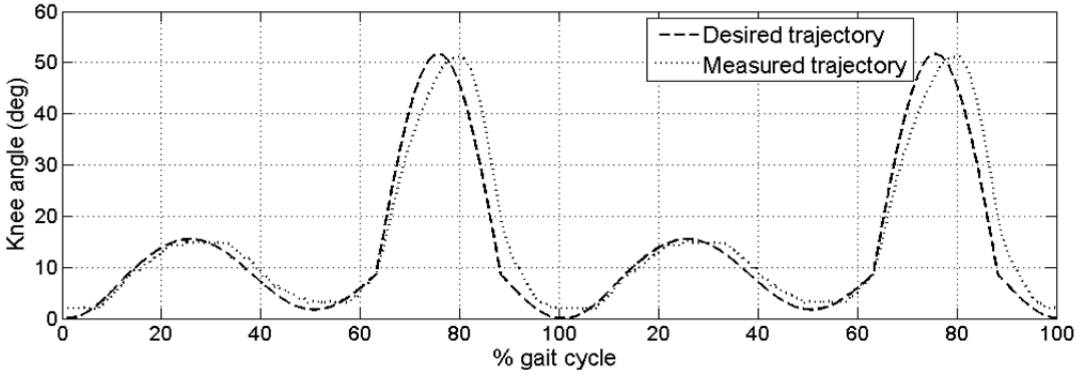

(b)

Figure 7-3. Average hip and knee sagittal plane joint angle trajectories with healthy subjects as a percentage of GC obtained during position control mode (trajectory tracking), averaged over all subjects for two GC. The deviations from the reference trajectories were kept to be minimum. The shown trajectories are for the values of forgetting rate ($\tau = 8s$) that still allows the robotic orthosis to move the subjects' limbs on reference trajectories. (a) Hip joint. (b) Knee joint.

During position control mode the maximum allowable angular deviations from desired hip and knee joint angle trajectories were below 10^{o} (maximum mean values depicted in Table 7-1). The mean values of robotic assistance ($|T_{rob}|$) averaged over all subjects during position control mode are presented in Table 7-1. With an inclusion of forgetting term ($\tau = 8s$), a decrease in robotic assistance was observed (*i.e.* 33.1 Nm to 26.3 Nm for hip joint and 31.21 Nm to 21.1 Nm for knee joint) for all subjects compared to the condition during which the forgetting term was not included ($\tau = \infty$) (values depicted in Table 7-1).

The desired and measured hip and knee joint angle trajectories during the zero assistance mode averaged over all subjects for two GC are shown in Fig. 7-4. The magnitude of angular deviations (trajectory tracking errors) during the zero assistance mode was higher compared to the position control mode (values depicted in Table 7-1). The reason behind the increase in angular deviations is that the robotic orthosis is passive, and subjects have more freedom to

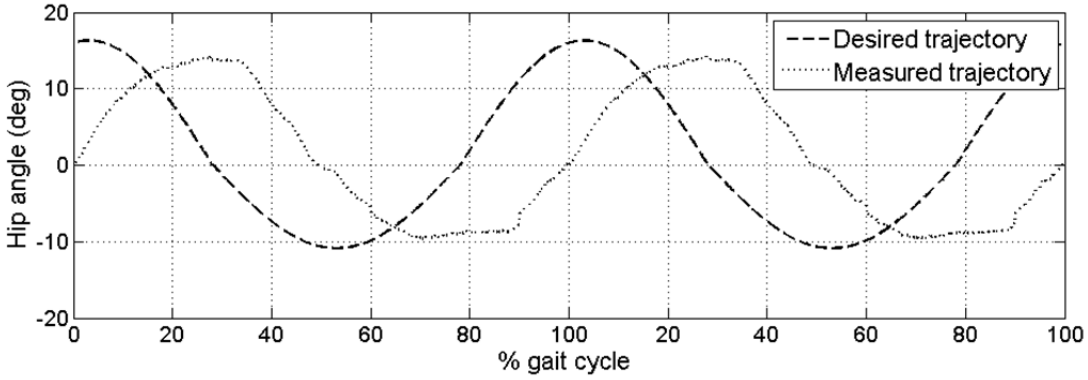

(a)

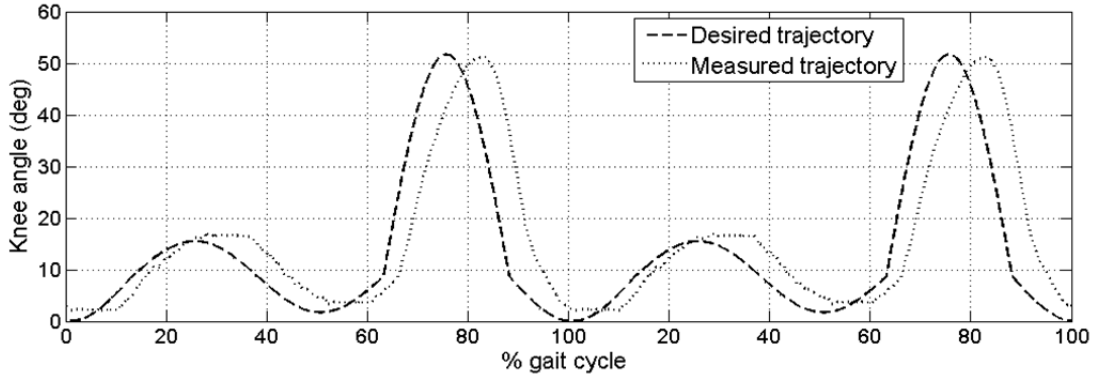

(b)

Figure 7-4. Average hip and knee sagittal plane joint angle trajectories with healthy subjects as a percentage of GC obtained during zero-impedance control or backdrive mode, averaged over all subjects for two GC. No robotic assistance was provided during this mode. (a) Hip joint. (b) Knee joint.

Table 7-1. Maximum Absolute Values of sagittal plane Joint Angular Deviations and Mean values of the controller output joint torque for Different Control Modes and Averaged Over Subjects during trajectory following experiment. The joint torque is the rough indicator of the robotic assistance provided to the subjects. Standard Deviations (±) are presented for within subject variability.

Gait parameter	Zero assistance mode	Position control mode	
		$\tau = \infty$	$\tau = 8s$
$\lvert\breve{\theta}_{hip}\rvert_{max}$	$18.78^{o}\pm7.5$	$2.96^{o}\pm1.7$	$4.22^{o}\pm2.1$
$\lvert\breve{\theta}_{knee}\rvert_{max}$	$28.24^{o}\pm10.2$	$6.31^{o}\pm2.05$	$7.1^{o}\pm2.5$
$\lvert T_{rob,hip}\rvert$	0	33.1 Nm±2.2	26.3 Nm±1.8
$\lvert T_{rob,knee}\rvert$	0	31.21 Nm±1.9	21.1 Nm±1.6

voluntarily drive the robotic orthosis. The purpose of the zero impedance control mode was to evaluate whether the robotic orthosis allows full range leg motions or not, therefore the deviations from reference joint angle trajectories should not be considered as trajectory

tracking errors. Furthermore, the deviations from reference trajectory can be explained due to individual differences among subjects (The reference trajectory was obtained from another subject). The robotic orthosis net torque at the joint level was zero during the zero assistance mode (Table 7-1).

7.5.2. AAN experiment

The AAN experiment was also performed for two modes. During the always active mode, the subjects were actively participating in the gait training process. The second condition of inactive to active mode was evaluated to see whether the robotic orthosis can reduce the applied joint torques if the subjects are actively participating in the gait training process. Both the always active and inactive to active modes were evaluated with no forgetting rate ($\tau = \infty$) and a forgetting rate ($\tau = 8s$) included in the AAN controller to evaluate the effect of forgetting rate. For the AAN experiment, the maximum joint angle deviations from the reference trajectories were also kept below 10^o by the robotic orthosis.

The robotic orthosis joint torques (T_{rob}) during the always active mode and inactive to active mode are shown in Fig. 7-5 and 7-6, respectively. With an inclusion of the forgetting term in the AAN controller, the robotic assistance (T_{rob}) decreased during the always active mode (Fig. 7-5), whereas without a forgetting term, the robotic orthosis applied higher joint torques, despite the fact that the subjects were actively contributing in the gait training process. The magnitude of maximum values of these robot applied joint torques averaged over all subjects are provided in Table 7-2.

In order to show that the robotic assistance decreases during AAN gait training, the robot torques (T_{rob}) during the inactive to active mode averaged over all subjects is presented for two GC (Fig. 7-6). During the GC1, the subjects were inactive and were not voluntarily participating in the robotic gait training process. During the GC2, the subjects were actively contributing in order to achieve the desired trajectories (Fig. 7-6). When the forgetting term ($\tau = 8s$) was included in the AAN controller, the robot applied torque decreases as the subjects started to participate in the robotic training process (Fig. 7-6). Without a forgetting term ($\tau = \infty$) the robot applied torques did not show a decreasing trend during the inactive to active mode. In other words, the robotic orthosis torque during the inactive to active mode without a forgetting term (Fig. 7-6) showed a similar pattern as observed in the always active mode without a forgetting term (Fig. 7-5). This shows that without the forgetting term, the

robotic orthosis did not decay the assistance torque (T_{rob}) during the AAN experiment and hence resulted in a reduction of the voluntary participation from the human subjects. The robotic assistance during the inactive to active mode (Fig. 7-6) converged to a steady state value, depending upon the value of forgetting rate and the amount of voluntary participation from the human subjects.

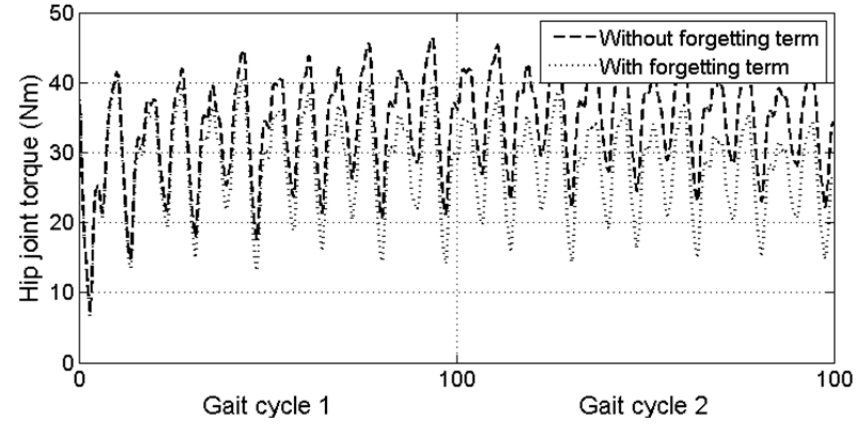

(a)

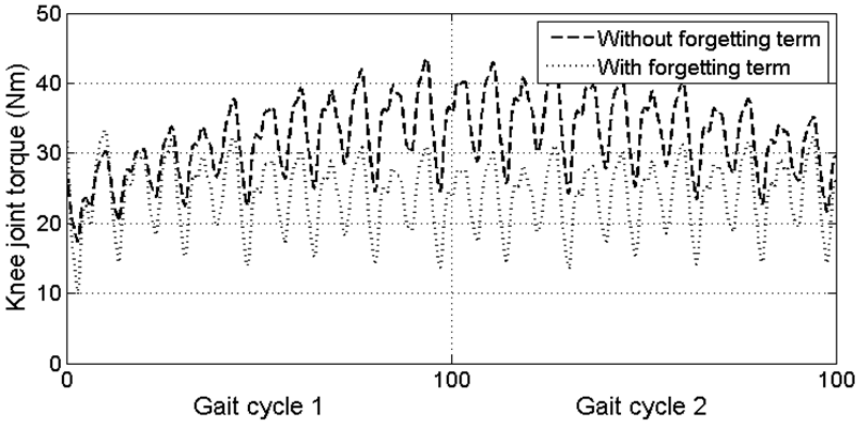

(b)

Figure 7-5. Robot applied torque at hip and knee sagittal plane joints of healthy subjects as a percentage of GC obtained during AAN experiment for always active condition, averaged over all subjects for two GC. Trajectories with a forgetting term ($\tau = 8s$) and without a forgetting term ($\tau = \infty$) are shown. (a) Hip joint. (b) Knee joint.

The maximum values of robotic assistance torque ($|T_{rob}|_{max}$) averaged over all subjects during the always active mode and inactive to active mode are presented in Table 7-2. For always active and inactive to active modes, values of only GC2 (Fig. 7-5 and 7-6) are presented (Table 7-2). With an inclusion of forgetting term, a decrease in robotic assistance was observed for all subjects as compared to the condition during which the forgetting term was not included ($\tau = \infty$) (values depicted in Table 7-2). The maximum mean values of

trajectory tracking errors averaged over all subjects during the always active mode and inactive to active mode are presented in Table 7-2 (error values of only GC 2 are provided). It was ensured during the AAN experiments that the deviations from reference joint angle trajectories must be below 10^{o}. If the trajectory tracking errors go beyond 10^{o}, the robotic orthosis should enhance its assistance torque.

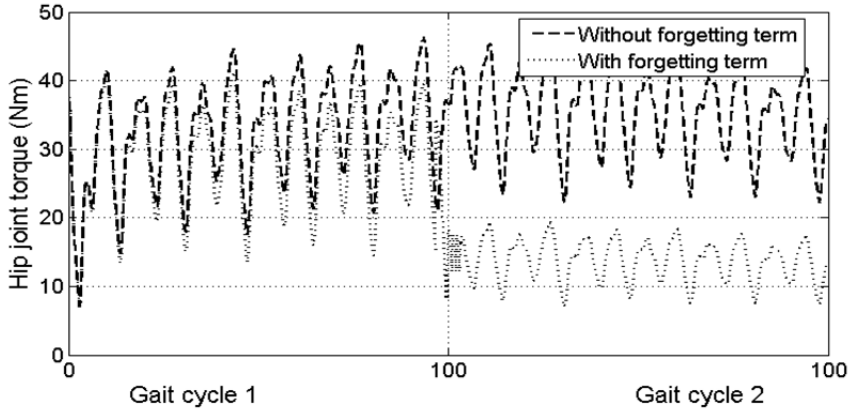

(a)

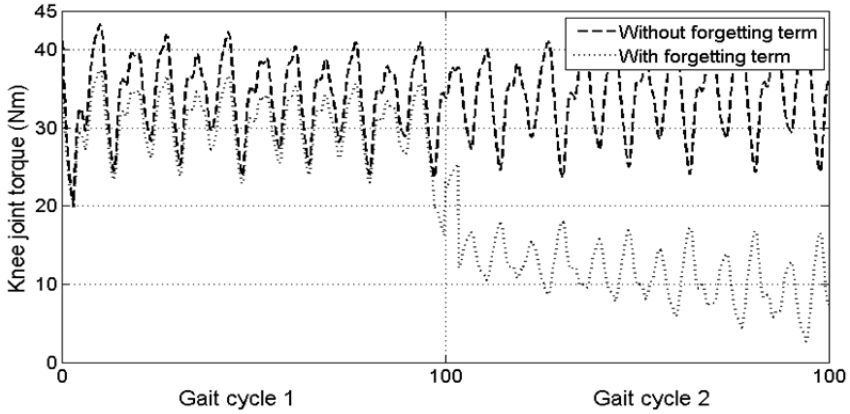

(b)

Figure 7-6. Robot applied torque at hip and knee sagittal plane joints of healthy subjects as a percentage of GC obtained during AAN experiment for inactive to active condition, averaged over all subjects for two GC. Trajectories with a forgetting term ($\tau = 8s$) and without a forgetting term ($\tau = \infty$) are shown. The subjects' remained inactive (passive) during GC1. At the end of GC1 the subjects' participated actively in the gait training process during GC2. (a) Hip joint. (b) Knee joint.

Table 7-2. Maximum Absolute Values of sagittal plane Joint Angular Deviations and Maximum value of the controller output joint torque for Different Control Modes and Averaged Over Subjects during assist-as-needed experiment. The joint torque is the rough indicator of the robotic assistance provided to the subjects. Standard Deviations (±) are presented for within subject variability. Values for GC2 presented in Fig. 7-5 and 7-6 are provided.

Gait parameter	Always active mode		Inactive to active mode	
	$\tau = \infty$	$\tau = 8s$	$\tau = \infty$	$\tau = 8s$
$\lvert\breve{\theta}_{hip}\rvert_{max}$	$3.16^{o}\pm2.4$	$6.52^{o}\pm1.82$	$4.62^{o}\pm3.71$	6.13 ± 2.9
$\lvert\breve{\theta}_{knee}\rvert_{max}$	$5.22^{o}\pm3.52$	$6.5^{o}\pm1.73$	$5.84^{o}\pm2.3$	6.95 ± 2.8
$\lvert T_{rob,hip}\rvert_{max}$	46.3 Nm±3.1	38.1 Nm±2.6	44.6 Nm±2.7	19.5 Nm±3.2
$\lvert T_{rob,knee}\rvert_{max}$	42.51 Nm±2.4	31.1 Nm±3.2	40.5 Nm±3.7	18.2 Nm±4.6

7.6. Discussion and Conclusion

In this work, an adaptive AAN controller was developed for the robot assisted gait training of neurologically impaired subjects. This controller provides seamless adaptive robotic assistance according to the disability level and stage of rehabilitation of neurologically impaired subjects. We believe that this kind of adaptive AAN robotic gait training is important for neurologically impaired subjects in order to maximize the therapeutic efficacy. A six DOF intrinsically compliant robotic orthosis was used to evaluate the performance of the adaptive AAN controller during the treadmill walking task (Chapter 2).

The adaptive AAN controller uses a CRVC control law as the basic position controller in order to provide reasonable trajectory tracking performance in the presence of structured uncertainties in the model of PMA. During position control mode, the maximum angular deviations from desired hip and knee joint angle trajectories must be below 10^{o}. These angular deviations are partly due to the structured uncertainties in the model of PMA [126]. However, this performance is in accordance with the other gait rehabilitation orthoses, such as LOKOMAT, for which the maximum trajectory tracking errors during the position control mode must be below 15^{o} [37]. The position control mode is important for the severely impaired subjects who are not capable of voluntarily participating in the gait training process during the early phases of rehabilitation. During the zero assistance mode, the angular deviations were higher compared to the position control mode. This phenomenon was observed, because the robotic orthosis was completely passive during the zero assistance

mode, and the subjects have the liberty to drive the robotic orthosis freely. This phenomenon has also been reported for the zero assistance mode of LOKOMAT [37].

The AAN controller works on the basis of an adaptive control law that learns in real time the subject's disability level and the voluntary participation. The AAN controller takes input in the form of trajectory tracking error and adjusts the robotic assistance to meet the needs of individual subjects based on their disability level and stage of gait rehabilitation. The model based component of the controller adapts in real time the robotic assistance, depending on the trajectory tracking errors. If tracking errors are small, the controller decays the robotic assistance and let the subjects complete the desired movements and vice versa. It was observed during the AAN experiment that the inclusion of forgetting factor in the adaptive AAN control scheme resulted in a variation in robot applied joint torque, depending on the subjects' voluntary participation. When the forgetting rate was not included in the adaptive AAN control scheme, the robotic orthosis did not decay the applied torques, even when the subjects were actively contributing towards the gait training process.

The adaptive AAN controller developed in this study is proven theoretically stable by using a Lyapunov-based stability analysis (Appendix A). The adaptive AAN controller implemented for the robotic gait training orthosis has the human torque component that is certainly time dependent. The presence of time dependent human torque component results in a system that is not globally asymptotically stable. However, the controller was shown to exhibit uniform ultimate boundedness, with the tracking errors limited by the bounds of the system dynamics and by the bounds of the torque output from the human subject. It was found experimentally that the controller who uses eq.(7.8) will converge to steady state tracking errors.

7.6.1. Related work and significance of present work

Various AAN robotic gait training strategies have been previously reported in literature [1, 6, 36, 79]. The most notable work regarding the AAN robotic gait training has been reported by the developers of LOKOMAT [37] and ALEX [6]. LOKOMAT's AAN gait training [37] is based on impedance control [66]. However, LOKOMAT was not originally built to function as an impedance controlled device [79]. The impedance values for the LOKOMAT assisted gait training are chosen by the physical therapist, which presents a problem in terms of providing seamless AAN gait training [66]. A force field control scheme [42, 109] has also been implemented by the developers of ALEX [6] and LOKOMAT [14,

71]. A similar decision by the physical therapist during the ALEX and LOKOMAT force field control scheme is also required [6]. The seamless AAN controller developed in this study can automatically adapt the robotic assistance in real time, according to the disability level and voluntary participation of human subject.

The LOKOMAT's impedance controller, force field controller [71], and ALEX's force field controller [6] also utilizes a feedforward term or a fixed dynamic model for gravity compensation [37]. This feedforward term or fixed model needs to be manually readjusted for individual subject according to his/her anthropometric parameters [65]. Also, this approach is not useful when the subjects have the capability to move their limbs against gravity during the later stages of gait rehabilitation. The AAN controller developed in this study provides a mean to automatically create the feedforward term across the joint space in real time, as well as automatically reduces it, as the subject contributes more towards the robotic gait training process. The LOKOMAT's impedance controller is also effectively valid for the swing phase of GC, as the load cell data used to estimate the human-robot interaction torque component is corrupted during the stance phase due to the horizontal ground reaction forces [37]. Contrary to the impedance control of LOKOMAT, the AAN controller developed in this study only works on the basis of kinematic data and is hence valid for the complete GC (100% GC). It is important to mention here that the available robotic gait training orthoses [6, 37] use force sensors to estimate human-robot interaction. The use of force sensors may limit the place and degree of interaction as well as increase the cost of robotic gait training orthoses [72]. The adaptive AAN control scheme developed in this work estimates the human-robot interaction without the use of force/torque sensors.

The impedance controller of LOKOMAT extracts the subject's active joint moment contributions from the remaining passive and kinetic effects by using an inverse dynamics algorithm [37]. The lower limb joint stiffness relationship [112, 113] used in the inverse dynamics algorithm [37] is most likely not quantitatively identical to that observed in a particular user. Contrary to the LOKOMAT's inverse dynamics algorithm, the adaptive AAN control scheme developed in this work presents a more generalized approach of the subject's voluntary (active) participation estimation as it only works on the basis of kinematic error.

PAM and POGO have used the concept of *triggered assistance* for providing AAN gait training [46]. However, this approach breaks the movement into a subject driven part and a robot driven part, rather than providing a seamless level of adaptive robotic assistance. In this

work we have developed a seamless adaptive control scheme for a PMA powered robotic orthosis in order to provide AAN gait training.

It is important to mention here that a seamless adaptive AAN control algorithm has also been developed for Pneu-Wrex by *Wolbrecht et al.* in task space for upper limb rehabilitation [65, 167]. Pneu-Wrex is a robotic orthosis for upper limb rehabilitation and is powered by pneumatic cylinders (cylinder- piston arrangement) [65, 167]. The AAN controller developed in the present study was implemented in joint space whereas the AAN control scheme for Pneu-Wrex has been implemented in task space. The adaptive AAN controller used in this study is different from the controller used by *Wolbrecht et al*. in a way that a PD controller has been used as a basic position controller for Pneu-Wrex [65, 167]; whereas in this study the robust CRVC was used as the basic position controller (Chapter 4). It was necessary to use the robust CRVC as the basic position controller in the overall AAN control scheme because of the structured uncertainties in the numerical model of PMA [129, 134].

7.6.2. Conclusions

This chapter presents a seamless adaptive AAN control scheme for the robot assisted gait training of neurologically impaired subjects. The overall AAN control architecture works on the basis of robust adaptive control scheme. The AAN control scheme learns in real time the disability level and effort of the human subject, and adapts the robotic assistance accordingly. The presented control scheme for seamless, adaptive AAN gait training was successfully evaluated on neurologically intact subjects. The experimental results showed that the robotic orthosis can adapt the applied joint torques based on the trajectory tracking errors, in a seamless manner. In order to establish the therapeutic efficacy of the adaptive, AAN gait training strategy, rigorous clinical trials with neurologically impaired subjects are necessary. This work will also help in further developing adaptive, AAN gait rehabilitation strategies for robotic orthoses powered by intrinsically compliant actuators.

Chapter 8. Conclusions

Robot assisted gait training may help in producing rapid improvements in functional gait parameters [168-170] of the subjects suffering from neurologic impairments, such as stroke [6, 81, 92] and SCI [37, 80, 109]. The robotic orthoses relieve the physical therapist from the laborious task of manual assistance and helps in delivering well controlled repetitive and prolonged gait training sessions at a reasonable cost [1, 2]. The subjectivity of manual assistance is eliminated by providing objective measurements of interaction forces and limb movements to assess the quantitative level of motor function recovery [2]. In this research, an intrinsically compliant and back-drivable robotic orthosis for gait rehabilitation of neurologically impaired subjects was developed. The robotic orthosis has six DOFs that allow naturalistic gait pattern. Hip and knee sagittal plane rotations of the robotic orthosis are powered by the antagonistic actuation of PMA.

A new trajectory tracking control scheme was developed to guide the subjects' limbs on reference physiological trajectories. This scheme is designed for the initial phases of gait rehabilitation of wheel chair bounded subjects. The proposed control scheme allows the robotic orthosis joint compliance to be controlled independently of the trajectory tracking control. The trajectory tracking control scheme works on the basis of robust control laws for handling the structured uncertainties that exist in the model of PMA. Two robust control laws, namely the BASMC and the CRVC, were proposed to guide the subjects' limbs to follow the defined reference physiological trajectories. Preliminary experiments of the trajectory tracking controller were performed on neurologically intact subjects. The robust control laws were able to guide the subjects' limbs on reference physiological trajectories with bounded tracking errors. The trajectory tracking performance of the robust control laws is in accordance with the trajectory tracking performance of commercial gait rehabilitation orthoses, such as LOKOMAT [37]. The CRVC carries all the advantages of the BASMC and mitigated the chattering effect by utilizing a novel feedback function that is continuous in time domain. The CRVC control law is smoother than the BASMC, eliminating the sliding manifold information using *signum* or *saturation* function. For that reason, the CRVC was used as a basic trajectory tracking (position) controller for the implementation of impedance and seamless adaptive, AAN controllers.

The 2-D dynamic model of the robot orthosis and the 2-D human lower limb musculoskeletal dynamic model were established to study the dynamic interaction between the device and subjects. These two models were used along with a custom inverse-dynamics algorithm [3, 107] and a quadratic minimization algorithm [144] to identify muscle activation patterns during robot assisted gait. The study of dynamic interaction between the device and subjects is vital for the design and control of robotic orthosis [39, 79]. The information obtained from the interaction of these models is also important for proper elucidation of clinical studies involving robotic gait training orthoses [108, 138, 139].

The trajectory tracking control of robotic orthosis forces the subject's limbs on predefined trajectories without taking into account his/her disability level [36, 37]. The disability level of subjects suffering from neurologic impairments varies from subject to subject and also for the same subject during the course of rehabilitation. The disability level of each subject need to be estimated, and the robotic orthosis torque needs to be adjusted accordingly so that the subject can contribute more towards the rehabilitation process [109]. Impedance control architecture was proposed and developed for providing interactive robotic gait training according to the disability level of neurologically impaired subjects. The CRVC was used as the basic position controller in the overall impedance control architecture. The robotic orthosis was operated in four gait training modes, namely position control, zero-impedance control, non-zero-impedance control with high compliance, and non-zero-impedance control with low compliance to evaluate the performance of impedance control scheme. Preliminary experiments of the impedance controller were performed on neurologically intact subjects. The experimental results show that an increase in robotic compliance encouraged the subjects to participate more actively towards the gait training process.

Impedance control of conventional robotic gait training orthosis [36, 37, 41] has several limitations. This research developed AAN control architecture for providing seamless adaptive robotic assistance during gait training process. The CRVC was used as the basic position controller in the overall adaptive AAN control scheme. The adaptive AAN controller takes into account the subject's disability level and voluntary participation, and adapts the robotic assistance accordingly, in a seamless manner in real time. The AAN controller takes input in the form of trajectory tracking error and adjusts the robotic assistance to meet the needs of individual subjects based on their disability level and stage of gait rehabilitation. The model based component of the controller adapts the robotic assistance in real time, depending on the trajectory tracking errors. If tracking errors are small, the controller decays

the robotic assistance and let the subjects complete the desired movements, and vice versa. An AAN experiment was designed to evaluate that whether the robotic orthosis can increase or decrease the assistance based on the extent of voluntary participation from human subjects. Preliminary experiments were performed with neurologically intact subjects to evaluate the performance of adaptive AAN control scheme. The experimental results were encouraging and show that the seamless, adaptive AAN controller is capable of varying the robotic assistance based on trajectory tracking errors in real time. This research is a step forward in the design and AAN control of robotic gait training orthoses powered by intrinsically compliant actuators.

8.1. Contributions

The major scientific contribution of this research includes the combination of an intrinsically compliant robotic orthosis mechanism with an AAN control scheme for providing seamless, customized robotic assistance. The contributions are further detailed as follows:

8.1.1. Robotic orthosis design

During the course of this research, the first prototype of an intrinsically compliant and back-drivable robotic gait training orthosis was developed. The robotic orthosis prototype provides a realistic stepping experience. PMA were used in the robotic orthosis design for powering the hip and knee sagittal plane rotations. PMA are intrinsically compliant and are suitable for providing safe contact with neurologically impaired subjects during the robot assisted gait training. According to the author's best knowledge, no multijoint intrinsically compliant robotic orthosis powered by PMA has been developed before for treadmill training of neurologically impaired subjects. The robotic orthosis powered, by intrinsically compliant actuators, is important for gait rehabilitation, because it allows after-effects to be measured [89]. More generally, a wide range of dynamic environments can be created by using the intrinsically compliant robotic gait training orthosis [2].

8.1.2. Trajectory tracking control

The purpose of the robotic gait training orthosis is to guide the limbs of severely impaired subjects on reference physiological trajectories. During the course of this research, a trajectory tracking control scheme based on the robust control laws was developed in order to

guide the subject's limbs on reference physiological trajectories, in the presence of structured uncertainties in the model of PMA. The novelty of the proposed control scheme is that the robotic orthosis joint compliance can be controlled independently of the trajectory tracking control. The trajectory tracking control scheme was successfully evaluated on neurologically intact subjects.

8.1.3. Modeling muscle activation patterns during robot assisted gait

The first ever dynamic models of robot assisted gait were developed in order to study the muscle activation patterns and the effect of cadence regulation on muscle activation patterns. A 2-D musculoskeletal model of human gait was developed along with a 2-D model of robotic orthosis. These models were used along with a custom inverse-dynamics algorithm [107] and a quadratic minimization algorithm [144] to identify muscle activation patterns during robot assisted gait. The information obtained from this simulation is important for proper elucidation of clinical studies involving robotic gait training orthoses [39, 79, 108, 138, 139].

8.1.4. Impedance control for interactive gait training

In order to overcome the limitations of impedance control of existing robotic gait training orthoses [36, 37, 41], an impedance control scheme was developed to provide interactive robot assisted gait training. The impedance control law modifies the robotic assistance based on the human subject's active joint torque contributions. Different levels of compliance can be selected by the physical therapist during the impedance control scheme according to the disability level and stage of rehabilitation of neurologically impaired subjects. The impedance control scheme was successfully evaluated on neurologically intact subjects. All the subjects showed greater deviations from the reference joint angle trajectories with an increase in robotic compliance. This happened because the impedance control scheme helped in enhancing subjects' voluntary participation in the gait training process. According to the author's best knowledge, the impedance control of robotic gait training orthoses powered by PMA has not been reported in literature before.

8.1.5. Assist-as-Needed control

In order to overcome the limitations of impedance control [36, 37, 41] and other AAN [6, 46, 132] control schemes, a new seamless adaptive, AAN control scheme was developed for the robot assisted gait training. The seamless adaptive, AAN control scheme estimates the

disability level of neurologically impaired subjects based on the kinematic error and adapts the robotic assistance accordingly. The presented control scheme for seamless adaptive, AAN gait training was successfully evaluated on neurologically intact subjects. The experimental results showed that the robotic orthosis can adapt the applied joint torques based on the trajectory tracking errors, in a seamless manner in real time. According to the author's best knowledge no seamless adaptive, AAN robotic gait training strategy has been reported in literature before.

8.2. Limitations

BWS was not used during all experiments presented in this thesis, as the test subjects had no neurologic impairment and did not require any external support. The use of BWS can be neglected during the evaluation of robotic gait training orthosis if the subjects have no neurologic impairments [105, 132]. However, BWS is required for the robot assisted gait training of neurologically impaired subjects. A fixed treadmill speed was used during all the presented experiments. In order to further enhance the voluntary participation of human subjects, the treadmill speed may be adapted according to individual subject's disability level and intention. A method for automatic treadmill speed adaptation has been proposed by Zitzewitz *et al.* [48]. Also, a fixed gait pattern recorded for a healthy subject was used during all experiments. This fixed pattern may not be suitable for the subjects having different types and levels of neurologic impairments. Different algorithms for automatic gait pattern adaptation have been proposed by Jezernik *et al.* [36]. The extent of adaptation of reference gait pattern is an important clinical research question with regard to robot assisted gait rehabilitation [37, 42]. A maximum kinematic error (trajectory tracking error) of 10^{o} was allowed during the AAN experiments in the present study. The robotic assistance was increased if the trajectory tracking errors go beyond 10^{o} during the AAN experiments. The extent of allowable trajectory tracking error depends on the subject's effort and disability level and is an important clinical research question [37, 42].

The robotic orthosis joints were assumed to be in alignment with the human subjects' anatomical joints during dynamic modeling. The misalignment of robotic orthosis joints with human subject joints is a major concern in the field of rehabilitation robotics. This misalignment can make the robot assisted training uncomfortable [117]. A spring was used to compensate the weight of the robotic orthosis, which will help in reducing the relative slip between the robotic orthosis and human subject anatomical joints [54]. However, this

misalignment still presents a problem and several research groups are working towards the design of robotic orthosis mechanisms that can help in achieving better alignment between robotic orthosis and human subject anatomical joints [117, 160, 171].

8.3. Suggestions for Future Work

In this work, an intrinsically compliant robotic orthosis and adaptive, AAN gait training strategies were developed and experiments were conducted with neurologically intact subjects. As this is a multi-disciplinary project and involves research in the fields of mechanical engineering, biomechanics, and physical therapy, there is an immense possibility of future work in several aspects. Following are some of the suggestions.

In the next design iteration, some of the mechanical design improvements that can be made to the robotic orthosis are: (1) to use light weight carbon fiber material to make the device light and strong, (2) to perform a finite element method (FEM) analysis to improve the design features, (3) to design mechanism that will help in better alignment of human subject anatomical joints with robotic orthosis joints. This will help to adjust the device or change device parameters quickly during the experiment, (4) the actuation of ankle joint can also be included in the improved design if it appears to be crucial from a clinical point of view.

A rigorous clinical study of seamless adaptive, AAN gait training strategy can be conducted with stroke and SCI subjects to explore its efficacy. In order to further enhance the voluntary participation of human subjects, the treadmill speed may be adapted according to individual subject's disability level and intention. Different algorithms for automatic gait pattern adaptation can be designed in order to enhance the voluntary participation of human subjects. Different methods for automatically adapting the body weight of neurologically impaired subjects can also be implemented. Comparison studies between AAN gait training with the robotic orthosis and conventional gait training like BWS treadmill training can also be done. It is important to mention here that such comparisons are difficult to perform as the robotic gait training orthosis kinematically constrains the limbs of human subjects as compared to the manually assisted BWS treadmill training. Also, the energy storing properties of the PMA can be studied in relation to the robotic gait training orthosis.

Appendix A. Stability Analysis of Adaptive Assist-as-Needed Control Scheme

Stability analysis is important for robot-human interaction. This section describes the Lyapunov stability analysis of the adaptive, AAN control scheme (Chapter 7). The analysis is based on the adaptive algorithms developed by *Spong* [166] and *Slotine* [122]. The Lyapunov function candidate considered for this study is

$$V(t) = \frac{1}{2}s^T M s + \frac{1}{2}\tilde{\theta}^T w(1+\lambda)\tilde{\theta} + \frac{1}{2}\Gamma\tilde{\beta}^T\tilde{\beta} \tag{A.1}$$

where s, M, λ, w and Γ are defined in the previous sections and $\tilde{\beta}$ is the parameter error defined as

$$\tilde{\beta} = \hat{\beta} - \beta \tag{A.2}$$

where $\hat{\beta}$ is the estimate of the parameters,β, as previously defined. Differentiating eq.(A.1) along system trajectories gives

$$\dot{V}(t) = \frac{1}{2}s^T \dot{M} s + s^T M \dot{s} + \tilde{\theta}^T w(1+\lambda)\dot{\tilde{\theta}} + \Gamma\tilde{\beta}^T\dot{\tilde{\beta}} \tag{A.3}$$

The system dynamics in eq.(7.1) can be redefined by using the sliding surface *s* in eq.(7.2) and reference trajectory *v* in eq.(7.3)

$$M\dot{s} + Cs + Y\beta = T_{rob} \tag{A.4}$$

Combining eq.(A.2), eq.(A.3) and eq.(A.4) yields

$$\dot{V}(t) = \frac{1}{2}s^T \dot{M} s + s^T\left(T_{rob} - Y\hat{\beta}\right) - s^T C s + \tilde{\theta}^T w(1+\lambda)\dot{\tilde{\theta}} + \tilde{\beta}^T(\Gamma\hat{\beta} + Y^T s) \tag{A.5}$$

Since $\dot{M} - 2C$ is skew symmetric

$$\dot{V}(t) = s^T\left(T_{rob} - Y\hat{\beta}\right) + \tilde{\theta}^T w(1+\lambda)\dot{\tilde{\theta}} + \tilde{\beta}^T(\Gamma\hat{\beta} + Y^T s) \tag{A.6}$$

Using the control law eq.(7.5) and the modified parameter update law eq.(7.12) in eq.(A.6) gives

$$\dot{V}(t) = -\tilde{\theta}^T \lambda w \tilde{\theta} - \dot{\tilde{\theta}}^T w \dot{\tilde{\theta}} - \tilde{\beta}^T \frac{1}{\tau}\Gamma Y^T (YY^T)^{-1} Y\hat{\beta} \tag{A.7}$$

The system is not asymptotically stable because the last term in eq.(A.7) may be positive. However, the system is stable in the form of uniform ultimate boundedness. In order to determine the stable boundary of the system, eq.(A.7) can be rewritten as

$$\dot{V}(t) = -e^T P e - \check{\beta}^T R \hat{\beta} \tag{A.8}$$

where

$$e = [\check{\theta}\ \dot{\check{\theta}}]^T$$

$$P = \begin{bmatrix} \lambda w & \vdots & 0 \\ \cdots & \vdots & \cdots \\ 0 & \vdots & w \end{bmatrix}$$

$$R = \frac{1}{\tau}\Gamma Y^T (Y Y^T)^{-1} Y$$

$\dot{V}(t) < 0$ when

$$e^T P e > -\check{\beta}^T R \hat{\beta} \tag{A.9}$$

which occurs whenever

$$\varsigma_{min}(P)||e||^2 > \max_{\hat{\beta}}(-\check{\beta}^T R \hat{\beta}) \tag{A.10}$$

where $\varsigma_{min}(P)$ is the minimum eigenvalue of P. The maximum of $-\check{\beta}^T R \hat{\beta}$ occurs when

$$\hat{\beta} = \frac{1}{2}\beta \tag{A.11}$$

Using eq.(A.11) into eq.(A.10) and solving for $||e||$ using the definition of *R* gives

$$||e|| > \frac{1}{2}\left(\frac{\beta^T R \beta}{\varsigma_{min}(P)}\right)^{1/2}$$

$$= \frac{1}{2}\left(\frac{1}{\tau}\frac{\beta^T \Gamma Y^T (Y Y^T)^{-1} Y \beta}{\varsigma_{min}(P)}\right)^{1/2} \tag{A.12}$$

Equation eq.(A.12) represents the boundary of the closed loop system by defining the maximum error for $\dot{V}(t) > 0$. Larger magnitude of e will have $\dot{V}(t) < 0$ and thus the closed loop human-robot system will converge to this boundary. The magnitude of error e will be small when the robot forgetting rate $1/\tau$ is small. So as $\tau \to \infty$ the adaptive controller remembers all it has learned about the parameters so that $e \to 0$. As $\varsigma_{max}(\Gamma Y^T (Y Y^T)^{-1} Y) = \varsigma_{max}(\Gamma)$, eq.(A.12) can be written as

$$||e|| > \frac{1}{2}|\beta|\left(\frac{1}{\tau}\frac{\varsigma_{max}(\Gamma)}{\varsigma_{min}(P)}\right)^{1/2} \tag{A.13}$$

Equation (A.13) shows that the kinematic tracking error bound is proportional to the actual parameters β of the system.

Appendix B. Bill of Materials

Parts for robotic gait training orthosis came from many sources, some of them were ordered for machining and some were made in the student machine shop. Following is the list of vendors from which most of the parts ordered online came from.

Vendor name	Vendor details	Web	Parts
Shadow Robots	Shadow Robot Company LTD. 251 Liverpool Road London, N1 1LX, UK.	www.shadowrobot.com	Pneumatic muscle actuators, Pressure sensors.
Futek	25 Flinders Parade North Lakes QLD 4509,Australia.	www.futek.com	Tension/Compression load cells.
Matrix	MATRIX S.p.A. C.so Vercelli 330, 10015 Ivrea (TO), Italy	matrix.to.it	2/2 solenoid pneumatic valves.
Landice	Landice, Inc. 111 Canfield Avenue Suite A1 Randolph, New Jersey, USA.	www.landice.com	Rehabilitation Treadmill.
dSPACE	dSPACE GmbH Rathenaustraße 26 33102 Paderborn, Germany.	dspaceinc.com	Dspace processing system.
RS	Auckland, N.Z.	newzealand.rs-online.com	Joint Encoders, amplifiers, resistors, etc.
CMI Springs	P.O.Box 3963 AUCKLAND, N.Z.	cmilimited.com.au	Springs
Walrus Limited	11 Donnor Place, Mt Wellington, Auckland, N.Z.	www.walrus.co.nz	Brace wear

All the metallic parts (aluminium) of the robotic orthosis were fabricated in the Machine Shop in Department of Mechanical Engineering, University of Auckland.

Appendix C. Publication List

The following publications have resulted from the research described in this thesis.

Book Chapter

1. **S. Hussain** and S. Q. Xie, "An Active Orthosis for Gait Rehabilitation," in *Mechatronics*, J. P. Davim, Ed, London, UK. : Wiley, 2011.

Peer Reviewed Journal Papers

2. **S. Hussain**, S. Q. Xie, and G. Liu, "Robot assisted treadmill training: Mechanisms and training strategies," *Medical Engineering & Physics,* vol. 33, pp. 527-533, 2011.
3. **S. Hussain**, S. Q. Xie, P. K. Jamwal, and J. Parsons, "An Intrinsically Compliant Robotic Orthosis for Treadmill Training," *Medical Engineering and Physics,* vol. 34, pp. 1448-1453, 2012.
4. **S. Hussain**, S. Q. Xie, and P. K. Jamwal "Robust Nonlinear Control of an Intrinsically Compliant Robotic Gait Training Orthosis," *IEEE Transactions on Systems, Man, and Cybernetics, Part A: Systems and Humans,* 2012 (In press) DOI: 10.1109/TSMCA.2012.2207111.
5. **S. Hussain**, S. Q. Xie, and P. K. Jamwal, " Effect of Cadence Regulation on Muscle Activation Patterns during Robot Assisted Gait: A Dynamic Simulation Study " *IEEE Transactions on Information Technology in Biomedicine*, 2012 (In press) DOI:10.1109/TITB.2012.2226596.
6. **S. Hussain,** S. Q. Xie and P. K. Jamwal, "An Impedance Controlled Robotic Orthosis for Interactive Gait Training" *IEEE Transactions on Systems, Man, and Cybernetics, Part B: Cybernetics,* 2012 (In press) DOI: 10.1109/TSMCB.2012.2222374.
7. **S. Hussain**, S. Q. Xie, and P. K. Jamwal, "Modeling Muscle Activation Patterns during Robot-Assisted Gait: A Dynamic Simulation Study, " *Computer Methods and Programs in Biomedicine*, 2012 (Under review).
8. **S. Hussain** and S. Q. Xie, "Assist-as-Needed Control of a Robotic Gait Training Orthosis," *IEEE Transactions on Systems, Man, and Cybernetics, Part B: Cybernetics,* 2012*,* 2012 (Under review).
9. **S. Hussain** and S. Q. Xie, "Control of an Intrinsically Compliant Robotic Orthosis for Gait Rehabilitation," *Automatica,* 2012 (Under review).

Peer Reviewed International Conference Papers

10. **S. Hussain** and S. Q. Xie, "Design and Control of a Compliant Active Orthosis for Gait Rehabilitation," *International Conference on Industrial Engineering and Application Shenzhen, China*, 2010.
11. **S. Hussain**, S. Q. Xie, and P. K. Jamwal "A Bio-Inspired Robotic Orthosis for Gait Rehabilitation," *IEEE International Conference on Biomedical Robotics and Biomechatronics, Roma, Italy*, 2012.
12. **S. Hussain** and S. Q. Xie, "Customized Robot Aided Gait Training for NeuroRehabilitation," *International Conference on NeuroRehabilitation, Toledo, Spain, 2012*.

Appendix D. Ethics Approval

CONSENT FORM

(Head of Department)

THIS FORM WILL BE HELD FOR A PERIOD OF 6 YEARS

Project title: Active Orthosis (robot) for Gait Rehabilitation
Name(s) of Researchers(s): Shahid Hussain, Prof. Shane Xie

I have read the Participant Information Sheet; have understood the nature of the research. I have had the opportunity to ask questions and have them answered to my satisfaction. I have given permission for this research on a voluntary basis.

- I grant permission for the researchers to recruit post graduate students and staff members of the department for this research.
- I grant permission for the researchers to advertise their research on departmental notice boards.
- I give assurance that participation/non-participation of students in this research will not affect their grades and relations with the university
- I give assurance that participation/non-participation of staff in this research will not affect their relations with the university
- I understand that this research will require physical interaction with a prototype robotic device.
- I understand that the data will be kept for 6 years, after which they will be destroyed.

Name _____

Signature _____ Date _____

APPROVED BY THE UNIVERSITY OF AUCKLAND HUMAN PARTICIPANTS ETHICS COMMITTEE ON 20/08/2010 for (3) years, Reference Number 2010/308.

CONSENT FORM

(Participants)

THIS FORM WILL BE HELD FOR A PERIOD OF 6 YEARS

Project title: Active Orthosis (robot) for Gait Rehabilitation

Name(s) of Researchers(s): Shahid Hussain, Prof. Shane Xie

I have read the Participant Information Sheet; have understood the nature of the research and why I have been selected. I have had the opportunity to ask questions and have them answered to my satisfaction. I have chosen to participate in this research on a voluntary basis.

- I agree to take part in this research
- I understand that participation in this research will require physical interaction with a prototype robotic device.
- I understand that there is a small possibility of injury should the prototype device malfunction, and I accept this risk.
- I understand that my identity will not be revealed in publications derived from this research.
- I understand that the information related to the experimental trial which I am involved in will be recorded using sensors on the prototype device and stored electronically with secure access.
- I understand that I am free to withdraw participation at any time, and to withdraw any data traceable to me up to three months after the collection of the data.
- I understand that participation in this research will not affect my grades or my relations with the university (where applicable).
- I agree / do not agree to be videotaped.
- I understand that the data will be kept for 6 years, after which they will be destroyed.
- I understand that I am only required to attend one 45 minute experimental trial.
- I agree to be informed of any incidental findings that arise from this research.

Name _____

Signature _____ Date _____

APPROVED BY THE UNIVERSITY OF AUCKLAND HUMAN PARTICIPANTS ETHICS COMMITTEE ON 20/08/2010 for (3) years, Reference Number 2010/308.

PARTICIPANT INFORMATION SHEET

(Head of Department)

Project title: Active Orthosis (robot) for Gait Rehabilitation

Name(s) of Researcher(s): Shahid Hussain, Prof. Shane Xie

Researcher Introduction

This research will be conducted by Shahid Hussain, a PhD student in the Department of Mechanical Engineering. The research is supervised by Prof. Shane Xie, in the Department of Mechanical Engineering.

Project Description and Invitation

This project aims to develop effective control algorithms for a robotic device designed to facilitate gait rehabilitation. The device is intended for use with patients suffering from musculoskeletal injuries at the lower limb or neurological diseases which results in gait functions. In particular, the part of the research where human participation is required is designed to evaluate the performance of the developed control algorithm. At the same time, information regarding the physical characteristics of the human robot interaction will also be identified to facilitate development of the controller and the robotic device.

We are seeking your permission to recruit participants from your department and therefore also the permission to use departmental notice boards for display of our advertisement poster. Potential participants are expected to be primarily post graduate students who have no existing lower limb or gait impairment, staff members however are also welcomed to participate. It is preferred that the participant is familiar or comfortable with the operation of robotic devices. All potential participants will be shown the experimental setup and briefed about the operation of the prototype before they commit to participation in the research.

Should you be willing to grant us the permission to proceed with this research we are also asking for your assurance that participation/non participation of students or staff will not affect their grades (for students) and relation with the university (for both students and staff)

Project Procedures

With the exception for the case where the participant is the researcher, participants will only be required to take part in one experimental trial. The duration of the trial is expected to span approximately half an hour. The experimental trial will be carried out in the Mechatronics laboratory at the University of Auckland's School of Engineering.

Before the experimental trials begin, the user will be given an explanation of the operation of the robotic devices, in particular the safety measures put in place to allow termination of the robot operation should an emergency situation arise. A brief demonstration of the prototype will also be given. The age, gender and body weight of the participant will also be collected so that allow the results can be normalized with respect to the body weight and related to the corresponding demographic groups.

After the briefing and collection of information, the participant's lower limb will be strapped in place on the prototype device. The experimental trials consists of two parts, the first involves the passive movement of the lower limb by the robotic device. During this part of the trial, the participant should relax his/her lower limb on the robotic device and allow the robot to move the lower limb passively along a predefined motion path. During this time, information regarding the orientation of the lower limb and the forces applied on the robot will be logged and analysed to allow computation of the lower limb kinematic and stiffness parameters.

In the second part of the trial, the participant will be required to move his/her lower limb actively in the directions given by the user interface. The robot will provide a resistance against the motion during this part of the trial. Again, sensor information on the robotic device will be logged and analysed. This part of the trial will allow determination of the active forces applied by the lower limb to the robot.

The participants may experience a small level of physical discomfort during a normal trial. However, should the level of discomfort exceeds that of the participant's liking, the participant can terminate the experimental trial by either indicating to the researcher or by using the emergency stop button provided. Since the actuators used in the prototype can produce significant forces, there is a possibility of injury should the hardware or software of the prototype malfunctions. This will be very unlikely as the prototype would have been tested extensively before the commencement of the experimental trial. In addition to that, the researcher or another individual will be present to provide aid if required. To ensure that prompt medical attention is available during emergencies, the trials will be conducted during the operating hours of the University Health Services clinic at the city campus.

Data Storage / Retention / Destruction / Future Use

As discussed in the previous section, data collected will be in the form of sensor readings which are used to compute the motion and force/moment observed during the experimental trial. This information will also be used to identify properties of the participant's lower limb. Additionally, the age, gender and body weight of the participants will also be recorded. All such data will be stored electronically on a computer hard drive kept in a secure location. The data will be store in such a way that a third party will not be able to identify the participant through the information stored on the data file. The information collected will be kept for a period of up to six years as reference for current and possibly future research. When no longer required, such data files will be destroyed through permanent deletion. If they be interested, participants can also arrange with the researcher a suitable time to have a discussion about any information derived from offline analysis of the collected data.

With the permission of the participant, a photograph/video of the experimental trial may also be taken using an electronic device. The photograph/video of the trial will also be stored electronically on a hard drive kept in a secure location. The video will be taken in such a way that it will provide minimal features which can be used to identify the individual.

Right to Withdraw from Participation

The participant may withdraw from participation at any time. The participant can also withdraw their data from the research within 3 months from the date of the experiment.

Anonymity and Confidentiality

The identity of the participant will be kept anonymous from all third parties. If the data collected is used in publications, participants will be referred to using a generic identifier such as “subject A”.

Funding

Funding has been obtained for the research. The source of the funding is the Faculty Research Development Fund of the Faculty of Engineering, project number: 3625057/9574.

Contact Details and Approval Wording

Researcher:

Shahid Hussain

Email: shus045@aucklanduni.ac.nz

Phone: 09 373-7599 extn. 87555

Supervisor:

Prof. Shane Xie

Email: s.xie@auckland.ac.nz

Phone: 09 373-7599 extn. 88143

Head of Department:

Prof. Gordon Mallinson

Email: g.mallinson@auckland.ac.nz

Phone: 09 373-7599 extn. 88148

For any queries regarding the ethical concerns you may contact the Chair, The University of Auckland Human Participants Ethics Committee, The University of Auckland, Office of the Vice Chancellor, Private Bag 92019, Auckland 1142. Telephone 09 373-7599 extn. 83711.

APPROVED BY THE UNIVERSITY OF AUCKLAND HUMAN PARTICIPANTS ETHICS COMMITTEE ON 20/08/2010 for (3) years, Reference Number 2010/308.

PARTICIPANT INFORMATION SHEET

(Participants)

Project title: Active Orthosis (robot) for Gait Rehabilitation

Name(s) of Researcher(s): Shahid Hussain, Prof. Shane Xie

Researcher Introduction

This research will be conducted by Shahid Hussain, a PhD student in the Department of Mechanical Engineering. The research is supervised by Prof. Shane Xie, in the Department of Mechanical Engineering.

Project Description and Invitation

This project aims to develop effective control algorithms for a robotic device designed to facilitate gait rehabilitation. The device is intended for use with patients suffering from musculoskeletal injuries or neurological diseases which impair gait functions. In particular, the part of the research where human participation is required is designed to evaluate the performance of the developed control algorithm. At the same time, information regarding the physical characteristics of the lower limb such as stiffness and lower limb kinematics will also be identified to facilitate development of the controller and the robotic device.

You are invited to participate in this research by carrying a series of exercises using a prototype of this gait rehabilitation device. Potential participants in this research are chosen from colleagues of the researcher who are healthy individuals over the age of 16 and have no existing gait impairment. It is preferred that you are familiar or comfortable with the operation of robotic devices. You will be shown the experimental setup and briefed about the operation of the prototype prior to your commitment to participation in this research. Your identity will be kept anonymous from third parties.

Project Procedures

You will only be required to take part in one experimental trial. The duration of the trial is expected to span approximately 45 minutes. The experimental trial will be carried out in the Mechatronics laboratory at the University of Auckland's School of Engineering.

Before the experimental trials begin, you will be given an explanation of the operation of the robotic devices, in particular the safety measures put in place to allow termination of the robot operation should an emergency situation arise. A brief demonstration of the prototype will also be given. Your age, gender and body weight will also be collected so that the results can be normalized with respect to the body weight and related to the corresponding demographic groups.

After the briefing and collection of information, your lower limb will be strapped in place on the prototype device and your trunk will be attached to a harness for body weight compensation. The experimental trials consists of two parts, the first involves the passive movement of the lower limb by the robotic device. During this part of the trial, you should relax your lower limb on the robotic device and allow the robot to move the lower limb passively along a predefined motion path. During this time, information regarding the orientation of the lower limb joints and the forces applied on the robot will

be logged and analysed to allow computation of the lower limb kinematic and stiffness parameters.

In the second part of the trial, you will be required to move your lower limb actively in the directions given by the user interface. The robot will provide a resistance against the motion during this part of the trial. Again, sensor information on the robotic device will be logged and analysed. This part of the trial will allow determination of the active forces applied by the lower limb to the robot.

You may experience a small level of physical discomfort during a normal trial. However, should the level of discomfort exceed that of the participant's liking, you can terminate the experimental trial by either indicating to the researcher or by using the emergency stop button provided. Since the actuators used in the prototype can produce significant forces, there is a possibility of injury should the hardware or software of the prototype malfunctions. This will be very unlikely as the prototype would have been tested extensively before the commencement of the experimental trial. In addition to that, the researcher or another individual will be present to provide aid if required. To ensure that prompt medical attention is available during emergencies, the trials will be conducted during the operating hours of the University Health Services clinic at the city campus.

Data Storage / Retention / Destruction / Future Use

As discussed in the previous section, data collected will be in the form of sensor readings which are used to compute the motion and force/moment observed during the experimental trial. This information will also be used to identify properties of the participant's lower limb joints. Additionally, your age, gender and body weight will also be recorded. All such data will be stored electronically on a computer hard drive kept in a secure location. The data will be stored in such a way that a third party will not be able to identify the participant through the information stored on the data file. The information collected will be kept for a period of up to six years as reference for current and possibly future research. When no longer required, such data files will be destroyed through permanent deletion. If you are interested, you can also arrange with the researcher a suitable time to have a discussion about any information derived from offline analysis of the collected data.

With your permission, a photograph/video of the experimental trial may also be taken using an electronic device. The photograph/video of the trial will also be stored electronically on a hard drive kept in a secure location. The video will be taken in such a way that it will provide minimal features which can be used to reveal your identity.

Right to Withdraw from Participation

You may withdraw from participation at any time. You can also withdraw their data from the research within 3 months from the date of the experiment.

Anonymity and Confidentiality

Your identity will be kept anonymous from all third parties. If the data collected is used in publications, you will be referred to using a generic identifier such as "subject A".

Participation in this research is entirely voluntary. Assurance from the head of department has been obtained such that neither your grades nor your relations with the university will be affected by agreement/refusal to participate in this research.

Incidental Findings

There is a small chance where anomaly may be found in the data collected regarding the characteristics of your lower limb. Should this occur, you will be informed and should consult a qualified health professional to verify such findings.

Compensation

In the unlikely event of a physical injury as a result of your participation in this study, you may be covered by ACC under the Injury Prevention, Rehabilitation, and Compensation Act 2001. ACC cover is not automatic, and your case will need to be assessed by ACC according to the provisions of the Injury Prevention, Rehabilitation, and Compensation Act 2001. If your claim is accepted by ACC, you still might not get any compensation. This depends on a number of factors, such as whether you are an earner or non-earner. ACC usually provides only partial reimbursement of costs and expenses, and there may be no lump sum compensation payable. There is no cover for mental injury unless it is a result of physical injury. If you have ACC cover, generally this will affect your right to sue the investigators.

If you have any questions about ACC, contact your nearest ACC office or the investigator.

You are also advised to check whether participation in this study would affect any indemnity cover you have or are considering, such as medical insurance, life insurance and superannuation.

Funding

Funding has been obtained for the research. The source of the funding is the Faculty Research Development Fund of the Faculty of Engineering, project number: 3625057/9574.

Contact Details and Approval Wording

Researcher:

Shahid Hussain

Email: shus045@aucklanduni.ac.nz

Phone: 09 373-7599 extn. 87555

Supervisor:

Assoc. Prof. Shane Xie

Email: s.xie@auckland.ac.nz

Phone: 09 373-7599 extn. 88143

Head of Department:

Prof. Gordon Mallinson

Email: g.mallinson@auckland.ac.nz

Phone: 09 373-7599 extn. 88148

For any queries regarding the ethical concerns you may contact the Chair, The University of Auckland Human Participants Ethics Committee, The University of Auckland, Office of the Vice Chancellor, Private Bag 92019, Auckland 1142. Telephone 09 373-7599 extn. 83711.

APPROVED BY THE UNIVERSITY OF AUCKLAND HUMAN PARTICIPANTS ETHICS COMMITTEE ON 20/08/2010 for (3) years, Reference Number 2010/308.

Poster

Participants wanted for experimental trials on Gait Rehabilitation Robot

Project title: Active Orthosis (robot) for Gait Rehabilitation
Names of Researchers: Shahid Hussain, Prof. Shane Xie

Human participants are currently being sought to take part in experimental trials for a research project. This research involves the development of a robotic device for gait rehabilitation. Invitation to participate in this research is extended to post graduate students and staff members who are healthy individuals with no lower limb impairment. The experimental trial will involve physical interaction between the participant and a prototype gait rehabilitation device.

The experimental trials are aimed at evaluating the controller performance of the gait rehabilitation robot. The trials will require the participant to undergo two types of rehabilitation exercises on the robot, the first involves the passive movement of the lower limb by the robotic device and the second requires the participants to actively move their lower limb against resistance provided by the robotic device. In terms of time commitment, participants are required to attend one experimental trial where the duration of each of these trials are expected to be about 45 minutes.

If you are interested in participating in this research and/or would like to learn more about the experimental trials, please contact the researchers through the contact details listed below.

Researcher (PhD student):
Shahid Hussain
Email: shus045@aucklanduni.ac.nz
Phone: 09 373-7599 extn. 87555

Supervisor:
Prof. Shane Xie
Email: s.xie@auckland.ac.nz
Phone: 09 373-7599 extn. 88143

Your help is very much appreciated. Thank you.
Funding has been obtained for the research. The source of the funding is the Faculty Research Development Fund of the Faculty of Engineering.

APPROVED BY THE UNIVERSITY OF AUCKLAND HUMAN PARTICIPANTS ETHICS COMMITTEE ON 20/08/2010 for (3) years, Reference Number 2010/308.

References

[1] S. Hussain, S. Q. Xie, and G. Liu, "Robot assisted treadmill training: Mechanisms and training strategies," *Medical Engineering & Physics,* vol. 33, pp. 527-533, 2011.

[2] D. J. Reinkensmeyer, J. L. Emken, and S. C. Cramer, "Robotics, motor learning, and neurologic recovery," *Annual Review of Biomedical Engineering,* vol. 6, pp. 497-525, 2004.

[3] D. A. Winter, *The Biomechanics and Motor Control of Human Gait: Normal, Elderly and Pathological*, 2nd ed. Waterloo: University of Waterloo Press, 1991.

[4] J. Perry and J. M. Burnfield, *Gait Analaysis: Normal and Pathological Function*, 2nd ed. NJ: Slack Inc., 1992.

[5] D. A. Winter, *Biomechanics and Motor Control of Human Movement* vol. 2nd ed. USA.: John Wiley & Sons, Inc., 1990.

[6] S. K. Banala, S. H. Kim, S. K. Agrawal, and J. P. Scholz, "Robot assisted gait training with active leg exoskeleton (ALEX)," *IEEE Transactions on Neural Systems and Rehabilitation Engineering,* vol. 17, pp. 2-8, 2009.

[7] G. Colombo, M. Joerg, R. Schreier, and V. Dietz, "Treadmill training of paraplegic patients using a robotic orthosis," *Journal of Rehabilitation Research and Development,* vol. 37, pp. 693-700, 2000.

[8] R. Bonita and R. Beaglehole, "Recovery of motor function after stroke," *Stroke,* vol. 19, pp. 1497-1500, 1988.

[9] T. E, M. NE, N. TA, C. E. 3rd, F. WC, N. CS, C. JS, and C. JE, "Technique to improve chronic motor deficit after stroke," *Archives of Physical Medicine and Rehabilitation,* vol. 74, pp. 347-354, 1993.

[10] B. FW, W. SH, and T. BS, "Effect of aging on human skeletal muscle and motor function," *Medicine and Science in Sports and Exercise,* vol. 26, pp. 556-560, 1994.

[11] www.heart.org *(Extracted on September 09, 2010)*.

[12] www.stroke.org.nz *(Extracted on April 13, 2012)*.

[13] www.catwalk.org.nz *(Extracted on February 19, 2012)*.

[14] A. Duschau-Wicke, A. Caprez, and R. Riener, "Patient-cooperative control increases active participation of individuals with SCI during robot-aided gait training," *Journal of NeuroEngineering and Rehabilitation,* vol. 7, 2010.

[15] http://scia.org.au/sci-research *(Extracted on June 14, 2012)*.

[16] S. Hesse, C. Bertelt, M. T. Jahnke, A. Schaffrin, P. Baake, M. Malezic, and K. H. Mauritz, "Treadmill training with partial body weight support compared with physiotherapy in nonambulatory hemiparetic patients," *Stroke,* vol. 26, pp. 976-981, 1995.

[17] M. Visintin, H. Barbeau, N. Korner-Bitensky, and N. E. Mayo, "A new approach to retrain gait in stroke patients through body weight support and treadmill stimulation," *Stroke,* vol. 29, pp. 1122-1128, 1998.

[18] Y. Laufer, R. Dickstein, Y. Chefez, and E. Marcovitz, "The effect of treadmill training on the ambulation of stroke survivors in the early stages of rehabilitation: A randomized study," *Journal of Rehabilitation Research and Development,* vol. 38, pp. 69-78, 2001.

[19] I. Teixeira da Cunha Filho, P. A. C. Lim, H. Qureshy, H. Henson, T. Monga, and E. J. Protas, "A comparison of regular rehabilitation and regular rehabilitation with supported treadmill ambulation training for acute stroke patients," *Journal of Rehabilitation Research and Development,* vol. 38, pp. 245-255, 2001.

[20] M. P. Murray, G. B. Spurr, and S. B. Sepic, "Treadmill vs. floor walking: Kinematics, electromyogram, and heart rate," *Journal of Applied Physiology,* vol. 59, pp. 87-91, 1985.

[21] S. L. Patterson, M. M. Rodgers, R. F. Macko, and L. W. Forrester, "Effect of treadmill exercise training on spatial and temporal gait parameters in subjects with chronic stroke: A preliminary report," *Journal of Rehabilitation Research and Development,* vol. 45, pp. 221-228, 2008.

[22] S. Hesse, M. Konrad, and D. Uhlenbrock, "Treadmill walking with partial body weight support versus floor walking in hemiparetic subjects," *Archives of Physical Medicine and Rehabilitation,* vol. 80, pp. 421-427, 1999.

[23] E. Hassid, D. Rose, J. Commisarow, M. Guttry, and B. H. Dobkin, "Improved gait symmetry in hemiparetic stroke patients induced during body weight-supported treadmill stepping," *Journal of Neurologic Rehabilitation,* vol. 11, pp. 21-26, 1997.

[24] V. L. J. Hendricks HT, Geurts AC, Zwarts MJ., "Motor Recovery after stroke: a systematic review of the literature.," *Phys Med Rehabil,* vol. 83, pp. 1629-37, 2002.

[25] A. L. Behrman and S. J. Harkema, "Locomotor training after human spinal cord injury: A series of case studies," *Physical Therapy,* vol. 80, pp. 688-700, 2000.

[26] L. Finch, H. Barbeau, and B. Arsenault, "Influence of body weight support on normal human gait: Development of a gait retraining strategy," *Physical Therapy,* vol. 71, pp. 842-856, 1991.

[27] G. Bolmsjo, H. Neveryd, and H. Eftring, "Robotics in rehabilitation," *IEEE Transactions on Rehabilitation Engineering,* vol. 3, pp. 77-83, 1995.

[28] S. A. Napper and R. L. Seaman, "Applications of robots in rehabilitation," *Robotics and Autonomous Systems,* vol. 5, pp. 227-239, 1989.

[29] N. Hogan, "Guest editorial: Rehabilitation applications of robotic technology," *Journal of Rehabilitation Research and Development,* vol. 37, 2000.

[30] S. K. Agrawal and A. Fattah, "Theory and design of an orthotic device for full or partial gravity-balancing of a human leg during motion," *IEEE Transactions on Neural Systems and Rehabilitation Engineering,* vol. 12, pp. 157-165, 2004.

[31] S. K. Banala, S. K. Agrawal, A. Fattah, V. Krishnamoorthy, W. L. Hsu, J. Scholz, and K. Rudolph, "Gravity-balancing leg orthosis and its performance evaluation," *IEEE Transactions on Robotics,* vol. 22, pp. 1228-1239, 2006.

[32] M. Vukobratovic, D. Hristic, and Z. Stojiljkovic, "Development of active anthropomorphic exoskeletons," *Medical and Biological Engineering,* vol. 12, pp. 66-80, 1974.

[33] A. S. a. J. G. Grundmann, "Design of a multi task exoskeletal walking device for paraplegics," *Biomechanics of Medical Devices,* pp. 569-644, 1981.

[34] Y. Stauffer, Y. Allemand, M. Bouri, J. Fournier, R. Clavel, P. Metrailler, R. Brodard, and F. Reynard, "The WalkTrainer - A new generation of walking reeducation device combining orthoses and muscle stimulation," *IEEE Transactions on Neural Systems and Rehabilitation Engineering,* vol. 17, pp. 38-45, 2009.

[35] A. Roy, H. I. Krebs, D. J. Williams, C. T. Bever, L. W. Forrester, R. M. Macko, and N. Hogan, "Robot-aided neurorehabilitation: A novel robot for ankle rehabilitation," *IEEE Transactions on Robotics,* vol. 25, pp. 569-582, 2009.

[36] S. Jezernik, G. Colombo, and M. Morari, "Automatic gait-pattern adaptation algorithms for rehabilitation with a 4-DOF robotic orthosis," *IEEE Transactions on Robotics and Automation,* vol. 20, pp. 574-582, 2004.

[37] R. Riener, L. Lunenburger, S. Jezernik, M. Anderschitz, G. Colombo, and V. Dietz, "Patient-cooperative strategies for robot-aided treadmill training: First experimental results," *IEEE Transactions on Neural Systems and Rehabilitation Engineering,* vol. 13, pp. 380-394, 2005.

[38] www.healthsouth.com *(Extracted on November 12, 2011).*

[39] J. F. Veneman, R. Kruidhof, E. E. G. Hekman, R. Ekkelenkamp, E. H. F. Van Asseldonk, and H. Van Der Kooij, "Design and evaluation of the LOPES exoskeleton robot for interactive gait rehabilitation," *IEEE Transactions on Neural Systems and Rehabilitation Engineering,* vol. 15, pp. 379-386, 2007.

[40] J. F. Veneman, R. Ekkelenkamp, R. Kruidhof, F. C. T. Van Der Helm, and H. Van Der Kooij, "A series elastic- and bowden-cable-based actuation system for use as torque actuator in exoskeleton-type robots," *International Journal of Robotics Research,* vol. 25, pp. 261-281, 2006.

[41] J. L. Emken, S. J. Harkema, J. A. Beres-Jones, C. K. Ferreira, and D. J. Reinkensmeyer, "Feasibility of manual teach-and-replay and continuous impedance shaping for robotic locomotor training following spinal cord injury," *IEEE Transactions on Biomedical Engineering,* vol. 55, pp. 322-334, 2008.

[42] N. Hogan, H. I. Krebs, B. Rohrer, J. J. Palazzolo, L. Dipietro, S. E. Fasoli, J. Stein, R. Hughes, W. R. Frontera, D. Lynch, and B. T. Volpe, "Motions or muscles? Some behavioral factors underlying robotic assistance of motor recovery," *Journal of Rehabilitation Research and Development,* vol. 43, pp. 605-618, 2006.

[43] J. L. Emken, J. H. Wynne, S. J. Harkema, and D. J. Reinkensmeyer, "A robotic device for manipulating human stepping," *IEEE Transactions on Robotics,* vol. 22, pp. 185-189, 2006.

[44] J. L. Emken and D. J. Reinkensmeyer, "Robot-enhanced motor learning: Accelerating internal model formation during locomotion by transient dynamic amplification," *IEEE Transactions on Neural Systems and Rehabilitation Engineering,* vol. 13, pp. 33-39, 2005.

[45] J. E. Bobrow and B. W. McDonell, "Modeling, identification, and control of a pneumatically actuated, force controllable robot," *IEEE Transactions on Robotics and Automation,* vol. 14, pp. 732-742, 1998.

[46] W. E. I. Daisuke Aoyagi, Susan J. Harkema, David J. Reinkensmeyer, James E. Bobrow., "A Robot and Control Algorithm That Can Synchronously Assist in Naturalistic Motion During Body-Weight-Supported Gait Training Following Neurologic Injury," *IEEE Transactions on Neural Systems And Rehabilitation Engineering,* vol. 15, pp. 387-400, 2007.

[47] M. Frey, G. Colombo, M. Vaglio, R. Bucher, M. Jörg, and R. Riener, "A novel mechatronic body weight support system," *IEEE Transactions on Neural Systems and Rehabilitation Engineering,* vol. 14, pp. 311-321, 2006.

[48] J. Von Zitzewitz, M. Bernhardt, and R. Riener, "A novel method for automatic treadmill speed adaptation," *IEEE Transactions on Neural Systems and Rehabilitation Engineering,* vol. 15, pp. 401-409, 2007.

[49] S. M. M. de Rossi, N. Vitiello, T. Lenzi, R. Ronsse, B. Koopman, A. Persichetti, F. Vecchi, A. J. Ijspeert, H. van der Kooij, and M. C. Carrozza, "Sensing pressure distribution on a lower-limb exoskeleton physical human-machine interface," *Sensors,* vol. 11, pp. 207-227, 2011.

[50] S. L. Patterson, L. W. Forrester, M. M. Rodgers, A. S. Ryan, F. M. Ivey, J. D. Sorkin, and R. F. Macko, "Determinants of Walking Function After Stroke: Differences by Deficit Severity," *Archives of Physical Medicine and Rehabilitation,* vol. 88, pp. 115-119, 2007.

[51] R. Bayat, H. Barbeau, and A. Lamontagne, "Speed and temporal-distance adaptations during treadmill and overground walking following stroke," *Neurorehabilitation and Neural Repair,* vol. 19, pp. 115-124, 2005.

[52] H. Barbeau, S. Nadeau, and C. Garneau, "Physical determinants, emerging concepts, and training approaches in gait of individuals with spinal cord injury," *Journal of Neurotrauma,* vol. 23, pp. 571-585, 2006.

[53] G. Kwakkel, R. C. Wagenaar, T. W. Koelman, G. J. Lankhorst, and J. C. Koetsier, "Effects of intensity of rehabilitation after stroke: A research synthesis," *Stroke,* vol. 28, pp. 1550-1556, 1997.

[54] S. Hussain, S. Q. Xie, P. K. Jamwal, and J. Parsons, "An Intrinsically Compliant Robotic Orthosis for Treadmill Training.," *Medical Engineering and Physics,* 2012 (In press) DOI:10.1016/j.medengphy.2012.02.003.

[55] P. S. Lum, C. G. Burgar, P. C. Shor, M. Majmundar, and M. Van der Loos, "Robot-assisted movement training compared with conventional therapy techniques for the rehabilitation of upper-limb motor function after stroke," *Archives of Physical Medicine and Rehabilitation,* vol. 83, pp. 952-959, 2002.

[56] P. S. Lum, D. J. Reinkensmeyer, and S. L. Lehman, "Robotic assist devices for bimanual physical therapy: preliminary experiments," *IEEE Transactions on Rehabilitation Engineering,* vol. 3, pp. 185-191, 1993.

[57] P. S. Lum, S. L. Lehman, and D. J. Reinkensmeyer, "Bimanual lifting rehabilitator: An adaptive machine for therapy of stroke patients," *IEEE Transactions on Rehabilitation Engineering,* vol. 3, pp. 166-173, 1995.

[58] K. J. Wisneski and M. J. Johnson, "Quantifying kinematics of purposeful movements to real, imagined, or absent functional objects: Implications for modelling trajectories for robot-assisted ADL tasks," *Journal of NeuroEngineering and Rehabilitation,* vol. 4, 2007.

[59] A. Montagner, A. Frisoli, L. Borelli, C. Procopio, M. Bergamasco, M. C. Carboncini, and B. Rossi, "A pilot clinical study on robotic assisted rehabilitation in VR with an arm exoskeleton device," in *2007 Virtual Rehabilitation, IWVR*, 2007, pp. 57-64.

[60] H. Vallery, E. H. F. Van Asseldonk, M. Buss, and H. Van Der Kooij, "Reference trajectory generation for rehabilitation robots: Complementary limb motion estimation," *IEEE Transactions on Neural Systems and Rehabilitation Engineering,* vol. 17, pp. 23-30, 2009.

[61] J. L. Emken, R. Benitez, and D. J. Reinkensmeyer, "Human-robot cooperative movement training: Learning a novel sensory motor transformation during walking with robotic assistance-as-needed," *Journal of NeuroEngineering and Rehabilitation,* vol. 4, 2007.

[62] J. L. Patton, M. E. Stoykov, M. Kovic, and F. A. Mussa-Ivaldi, "Evaluation of robotic training forces that either enhance or reduce error in chronic hemiparetic stroke survivors," *Experimental Brain Research,* vol. 168, pp. 368-383, 2006.

[63] L. E. Kahn, P. S. Lum, W. Z. Rymer, and D. J. Reinkensmeyer, "Robot-assisted movement training for the stroke-impaired arm: Does it matter what the robot does?," *Journal of Rehabilitation Research and Development,* vol. 43, pp. 619-629, 2006.

[64] A. Kaelin-Lane, L. Sawaki, and L. G. Cohen, "Role of voluntary drive in encoding an elementary motor memory," *Journal of Neurophysiology,* vol. 93, pp. 1099-1103, KAE 05 2005.

[65] E. T. Wolbrecht, V. Chan, D. J. Reinkensmeyer, and J. E. Bobrow, "Optimizing compliant, model-based robotic assistance to promote neurorehabilitation," *IEEE Transactions on Neural Systems and Rehabilitation Engineering,* vol. 16, pp. 286-297, 2008.

[66] N. Hogan, "Impedance Control: An approach to manipulation," *J. Dynamic Syst. Meas. Control,* vol. 107, pp. 1-23, 1985.

[67] J. Hoogen, R. Riener, and G. Schmidt, "Control aspects of a robotic haptic interface for kinesthetic knee joint simulation," *Control Engineering Practice,* vol. 10, pp. 1301-1308, 2002.

[68] M. Lotze, C. Braun, N. Birbaumer, S. Anders, and L. G. Cohen, "Motor learning elicited by voluntary drive," *Brain,* vol. 126, pp. 866-872, 2003.

[69] A. J. F. Lance L. Cai, Chad K. Otoshi, Yong qiang Liang, Joel W. Burdick, Roland R. Roy and V. Reggie Edgerton, "Implications of assist-as-needed robotic step training after a complete spinal cord injury on intrinsic strategies of motor learning.," *Journal of NeuroScience,* vol. 20, pp. 10564-10568, 2006.

[70] R. Colombo, F. Pisano, S. Micera, A. Mazzone, C. Delconte, M. Chiara Carrozza, P. Dario, and G. Minuco, "Robotic techniques for upper limb evaluation and rehabilitation of stroke patients," *IEEE Transactions on Neural Systems and Rehabilitation Engineering,* vol. 13, pp. 311-324, 2005.

[71] J. v. Z. Alexander Duschau Wicke, Andrea Caprez, Lars Lunenburger, Robert Riener, "Path Control: A Method for Patient-Cooperative Robot Aided Gait Rehabilitation " *IEEE Transactions on Neural Systems And Rehabilitation Engineering,* vol. 18, pp. 38-48, 2010.

[72] M. S. Erden and T. Tomiyama, "Human-intent detection and physically interactive control of a robot without force sensors," *IEEE Transactions on Robotics,* vol. 26, pp. 370-382, 2010.

[73] D. Campolo, D. Accoto, D. Formica, and E. Guglielmelli, "Intrinsic constraints of neural origin: Assessment and application to rehabilitation robotics," *IEEE Transactions on Robotics,* vol. 25, pp. 492-501, 2009.

[74] V. Magagnin, A. Porta, L. Fusini, V. Licari, I. Bo, M. Turiel, F. Molteni, S. Cerutti, and E. G. Caiani, "Evaluation of the autonomic response in healthy subjects during treadmill training with assistance of a robot-driven gait orthosis," *Gait & Posture,* vol. 29, pp. 504-508, 2009.

[75] V. Magagnin, I. Bo, M. Turiel, M. Fornari, E. G. Caiani, and A. Porta, "Effects of robot-driven gait orthosis treadmill training on the autonomic response in rehabilitation-responsive stroke and cervical spondylotic myelopathy patients," *Gait & Posture,* vol. 32, pp. 199-204, 2010.

[76] A. C. Lo, V. C. Chang, M. A. Gianfrancesco, J. H. Friedman, T. S. Patterson, and D. F. Benedicto, "Reduction of freezing of gait in Parkinson's disease by repetitive robot-

assisted treadmill training: A pilot study," *Journal of NeuroEngineering and Rehabilitation,* p. 51, 2010.

[77] T. G. Hornby, D. H. Zemon, and D. Campbell, "Robotic-assisted, body-weight-supported treadmill training in individuals following motor incomplete spinal cord injury," *Physical Therapy,* vol. 85, pp. 52-66, 2005.

[78] S. H. Kim, S. K. Banala, E. A. Brackbill, S. K. Agrawal, V. Krishnamoorthy, and J. P. Scholz, "Robot-assisted modifications of gait in healthy individuals," *Experimental Brain Research,* vol. 202, pp. 809-824, 2010.

[79] E. H. F. Van Asseldonk, J. F. Veneman, R. Ekkelenkamp, J. H. Buurke, F. C. T. Van Der Helm, and H. Van Der Kooij, "The effects on kinematics and muscle activity of walking in a robotic gait trainer during zero-force control," *IEEE Transactions on Neural Systems and Rehabilitation Engineering,* vol. 16, pp. 360-370, 2008.

[80] S. Jezernik, R. Schärer, G. Colombo, and M. Morari, "Adaptive robotic rehabilitation of locomotion: A clinical study in spinally injured individuals," *Spinal Cord,* vol. 41, pp. 657-666, 2003.

[81] B. Husemann, F. Müller, C. Krewer, S. Heller, and E. Koenig, "Effects of locomotion training with assistance of a robot-driven gait orthosis in hemiparetic patients after stroke: A randomized controlled pilot study," *Stroke,* vol. 38, pp. 349-354, 2007.

[82] J. F. Israel, D. D. Campbell, J. H. Kahn, and T. G. Hornby, "Metabolic costs and muscle activity patterns during robotic- and therapist-assisted treadmill walking in individuals with incomplete spinal cord injury," *Physical Therapy,* vol. 86, pp. 1466-1478, 2006.

[83] K. P. Westlake and C. Patten, "Pilot study of Lokomat versus manual-assisted treadmill training for locomotor recovery post-stroke," *Journal of NeuroEngineering and Rehabilitation,* vol. 6, 2009.

[84] A. Mayr, M. Kofler, E. Quirbach, H. Matzak, K. Fröhlich, and L. Saltuari, "Prospective, blinded, randomized crossover study of gait rehabilitation in stroke patients using the Lokomat gait orthosis," *Neurorehabilitation and Neural Repair,* vol. 21, pp. 307-314, 2007.

[85] T. G. Hornby, D. D. Campbell, J. H. Kahn, T. Demott, J. L. Moore, and H. R. Roth, "Enhanced gait-related improvements after therapist- versus robotic-assisted locomotor training in subjects with chronic stroke: A randomized controlled study," *Stroke,* vol. 39, pp. 1786-1792, 2008.

[86] J. Hidler, D. Nichols, M. Pelliccio, K. Brady, D. D. Campbell, J. H. Kahn, and T. G. Hornby, "Multicenter randomized clinical trial evaluating the effectiveness of the Lokomat in subacute stroke," *Neurorehabilitation and Neural Repair,* vol. 23, pp. 5-13, 2009.

[87] T. G. Sugar, J. He, E. J. Koeneman, J. B. Koeneman, R. Herman, H. Huang, R. S. Schultz, D. E. Herring, J. Wanberg, S. Balasubramanian, P. Swenson, and J. A. Ward, "Design and control of RUPERT: A device for robotic upper extremity repetitive therapy," *IEEE Transactions on Neural Systems and Rehabilitation Engineering,* vol. 15, pp. 336-346, 2007.

[88] H. Vallery, J. Veneman, E. van Asseldonk, R. Ekkelenkamp, M. Buss, and H. van Der Kooij, "Compliant actuation of rehabilitation robots," *IEEE Robotics and Automation Magazine,* vol. 15, pp. 60-69, 2008.

[89] H. I. Krebs, B. T. Volpe, M. L. Aisen, and N. Hogan, "Increasing productivity and quality of care: Robot-aided neuro-rehabilitation," *Journal of Rehabilitation Research and Development,* vol. 37, pp. 639-652, 2000.

[90] V. R. Ham, T. G. Sugar, B. Vanderborght, K. W. Hollander, and D. Lefeber, "Compliant actuator designs: Review of actuators with passive adjustable compliance/controllable stiffness for robotic applications," *IEEE Robotics and Automation Magazine,* vol. 16, pp. 81-94, 2009.

[91] J. A. Blaya and H. Herr, "Adaptive Control of a Variable-Impedance Ankle-Foot Orthosis to Assist Drop-Foot Gait," *IEEE Transactions on Neural Systems and Rehabilitation Engineering,* vol. 12, pp. 24-31, 2004.

[92] J. S. Sulzer, R. A. Roiz, M. A. Peshkin, and J. L. Patton, "A highly backdrivable, lightweight knee actuator for investigating gait in stroke," *IEEE Transactions on Robotics,* vol. 25, pp. 539-548, 2009.

[93] K. Kong, J. Bae, and M. Tomizuka, "Control of rotary series elastic actuator for ideal force-mode actuation in human-robot interaction applications," *IEEE/ASME Transactions on Mechatronics,* vol. 14, pp. 105-118, 2009.

[94] K. Kong and D. Jeon, "Design and control of an exoskeleton for the elderly and patients," *IEEE/ASME Transactions on Mechatronics,* vol. 11, pp. 428-432, 2006.

[95] A. H. A. Stienenw, E. E. G. Hekman, H. T. Braak, A. M. M. Aalsma, F. C. T. Van Der Helm, and H. Van Der Kooij, "Design of a rotational hydroelastic actuator for a powered exoskeleton for upper limb rehabilitation," *IEEE Transactions on Biomedical Engineering,* vol. 57, pp. 728-735, 2010.

[96] C. P. Chou and B. Hannaford, "Measurement and modeling of McKibben pneumatic artificial muscles," *IEEE Transactions on Robotics and Automation,* vol. 12, pp. 90-102, 1996.

[97] D. Shin, I. Sardellitti, Y. L. Park, O. Khatib, and M. Cutkosky, "Design and control of a bio-inspired human-friendly robot," *International Journal of Robotics Research,* vol. 29, pp. 571-584, 2010.

[98] J. Ueda, D. Ming, V. Krishnamoorthy, M. Shinohara, and T. Ogasawara, "Individual muscle control using an exoskeleton robot for muscle function testing," *IEEE Transactions on Neural Systems and Rehabilitation Engineering,* vol. 18, pp. 339-350, 2010.

[99] D. P. Ferris, K. E. Gordon, G. S. Sawicki, and A. Peethambaran, "An improved powered ankle-foot orthosis using proportional myoelectric control," *Gait and Posture,* vol. 23, pp. 425-428, 2006.

[100] S. K. Banala, "Lower extremity exoskeltons for gait rehabilitation of motor-impaired patients," PhD, Mechanical Engineering, University of Delaware, 2008.

[101] S. J. Olney and C. Richards, "Hemiparetic gait following stroke. Part I: Characteristics," *Gait and Posture,* vol. 4, pp. 136-148, 1996.

[102] A. Lamontagne, C. L. Richards, and F. Malouin, "Coactivation during gait as an adaptive behavior after stroke," *Journal of Electromyography and Kinesiology,* vol. 10, pp. 407-415, 2000.

[103] W. K. Durfee and A. Rivard, "Design and simulation of a pneumatic, stored-energy, hybrid orthosis for gait restoration," *Journal of Biomechanical Engineering,* vol. 127, pp. 1014-1019, 2005.

[104] J. H. Buurke, A. V. Nene, G. Kwakkel, V. Erren-Wolters, M. J. Ijzerman, and H. J. Hermens, "Recovery of gait after stroke: What changes?," *Neurorehabilitation and Neural Repair,* vol. 22, pp. 676-683, 2008.

[105] J. M. Hidler and A. E. Wall, "Alterations in muscle activation patterns during robotic-assisted walking," *Clinical Biomechanics,* vol. 20, pp. 184-193, 2005.

[106] T. Klarner, H. K. Chan, J. M. Wakeling, and T. Lam, "Patterns of muscle coordination vary with stride frequency during weight assisted treadmill walking," *Gait and Posture,* vol. 31, pp. 360-365, 2010.

[107] N. D. Neckel, N. Blonien, D. Nichols, and J. Hidler, "Abnormal joint torque patterns exhibited by chronic stroke subjects while walking with a prescribed physiological gait pattern," *Journal of NeuroEngineering and Rehabilitation,* vol. 5, 2008.

[108] J. Hidler, W. Wisman, and N. Neckel, "Kinematic trajectories while walking within the Lokomat robotic gait-orthosis," *Clinical Biomechanics,* vol. 23, pp. 1251-1259, 2008.

[109] L. L. Cai, A. J. Fong, C. K. Otoshi, Y. Liang, J. W. Burdick, R. R. Roy, and V. R. Edgerton, "Implications of assist-as-needed robotic step training after a complete spinal cord injury on intrinsic strategies of motor learning," *Journal of NeuroScience,* vol. 26, pp. 10564-10568, 2006.

[110] M. A. Lemay, N. Hogan, and J. W. A. Van Dorsten, "Issues in impedance selection and input devices for multijoint powered orthotics," *IEEE Transactions on Rehabilitation Engineering,* vol. 6, pp. 102-105, 1998.

[111] H. M, "Muscle tone abnormalities," *Rehabilitation Nursing,* vol. 22, pp. 118-23, 1997.

[112] R. Riener and T. Edrich, "Identification of passive elastic joint moments in the lower extremities," *Journal of Biomechanics,* vol. 32, pp. 539-544, 1999.

[113] T. Edrich, R. Riener, and J. Quintern, "Analysis of passive elastic joint moments in paraplegics," *IEEE Transactions on Biomedical Engineering,* vol. 47, pp. 1058-1065, 2000.

[114] M. Wu, T. G. Hornby, J. M. Landry, H. Roth, and B. D. Schmit, "A cable-driven locomotor training system for restoration of gait in human SCI," *Gait and Posture,* vol. 33, pp. 256-260, 2011.

[115] D.A.Winter, "Biomechancis of Human Movement," *Toronto, ON, Canada: John Wiley & Sons.,* 1979.

[116] T. Yakimovich, J. Kofman, and E. D. Lemaire, "Design and evaluation of a stance-control knee-ankle-foot orthosis knee joint," *IEEE Transactions on Neural Systems and Rehabilitation Engineering,* vol. 14, pp. 361-369, 2006.

[117] A. Schiele and F. C. T. Van Der Helm, "Kinematic design to improve ergonomics in human machine interaction," *IEEE Transactions on Neural Systems and Rehabilitation Engineering,* vol. 14, pp. 456-469, 2006.

[118] K. E. Gordon, G. S. Sawicki, and D. P. Ferris, "Mechanical performance of artificial pneumatic muscles to power an ankle-foot orthosis," *Journal of Biomechanics,* vol. 39, pp. 1832-1841, 2006.

[119] S. L. Delp, F. C. Anderson, A. S. Arnold, P. Loan, A. Habib, C. T. John, E. Guendelman, and D. G. Thelen, "OpenSim: Open-source software to create and analyze dynamic simulations of movement," *IEEE Transactions on Biomedical Engineering,* vol. 54, pp. 1940-1950, 2007.

[120] G. T. Yamaguchi, *Dynamic Modeling of Musculoskeletal Motion - A Vectorized Approach for Biomechanical Analysis in Three Dimensions*, 1st ed. Massachusetts, USA: Kluwer academic publishers, 2001.

[121] L.-W. Tsai, *Robot Analysis:The Mechanics of Serial and Parallel Manipulators*: John Wiley & Sons, 1999.

[122] J.-J. E. Slotine and W. Li, *Applied NonLinear Control*. NJ: Prentice-Hall, Inc 1991.

[123] B. Tondu and P. Lopez, "Modeling and control of McKibben artificial muscle robot actuators," *IEEE Control Systems Magazine,* vol. 20, pp. 15-38, 2000.

[124] M. Doumit, A. Fahim, and M. Munro, "Analytical modeling and experimental validation of the braided pneumatic muscle," *IEEE Transactions on Robotics,* vol. 25, pp. 1282-1291, 2009.

[125] G. K. Klute and B. Hannaford, "Accounting for elastic energy storage in McKibben artificial muscle actuators," *Journal of Dynamic Systems, Measurement and Control, Transactions of the ASME,* vol. 122, pp. 386-388, 2000.

[126] D. B. Reynolds, D. W. Repperger, C. A. Phillips, and G. Bandry, "Modeling the dynamic characteristics of pneumatic muscle," *Annals of Biomedical Engineering,* vol. 31, pp. 310-317, 2003.

[127] T. Y. Choi and J. J. Lee, "Control of manipulator using pneumatic muscles for enhanced safety," *IEEE Transactions on Industrial Electronics,* vol. 57, pp. 2815-2825, 2010.

[128] V. M. Zatsiorsky and V. N. Seluyanov, "Mass and inertia characteristics of the main segments of the human body," 1983, pp. 1152-1159.

[129] J. H. Lilly and P. M. Quesada, "A two-input sliding-mode controller for a planar arm actuated by four pneumatic muscle groups," *IEEE Transactions on Neural Systems and Rehabilitation Engineering,* vol. 12, pp. 349-359, 2004.

[130] T. Y. Choi, B. S. Choi, and K. H. Seo, "Position and compliance control of a pneumatic muscle actuated manipulator for enhanced safety," *IEEE Transactions on Control Systems Technology,* vol. 19, pp. 832-842, 2011.

[131] R. Q. Van Der Linde, "Design, analysis, and control of a low power joint for walking robots, by phasic activation of McKibben muscles," *IEEE Transactions on Robotics and Automation,* vol. 15, pp. 599-604, 1999.

[132] S. K. Banala, S. K. Agrawal, S. H. Kim, and J. P. Scholz, "Novel gait adaptation and neuromotor training results using an active leg exoskeleton," *IEEE/ASME Transactions on Mechatronics,* vol. 15, pp. 216-225, 2010.

[133] X. Shen, "Nonlinear model-based control of pneumatic artificial muscle servo systems," *Control Engineering Practice,* vol. 18, pp. 311-317, 2010.

[134] J. H. Lilly and L. Yang, "Sliding mode tracking for pneumatic muscle actuators in opposing pair configuration," *IEEE Transactions on Control Systems Technology,* vol. 13, pp. 550-558, 2005.

[135] J. H. Lilly, "Adaptive tracking for pneumatic muscle actuators in bicep and tricep configurations," *IEEE Transactions on Neural Systems and Rehabilitation Engineering,* vol. 11, pp. 333-339, 2003.

[136] M. Van Damme, B. Vanderborght, B. Verrelst, R. Van Ham, F. Daerden, and D. Lefeber, "Proxy-based sliding mode control of a planar pneumatic manipulator," *International Journal of Robotics Research,* vol. 28, pp. 266-284, 2009.

[137] K. Kyoungchul, M. Hyosang, J. Doyoung, and M. Tomizuka, "Control of an Exoskeleton for Realization of Aquatic Therapy Effects," *Mechatronics, IEEE/ASME Transactions on,* vol. 15, pp. 191-200, 2010.

[138] F. E. Zajac, R. R. Neptune, and S. A. Kautz, "Biomechanics and muscle coordination of human walking: Part I: Introduction to concepts, power transfer, dynamics and simulations," *Gait and Posture,* vol. 16, pp. 215-232, 2002.

[139] F. E. Zajac, R. R. Neptune, and S. A. Kautz, "Biomechanics and muscle coordination of human walking: Part II: Lessons from dynamical simulations and clinical implications," *Gait and Posture,* vol. 17, pp. 1-17, 2003.

[140] M. G. Pandy and T. P. Andriacchi, "Muscle and joint function in human locomotion," *Annual Review of Biomedical Engineering,* vol. 12, pp. 401-433, 2010.

[141] J. Hicks, A. Arnold, F. Anderson, M. Schwartz, and S. Delp, "The effect of excessive tibial torsion on the capacity of muscles to extend the hip and knee during single-limb stance," *Gait and Posture,* vol. 26, pp. 546-552, 2007.

[142] K. M. Steele, A. Seth, J. L. Hicks, M. S. Schwartz, and S. L. Delp, "Muscle contributions to support and progression during single-limb stance in crouch gait," *Journal of Biomechanics,* vol. 43, pp. 2099-2105, 2010.

[143] C. A. Crabtree and J. S. Higginson, "Modeling neuromuscular effects of ankle foot orthoses (AFOs) in computer simulations of gait," *Gait and Posture,* vol. 29, pp. 65-70, 2009.

[144] J. J. Moré and G. Toraldo, "Algorithms for bound constrained quadratic programming problems," *Numerische Mathematik,* vol. 55, pp. 377-400, 1989.

[145] R. D. Crowninshield and R. A. Brand, "A physiologically based criterion of muscle force prediction in locomotion," *Journal of Biomechanics,* vol. 14, pp. 793-801, 1981.

[146] M. G. Pandy, "Computer modeling and simulation of human movement," *Annual Review of Biomedical Engineering,* vol. 3, pp. 245-273, 2001.

[147] K. G. M. Gerritsen, A. J. Van Den Bogert, and B. M. Nigg, "Direct dynamics simulation of the impact phase in heel-toe running," *Journal of Biomechanics,* vol. 28, pp. 661-668, 1995.

[148] J. A. Friederich and R. A. Brand, "Muscle fiber architecture in the human lower limb," *Journal of Biomechanics,* vol. 23, pp. 91-95, 1990.

[149] A. L. Hof, H. Elzinga, W. Grimmius, and J. P. K. Halbertsma, "Speed dependence of averaged EMG profiles in walking," *Gait & Posture,* vol. 16, pp. 78-86, 2002.

[150] A. R. den Otter, A. C. H. Geurts, T. Mulder, and J. Duysens, "Speed related changes in muscle activity from normal to very slow walking speeds," *Gait & Posture,* vol. 19, pp. 270-278, 2004.

[151] R. R. Neptune, K. Sasaki, and S. A. Kautz, "The effect of walking speed on muscle function and mechanical energetics," *Gait & Posture,* vol. 28, pp. 135-143, 2008.

[152] F. C. Anderson and M. G. Pandy, "Individual muscle contributions to support in normal walking," *Gait and Posture,* vol. 17, pp. 159-169, AND 03 2003.

[153] H. Geyer and H. Herr, "A Muscle-reflex model that encodes principles of legged mechanics produces human walking dynamics and muscle activities," *IEEE Transactions on Neural Systems and Rehabilitation Engineering,* vol. 18, pp. 263-273, 2010.

[154] F. E. Zajac, "Understanding muscle coordination of the human leg with dynamical simulations," *Journal of Biomechanics,* vol. 35, pp. 1011-1018, 2002.

[155] K. J. Agarwal-Harding, M. H. Schwartz, and S. L. Delp, "Variation of hamstrings lengths and velocities with walking speed," *Journal of Biomechanics,* vol. 43, pp. 1522-1526, 2010.

[156] M. D. Fox and S. L. Delp, "Contributions of muscles and passive dynamics to swing initiation over a range of walking speeds," *Journal of Biomechanics,* vol. 43, pp. 1450-1455, 2010.

[157] J. Hidler and N. Neckel, "Inverse-dynamics based assessment of gait using a robotic orthosis," *Conference proceedings : ... Annual International Conference of the IEEE Engineering in Medicine and Biology Society. IEEE Engineering in Medicine and Biology Society. Conference,* vol. 1, pp. 185-188, 2006.

[158] E. M. Arnold, S. R. Ward, R. L. Lieber, and S. L. Delp, "A model of the lower limb for analysis of human movement," *Annals of Biomedical Engineering,* vol. 38, pp. 269-279, 2010.

[159] T. S. Bae, P. Loan, K. Choi, D. Hong, and M. S. Mun, "Estimation of muscle response using three-dimensional musculoskeletal models before impact situation: a simulation study," *Journal of Biomechanical Engineering,* vol. 132, p. 121011, 2010.

[160] A. H. A. Stienen, E. E. G. Hekman, F. C. T. van der Helm, and H. van der Kooij, "Self-aligning exoskeleton axes through decoupling of joint rotations and translations," *IEEE Transactions on Robotics,* vol. 25, pp. 628-633, 2009.

[161] Y. Xu, "Chattering free robust control for nonlinear systems," *IEEE Transactions on Control Systems Technology,* vol. 16, pp. 1352-1359, 2008.

[162] B. Armstrong-Hélouvry, P. Dupont, and C. C. D. Wit, "A survey of models, analysis tools and compensation methods for the control of machines with friction " *Automatica,* vol. 30, pp. 1083-1138, 1994.

[163] A. Albu-Schäffer, W. Bertleff, B. Rebele, B. Schäfer, K. Landzettel, and G. Hirzinger, "ROKVISS - Robotics component verification on ISS current experimental results on parameter identification," in *IEEE International Conference on Robotics and Automation*, 2006, pp. 3879-3885.

[164] M. Mahvash and A. M. Okamura, "Friction compensation for a force-feedback telerobotic system," in *IEEE International Conference on Robotics and Automation*, 2006, pp. 3268-3273.

[165] D. J. Reinkensmeyer, D. Aoyagi, J. L. Emken, J. A. Galvez, W. Ichinose, G. Kerdanyan, S. Maneekobkunwong, K. Minakata, J. A. Nessler, R. Weber, R. R. Roy, R. De Leon, J. E. Bobrow, S. J. Harkema, and V. Reggie Edgerton, "Tools for understanding and optimizing robotic gait training," *Journal of Rehabilitation Research and Development,* vol. 43, pp. 657-670, 2006.

[166] M. W. Spong and M. Midyasagar, *Robot Dynamics and Control* New York Wiley, 1989.

[167] E. T. Wolbrecht, D. J. Reinkensmeyer, and J. E. Bobrow, "Pneumatic control of robots for rehabilitation," *International Journal of Robotics Research,* vol. 29, pp. 23-38, 2010.

[168] C. M. Dean, C. L. Richards, and F. Malouin, "Walking speed over 10 metres overestimates locomotor capacity after stroke," *Clinical Rehabilitation,* vol. 15, pp. 415-421, 2001.

[169] H. P. Von Schroeder, R. D. Coutts, P. D. Lyden, E. Billings Jr, and V. L. Nickel, "Gait parameters following stroke: A practical assessment," *Journal of Rehabilitation Research and Development,* vol. 32, pp. 25-31, 1995.

[170] S. J. Olney, M. P. Griffin, T. N. Monga, and I. D. McBride, "Work and power in gait of stroke patients," *Archives of Physical Medicine and Rehabilitation,* vol. 72, pp. 309-314, 1991.

[171] N. Jarrasse and G. Morel, "Connecting a Human Limb to an Exoskeleton," *IEEE Transactions on Robotics,* vol. 28, pp. 697-709, 2012.